UNIVERSIDADE ESTADUAL PAULISTA
"JÚLIO DE MESQUITA FILHO"
Câmpus de São José do Rio Preto

Mayara Aparecida Rocha Garcia

Atividade Antimicrobiana de Aminochalconas contra Células Planctônicas e Biofilmes

São José do Rio Preto
2021

Mayara Aparecida Rocha Garcia

Atividade Antimicrobiana de Aminochalconas contra Células Planctônicas e Biofilmes

Tese apresentada como parte dos requisitos para obtenção do título de Doutor em Química, junto ao Programa de Pós-Graduação em Química, do Instituto de Biociências, Letras e Ciências Exatas da Universidade Estadual Paulista "Júlio de Mesquita Filho", Câmpus de São José do Rio Preto.

Financiadora: Capes

Orientador: Prof. Dr. Luis Octavio Regasini
Coorientador: Janaína de Cássia Orlandi Sardi

São José do Rio Preto
2021

Garcia, Mayara Aparecida Rocha

G216a Atividade Antimicrobiana de Aminochalconas contra Células Planctônicas e Biofilmes / Mayara Aparecida Rocha Garcia. -- São José do Rio Preto, 2021

256 p.

Tese (doutorado) - Universidade Estadual Paulista (Unesp), Instituto de Biociências Letras e Ciências Exatas, São José do Rio Preto

Orientador: Luis Octavio Regasini Coorientadora: Janaína de Cássia Orlandi Sardi

1. Química farmacêutica. 2. Chalconas. 3. Antimicrobianos. 4. Biofilme. I. Título.

Mayara Aparecida Rocha Garcia

Atividade Antimicrobiana de Aminochalconas contra Células Planctônicas e Biofilmes

Tese apresentada como parte dos requisitos para obtenção do título de Doutor em Química, junto ao Programa de Pós-Graduação em Química, do Instituto de Biociências, Letras e Ciências Exatas da Universidade Estadual Paulista "Júlio de Mesquita Filho", Câmpus de São José do Rio Preto.

Financiadora: Capes

Comissão Examinadora

Prof. Dr. Luis Octavio Regasini
UNESP – Câmpus de São José do Rio Preto
Orientador

Profª. Drª. Lídia Moreira Lima
UFRJ – Universidade Federal do Rio de Janeiro

Profª. Drª. Wanda Pereira Almeida
UNICAMP – Universidade Estadual de Campinas

Profª. Drª. Vera Aparecida de Oliveira Tiera
UNESP – Câmpus de São José do Rio Preto

Profª. Drª. Amanda Danuello Pivatto
UFU – Universidade Federal de Uberlândia

São José do Rio Preto
24 de novembro de 2021

AGRADECIMENTOS

À Deus pelas oportunidades concedidas até aqui.

Ao meu orientador, Luís Octavio, pelos ensinamentos e orientação.

A minha mãe biológica, Maria de Fátima, pelo amor, dedicação e ensinamentos que me trouxeram à esse título, apesar das dificuldades Sem ela nada seria possível.

A minha mãe de criação, Teresa Vita, pela dedicação e carinho que me tornaram a pessoa que sou e me fizeram alcançar sonhos. Todo apoio e motivação foram fundamentais para esse título.

A minha irmã e amiga, Yara, pelo apoio nos momentos de fraqueza.

À memória de meu irmão, André, por todo amor e carinho dedicados enquanto vivo. Ao Prof. Dr. Pedro Rosalen e Drª. Janaína de Cássia Orlandi Sardi, por todo o suporte e apoio na minha ida a Piracicaba para realização dos ensaios biológicos.

Ao Prof. Dr. Fernando Rogério Pavan, pelo apoio na realização dos ensaios em micobactérias.

Ao Fábio pela realização dos espectros de RMN.

Ao Conselho Nacional de Desenvolvimento Científico e Tecnológico (CNPq), a Fundação de Amparo à Pesquisa do Estado de São Paulo (FAPESP), Pró-Reitoria de Pesquisa da Unesp (PROPe-Unesp) e a Pró-Reitoria de Pós Graduação (PROPG-Unesp).

O presente trabalho foi realizado com apoio da Coordenação de Aperfeiçoamento de Pessoal de Nível Superior – Brasil (CAPES) – Código de Financiamento 88887.144249/2017-00.

RESUMO

As infecções nosocomiais são uma das principais causas de mortalidade em todo mundo. O surgimento de agentes antimicrobianos inovadores vem se tornando uma necessidade, uma vez que as altas taxas de infecções são devidas ao aumento da resistência bacteriana. Este trabalho teve como objetivo a síntese de aminochalconas e sua avaliação contra *Staphyloccous aureus* e *Candida albicans*, sendo determinados os valores de concentração inibitória mínima (CIM), concentração bactericida mínima (CBM) e concentração fungicida mínima (CFM). As aminochalconas foram sintetizadas por reação de condensação aldólica de Claisen-Schmidt em catálise básica. A potencialização do efeito antimicrobiano das aminochalconas foi alcançada por meio do emprego do Método Manual de Topliss, o qual preconiza substituintes em anéis aromáticos, segundo seus efeitos estereoeletrônicos e hidrofobicidade. A chalcona **3f** (3'-amino-4-bromochalcona) mais ativa contra *S. aureus* sensível e resistente à meticilina (MSSA e MRSA) exibiu CIM de 1,95 µg/mL para MSSA e 7,80 µg/mL para MRSA, foi selecionada para avaliação da sua combinação com antibióticos, atividade anti-adesão, antibiofilme e toxicidade *in vivo* usando larvas de *Gallera* m*ellonella*. Além disso, as aminochalconas foram avaliadas quanto a atividade antibacteriana contra outras espécies e *Mycobacterium tuberculosis*. O tratamento com **3f** diminuiu a adesão de MSSA e MRSA aos queratinócitos humanos, além de atividade antibiofilme similar à vancomicina. Demonstrou baixa toxicidade a 10 × CIM após 72 horas, com morte de 20% das larvas de *G. mellonella*. A aminochalcona mais ativa contra *Candida albicans* também foi selecionada para avaliação antibiofilme, anti-adesão, e tempo de morte desse fungo, além do estudo de mecanismo de ação e toxicidade em *G. mellonella*. A chalcona **3n** (3'amino-3-fluorchalcona) demonstrou CIM de 3,90 µg/mL contra *C. albicans* e foi selecionada para os ensaios posteriores, demonstrando ação fungicida no ensaio de tempo-morte. Demonstrou atividade antibiofilme e anti-adesão similar a anfotericina B. Além disso, **3n** demonstrou interação com ergosterol de membrana, sendo um possível mecanismo de ação dessa chalcona. A baixa toxicidade a 100 × CIM foi responsável pela morte de 20% das larvas de *G. mellonella*.

Palavras-chave: chalcona, antimicrobiano, biofilme.

ABSTRACT

Nosocomial infections are one of the main causes of mortality worldwide. The emergence of innovative antimicrobial agents is becoming a necessity, since the high rates are due to the increase in bacterial resistance. The objective of this work was the synthesis of aminochalcones and their evaluation against *Staphyloccous aureus* and *Candida albicans*, being determined the values of minimum inhibitory concentration (MIC), minimum bactericidal concentration (MBC) and minimum fungicidal concentration (MFC). Aminochalcones were synthesized by the Claisen-Schmidt aldol condensation reaction in basic catalysis. The potentiation of the antimicrobial effect of aminochalcones was achieved through the use of the Topliss' Manual Method, which recommends substituents in aromatic rings, according to their stereoelectronic effects and hydrophobicity. Chalcone **3f** (3'-amino-4-bromochalcone) more active against methicillin-sensitive and resistant *S. aureus* (MSSA and MRSA) exhibited MIC of 1.95 µg/mL for MSSA and 7.80 µg/mL for MRSA, was selected for evaluation of its combination with antibiotics, anti-adhesion activity, anti-biofilm and *in vivo* toxicity using *Gallera mellonella* larvae. In addition, aminochalcones were evaluated for antibacterial activity against other species and *Mycobacterium tuberculosis*. Treatment with **3f** decreased the adhesion of MSSA and MRSA to human keratinocytes, in addition to antibiofilm activity similar to vancomycin. It demonstrated low toxicity at 10 × MIC after 72 hours, with 20% death of *G. mellonella* larvae. The most active aminochalcone against *Candida albicans* was also referred for anti-biofilm, anti-adhesion, and time of death evaluation of this fungus, in addition to the study of its mechanism of action and toxicity in *G. mellonella*. Chalcone **3n** (3'amino-3-fluorochalcone) demonstrated MIC of 3.90 µg/mL against *C. albicans* and was selected on to further tests, demonstrating fungicidal action in the time-death test. It demonstrated anti-biofilm and anti-adhesion activity similar to amphotericin B. In addition, sophisticated 3n with membrane ergosterol, being a possible mechanism of action of this chalcone. Low toxicity at 100 × MIC was responsible for the death of 20% of *G. mellonella* larvae.

Keywords: chalcone, antimicrobial, biofilm.

LISTA DE FIGURAS

Capítulo I

Capítulo II

Capítulo III

LISTA DE ESQUEMAS

Capítulo II

LISTA DE TABELAS

Capítulo II

Capítulo III

LISTA DE ABREVIATURAS E SIGLAS

ABSSSI – acute bacteria skin and skin structure infections
ATCC – American Type Culture Collection
CIM - Concentração Inibitória Mínima
CFU/mL – colony-forming unities per mL
CLSI – Clinical and Laboratory Standards Institute
DMEM – Dulbecco's Modified Eagle's Medium
eDNA – DNA extracelular
EPS – exopolissacarídeo
FIC – fractional inhibitory concentration
Hla – alpha-hemolysin
HPLC – High Performance Liquid Chromatography
MBC – Minimum Bactericidal Concentration
MFC – Minimum Fungicidal Concentration
MIC – Minimum Inhibitory Concentration
MMT – Manual Method Topliss
MRSA – Methicillin-resistant *Staphylococcus aureus*
MS – mass spectra
MSSA – Methicillin-sensitive *Staphylococcus aureus*
OMS – Organização Mundial da Saúde
PBS – phosphate buffered saline
Srt A – sortase A
TSA – Tryptic Soy Agar
TSB – Tryptic Soy Broth
VISA - Vancomycin-Intermediate *Staphylococcus aureus*
VRSA - Vancomycin-Resistant *Staphylococcus aureus*

LISTA DE SÍMBOLOS

σ – eletronic effect

π – lipophilic effect

E_S – steric effect

^{1}H NMR – ^{1}H Nuclear Magnetic Resonance

^{13}C NMR – ^{13}C Nuclear Magnetic Resonance

δ – chemical shift

s – singlet

m - multiplet

d – doublet

dd – doublet of doublets

ddd – doublet of doublet of doublets

J - coupling constant

λ_{max} – maximum wavelength

Log *P*o/w – partition coefficient *n*-octanol/water

SUMÁRIO

CAPÍTULO I

1. INTRODUÇÃO

1.1 Infecções microbianas

As infecções hospitalares (infecções nosocomiais) ocorrem em pacientes sob tratamento médico em um hospital ou outro estabelecimento de saúde. Essas infecções podem acontecer durante os cuidados de saúde ou até após a alta médica. Dispositivos médicos empregados nos cuidados de saúde estão associados a estas infecções, sendo que população mais atingida é a que se encontra em unidades de terapia intensiva e pacientes submetidos a procedimentos cirúrgicos (Khan et al., 2015).

As bactérias são os patógenos mais comuns causadores de infecções nosocomiais. Alguns pertencem a microbiota humana e causam infecção em condições em que o paciente encontra-se com sistema imunológico afetado (Khan et al., 2017).

Staphylococcus aureus é uma espécie bacteriana causadora de infecções hospitalares e que leva a uma alta mortalidade em crianças e adultos. *S. aureus* pode causar infecções menos graves como impetigo e foliculite até infecções mais graves como pneumonia necrosante e sepse (Tong et al., 2015).

Os fungos agem como patógenos oportunistas causando infecções nosocomiais em pacientes imunocomprometidos. *Candida albicans* está presente na microbiota humana e coloniza trato gastrointestinal, trato reprodutivo, boca e pele (Achkar e Fries, 2010; Ganguly e Mitchell, 2011). Mudanças no pH, uso de antibióticos e imunodepressão podem permitir a infecção por *C. albicans* e que variam desde afecções dérmicas até disseminadas na corrente sanguínea, causando altas taxas de mortalidade (Calderoni e Fonzi, 2001).

Os antimicrobianos revolucionaram a prática clínica, possibilitando avanços em toda medicina, uma vez que tornaram os procedimentos cirúrgicos e tratamentos hospitalares mais seguros. Porém, desde a descoberta dos principais grupos de antimicrobianos conhecidos, o crescente desafio nos cuidados da saúde vem atribuído a resistência microbiana e ausência de acesso à antimicrobianos eficazes (Marstson et al., 2016; Balouiri et al., 2016).

A resistência microbiana é um fenômeno causado pelo uso irracional de agentes antimicrobianos, incluindo automedicação, doses incorretas e uso prolongado ou atenuado. Essa prática vem se intensificando, tornando a resistência uma ameaça global na saúde pública (Roca et al., 2015). A resistência ameaça o controle eficaz dos microorganismos, causando infecções mais graves como pneumonia e infecções no sangue. *S. aureus* resistente

a meticilina (MRSA) e bactérias multiresistentes são responsáveis pela elevada taxa de infecçõs nosocomiais no mundo. A OMS destacou a resistência a antibióticos como uma das três principais ameaças a saúde pública do século (OMS, 2014).

1.2 Biofilmes microbianos

Os biofilmes são formados por uma comunidade de microorganismos incorporados em uma matriz polimérica que são aderentes entre si e em uma superfície (Vert et al., 2012). Devido ao comportamento coletivo, as células de biofilme possuem maior resistência às ameaças externas do que em células planctônicas, causando infecções mais resistentes a antibióticos, requerindo muitas vezes tratamento por associação de fármacos (Drescher et al., 2014; Kristian et al., 2004).

A formação de biofilme é dividida em três fases: adesão, maturação e dispersão (Figura 1). Inicialmente, as células planctônicas ligam-se a superfícies abióticas ou bióticas. Em superfícies abióticas, a adesão é mediada por interações hidrofóbicas ou eletrostáticas. A ligação em superficies bióticas, como tecido humano, envolve interações mais específicas, como ligações com proteínas da matriz humana (Otto, 2013). A maturação consiste no desenvolvimento da estrutura multicelular, pelo aumento de mediadores bacterianos, a cooperação celular e a desaceleração do metabolismo, produzindo uma matriz extracelular polimérica. A maturação inicia quando as células criam agregação intercelular por meio da produção da matriz, que agrega os microorganismos entre si e na superfície. A matriz é constituída de exopolissacarídeos (EPS), proteínas e DNA extracelular (eDNA), que são responsáveis pela maturação do biofilme, resultando em uma comunidade organizada (O'Toole et al., 2000). Após a estruturação do biofilme pode ocorrer o desprendimento de células ou aglomerados celulares presentes no biofilme sob condições favoráveis, espalhando as células por meio do sangue e fluidos corporais para outros locais de infecção, gerando disseminação sistêmica (Otto, 2013). O desprendimento é causado por forças mecânicas, interrupção da produção do material e produção de enzimas e surfactantes capazes de destruir a matriz extracelular (Periasamy et al., 2012).

A resistência antibiótica de biofilmes contribui para o desenvolvimento prolongado de infecções associadas a adesão em dispositivos médicos ou tecidos humanos danificados. Nos biofilmes, o mecanismo de resistência é diferente de células planctônicas, as quais conferem

resistência por plasmídeos ou mutações (Stewart e Costerton, 2001). Foi relatado que a resistência a biofilmes é maior que a resistência a antibióticos em células planctônicas (Stewart, 2002).

Os mecanismos de resistência de biofilmes estão sendo elucidados e já existem três hipóteses principais:

i) penetração lenta ou incompleta: não há barreiras genéricas para a difusão de antibióticos por meio da matriz do biofilme, porém, se o antibiótico for desativado no biofilme, a penetração é retardada. Anderl e colaboradores, demonstraram que a ampicilina pode penetrar em um biofilme formado por *Klebsiella pneumoniae* negativa para β-lactamase, mas não penetra em um biofilme formado por cepa sensível β-lactamase positiva. Na cepa sensível o antibiótico é desativado nas camadas superficiais mais rapidamente do que difunde (Anderl et al., 2000). Além disso, antibióticos carregados positivamente ligam-se a polímeros carregados negativamente na matriz do biofilme, resultando em uma penetração retardada (Shigeta et al., 1997).

ii) fenótipo resistente: população de microganismos formam um estado fenotípico único e protegido, semelhante a formação de esporos. Com a penetração de antibióticos a maioria das bactérias do biofilme é morta, porém, as sobreviventes persistem apesar da exposição contínua ao antibiótico. Isso sustenta a hipótese de um estado esporular demonstrado por algumas células bacterianas (Brooun et al., 2000).

iii) alteração do microambiente: estudos demonstraram que o oxigênio pode ser completamente consumido nas camadas superficiais do biofilme, levando a nichos anaeróbicos nas camadas profundas. Alguns antibióticos, como os aminoglicosídeos, são menos eficazes em condições anaeróbicas do que em aeróbicas (De Beer, 1994). Alternativamente, a depleção de um substrato ou acúmulo de resíduos leva a bactéria a um estado de não crescimento, o que inibe a ação de antibióticos que visam a síntese da parede celular, como a penilicina, uma vez que atuam somente com o crescimento bacteriano (Stewart and Costerton, 2001).

As infecções por biofilme são geralmente atribuídas a bactérias oportunistas que são hábeis na formação de biofilmes e por isso podem persistir por um longo tempo (Stewart and Costerton, 2001).

Figura 1. Ciclo de vida de biofilme. Adaptado de Reffuveille et al., 2017.

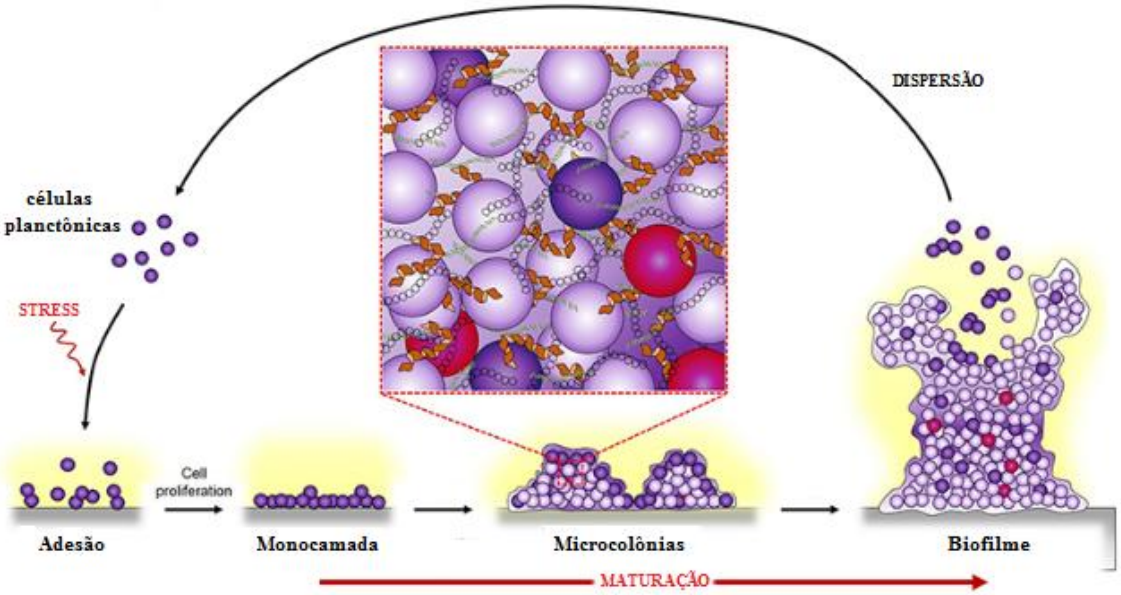

1.3 Chalconas

Chalconas são conhecidas como estruturas privilegiadas na Química Medicinal, exibindo um esqueleto carbônico formado por duas arilas (anéis A e B) separadas por uma ponte *trans*-enônica (Figura 2), que pode incorporar diferentes moléculas com várias atividades (Zhuang, 2017).

Figura 2. Núcleo chalcônico

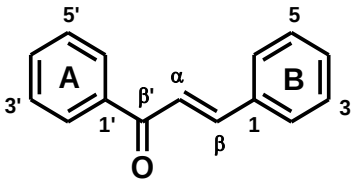

Sivakumar e colaboradores descreveram a ação antibacteriana da 4-metóxi-3'-hidroxichalcona (**1**) (Figura 3), contra *S. aureus*, a qual promoveu morte bacteriana à 0,244 µM. Análises de microscopia eletrônica indicaram que **1** promoveu morte bacteriana por meio de danos à parede celular (Silvakumar et al., 2009).

Figura 3. Estrutura da 3-hidróxi-4’-metoxichalcona contra *Staphylococcus aureus*

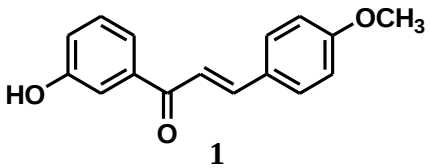

1

A ação de chalconas contra formação de biofilme de *S. aureus* foi demonstrada por Bozic e colaboradores. A chalcona **2** exibiu efeito na inibição da formação de biofilme de MRSA na concentração de 6,25 µg/mL (Bozic et al., 2014).

Figura 4. Chalcona com atividade anti-biofilme de Staphylococcus *aureus*

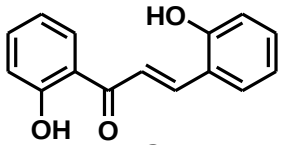

2

Xu e colaboradores revisaram o potencial antibacteriano de chalconas, descrevendo seu amplo espectro de ação. Em seu artigo de revisão, demonstraram que análogos com substituintes retiradores de elétrons no anel B (Cl, Br e F) são mais ativos quando comparados à substituintes doadores de elétrons (CH_3 e OCH_3) (Xu et al., 2019).

Para avaliar e efeito sinérgico de chalconas, Wang e colaboradores, sintetizaram 24 chalconas hidroxiladas e avaliaram sua ação associada ao fluconazol contra *C. albicans* resistente ao fluconazol. Entre as chalconas avaliadas a 2’-hidroxi-4’-metoxichalcona (**3**) exibiu o efeito mais potente *in vitro* (Wang et al., 2016).

Figura 5. Chalcona com efeito sinérgico contra *Candida albicans*

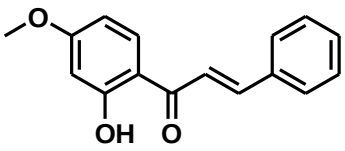

3

Messier e colaboradores, investigaram a atividade antibiofilme de *C. albicans* da 4-hidroxicordoina (**4**), demonstrando que a formação de biofilme foi fortemente inibida (85%) na concentração de 20 µg/mL. Além disso, demonstrou-se por microscopia que concentrações entre 50 e 200 µg/mL causaram inibição na transição levedura-hifa (Messier et al., 2011).

Figura 6. Estrutura da 4-hidroxicordoina com efeito contra *Candida albicans*

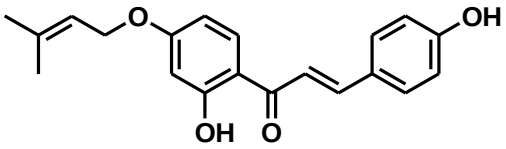

4

Nowakoswska revisou o potencial anti-infectivo de chalconas, descrevendo a ação antibacteriana e antifungica dessa classe de compostos. A licochalcona A (**5**) demonstrou efeito contra cepas de MRSA com valores de CIM entre 6,25 e 16 µg/mL (Nowakoswska, 2007).

Figura 7. Licochalcona A contra MRSA

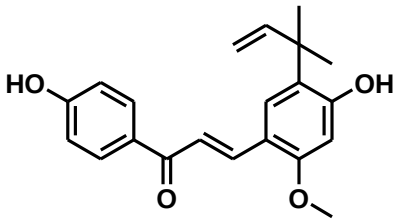

5

Alguns relatos descrevem a atividade antimicrobiana de aminochalconas (Irfan et al., 2020). Suwito, avaliou a atividade de uma série de 4'-aminochalconas contra *S. aureus* e *C. albicans*. A chalcona **6** demonstrou maior potência contra *S. aureus* com zonas de inibição similares a sulfamerazina, e as chalconas **7** e **8** maior potência contra *C. albicans* (Figura 8) (Suwito, 2016).

Figura 8. 4'-Aminochalconas antibacterianas **6** – **8**

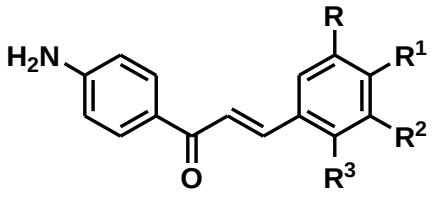

6 R = R^3 = OCH_3; R^1 = R^2 = H
7 R = OCH_3; R^1 = R^2 = R^3 = H
8 R = R^2 = R^3 = H; R^1 = OCH_3

1.4 Método Manual de Topliss

A descoberta e desenvolvimento de fármacos é um processo complexo e duradouro, tendo a química medicinal, papel crucial nesse ramo (Guido, Andricopulo e Oliva, 2010). A fim de aperfeiçoar propriedades farmacodinâmicas, a seleção de substituintes em anéis

aromáticos corrobora para aumento de potência, além de fornecer informações preliminares de relação estrutura-atividade. O substituinte em um sistema arílico pode alterar o efeito farmacológico, baseado na modificação de propriedades físico-químicas como lipofilia e efeito eletrônico. Topliss aplicou os métodos de Hansch para o planejamento de fármacos, na busca por moléculas bioativas com alvo molecular desconhecido (Topliss, 1977).

Baseado em fatores eletrônicos (σ), lipofílicos (π) e estéricos (E_S), Topliss desenvolveu um método prático para escolha de substituintes em anéis aromáticos, titulado Método Manual de Topliss. Um grupo inicial de cinco análogos é selecionado para síntese e consiste nos substituintes: H, 4-Cl, 4-OCH_3, 4-CH_3 e 3,4-diCl. Posteriormente, faz-se a comparação da atividade biológica destas substâncias e define-se uma ordem de potência, permitindo uma dedução quanto aos possíveis parâmetros operativos. Com isso, segue-se para as novas seleções de substituintes baseado nos parâmetros de maior influência sobre a atividade biológica.

1.5 Biosisosterismo

Bioisósteros são substâncias que apresentam propriedades físicas ou químicas semelhantes, exibindo propriedades biológicas similares. É uma ferramenta usada para modificação racional de compostos, produzindo leads, pois permite aprimorar as propriedades físicas ou biológicas, reduzir a toxicidade e alterar o metabolismo de um composto (Meanwell, 2011). Eles podem ser classificados em isósteros clássicos e não-clássicos, de acordo com os fatores estereoeletrônicos. Os isósteros não-clássicos não obedecem à definição eletrônica e estérica dos isósteros clássicos, além de não terem o mesmo número de átomos que o substituinte para o qual são usados como substituto (Brown, 2014).

Tieu e colaboradores avaliaram a atividade de inibidores da proteína ligase de biotina de *S. aureus* usando a ferramenta de biosisosterismo (Figura 9). A substituição isostérica de triazóis por oxadiazóis, forceceu inibidores potentes dessa proteína (Tieu et al., 2014).

Figura 9. Troca bioisosterica de inibidores da proteína ligase de biotina de *Staphylococcus aureus*

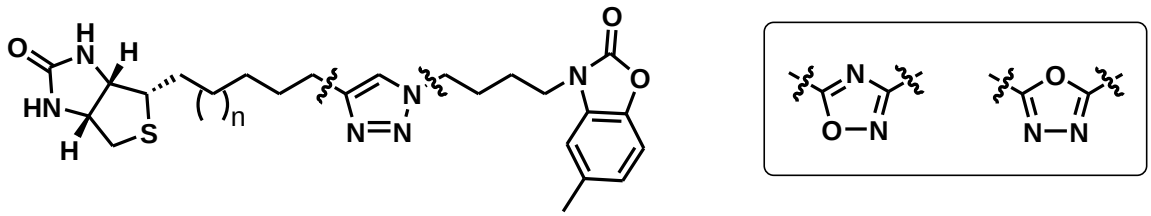

2. OBJETIVOS

2.1 Objetivo geral

O objetivo geral deste trabalho foi a síntese de aminochalconas, bem como a sua avaliação antimicrobiana.

2.2 Objetivos específicos

A) Síntese, purificação e identificação de 2', 3' e 4'-aminochalconas;
B) Avaliação da atividade antibacteriana das aminochalconas contra *Staphylococcus aureus* sensível e resistente à meticilina (MSSA e MRSA);
C) Avaliação da combinação entre meticilina ou vancomicina com a aminochalcona mais ativa contra MSSA e MRSA;
D) Avaliação da atividade inibitória da aminochalcona mais ativa contra adesão de MSSA e MRSA em queratinócito humano;
E) Avaliação da atividade antibiofilme da aminochalcona mais ativa contra MSSA e MRSA;
F) Avaliação da toxicidade da aminochalcona mais ativa contra MSSA e MRSA em modelo alternativo de *Gallera mellonella*;
G) Avaliação da atividade antibacteriana da aminochalcona mais ativa contra outras espécies bacterianas e *Mycobacterium tuberculosis*;
H) Avaliação da atividade antifúngica das aminochalconas contra *Candida albicans*;
I) Avaliação da combinação entre anfotericina B e a aminochalcona mais ativa contra *C. albicans*;
J) Avaliação do tempo de morte de *C. albicans* da aminochalcona mais ativa;

K) Avaliação da atividade inibitória da aminochalcona mais ativa contra adesão de *C. albicans* em queratinócito humano;
L) Avaliação da atividade antibiofilme da aminochalcona mais ativa contra *C. albicans*;
M) Estudo do mecanismo de ação usando sorbitol e ergosterol da aminochalcona mais ativa;
N) Avaliação da toxicidade da aminochalcona mais ativa contra *C. albicans* em *Gallera mellonella*.
O) Avaliação da atividade antifúngica da aminochalcona mais ativa contra *C. tropicallis, C. parapsilosis, C. glabrata* e *C. krusei*.

3. REFERÊNCIAS BIBLIOGRÁFICAS

ACHKAR, J. M.; FRIES, B. C. *Candida* Infections of the Genitourinary Tract. Clinical Microbiology Reviews, v. 23, p. 253–273, 2010.

ANDERL, J. N.; FRANKLIN, M. J.; STEWART, P. S. Role of Antibiotic Penetration Limitation in *Klebsiella pneumoniae* Biofilm Resistance to Ampicillin and Ciprofloxacin. Antimicrobial Agents and Chemotherapy, v. 44, p. 1818–1824, 2000.

BALOUIRI, M.; SADIKI, M.; IBNSOUDA, S. K. Methods for *in vitro* evaluating antimicrobial activity: A review. Journal of Pharmaceutical Analysis, v. 6, p. 71–79, 2016.

BOZIC, D. D. et al. Newly-synthesized chalcones-inhibition of adherence and biofilm formation of methicillin-resistant *Staphylococcus aureus*. Brazilian Journal of Microbiology, v. 45, p. 263–270, 2014.

BROOUN, A.; LIU, S.; LEWIS, K. A Dose-Response Study of Antibiotic Resistance in *Pseudomonas aeruginosa* Biofilms. Antimicrobial Agents and Chemotherapy, v. 44, p. 640–646, 2000.

BROWN, N. Bioisosteres and Scaffold Hopping in Medicinal Chemistry. Molecular Informatics, p. 1–5, 2014.

CALDERONE, R. A.; FONZI, W. A. Virulence factors of *Candida albicans*. Trends in Microbiology, v. 9, p. 327–335, 2001.

DE BEER, D. et al. Effects of biofilm structures on oxygen distribution and mass transport. Biotechnology and Bioengineering, v. 43, p. 1131–1138, 1994.

DRESCHER, K. et al. Solutions to the Public Goods Dilemma in Bacterial Biofilms. Current Biology, v. 24, p. 50–55, 2014.

GANGULY, S.; MITCHELL, A. P. Mucosal biofilms of *Candida albicans*. Current Opinion in Microbiology, v. 14, p. 380–385, 2011.

GUIDO, R. V. C.; ANDRICOPULO, A. D.; OLIVA, G. Planejamento de fármacos, biotecnologia e química medicinal: aplicações em doenças infecciosas. Revista Estudos Avançados, v. 24, p. 66–73, 2010.

IRFAN, R.; MOUSAVI, S.; ALAZMI, M.; SALEEM, R. S. Z. A comprehensive review of aminochalcones. Molecules, v. 25, 2020.

KHAN, H. A.; AHMAD, A.; MEHBOOB, R. Nosocomial infections and their control strategies. Asian Pacific Journal of Tropical Biomedicine, v. 5, p. 509–514, 2015.

KHAN, H. A.; BAIG, F. K.; MEHBOOB, R. Nosocomial infections: Epidemiology, prevention, control and surveillance. Asian Pacific Journal of Tropical Biomedicine, v. 7, p. 478–482, 2017.

KRISTIAN, S. A. et al. The ability of biofilm formation does not influence virulence of *Staphylococcus aureus* and host response in a mouse tissue cage infection model. Microbial Pathogenesis, v. 36, p. 237–245, 2004.

MARSTON, H. D. et al. Antimicrobial Resistance. JAMA, v. 316, p. 1193, 2016.

MEANWELL, N. A. Synopsis of Some Recent Tactical Application of Bioisosteres in Drug Design. Journal of Medicinal Chemistry, v. 54, p. 2529–2591, 2011.

MESSIER, C. et al. Inhibition of *Candida albicans* biofilm formation and yeast-hyphal transition by 4-hydroxycordoin. Phytomedicine, v. 18, p. 380–383, 2011.

NOWAKOWSKA, Z. A review of anti-infective and anti-inflammatory chalcones. European Journal of Medicinal Chemistry, v. 42, p. 125–137, 2007.

O'TOOLE, G.; KAPLAN, H. B.; KOLTER, R. Biofilm Formation as Microbial Development. Annual Review of Microbiology, v. 54, p. 49–79, 2000.

OTTO, M. Staphylococcal Infections: Mechanisms of Biofilm Maturation and Detachment as Critical Determinants of Pathogenicity. Annual Review of Medicine, v. 64, p. 175–188, 2013.

PERIASAMY, S. et al. How *Staphylococcus aureus* biofilms develop their characteristic structure. Proceedings of the National Academy of Sciences, v. 109, p. 1281–1286, 24 2012.

REFFUVEILLE, F. et al. Staphylococcus aureus Biofilms and their Impact on the Medical Field. In: ENANY, S.; CROTTY ALEXANDER, L. E. (Eds.). . The Rise of Virulence and Antibiotic Resistance in *Staphylococcus aureus*. [s.l.] InTech, 2017.

ROCA, I. et al. The global threat of antimicrobial resistance: science for intervention. New Microbes and New Infections, v. 6, p. 22–29, 2015.

SHIGETA, M. et al. Permeation of Antimicrobial Agents through *Pseudomonas aeruginosa* Biofilms: A Simple Method. Chemotherapy, v. 43, p. 340–345, 1997.

SIVAKUMAR, P. M.; PRIYA, S.; DOBLE, M. Synthesis, Biological Evaluation, Mechanism of Action and Quantitative Structure-Activity Relationship Studies of Chalcones as Antibacterial Agents. Chemical Biology & Drug Design, v. 73, p. 403–415, 2009.

STEWART, P. S. Mechanisms of antibiotic resistance in bacterial biofilms. International Journal of Medical Microbiology, v. 292, p.107–113, 2002.

STEWART, P. S.; WILLIAM COSTERTON, J. Antibiotic resistance of bacteria in biofilms. The Lancet, v. 358, p. 135–138, 2001.

SUWITO, H. et al. Antimicrobial Activities and *In silico* Analysis of Methoxy Amino Chalcone Derivatives. Procedia Chemistry, v. 18, p. 103–111, 2016.

TIEU, W. et al. Heterocyclic acyl-phosphate bioisostere-based inhibitors of *Staphylococcus aureus* biotin protein ligase. Bioorganic & Medicinal Chemistry Letters, v. 24, p. 4689–4693, 2014.

TONG, S. Y. C. et al. *Staphylococcus aureus* Infections: Epidemiology, Pathophysiology, Clinical Manifestations, and Management. Clinical Microbiology Reviews, v. 28, p. 603–661, 2015.

TOPLISS, J. G. A manual method for applying the Hansch approach to drug design. Journal of Medicinal Chemistry, v. 20, p. 463–469, 1977.

VERT, M. et al. Terminology for biorelated polymers and applications (IUPAC Recommendations 2012). Pure and Applied Chemistry, v. 84, p. 377–410, 2012.

WANG, Y.-H. et al. The synthesis and synergistic antifungal effects of chalcones against drug resistant *Candida albicans*. Bioorganic & Medicinal Chemistry Letters, v. 26, p. 3098–3102, 2016.

WORLD HEALTH ORGANIZATION (ED.). Antimicrobial resistance: global report on surveillance. Geneva, Switzerland: World Health Organization, 2014.

XU, M. et al. Chalcone derivatives and their antibacterial activities: Current development. Bioorganic Chemistry, v. 91, p. 103133, 2019.

ZHUANG, C. et al. Chalcone: A Privileged Structure in Medicinal Chemistry. Chemical Reviews, v. 117, p. 7762–7810, 2017.

CAPÍTULO II

Artigo publicado na *Bioorganic Chemistry*

Design, synthesis and antibacterial activity of chalcones against MSSA and MRSA planktonic cells and biofilms

Mayara A. R. Garcia[a], Reinaldo S. Theodoro[a], Janaína de C. O. Sardi[b], Mariana B. Santos[a], Gabriela M. Ayusso[c], Fernando R. Pavan[c], Alan R. Costa[d], Lucas M. Santa Cruz[d], Pedro L. Rosalen[b], Luis O. Regasini[a,*]

[a]*Department of Chemistry and Environmental Sciences, Institute of Biosciences, Humanities and Exact Sciences, São Paulo State University, São José do Rio Preto, SP, Brazil.*

[b]*Department of Physiological Sciences, Piracicaba Dental School, University of Campinas, Piracicaba, SP, Brazil.*

[c]*Department of Biological Sciences, School of Pharmaceutical Sciences, São Paulo State University, Araraquara, SP, Brazil*

[d]*Núcleo de Contaminantes Orgânicos, Instituto Adolfo Lutz, São Paulo, SP, Brazil*

*** Corresponding author.**

E-mail addresses: luis.regasini@unesp.br (LO Regasini)

ABSTRACT

Staphylococcus aureus is the one of the most successful modern pathogens. The same bacterium that lives as a skin and mucosal commensal can be transmitted in health-care environments, causing acute bacterial infections. Methicillin-resistant *S. aureus* (MRSA) has emerged and disseminated around the world, belonging to 12 deadliest drug-resistant bacteria according to World Health Organization. Thus, there is a great challenge for a discovery of novel anti-*Staphylococcus aureus* compounds, which should act againt MRSA. Herein, we designed and synthesized a series of 17 chalcones, substituted by amino group on ring A, which were evaluated against methicillin-susceptible *S. aureus* (MSSA) and MRSA planktonic cells. The antibacterial potency was improved by substituents on ring B, which were designed according to Topliss' manual method. 4-bromo-3'-aminochalcone (**5f**) was the most active, demonstrating minimum inhibitory concentration (MIC) values of 1.9 μg mL^{-1} and 7.8 μg mL^{-1}against MSSA and MRSA, respectively. The association of **5f** with vancomycin demonstrated synergistic effect against MSSA and MRSA, with Fractional Inhibiroty Concentration Index (FICI) values of 0.4 and 0.3, respectively. Subinhibitory concentration of **5f** inhibited the MSSA and MRSA adhesion to human keratinocytes. Chalcone **5f** was able to reduce MSSA and MRSA biofilm formation, as well as acts on preformed biofilm in concentration-dependent mode. Scanning electron microscopy analyses confirmed severe perturbations of **5f** on MSSA and MRSA biofilm architecture. The acute toxicity assay, using *Galleria mellonella*, indicated low toxic effect of **5f**, after 72 h of treatment, displaying lethality to 20% and 30% larvae at 7.8 μg $mL^{-1}$and 78.0 μg mL^{-1}, respectively. In addition, the antibacterial activity spectrum of **5f**indicated action against planktonic cells of *Enterococcus faecalis* (MIC =7.8 μg mL^{-1}), *Acinetobacter baumannii* (MIC = 15.6 μg mL^{-1}) and *Mycobacterium tuberculosis* (MIC = 5.7 μg mL^{-1}). Altogether, these results open new avenues for **5f** as an anti-*Staphylococcus aureus* agent, with potential applications as antibacterial drug, adjunct of antibiotics and medical devices coating.

Keywords: Chalcone, *Staphylococcus aureus*, MRSA, Biofilm, Antibacterial, Topliss.

1. Introduction

*Staphylococcus aureus*is a well-adapted Gram-positivebacterium to community-settingsand health-care environments. It is a human commensal and etiologic agent of endocarditis, osteoarticular infections, pneumonia, acute bacterial skin and skin structure infections (ABSSSI) and bacteremia. With rise of clinical practice in health-care environments, *S. aureus* became a central cause of nosocomial infections, which were firstly treated with penicillin [1]. However, the emergence of penicillin-resistant strains of *S. aureus*, which encodes gene *blaZ* and expresses β-lactamase, improved the search for efficient semi-synthetic β-lactams. Among these, methicillin, apenicillin bearing steric hindrance *ortho*-dimethoxyphenyl motif, conferred short-lived relief [2]. Within 1–2 years of clinical methicillinuse, strains with gene *mecA* were able to resist to methicillin treatments, which were named as Methicillin-Resistant *Staphylococcus aureus* (MRSA). This gene encodes penicillin-binding protein 2a (PBP2a), which is responsible for peptidoglycan layer biosynthesis and has low affinity for β-lactams [3, 4].

Vancomycin has been the drug of choice for systemic MRSA infections in hospitalized patients. However, MRSA has acquired resistance to vancomycin, corroborating two main phenotypes: vancomycin intermediate-resistant *S. aureus*, (VISA) and vancomycin-resistant *S. aureus* (VRSA), which were detected in 1997 and 2002, respectively [1, 5]. The emergence of VISA and VRSA strains has been related to vancomycin-treatment failures and *vanA* gene transferred from *Enterococcus faecalis*, respectively [6]. Additionally, the MRSA infections can be treated by conventional antibacterial drugs, including antifolates (trimethoprim-sulfamethoxazole), protein biosynthesis inhibitors (linezolid) and cell membrane disruptors (daptomycin) [7]. In 2018, the USA Food and Drug Administration approved the omadacycline, which is the most recent drug to treat complicated ABSSSI caused by MRSA. Its structure belongs to aminomethylcycline subclass of tetracyclines and its mode of action involved the 30S ribosomal subparticle blockade, a well-known antibacterial target [8].

Chalcones (or 1,3-diaryl-2-propen-1-ones) are recognized as privileged scaffolds by drug discovery due to simple synthesis and versatile skeleton to derive structure-activity relationships [9]. Some naturally-occurring and synthetic chalcones have been approved for clinical trials, demonstrating good pharmacokinetics properties and are well-tolerated by humans. Among these, metochalcone (**1**) and sofalcone (**2**) were marketed as choleretic and anti-ulcer/mucoprotective drugs, respectively [10]. Zhang and co-authors reported the effect

of chalcone with unsubstituted rings A and B (**3**) against USA 300, a community-associated methicillin-resistant *Staphylococcus aureus* (CA-MRSA). Chalcone **3** was able to inhibit sortase A (SrtA) and alpha-hemolysin (Hla), proteins responsible for anchoring virulence-related surface proteins and pore-forming in host cell, respectively. Additionally, chalcone **3** down-regulated *hla* gene at transcriptional level, reducing Hla expression and the mortality of infected mice by USA 300 [11]. (Fig. 1).

In our continuing search for novel antibacterial drugs from chalcone-based framework, we designed and synthesized a series of 17 chalcones as well as evaluated their antibacterial activity against MSSA and MRSA planktonic cells. The most active compound, 4-bromo-3'-aminochalcone (**5f**), was selected for detailed bioassays, including its antibacterial effect associated with methicillin and vancomycin against MSSA and MRSA planktonic cells. Also, we investigated the antibacterial activity of **5f** against MSSA and MRSA biofilm formation and pre-formed biofilms. The inhibition of **5f**on MSSA and MRSA adhesion to human skin cells and its *in vivo* acute toxicity using *Galleria mellonella* larvae were also carried out. In addition, the antibacterial spectrum of **5f** was tested against another Gram-positive species, two Gram-negative species and *Mycobacterium tuberculosis*.

2. Materials and methods

2.1. Design

In vitro and *in vivo* antibacterial activities of **3** against MRSA, described by Zhang and co-workers, encouraged us to investigate it in our bioassays [11]. However, **3** was not soluble in culture medium in concentrations required by biofilm experiments. Thus, we decided to design analogs of **3** with higher solubility in water, using derivatives with amino group as substituent on ring A. The selection by amino group was based on its ability to establish strong hydrogen bonds with water and its alkaline properties. According to Nostro and collaborators, higher pH values were able to reduce staphylococcal biofilm formation [12]. In order to improve the antibacterial potency, we adopted the Topliss' manual method, which is based on Hansch approach to drug design [13, 14]. We investigated an initial set of five aminochalcones with unsubstituted ring B and substituted at *p*-Cl, *m*,*p*-diCl, *p*-Me and *p*-OMe positions. The potency ranking in this first set was compared to tabulated potency ranking, which is calculated for parameters correlated to hydrophobic (π), electronic (σ) and steric effects (Es). From this comparison, the probable operative physicochemical parameters were

deduced and a second set of chalcones was designed, aiming more potent antibacterial analogs.

2.2. Synthesis

Reagents and solvents were purchased from Merck®. Series of 17 chalcones was synthesized by Claisen-Schmidt aldol condensation, according to protocol reported by Santos and coauthors, with minor modifications [15]. Reactions were carried out at room temperature using 5.0 mmol of respective benzaldehyde derivatives and 5.0 mmol of respective aminoacetophenones, which were dissolved in ethanol (50 mL). Sodium hydroxide in ethanol (1 mol L^{-1}) was added as catalyst solution. Reagents conversion was monitored by thin layer chromatography. Crude products were poured onto ice from distilled and deionized water and filtered. All compounds were purified over silica gel chromatography column eluted with mixtures of hexane and ethyl acetate. Melting point of chalcones was measured on open capillaries on Melt Temperature apparatus MS Tecnopon PFM-II. UV-Vis spectra and chromatograms were obtained in High Performance Liquid Chromatography with Diode Array Detector (HPLC-DAD) Agilent Technologies® 1220 Infinity equipment, photodiode array system (Agilent Tecnologies® Model 1260 Infinity) and Agilent Zorbax Eclipse Plus C-18® column (250 mm × 4.6 mm, 5 µL) using methanol:water (3:1) as mobile phase (1.0 mL/min). NMR spectra were obtained in two spectrometers: BrukerAvance III (600 MHz) and BrukerAvance III (400 MHz), using deuterated dimethyl sulfoxide (DMSO- d_6) as internal reference. Low mass spectrometry by electrospray ionization spectra were performed on Bruker® Amazon ESI-IT.

2.3. Antibacterial assay against MSSA and MRSA

Two *Staphylococcus aureus* strains were used in anti-staphylococcal assay, including methicillin-susceptible *Staphylococcus aureus* ATCC 25923 (MSSA) and methicillin-resistant *Staphylococcus aureus* ATCC 33591 (MRSA). Both strains were maintained as frozen stocks at –80 ºC until use. For the assays, the strains were subcultured onto trypticase soy agar (TSA- BD Difco™) and a single colony was inoculated into trypticase soy broth (TSB- BD Difco™) medium and incubated at 37 ºC for 24 h [16]. Minimum inhibitory concentration (MIC) was determined according to the M07-A9 of the Clinical and Laboratory Standards Institute (CLSI) with minor adaptations [17]. The strains were seeded on brain

heart infusion agar (BHI- BD Difco™) at 37 °C for 24 h. From this culture, the inoculum was dispersed in Miller Hynton broth (MH - BD Difco™) to obtain suspension between 2.5 and 5.0 × 10^4 CFU mL^{-1}, which was distributed in 96-well plates. Inoculum absorbance was confirmed by Spectrophotometer Unico 1100RS. Plates were incubated at 37 °Cfor 24 h and MIC values were established as the concentration capable of inhibition of bacterial growth after visual readings. Vancomycin (Merck®) was used as reference antibacterial drug, 2% DMSO (v/v vehicle) was used as negative control and culture medium free of any other agent was included to check the sterility. Minimum bactericidal concentration (MBC) was determined by transferring each 96-well microplate concentration to plate with BHI agar and subsequent incubation at 37 °C for 24 h. MBC value was defined as the lowest concentration that did not allow bacterial growth visible on the solid medium.

2.4. Checkerboard assay

Combination effect of **5f** with two antibacterial drugs, vancomycin (Merck®) and methicillin (Merck®), was evaluated by the microdilution broth checkerboard method [18, 19]. The following combinations were tested: vancomycin (from 4.0 to 0.0062 µg mL^{-1}), methicillin (from 4.0 to 0.0062 µg mL^{-1}) along with chalcone **5f** (from 62.5 to 0.12 µg mL^{-1}). For test, vancomycin and methicillin were dissolved according to instructions of manufacturer. The medium was distributed in 96-well plates with a final inoculum suspension between 2.5 and 5.0 ×10^4 CFU mL^{-1}. The plates were incubated at 37 °C with microplate readings at 490 nm after 24 h. Fractional inhibitory concentration index (FICI) was calculated using the equation: ΣFIC = FICA + FICB, where the FIC is the ratio of the MIC of the drug in combination with the MIC alone. A synergistic combination was defined as FICI ≤ 0.5, an additive combination was defined as 0.5 < FICI < 1.0, an indifferent combination was defined as 1.0 < FICI < 4.0 and an antagonistic combination as FICI > 4 [19].

2.5. Anti-adhesion assay

In order to determine the anti-adhesion activity of **5f**, immortalized human keratinocytes (HaCaT cells) were obtained from the Bank of Cells of Rio de Janeiro (Rio de Janeiro, Brazil). Cell culture and anti-adhesion assay were performed as described by Emeri and co-authors, with minor modifications [20]. Cells were maintained in Dulbecco's medium (DMEM) supplemented with 10% fetal bovine serum plus 100 UmL^{-1} penicillin, 100 µg mL^{-}

[1]streptomycin sulfate and 200 mM L-glutamine at 37°C under 5% CO_2 atmosphere. Two curves at 1, 2 and 3 h were plotted to establish MSSA and MRSA adhesion to HaCaT cells. The adhesion assay was carried out using 24-well plates containing 1×10^5 cells/well. After cell monolayers formation, aliquots of 500 µL staphylococcal inocula (5×10^3 CFU mL^{-1}) were added to each well. The plates were incubated at 37 °C under 5% CO_2 atmosphere for the previously mentioned times. After each incubation time, HaCaT cells were washed threetimes with sterile phosphate-buffered saline (PBS) and trypsinized. Aliquots of 100 µL were plate for CFU measurement onto TSA plates and incubated at 37 °C for 24 h. The effect of **5f** towards MSSA and MRSA adhesion on HaCaT cells were tested at its MIC/2 values, 1.0 µg mL^{-1} and 3.9 µg mL^{-1}, respectively. The subinhibitory concentration was selected as it ensures staphylococcal growth and survival were not severely affected by **5f**. After the adhesion periods of 1, 2 and 3 h, the cells were washed three times with sterile PBS, trypsinized and plated for CFU measurements on TSA plates. The percentage of inhibition of adhesion was established based on the final number of adhered bacteria in comparison to an untreated group (bacteria + cells + DMEM) indicating 100% bacterial adhesion. In order to check if **5f** directly acts on adhesion bacterial to HaCaT cells instead of causes HaCaT viability reduction, we included a test with HaCaT cells treated **5f** at its MIC/2 value. The percentage of inhibition of adhesion was calculated based on final number of adhered staphylococcal in relation to an untreated control indicating 100% bacterial adhesion.

2.6. Biofilm formation inhibition assay

Assay of biofilm formation inhibition was performed according to protocol described by Sardi and collaborators, with minor modifications [16]. In order to investigate the effect of **5f** and vancomycin towards MSSA and MRSA biofilm formation, an aliquot of 100 µL staphylococcal inoculum (1×10^7 CFU) was transferred to 96-well plates and incubated at 37° C for 2 h, allowing cell adhesion [21]. Cell suspension was aspirated from the wellsand 100 µLTrypticase Soy Broth plus 0.1% glucose (TSB-g) with **5f** and vancomycin at their MIC and 10×MIC values were added to the wells. The dishes were incubated at 37 °C. After 24 h, the plates were washed with PBS to remove planktonic and dead cells. A total 100 µL transferred to a tube with 900 µL of PBS and serial dilutions were performed. 20 µL of each suspension was added to TSA plates. The percentage of CFU was determined in comparison tothe untreated MSSA and MRSA biofilms.

2.7. Preformed biofilm inhibition assay

Assay of preformed biofilm inhibition was carried out according to protocol described by Sardi and collaborators, with minor modifications [16]. An aliquot of 100 μL inoculum was added to TSB-g. The medium was distributed into polystyrene 96-well plates with a final inoculum concentration of 1×10^7 CFU mL^{-1}. The plates were incubated at 37 °C for 24 h, allowing biofilm formation [22]. Following preformed biofilms, the wells were washed three times with 200 μL sterile saline (0.85%) to remove planktonic and dead cells. An aliquot of 100 μL TSB-g containing **5f** and vancomycin at their MIC and 10×MIC values were added to the wells. TBS-g was added to wells with and without staphylococcal inoculum as controls. The plates were incubated at 37 °C. After 24 h, the plates were washed with PBS. Biofilms were scraped from the bottom of the wells using 100 μL micropipette, allowing cellular agglomeration dissociation. A volume of 100 μL containing cell suspension was aspirated from the wells, transferred to a tube containing 900 μL PBS and vortexed for 3 minutes. Serial dilutions were performed and 100 μL of each suspension was plated onto TSA plates. The survival (percentage of CFU) was established in comparison to untreated biofilms.

2.8. Biofilm architecture perturbation assay

Perturbations of **5f** and vancomycin on MSSA and MRSA biofilm architecture were evaluated by scanning electron microscopy (SEM) analysis. Biofilms were grown for 24 h at 37 ºC on tissue-culture-treated chamberedglass slides (Corning BD Falcon), washed three times with PBS to remove non adhered cells, and treated with **5f** and vancomycin at their MIC and 10 × MIC values. A negative control group with untreated biofilm was also included. After 24 h, the samples were washed three times and maintained in 2.5% glutaraldehyde/PBS (v/v pH 7.4) for 2 h at room temperature. The slides were serially dehydrated with ethanol (from 50 to 100 %) for 2 minutes, coated with gold at 40mA (BAL-TEC SCD 050) and observed using a scanning electron microscope (Jeon JSM 5600LV) [23].

2.9. Acute toxicity assay

In vivo assay was performed to test the acute toxicity of **5f** and vancomycin as described by Megaw and collaborators with minor modifications [24]. A total of 50 healthy larvae, with weigh ranging from 200 to 300 mg, were randomly selected and separated in five

groups with 10 individuals: **5f** (MIC, 7.8 μg mL^{-1} or 0.31 mg/kg/larvae), **5f** (10 × MIC, 78 μg mL^{-1} or 3.12 mg/kg/larvae), vancomycin (MIC, 2.0 μg mL^{-1} or 0.02 mg/kg/larvae), vancomycin (10 × MIC, 20 μg mL^{-1} or 0,2 mg/kg/larvae), and vehicle control (DMSO). The values of concentrations adopted in acute toxicity assay were based on MIC values exhibited by **5f** and vancomycin MSSA. The larvae were chilled on ice for 20 minutes and had their prolegs cleaned with 70% ethanol. Five-microliters of **5f** solutions in DMSO, vancomycin solutions in DMSO as well as DMSO were injected into the hemocoel of each larva through the last left proleg by a trained operator using a 10 μL Hamilton syringe (Hamilton, Reno, NV). After injection, the larvae were maintainedat 37° C in dark. The larvae survival was monitored at selected intervals (8 h) during 72 h. The larvae that did not movement upon touch and with high melanization levels were counted as dead.

2.10. Additional antibacterial and antimycobacterial assays

In order to investigate the antibacterial spectrum of action of **5f**, additional strains were used, including another Gram-positive species, *Enterococcus faecalis* ATCC 29212, as well as two Gram-negative species, *Acinetobacter baumannii* ATCC 14803 and *Pseudomonas aeruginosa* ATCC 27853. MIC values were determined according to the M07-A9 (2012) of the Clinical and Laboratory Standards Institute (CLSI) with minor adaptations [17]. The strains were seeded on BHI agar at 37 °C for 24 h. From this culture, the inoculum was diluted in Miller Hynton broth (MH) to obtain suspensions between 2.5 and 5.0 × 10^4 $CFUmL^{-1}$, which was distributed in 96-well plates. Vancomycin and ciprofloxacin were used as reference antibacterial drugs. Compounds were diluted in DMSO and added to the wells at concentrations ranging from 62.5 to 0.48 μg mL^{-1} [25]. Plates were incubated at 37 °C with microplate visual readings after 24 h. MIC was established as the concentration capable of 100% inhibition of bacterial growth. MBC was determined by transferring each 96-well microplate concentration to plate with BHI agar and subsequent incubation at 37 °C for 24 h. MBC value was defined as the lowest concentration that did not allow bacterial growth visible on the solid medium.

The strain used in antimycobacterial activity assay was *Mycobacterium tuberculosis* H37Rv (ATCC 27294). The inoculum was incubated in shaker at 37 °C at 120 rpm for seven days until a turbidity of 1.0 was reached. The mycobacterial suspension was diluted to 3.0 × 10^5 CFU mL^{-1} and distributed into 96-well plates. Isoniazid was used as reference antitubercular drug. Compounds were solubilized in DMSO in concentrations ranging from

25.0 to 0.09 μg mL^{-1} and added to the wells. Plates were incubated at 37 °C with5% CO_2 for seven days. 30 μL of resazurin was added to the wells with fluorescence spectrometer reading at 530 and 590 nm after 24 h [26].

2.11. Statistical analysis

All assays were performed in triplicate for three independent experiments using the GraphPad Prism version 5.0. The data concerning the biofilm assays were analyzed by one-way analysis of variance (ANOVA) with Tukey's multiple comparison test, with a significance level of 5%. For the *G. mellonella* toxicity model, Kaplan-Meier killing curves were plotted on GraphPad Prism version 5.0 and estimations of differences in survival were compared using log-rank test.

3. Results and discussion

3.1. Design and synthesis

We designed three series of 17 chalcones substituted by amino group and substituents indicated by Topliss' manual method on rings A and B, respectively. Chalcones were synthesized by Claisen-Schmidt reaction with isolated yields ranging from 55% to 90% (Scheme 1). Benzaldehyde derivatives substituted by electron-releasing groups (methyl and methoxyl) led to higher isolated yields than those substituted by electron-withdrawing atoms/groups (chlorine, bromine and nitro). Similar electronic effect contributions of substituents on the benzaldehyde derivatives reactivity were described by Bahekar and co-authors, who described the synthesis of antifilarialsulphonamide chalcones using Claisen-Schmidt reaction [27].

Structure of chalcones was identified by ^{1}H NMR, ^{13}C NMR, MS and UV spectral data analyses. All NMR parameters, including hydrogen and carbon chemical shifts (δ_H and δc in ppm), integrations, multiplicities and coupling constants (*J* in Hz) corresponded to designed structures and compared to former literature reports. Two typical aminochalcone signals in ^{1}H NMR spectra were diagnosed: (*i*) a pair of doublets with *J* values ranging from 15.0 Hz to 15.7 Hz (7.38 ppm $\leq \delta_H \leq$ 8.08ppm), attributed to two hydrogens of carbon-carbon double bond with *E* configuration and (*ii*) broad singlets with δ_H values in ~7.4 ppm, ~5.4 ppm and ~6.2 ppm, related to two hydrogens of amino group at positions 2', 3' and 4',

respectively. In ^{13}C NMR spectra, resolved ketone signals were registered in 186.1 ppm ≤ δ_C ≤ 191.0 ppm. The δ_C values of ketone were shifted to down field due to conjugation of carbonyl with ring A as well as carbon-carbon double bond-ring B system. MS spectra exhibited base peaks attributed to protonated molecule $[M+H]^+$, isotopic peaks attributed to molecule [M + 2] and [M + 4] and characteristic dissociation chalcone peaks, including acylium-type and tropyllium-type. UV-Vis demonstrated λ_{max} values ranging from 302 nm to 36 8nm, evidencing a chromophoric π-electrons system. HPLC-PAD data analyses of peak area indicated the chalcone purities, which ranging from 95% to 100%. All spectra and chromatograms are presented in supplemental material.

(*E*)-1-(2'-aminophenyl)-3-phenylprop-2-en-1-one) (4a). Molecular formula: $C_{15}H_{13}NO$. Yellow solid: Yield: 82%; mp = 61 – 63 ºC. λ_{max}: 304 nm. Purity: 98%. ^1H NMR (600 MHz, DMSO-d_6) δ 6.59 (ddd, *J* = 1.2, 8.0 and 8.0; H-5'), 6.80 (dd, *J* = 1.0 and 8.0; H-3'), 7.29 (ddd, *J* = 1.2, 8.0 and 8.0; H-4'), 7.41 (br s, 2H, NH_2), 7.44 (m, H-3, H-4 and H-5), 7.63 (d, *J* = 15.6; H-α), 7.86 (dd, *J* = 1.2 and 7.5; H-2 and H-6), 7.95 (d, *J* = 15.6; H-β), 8.09 (dd, *J* = 1.2 and 8.0; H-6'). ^{13}C NMR (150 MHz) δ 114.9 (C-3'), 117.3 (C-5'), 117.9 (C-α), 123.8 (C-4), 129.1 (C-2 and C-6), 129.3 (C-3 and C-5), 130.6 (C-1'), 131.9 (C-6'), 134.8 (C-1), 135.5 (C-4'), 142.4 (C-β), 152.5 (C-2'), 191.0 (C-β'). MS (Mwt.: 223.10): *m*/*z* 224.03 ($[M + H]^+$, bp) [28].

(*E*)-1-(2'-aminophenyl)-3-(4-chlorophenyl)prop-2-en-1-one) (4b). Molecular formula: $C_{15}H_{12}ClNO$. Yellow solid: Yield: 88%; mp = 93 – 95 ºC. λ_{max}: 308 nm. Purity: 100%. ^1H NMR (600 MHz, DMSO-d_6) δ 6.59 (ddd, *J* = 1.2, 7.6 and 7.6; H-5'), 6.80 (d, *J* = 7.6; H-3'), 7.29 (ddd, *J* = 1.2, 7.6 and 7.6; H-4'), 7.42 (br s, 2H, NH_2), 7.51 (d, *J* = 8.5; H-2 and H-6), 7.61 (d, *J* = 15.5; H-α), 7.90 (d, *J* = 8.5; H-3 and H-5), 7.98 (d, *J* = 15.5; H-β), 8.09 (dd, *J* = 1.2 and 7.6; H-6'). ^{13}C NMR (150 MHz) δ 114.9 (C-3'), 117.4 (C-5'), 117.8 (C-α), 124.6 (C-1'), 129.4 (C-2 and C-6), 130.8 (C-3 and C-5), 131.9 (C-6'), 134.5 (C-1), 134.9 (C-4), 135.0 (C-4'), 140.9 (C-β), 152.6 (C-2'), 190.8 (C-β'). MS (Mwt.: 257.06): *m*/*z* 258.01 ($[M + H]^+$, bp); *m*/*z* 260.01 ([M + 2], ip); [28, 29].

(*E*)-1-(2'-aminophenyl)-3-(3,4-dichlorophenyl)prop-2-en-1-one (4c). Molecular formula: $C_{15}H_{11}Cl_2NO$. Yellow solid: Yield:90%; mp = 95 – 97 ºC. λ_{max}: 302 nm. Purity: 100%. ^1H NMR (400 MHz, DMSO-d_6) δ 6.60 (ddd, *J* = 1.1, 7.6 and 7.6; H-5'), 6.80 (dd, *J* = 1.1 and 7.6; H-3'), 7.31(ddd, J = 1.1, 7.6 and 7.6; H-4'), 7.44 (br s, 2H, NH_2), 7.58 (d, *J* = 15.5; H-α), 7,70 (d, *J* = 8.3; H-2), 7.85 (dd, *J* = 1.5 and 8.3; H-6), 8.07 (d, *J* = 15.5; H-β), 8,13 (dd, *J* = 1.5 and 8.3; H-5), 8,26 (d, *J* = 1.1; H-6').^{13}C NMR (150 MHz) δ 114.9 (C-3'), 117.4 (C-5'), 117.7 (C-α), 125.9 (C-6), 129.4 (C-2), 130.4 (C-1'), 131.4 (C-5), 132.1 (C-6'),

132.2 (C-4), 132.6 (C-3), 135.0 (C-1), 136.5 (C-4'), 139.6 (C-β), 152.7 (C-2'), 190.6 (C-β'). MS (Mwt.: 292.16): *m/z* 291.98 ([M + H]$^+$, bp); *m/z* 293.98 ([M + 2], ip); *m/z* 295.98 ([M + 4], ip) [30].

(*E*)-1-(2'-aminophenyl)-3-(4-methylphenyl)prop-2-en-1-one (4d). Molecular formula: $C_{16}H_{15}NO$. Yellow solid: Yield: 85%; mp = 95 – 97 ºC. λ_{max}: 315 nm. Purity: 100%. ^{1}H NMR (600 MHz, DMSO-d_6) δ2.35 (s, 4-CH_3), 6.59 (ddd, *J* = 1.0, 8.0 and 8.0; H-5'), 6.80 (dd, *J* = 1.0 and 8.0; H-3'), 7.27 (d, *J* = 7.8; H-3 and H-5), 7.28 (ddd, *J* = 1.0, 8.0 and 8.0; H-4') 7.40 (br s, 2H, NH_2), 7.61 (d, *J* = 15.5; H-α), 7.75 (d, *J* = 7.8; H-2 and H-6), 7.91 (d, *J* = 15.5; H-β), 8.09 (dd, *J* = 1.0 and 8.0; H-6'). ^{13}C NMR (150 MHz) δ 21.5 (4-CH_3), 114.9 (C-3'), 117.3 (C-5'), 118.0 (C-α), 122.7 (C-1'), 129.1 (C-2 and C-6), 130.0 (C-3 and C-5), 131.8 (C-6'), 132.8 (C-1), 134.7 (C-4'), 140.5 (C-4), 142.5 (C-β), 152.5 (C-2'), 191.0 (C-β'). MS (Mwt.: 237.11): *m/z* 238.05 ([M + H]$^+$, bp) [31, 32, 33, 34].

(*E*)-1-(2'-aminophenyl)-3-(4- methoxyphenyl)prop-2-en-1-one) (4e). Molecular formula: $C_{16}H_{15}NO_2$. Yellow solid: Yield: 93%; mp = 70 – 72 ºC. λ_{max}: 334 nm. Purity: 100%. ^{1}H NMR (600 MHz, DMSO-d_6) δ 3.82 (s, 4-OCH_3), 6.59 (ddd, *J* = 1.0, 7.0 and 7.0; H-5'), 6.79 (d, *J* = 7.0; H-3'), 7.01 (d, *J* = 8.7; H-3 and H-5), 7.28 (ddd; *J* = 1.0, 7.0 and 7.0; H-4'), 7.37 (br s, 2H, NH_2), 7.61 (d, *J* = 15.5; H-α), 7.81 (d, *J* = 15.5; H-β), 7.82 (d, *J* = 8.7; H-2 and H-6), 8.08 (d, *J* = 7.0; H-6'). ^{13}C NMR (150 MHz) δ 55.8 (4-OCH_3), 114.8 (C-3 and C-5), 114.9 (C-3'), 117.3 (C-5'), 118.1 (C-α), 121.2 (C-1), 128.1 (C-1'), 130.9 (C-2 and C-6), 131.8 (C-6'), 134.6 (C-4'), 142.4 (C-β), 152.4 (C-2'), 161.4 (C-4), 191.0 (C-β'). MS (Mwt.: 253.11): *m/z* 254.06 ([M + H]$^+$, bp) [29].

(*E*)-1-(3'-aminophenyl)-3-phenylprop-2-en-1-one) (5a). Molecular formula: $C_{15}H_{13}NO$. Yellow solid: Yield: 55%; mp = 112 – 114 ºC. λ_{max}: 309 nm. Purity: 100%. ^{1}H NMR (600 MHz, DMSO-d_6) δ 5.36 (s, 3-NH_2), 6.86 (ddd, *J* = 1.0, 1.6 and 8.0; H-4'), 7.22 (dd, *J* = 8.0 and 8.0; H-5'), 7.27 (dd, *J* = 1.6 and 1.6; H-2'), 7.32 (ddd, *J* = 1.0, 1.6 and 8.0; H-6'), 7.46 (dd, *J* = 2.0 and 6.0; H-3, H-4 and H-5), 7.68 (d, *J* = 15.7; H-α), 7.78 (d, *J* = 15.7; H-β), 7.84 (dd, *J* = 2.0 and 6.0; H-2 e H-6). ^{13}C NMR (150 MHz) δ113.4 (C-2'), 116.8 (C-6'), 119.1 (C-α), 122.9 (C-4'), 129.2 (C-2 and C-6), 129.4 (C-3 and C-5), 129.7 (C-4), 131.0 **(**C-5'), 135.2 (C-1), 138.8 (C-1'), 143.8 (C-β), 149.6 (C-3'), 190.1 (C-β'). MS (Mwt.: 223.10): *m/z* 224.04 ([M + H]$^+$, bp) [35].

(*E*)-1-(3'-aminophenyl)-3-(4-chlorophenyl)prop-2-en-1-one) (5b). Molecular formula: $C_{15}H_{12}ClNO$. Yellow solid: Yield: 75%; mp = 110 – 112 ºC. λ_{max}: 313 nm. Purity: 98%. ^{1}H NMR (600 MHz, DMSO-d_6) δ 5.38 (3-NH_2), 6.85 (dd, *J* = 1.8 and 7.8; H-4'), 7.21 (dd, *J* = 7.8 and 7.8; H-5'), 7.26 (d, *J* = 1.8; H-2'), 7.34 (d, *J* = 7.8; H-6'), 7.53 (d, *J* = 8.5; H-

2 and H-6),7.68 (d, *J* = 15.7; H-α), 7.83 (d, *J* = 15.7; H-β), 7.90 (d, *J* = 8.5; H-3 and H-5). ^{13}C NMR (150 MHz) δ 113.4 (C-2'), 116.9 (C-6'), 119.2 (C-α), 123.6 (C-4'), 129.4 (C-2 and C-6), 129.7 (C-5'), 130.9 (C-3 and C-5), 134.2 (C-1), 135.4 (C-4), 138.7 (C-1'), 142.3 (C-β), 149.6 (C-3'), 189.9 (C-β'). MS (Mwt.: 257.06): *m/z* 258.01 ([M + H]$^+$, bp); *m/z* 260.01 ([M + 2], ip) [36, 37].

(*E*)-1-(3'-aminophenyl)-3-(3,4-dichlorophenyl)prop-2-en-1-one (5c). Molecular formula: $C_{15}H_{11}Cl_2NO$. Yellow solid: Yield: 80%; mp = 120 –122 ºC. λ_{max}: 306 nm. Purity: 95%. ^{1}H NMR (600 MHz, DMSO-d_6) δ6.90 (d, *J* = 7.7; H-4'), 7.24 (dd, *J* = 7.7 and 7.7; H-5'), 7.30 (d, *J* = 1.0; H-2'), 7.41(d, *J* = 7.7; H-6'), 7.65 (d, *J* = 15.7; H-α), 7.70 (d, *J* = 8.4; H-6), 7.84 (d, *J* = 8.4; H-5), 7.90 (d, *J* = 15.7; H-β), 8.22 (d, *J* = 1.1; H-2). ^{13}C NMR (150 MHz) δ 113.3 (C-2'), 117.1 (C-6'), 119.4 (C-α), 124.9 (C-4'), 129.5 (C-6), 129.7 (C-2), 130.6 (C-5'), 131.5 (C-5), 132.3 (C-4), 133.0 (C-3), 136.2 (C-1), 138.6 (C-1'), 141.0 (C-β), 149.7 (C-3'), 189.8 (C-β'). MS (Mwt.: 292.16): *m/z* 291.99 ([M + H]$^+$, bp); *m/z* 293.98 ([M + 2], ip); *m/z* 295.98 ([M + 4], ip). MS/MS: *m/z* 291.98 ([M + H]$^+$), 273.96 ([M - OH]), 198.89 (acylium B, Ar' = 3,4-dichlorophenyl, bp).

(*E*)-1-(3'-aminophenyl)-3-(4-methylphenyl)prop-2-en-1-one (5d). Molecular formula: $C_{16}H_{15}NO$. Yellow solid: Yield: 71%; mp = 103 – 105 ºC. λ_{max}: 321 nm. Purity: 100%. ^{1}H NMR (600 MHz, DMSO-d_6) δ2.36 (s, 4-CH_3), 5.37 (s, 3'-NH_2), 6.84 (dd, *J* = 1.8 and 7.8; H-4'), 7.21 (dd, *J* = 7.8 and 7.8; H-5'), 7.27 (d, *J* = 1.8; H-2'), 7.28 (d, *J* = 8.1; H-3 and H-5), 7.32 (d, *J* = 7.8; H-6'), 7.67 (d, *J* = 15.3; H-α), 7.74 (d, *J* = 15.3; H-β), 7.75 (d, *J* = 8.1; H-2 and H-6). ^{13}C NMR (150 MHz) δ 21.6 (4-CH_3), 113.4 (C-2'), 116.8 (C-6'), 119.0 (C-α), 121.8 (C-4'), 129.2 (C-2 and C-6), 129.7 (C-5'),130.0 (C-3 and C-5), 132.5 (C-1), 138.9 (C-4), 141.0 (C-1'), 143.9 (C-β), 149.6 (C-3'), 190.0 (C-β'). MS (Mwt.: 237.11): *m/z* 238.05 ([M + H]$^+$, bp) [37].

(*E*)-1-(3'-aminophenyl)-3-(4-methoxyphenyl)prop-2-en-1-one) (5e). Molecular formula: $C_{16}H_{15}NO_2$. Yellow solid: Yield: 62%; mp = 122 – 124 ºC.λ_{max}: 341 nm. Purity: 100%. ^{1}H NMR (600 MHz, DMSO-d_6) δ3.88 (s, 4-OCH_3), 6.95 (d, *J* = 8.8; H-3 and H-5), 7.31 (d, *J* = 7.7; H-4'), 7.37 (d, *J* = 2.0; H-2'), 7.38 (d, *J* = 15.6; H-α), 7.41 (d, *J* = 2.0; H-6'), 7.42 (d, *J* = 7.7; H-5'), 7.61 (d, *J* = 8.8; H-2 and H-6), 7.78 (d, *J* = 15.6; H-β). ^{13}C NMR (150 MHz) δ 55.4 (4-OCH_3), 114.4 (C-3 and C-5), 114.6 (C-2'), 118.9 (C-6'), 119.4 (C-α), 120.1 (C-4'), 127.7 (C-1), 129.4 (C-5'), 130.2 (C-2 and C-6), 139.6 (C-1'), 144.5 (C-β), 146.6 (C-3'), 161.6 (C-4), 190.5 (C-β'). MS (Mwt.: 253.11): *m/z* 254.06 ([M + H]$^+$, bp) [29].

(*E*)-1-(3'-aminophenyl)-3-(4-bromophenyl)prop-2-en-1-one (5f). Molecular formula: $C_{15}H_{12}BrNO$. Yellow solid: Yield: 75%; mp = 115 – 117 ºC. λ_{max}: 315 nm. Purity:

100%. ^{1}H NMR (400 MHz, DMSO-d_6) δ5.37 (s, 3'-NH_2),6.84 (dd, *J* = 2.0 and 7.7; H-4'), 7.20 (dd, *J* = 7.7 and 7.7; H-5'), 7.26 (dd, *J* = 2.0 and 2.0; H-2'), 7.34 (d, *J* = 7.7; H-6'), 7.65 (d, *J* = 15.0; H-α), 7.66 (d, *J* = 8.7; H-2 and H-6), 7.82 (d, *J* = 8.7; H-3 and H-5), 7.83 (d, *J* = 15.0; H-β). ^{13}C NMR (150 MHz) δ 113.3 (C-2'), 116.9 (C-6'), 119.2 (C-α), 123.7 (C-4'), 124.3 (C-4), 129.7 (C-5'), 131.1 (C-2 and C-6), 132.4 (C-3 and C-5), 134.5 (C-1), 138.7 (C-1'), 142.4 (C-β), 149.7 (C-3'), 189.9 (C-β'). MS (Mwt.: 302.17): *m/z* 301.98 ([M + H]$^+$, bp); *m/z* 303.97 ([M + 2], ip). MS/MS: m/z 301.99 ([M + H]$^+$), 283.96 ([M - OH]), 208.88 (acylium B, Ar' = 3-bromophenyl, bp) [38].

(*E*)-1-(3'-aminophenyl)-3-(4-nitrophenyl)prop-2-en-1-one (5g). Molecular formula: $C_{15}H_{12}N_2O_3$. Orange solid: Yield: 70%; mp = 143 – 145 ºC. λ_{max}: 316 nm. Purity: 100%. ^{1}H NMR (400 MHz, DMSO-d_6) δ5.40 (s, 3'-NH_2), 6.88 (dd, *J* = 2.0 and 7.8; H-4'), 7.23 (dd, *J* = 7.8 and 7.8; H-5'), 7.28 (dd, *J* = 2.0 and 2.0; H-2'), 7.38 (d, *J* = 7.8; H-6'), 7.77 (d, *J* = 15.7; H-α), 8.00 (d, *J* = 15.7; H-β), 8.14 (d, *J* = 8.3; H-2 and H-6), 8.22 (d, *J*= 8.3; H-3 and H-5). ^{13}C NMR (150 MHz) δ113.3 (C-2'), 117.1 (C-6'), 119.5 (C-α), 124.4 (C-3 and C-5), 126.9 (C-4'), 129.8 (C-5'), 130.2 (C-2 and C-6), 138.4 (C-1'), 140.9 (C-1), 141.8 (C-β), 148.5 (C-4), 149.7 (C-3'), 189.9 (C-β'). MS (Mwt.: 268.27): *m/z* 269.04 ([M + H]$^+$, bp). MS/MS: m/z 269.02 ([M + H]$^+$), 251.01 ([M - OH]), 175.94 (acylium B, Ar' = 3-nitrophenyl, bp) [29].

(*E*)-1-(4'-aminophenyl)-3-phenylprop-2-en-1-one) (6a). Molecular formula: $C_{15}H_{13}NO$. Yellow solid: Yield: 60%; mp = 89 – 92 ºC. λ_{max}: 360 nm. Purity: 96%. ^{1}H NMR (600 MHz, DMSO-d_6) δ6.20 (s, 4'-NH_2), 6.63 (d, *J* = 8.6; H-3' and H-5'), 7.44 (m; H-3, H-4 and H-5), 7.62 (d, *J* = 15.6; H-α), 7.84 (d, *J* = 7.4; H-2 and H-6), 7.88 (d, *J* = 15.6; H-β), 7.93 (d, *J* = 8.6; H-2' and H-6'). ^{13}C NMR (150 MHz) δ 113.2 (C-3' and C-5'), 122.8 (C-α), 125.7 (C-1'), 129.0 (C-2 and C-6), 129.3 (C-3 and C-5), 130.5 (C-4), 131.6 (C-2' and C-6'), 135.6 (C-1), 141.9 (C-β), 154.4 (C-4'), 186.3 (C-β'). (Mwt.: 223.10): *m/z* 224.04 ([M + H]$^+$, bp) [28, 39].

(*E*)-1-(4'-aminophenyl)-3-(4-chlorophenyl)prop-2-en-1-one) (6b). Molecular formula: $C_{15}H_{12}ClNO$. Yellow solid: Yield: 79%; mp = 154 – 157 ºC. λ_{max}: 363 nm. Purity: 99%. ^{1}H NMR (600 MHz, DMSO-d_6) δ 6.20 (s, 4'-NH_2), 6.62 (d, *J* = 8.8; H-3' and H-5'), 7.50 (d, *J* = 7.4; H-2 and H-6), 7.60 (d, *J* = 15.6; H-α), 7.88 (d, *J* = 7.4; H-3 and H-5), 7.90 (d, *J* = 15.6; H-β), 7.93 (d, *J* = 8.8; H-2' and H-6'). ^{13}C NMR (150 MHz) δ 113.2 (C-3' and C-5'), 123.6 (C-α), 125.6 (C-1'), 129.3 (C-2 and C-6), 130.7 (C-3 and C-5), 131.7 (C-2' and C-6'), 134.6 (C-1), 134.9 (C-4), 140.4 (C-β), 154.5 (C-4'), 186.2 (C-β').). MS (Mwt.: 257.06): *m/z* 258.01 ([M + H]$^+$, bp); *m/z* 260.01 ([M + 2], ip) [28, 39].

(*E*)-1-(4'-aminophenyl)-3-(3,4-dichlorophenyl)prop-2-en-1-one (6c). Molecular formula: $C_{15}H_{11}Cl_2NO$. Yellow solid: Yield: 82%; mp = 181 – 183 ºC. λ_{max}: 370 nm. Purity: 100%. ^{1}H NMR (600 MHz, DMSO-d_6) δ6.21 (s, 4'-NH_2), 6.63 (d, *J* = 8.5; H-3' and H-5'), 7.57 (d, *J* = 15.5; H-α), 7.69 (d, *J* = 8.3; H-5), 7.82 (dd, *J* = 1.5 and 8.3; H-6), 7.95 (d; *J* = 8.5; H-2' and H-6'), 7.97 (d, *J* = 15.5; H-β), 8.23 (d; *J* = 1.5; H-2). ^{13}C NMR (150 MHz) δ113.2 (C-3' and C-5'), 125.0 (C-α), 125.5 (C-1'), 129.2 (C-5), 130.2 (C-2), 131.4 (C-6), 131.8 (C-2' and C-6'), 132.2 (C-4), 132.5 (C-3), 136.5 (C-1), 139.2 (C-β), 154.6 (C-4'), 186.1 (C-β'). MS (Mwt.: 292.16): *m/z* 291.99 ([M + H]$^+$, bp); *m/z* 293.99 ([M + 2], ip); *m/z* 295.98 ([M + 4], ip) [40].

(*E*)-1-(4'-aminophenyl)-3-(4-methylphenyl)prop-2-en-1-one (6d). Molecular formula: $C_{16}H_{15}NO$. Yellow solid: Yield: 73%; mp = 130 – 134 ºC. λ_{max}: 361 nm. Purity: 99%. ^{1}H NMR (600 MHz, DMSO-d_6) δ 2.34 (s, 4-CH_3), 6.16 (s, 4'-NH_2), 6.62 (d, *J* = 8.5; H-3' and H-5'), 7.26 (d, *J* = 7.9; H-3 and H-5), 7.59 (d, *J* = 15.5; H-α), 7.73 (d, *J* = 7.9; H-2 and H-6), 7.82 (d, *J* = 15.5; H-β), 7.93 (d, *J* = 8.5; H-2' and H-6'). ^{13}C NMR (150 MHz) δ 21.5 (4-CH_3), 113.2 (C-3' and C-5'), 121.8 (C-α), 125.8 (C-1'), 129.0 (C-2 and C-6), 129.9 (C-3 and C-5), 131.6 (C-1), 132.9 (C-2' and C-6'), 140.4 (C-4), 141.9 (C-β), 154.3 (C-4'), 186.3 (C-β'). MS (Mwt.: 237.11): m/z 238.06 ([M + H]$^+$, bp) [39].

(*E*)-1-(4'-aminophenyl)-3-(4- methoxyphenyl)prop-2-en-1-one) (6e). Molecular formula: $C_{16}H_{15}NO_2$. Yellow solid: Yield: 66%; mp = 109 – 113 ºC. λ_{max}: 368 nm. Purity: 99%. ^{1}H NMR (600 MHz, DMSO-d_6) δ 3.81 (s, 4-OCH_3), 6.13 (s, 4'-NH_2), 6.61 (d, *J* = 8.7; H-3' and H-5'), 7.00 (d, *J* = 8.8; H-3 and H-5), 7.58 (d, *J* = 15.5; H-α), 7.73 (d, *J* = 15.5; H-β), 7.80 (d, *J* = 8.8; H-2 and H-6), 7.91 (d, *J* = 8.7; H-2' and H-6'). ^{13}C NMR (150 MHz) δ 55.8 (4-OCH_3), 113.2 (C-3 and C-5), 114.8 (C-3' and C-5'), 120.3 (C-α), 125.9 (C-1), 128.2 (C-1'), 130.8 (C-2 and C-6), 131.5 (C-2' and C-6'), 141.8 (C-β), 154.2 (C-4'), 161.3 (C-4), 186.4 (C-β'). MS (Mwt.: 253.11): *m/z* 254.06 ([M + H]$^+$, bp) [39].

3.2. Antibacterial activity against MSSA and MRSA planktonic cells

All chalcones were submitted to antibacterial evaluations against MSSA and MRSA planktonic cells, furnishing the MIC and MBC values (Table 1). The bioactivity comparison of three series suggests 3'-aminochalcones (**5a**–**5e**) were more active than 2'-aminochalcones (**4a**–**4e**) and 4'-aminochalcones (**6a**–**6e**), evidencing the key role of amino group position to antibacterial potency (Scheme 2). 2'-aminochalcones **4a**–**4c** were active with MIC values of 15.6–62.5 µg mL^{-1} and 7.8–62.5 µg mL^{-1} against MSSA and MRSA, respectively. 2'-

aminochalcones **4d** and **4e** as well as 4'-aminochalcones **6a**–**6e** were considered inactive, with MIC ≥ 62.5 μg mL^{-1}.

3'-Aminochalcones exhibited MIC values of 1.95–62.5 μg mL^{-1} and 15.6–62.5 μg mL^{-1} against MSSA and MRSA, respectively. According to the MIC values against MSSA, the potency ranking for this first set of 3'-aminochalcones was: 3,4-diCl (**5c**) > 4-Cl (**5b**) > 4-CH_3 (**5d**) > H (**5a**) = 4-OCH_3 (**5e**) (Scheme 2). Analyzing the influence of electron density on ring B toward anti-MSSA activity, electron-withdrawing substituent (Cl) was more effective than electron-releasing groups by inductive (4-CH_3) and mesomeric effects (4-OCH_3). Also, hydrophobicity influenced anti-MSSA activity as indicated by potency ranking. Based on comparison Topliss' manual method, π was indicated as the main parameter for the selection of substituents and anti-MSSA analogs. As show in Scheme 2, according to anti-MRSA evaluations, the antibacterial effect was orchestrated by electron-withdrawing atoms and the potency ranking was: 4-Cl (**5b**) = 3,4-diCl (**5c**) > H (**5a**) > 4-CH_3 (**5d**) = 4-OCH_3 (**5e**), suggesting σ as the pivotal parameter. Altogether, anti-MSSA and anti-MRSA activities indicated π and σ preponderant parameters, respectively. We evaluated two additional analogs 4-bromo-3'-aminochalcone (**5f**) and 4-nitro-3'-aminochalcone (**5g**), which were suggested by tabulated potency ranking, following preconized physicochemical parameters. Moreover, *para*-bromo and *para*-nitro substituents are able to increase the σ and πvalues of chalcone nucleus. Compounds **5f** and **5g** were active against MSSA, with MIC values of 1.9 μg mL^{-1} and 3.9 μg mL^{-1}, respectively. These MIC values are comparable to vancomycin, which was used as reference antibacterial drug and demonstrated MIC value of 1.0 against MSSA (Table 1). The major contribution of two additional compounds was to MRSA growth inhibition, which displayed the lowest MIC values (7.8 μg mL^{-1}). In brief, the easy use of Topliss' manual method was useful to improve the antibacterial potency of 3'-aminochalcones, which possess unknown molecular targets. Also, Jorge and co-authors improved the antibacterial activity of benzofuroxan derivatives against VISA and VRSA planktonic cells using Topliss' decision tree, which is closely similar to Topliss' manual method [41]. Altogether, SAR data indicated two main structural features that collaborate with antibacterial activity of chalcones, including the essentiality of amino group position on ring A (potency order: 3′-NH_2 > 2′- NH_2 > 4′-NH_2) and the presence of hydrophobic and electron- withdrawing groups at position 4 of ring B (potency order: Br > NO_2 > Cl > Me > OMe) (Scheme 2).

3'-Aminochalcones were able to kill staphylococcal cells, exhibiting MBC values of 3.9–31.2 μg mL^{-1} and 7.8–31.2 μg mL^{-1} against MSSA and MRSA, respectively. Chalcone **5f** presented the most potent bactericidal effect, with MBC values of 3.9 μg mL^{-1} and 7.8 μg mL^{-1}

[1] against MSSA and MRSA, respectively. Several antibacterial studies of chalcones were revised by Xu and co-authors, who suggested those compounds have an excellent potential for the discovery and development of antibacterial drugs, highlighting a good number of clinical candidates in the near future [42]. Nevertheless, few chalcones have presented effect against resistant strains of *S. aureus*, including MRSA. Chen and co-workers synthesized a series of chalcones hybridized with rhodanine-3-acetic acid moiety, which were active against MRSA and QRSA (quinolone-resistant *Staphylococcus aureus*). Among those compounds, the most potent was the 2',4'-dichlorinated chalcone derivative, that exhibits MIC value of 2.0 μg mL^{-1} against MRSA and QRSA clinical isolates [43]. In summary, the lowest MIC and MBC values displayed by **5f** encouraged us to select it for detailed antibacterial investigations using MSSA and MRSA.

3.3. Checkerboard assay

We evaluated the effect of the combination of chalcone 5f with methicillin and vancomycin against MSSA and MRSA planktonic cells (Table 2). The combination with 5f decreased MIC value of vancomycin from 1.0 to 0.1 μg mL-1 and from 2.0 to 0.2 μg mL-1 against MSSA and MRSA, respectively. The 10-fold reduction of vancomycin MIC values may be a therapeutic advantage, which could lead to administration of lower doses of vancomycin, 5f or both. In this context, the high doses of vancomycin administered against infections can cause severe side effects, including phlebitis, nephrotoxicity, ototoxicity, neutropenia and thrombocytopenia [44]. Moreover, the combination of 5f and vancomycin displayed FICI values of 0.3 and 0.2 against MSSA and MRSA, respectively evidencing synergistic association.

In addition, the absence of antagonistic effect evidenced for both combinations, reinforces 5F as a possible antibacterial candidate for the treatment of MSSA / MRSA, because it does not interfere negatively in the tested antimicrobials. Indicating that the combined use in vivo could result in improved prognosis, through the use of therapeutic strategies that use more than one form of drug administration.

Since the discovery of penicillin G and prontosil rubrum, the resistance to antibiotics has been a health public problem, representing the central factor to the discovery of new antibacterial agents [45]. In order to avoid the resistance development to individual antibiotic use, the association of antibiotics with synergistic effect has been used by therapeutics [46]. Among these, sulfamethoxazole-trimethoprim is an ancient and effective combination, which

is administered against MRSA infections [7]. Some synthetic chalcones were tested with antibacterial drugs and demonstrated synergistic combination. Tran and co-authors described a FICI value of 0.3 as result of vancomycin and a pyridinic chalcone against MRSA [47]. Vásquez-Martínez and collaborators described a MIC reduction of methicillin against MRSA when combined with two catecholic chalcones (FIC values of 0.4 and 0.5), evidencing a synergistic combination [48]. Interestingly, our combination between **5f** and methicillin was additive, with FICI values of 0.7 and 1.0 against MSSA and MRSA, respectively.

3.4. Anti-adhesion assay

S. aureus is a common skin and mucosa colonizer in ~20% of individuals and its typical infections involve cutaneous lesions [49]. Thus, we investigated the inhibition of **5f** against staphylococcal adhesion on human keratinocytes. The inhibitory effect of MSSA and MRSA adhesion on HaCaT cells were tested in three times and subinhibitory concentration (1/2 MIC value). The results indicatedtreatment with **5f** at 1.0 μg $mL^{-1}$and 3.9 μg mL^{-1}against MSSA and MRSA, respectively led to a significant decrease in adhesion to HaCat cells ($P < 0.05$) over time compared to the untreated cells (Fig. 2). The greatest inhibitory effects against MSSA and MRSA were at 1 hour and 2 h, respectively. In order to verify whether **5f** demonstrated toxicity against HaCaTcells, which could interfereon anti-adhesion assay results, the cell viability was measured by MTT assay. At MIC/2 value, **5f** demonstrated low HaCaT toxicity, furnishing 94% cell viability. In concluding, anti-adhesion effect of **5f** on MRSA and MSSA is relevant to staphylococcal infection, because *S. aureus* adhesion is the early step for successful infection to surface host cells [50, 51]. The initial infection dynamics includes specific surface staphylococcal and human matrix proteins, including bacterial covalently-bound surface proteins [microbial surface components recognizing adhesive matrix (MSCRAMMs), sortase and clumping factors A and B] [52, 53], bacterial non-covalently surface proteins [secretable expanded repertoire adhesive molecules (SERAMs) and Atl-type autholysins) [54] as well as extracellular matrix proteins, mainly fibronectin, collagen and cytokeratin 10 [55].

3.5. Antibiofilm assays

Biofilms have been defined as sessile community which is embedded in extracellular polymeric matrix, forming aggregates attached to an abiotic or biotic surface, or non-attached

(free-floating aggregates). In this context, cells in biofilms and planktonic cells present notable differences with respect to their metabolism, gene transcription and protein expression [56, 57]. *S. aureus* is able to produce strong biofilms, generating severe and antibiotic-resistant infections, mainly in chronic skin ulcers in diabetes patients and acute burn wounds [58, 59]. Several therapeutic strategies to combat prolonged and recurrent biofilm infections have investigated, including antibacterial peptides, vaccines, biofilm-degrading enzymes, bacteriophages, quorum-sense blockers and small molecules. Most of them are still in the preclinical stage [57]. Our group has dedicated efforts in the search of small molecules with antibiofilm activity against *S. aureus* and *Streptococcus mutans*, including diacetylcurcumin [16] and pentylcaffeate [20]. Herein, we evaluated the effects of **5f** on MSSA and MRSA biofilm formation and preformed biofilm.

Chalcone **5f** and vancomycin was evaluated for their ability to inhibit biofilm formation at respective MIC and 10 × MIC values (Fig. 3). We performed a quantitative assay for determination of CFU mL^{-1} after initial biofilm formation. Treatment with **5f** and vancomycin atMIC values did not inhibit the MSSA and MRSA biofilm formation. On the other hand, treatment with **5f** and vancomycin at 10 × MIC values caused a significant decrease of MSSA and MRSA biofilm formation as compared to the untreated groups ($P < 0.05$). At 10 × MIC the inhibitory effect against biofilm formation of **5f** was higher than vancomycin, with a reduction of 8 $\log_{10}$ CFU mL^{-1} and 7 $\log_{10}$ CFU mL^{-1} against MSSA and MRSA, respectively when both were compared to the untreated control. During initial biofilm formation, the proliferation of microcolonies is accompanied by intense production of polysaccharide intercellular adhesin (PIA), surface-located proteins, teichoic acids and extracellular DNA, forming biofilm matrix [50, 60]. This slimy material is responsible to high adherence, conferring to biofilms ahighertolerance toantibacterial drugs and immune defenses than planktonic cells [61, 62]. The activity of **5f** against *S. aureus* biofilm formation can cause damage intogummy matrix, separating thecellular clusters and facilitating the access to individual cells as well as their viability.

In order to evaluate the effect of chalcone **5f** and vancomycin against MSSA and MRSA preformed biofilm, we carried out a quantitative assay for determination of CFU mL^{-1}. Compounds were tested at respective MIC and 10 × MIC values. Both concentrations of **5f** led to a significant decrease of MSSA and MRSA biofilm survival ($P < 0.05$) as compared to untreated biofilm, with better result at 10 × MIC value (Fig. 4). In contrast, vancomycin was able to reduce preformed biofilm survival at 10 × MIC value ($P < 0.05$). The mature biofilms demonstrate organized morphology with mushroom-like towers and fluid-filled channels,

which are maintained by strong adhesive factors [63]. On the other hand, the action of hydrolases (mainly proteases and nucleases) and phenol-soluble modulins (PSMs) disrupt covalent bounds and non-covalent interactions, respectively, causing detachment and dispersal of cell clusters [64, 65]. Chalcone **5f** was able to decrease preformed biofilm survival, avoiding complete biofilm maturation and dispersal. This behavior of **5f** may be useful to combat preformed biofilm on implanted medical devices, because dispersal can result in *Staphylococcus aureus* bacteremia (SAB), which has been associated with significant levels of nosocomial mortality [66].

Scanning electron microscopy (SEM) analyses were carried out to confirm the destructive effects of **5f** and vancomycin on the structure and integrity of MSSA and MRSA biofilms (Fig. 5). Untreated MSSA and MRSA biofilms demonstrated heavily colonized with the formation of grape-like structures of dividing and normally-shaped bacteria. Chalcone **5f** and vancomycin affected MSSA and MRSA biofilm structures, damaging their architecture and culminating in amorphous cellular clusters. The damaging effects of **5f** and vancomycin were similar, causing a significant reduction in the biofilm population, which corroborates the quantitative analyses colony count assay (Fig. 5). The concentration-dependent effect was observed for **5f** and vancomycin. Bacterial clusters were rarely observed in treated cultures by **5f** and vancomycin at 10 × MIC. Qualitative observations suggested the MRSA biofilms were moresusceptible to vancomycin than **5f**. Several authors have revised the activity of chalcones with diverse structural pattern against *S. aureus* planktonic cells [10, 42, 67, 68]. However, few investigations have usedcells in biofilms, which are similar to environment of sthaphylococcal infections. Bozic and co-authors reported a chalcone with hydroxyl groups at positions 2’ (ring A) and 4 (ring B) with antibiofilm activity against MRSA, including ATCC 43300 and 30 clinical isolates from blood, sputum, urine and a panel of swabs [69].

3.6. Acute toxicity assay

Galleria mellonela has been used as a consolidated model to *in vivo* tests of toxicity and anti-infective activity [70, 71]. Their larvae present high structural and functional similarities to mammal complexity, including innate immune response, as well are well-accepted as an ethical alternative for *in vivo* investigations [72]. The acute toxicity of **5f** and vancomycin was evaluated using *G. mellonella* larvae (Fig. 6). The larvae survival after treatment with vehicle control was 100% over a period of 72 h. After 72 h of intra-haemocoelic administration, chalcone **5f** did not cause significant acute toxicity, exhibiting

20% and 30% larval mortality at MIC and 10 × MIC values, respectively. Also, vancomycin was not toxic to *G. mellonella* larvae, demonstrating 0% and 20% larval mortality at MIC and 10 × MIC values.

3.7. Additional antibacterial and antimycobacterial assays

In order to assess the antibacterial spectrum, chalcone **5f** was evaluated againstanother Gram-positive, two Gram-negative and mycobacterium species. Chalcone **5f** was active against *E. faecalis* and *A. baumannii* planktonic cells, exhibiting MIC values of 7.8 and 15.6 μg mL^{-1}, respectively. Against these bacterial species, vancomycin demonstrated MIC value of 1.0 μg mL^{-1}. On the other hand, **5f** was not active against *P. aeuruginosa* planktonic cells, with MIC and MBC values higher than 62.5μg mL^{-1}, while ciprofloxacin demonstrated MIC value of 0.6 μg mL^{-1}. The growth of *M. tuberculosis* was moderately affected by **5f** (MIC = 5.7 μg mL^{-1}) when compared with isoniazid (MIC = 0.3). In 2017, the World Health Organization (WHO) reported a ranking with 12 deadliest drug-resistant bacteria [73]. In this context, **5f** demonstrated activity against *A. baumannii* and MRSA, which are included incritical priority and high priority groups, respectively.

4. Conclusions

In summary, we designed, synthesized and evaluated a series of 17 chalcones against MSSA and MRSA planktonic cells. Preliminary structure-activity relationship investigations suggested amino group and hydrophobic substituents on rings A and B, respectively demonstrated a key role on the antibacterial activity. 3'-amino-4-bromochalcone (**5f**) was the most active compound and selected for detailed bioassays. The combination of **5f** and vancomycin exhibited synergistic effect against MSSA and MRSA planktonic cells. The adhesion of MSSA and MRSA on human keratinocytes was reduced by subinhibitory concentrations of **5f**. In addition, **5f** has effect against MSSA and MRSA biofilm formation and preformed biofilms, perturbating their architecture. Acute toxicity using *G. mellonella* indicate low percentage of larval mortality after 72 h of treatment with **5f**. Moreover, the antibacterial activity of **5f** was confirmed against *E. faecalis, A. baumannii* and *M. tuberculosis*, evidencing its broad antibacterial spectrum. Altogether our findings open new avenues for **5f** as an anti-*Staphylococcus aureus* agent, with potential applications as antibacterial drug, adjunct of antibiotics and medical devices coating.

CRediT autorship contribution statement

Mayara A.R. Garcia: Data curation, Formal analysis, Methodology, Writing – original draft. **Reinaldo S. Theodoro:** Data curation, Formal analysis, Methodology. **Janaina C.O. Sardi:** Data curation, Formal analysis, Funding acquisition, Methodology, Resources, Writing – re- view & editing. **Mariana B. Santos:** Data curation, Formal analysis, Methodology. **Gabriela M. Ayusso:** Data curation, Formal analysis, Methodology. **Fernando R. Pavan:** Resources, Funding acquisition, Investigation, Supervision, Writing – review & editing. **Alan R. Costa:** Data curation, Formal analysis, Methodology. **Lucas M. Santa Cruz:** Data curation, Formal analysis, Methodology. **Pedro L. Rosalen:** Re- sources, Funding acquisition, Investigation, Supervision, Writing – re- view & editing. **Luis O. Regasini:** Resources, Funding acquisition, Investigation, Supervision, Writing – original draft, Writing – review & editing.

Declarations of Competing Interest

The authors declare that they have no known competing financial interests or personal relationships that could have appeared to influence the work reported in this paper.

Acknowledgements

The authors gratefully acknowledge financial support from the Co- ordination for the Improvement of Higher Education Personnel (CAPES), the National Research Council (CNPq) (Grants 471129/2013-5; 306251/2016-7, 429322/2018-6 and 309957/2019-2), and the São Paulo Research Foundation (FAPESP) (Grants 2014/18330-0 and 2018/ 15083-2). Also, we would like to thank the National Institute for Science and Technology of Biodiversity and Natural Products (INCT-BioNat) for MS experiments (Grants Fapesp 2014/50926-0 and CNPq 465337/ 2014-0), the Multiuser Centre for Biomolecular Innovation (CMIB/ Fapesp Grant 2009/53989-4) for NMR experiments. MAR thanks INCT- BioNat and CAPES (Finance code 001) for her scholarship.

References

[1] McGuinness, W.A., Malachowa, N., DeLeo, F.R. Vancomycin Resistance in *Staphylococcus aureus*. Yale J. Biol. Med. 90 (2017) 269–281.

[2] Harkins, C.P., Pichon, B., Doumith, M., Parkhill, J., Westh, H., Tomasz, A., de Lencastre, H., Bentley, S.D., Kearns, A.M., Holden, M.T.G. Methicillin-resistant *Staphylococcus aureus* emerged long before the introduction of methicillin into clinical practice. Genome Biol. 18 (2017) 130. https://doi.org/10.1186/s13059-017-1252-9

[3] Hartman, B.J., Tomasz, A. Low-affinity penicillin-binding protein associated with beta-lactam resistance in *Staphylococcus aureus*. J. Bacteriol. 158 (1984) 513–516. https://doi.org/10.1128/JB.158.2.513-516.1984

[4] Katayama, Y., Ito, T., Hiramatsu, K. A new class of genetic element, staphylococcus cassette chromosomemec, encodes methicillin resistance in *Staphylococcus aureus*. Antimicrob. AgentsChemother. 44 (2000) 1549–1555. https://doi.org/10.1128/aac.44.6.1549-1555.2000

[5] Gardete, S., Tomasz, A. Mechanisms of vancomycin resistance in *Staphylococcus aureus*. J. Clin. Invest. 124 (2014) 2836–2840. https://doi.org/10.1172/JCI68834

[6] Weigel, L.M. Genetic Analysis of a High-Level Vancomycin-Resistant Isolate of *Staphylococcus aureus*. Science 302 (2003) 1569–1571. https://doi.org/10.1126/science.1090956

[7] Wright, G.D., 2010. Q&A: Antibiotic resistance: where does it come from and what can we do about it? BMC Biol. 8, 123. https://doi.org/10.1186/1741-7007-8-123

[8] Mullard, A. 2018 FDA drug approvals. Nat. Rev. Drug. Discov. 18 (2019) 85–89. https://doi.org/10.1038/d41573-019-00014-x

[9] Zhuang, C., Zhang, Wen, Sheng, C., Zhang, Wannian, Xing, C., Miao, Z., 2017. Chalcone: a privileged structure in medicinal chemistry. Chem. Rev. 117, 7762–7810. https://doi.org/10.1021/acs.chemrev.7b00020

[10] Sahu, N.K., Balbhadra, S.S., Choudhary, J., Kohli, D.V. Exploring pharmacological significance of chalcone scaffold: a review. Curr. Med. Chem. 19 (2012) 209–225. https://doi.org/10.2174/092986712803414132

[11] Zhang, B., Teng, Z., Li, X., Lu, G., Deng, X., Niu, X., Wang, J. Chalcone attenuates *staphylococcus aureus* virulence by targeting sortase a and alpha-hemolysin. Front. Microbiol. 8 (2017) 1715. https://doi.org/10.3389/fmicb.2017.01715

[12] Nostro, A., Cellini, L., Di Giulio, M., D'Arrigo, M., marino, A., Blanco, A.R., Favaloro, A., Cutroneo, G., Bisignano, G. Effect of alkaline pH on staphylococcal biofilm formation. APMIS. 120 (2012) 733–742. https://doi.org/10.1111/j.1600-0463.2012.02900.x.

[13] Topliss, J.G. A manual method for applying the Hansch approach todrug design. J. Med. Chem. 20 (1977) 463–469. https://doi.org/10.1021/jm00214a001

[14] Tavares, L.C. QSAR: the Hansch's approach. Quim. Nova. 27 (2004) 655–660. https://doi.org/ 10.1590/S0100-40422004000400018

[15] Santos, M.B., Anselmo, D.B., Oliveira, J.G., Jardim-Perassi, B.V., Monteiro, D.A., Silva, G., Gomes, E., Fachin, A.L., Marins, M., Zuccari, D.A.P.C., Regasini, L.O. Antiproliferative activity and p53 up regulation effects of chalcones on humanbreast cancer cells. J. Enzyme Inhib.Med.Chem. 34 (2019) 1093–1099. https://doi.org/10.1080/14756366.2019.1615485

[16] Sardi, J.C.O., Polaquini, C.R., Freires, I.A., Galvão, L.C. de C., Lazarini, J.G., Torrezan, G.S., Regasini, L.O., Rosalen, P.L. Antibacterial activity of diacetylcurcumin against *Staphylococcus aureus* results in decreased biofilm and cellular adhesion. J. Med. Microbiol. 66 (2017) 816–824. https://doi.org/10.1099/jmm.0.000494

[17] Cockerill, F.R. Methods for Dilutions Antimicrobial Susceptibility Tests for Bacteria That Grow Aerobically: Approved Standard. CLSI. 32 (2012).

[18] Odds, F.C. Synergy, antagonism, and what the chequerboard puts between them. J. Antimicrob. Chemother. 52 (2003) 1–1. https://doi.org/10.1093/jac/dkg301

[19] Sangalli-Leite, F., Scorzoni, L., Silva, A.C.A.P., Silva, J. F., Oliveira, H.C., Singulani, J.L., Gullo, F.P., Silva, R.M., Regasini, L.O., Silva, D.H.S., Bolzani, V.S., Fusco-Almeida, A.M., Mendes-Giannini, M.J.S. Synergistic effect of pedalitinand amphotericin B against *Cryptococcus neoformans* by *in vitro* and *in vivo* evaluation. Int. J. Antimicrob. Agents 48 (2016) 504–511. https://doi.org/10.1016/j.ijantimicag.2016.07.025

[20] Emeri,F.T.A.S., Rosalen, P.L., Paganini, É.R., Garcia, M.A.R., Nazaré, A.C., Lazarini, J.G., Alencar, S.M. de, Regasini, L.O., Sardi, J. de C.O. Antimicrobial activity of nitrochalcone and pentyl
caffeate against hospital pathogens results in decreased microbial adhesion and biofilm formation. Biofouling 35 (2019) 129–142. https://doi.org/10.1080/08927014.2019.1574763

[21] Stepanović, S., Vuković, D., Hola, V., Bonaventura, G.D., Djukić, S., Ćirković, I., Ruzicka, F. Quantification of biofilm in microtiter plates: overview of testing conditions and practical recommendations for assessment of biofilm production by staphylococci. APMIS. 115 (2007) 891–899. https://doi.org/10.1111/j.1600-0463.2007.apm_630.x

[22] Ibarra-Trujillo, C., Villar-Vidal, M., Gaitán-Cepeda, L.A., Pozos-Guillen, A., Mendoza-de Elias, R., Sánchez-Vargas, L.O. Ensayo de formación y cuantificación de biopelículas mixtas de *Candida albicans* y *Staphylococcus aureus*. Ver. Iberoam. Micol. 29 (2012) 214–222. https://doi.org/10.1016/j.riam.2012.02.003

[23] Freires, I. de A., Murata, R.M., Furletti, V.F., Sartoratto, A., Alencar, S.M. de, Figueira, G.M., de Oliveira Rodrigues, J.A., Duarte, M.C.T., Rosalen, P.L. *Coriandrums ativum L*. (Coriander) Essential Oil: Antifungal Activity and Mode of Action on *Candida spp*., and Molecular Targets Affected in Human Whole-Genome Expression. PLoS ONE 9 (2014) e99086. https://doi.org/10.1371/journal.pone.0099086

[24] Megaw, J., Thompson, T.P., Lafferty, R.A., Gilmore, B.F. *Galleria mellonella* as a novel in vivo model for assessment of the toxicity of 1-alkyl-3-methylimidazolium chloride ionic liquids. Chemosphere 139 (2015) 197–201. https://doi.org/10.1016/j.chemosphere.2015.06.026

[25] Scorzoni, L., Benaducci, T., Almeida, A.M.F., Silva, D.H.S., Bolzani, V. da S., Gianinni, M.J.S.M. The use of standard methodology for determination of antifungal activity of natural products against medical yeasts *Candida* sp.and *Cryptococcus* sp. Braz. J. Microbiol. 38 (2007) 391–397. https://doi.org/10.1590/S1517-83822007000300001

[26] Palomino, J.-C., Martin, A., Camacho, M., Guerra, H., Swings, J., Portaels, F. Resazurin microtiter assay plate: simple and inexpensive method for detection of drug resistance in *mycobacterium tuberculosis*. Antimicrob. AgentsChemother. 46 (2002) 2720–2722. https://doi.org/10.1128/AAC.46.8.2720-2722.2002

[27] Bahekar, S.P., Hande, S.V., Agrawal, N.R., Chandak, H.S., Bhoj, P.S., Goswami, K., Reddy, M.V.R. Sulfonamidechalcones: Synthesis and *in vitro* exploration for therapeutic potential against *Brugiamalayi*. Eur.J. Med.Chem. 124 (2016) 262–269. https://doi.org/10.1016/j.ejmech.2016.08.042

[28] Mai, C.W., Yaeghoobi, M., Abd-Rahman, N., Kang, Y.B., Pichika, M.R. Chalcones with electron-with drawing and electron-donating substituents: Anticancer activity against TRAIL resistant cancer cells, structure–activity relationship analysis and regulation of apoptotic proteins. Eur.J. Med.Chem.77 (2014) 378–387. https://doi.org/10.1016/j.ejmech.2014.03.002

[29] Malbari, K., Gonsalves, H., Chintakrindi, A., Gohil, D., Joshi, M., Kothari, S., Srivastava, S., Chowdhary, A., Kanyalkar, M. In search of effective H1N1 neuraminidase inhibitorby molecular docking, antiviral evaluation and membrane interaction studies using NMR. Acta. Virol. 62 (2018) 179–190. https://doi.org/10.4149/av_2018_209

[30] Zhao, F., Zhao, Q.-J., Zhao, J.-X., Zhang, D.-Z., Wu, Q.-Y., Jin, Y.-S. Synthesis and cdc25B inhibitory activity evaluation of chalcones. Chem. Nat.Compd. 49 (2013) 206–214. https://doi.org/10.1007/s10600-013-0563-7

[31] Xia, Y., Yang, Z-Y., Xia, P., Bastow, K.F., Nakanishi, Y., Lee, K-H. Antitumor agents. Part 202: Novel 2′-amino chalcones: design, synthesis and biological evaluation. Bioorg. Med. Chem. Lett. 10 (2000) 699–701. doi: 10.1016/S0960-894X(00)00072-X.

[32] Sun, F., Zhao, X., Shi, D. An efficient one-step synthesis of 2-arylquinolin-4(1H)-ones with the aidof a low-valenttitanium reagent. TetrahedronLett. 52 (2011) 5633–5635. https://doi.org/10.1016/j.tetlet.2011.08.089

[33] Ravi, M., Chauhan, P., Singh, S., Kant, R., Yadav, Prem.P. p-TsOH-promoted synthesis of (E)-6-phenyl-7-styryl-5,6-dihydrodibenzo[b,h][1,6]naphthyridines via cascade intramolecular aza-Michael addition/Friedlander condensation of 2′-aminochalcones in a SDS/H_2O system. RSC Adv. 6 (2016) 48774–48778. https://doi.org/10.1039/C6RA04837D

[34] Santos, M.B., Pinhanelli, V.C., Garcia, M.A.R., Silva, G., Baek, S.J., França, S.C., Fachin, A.L., Marins, M, Regasini, L.O. Antiproliferative and pro-apoptotic activities of 2'- and 4'-aminochalcones against tumor canine cells. Eur. J. Med. Chem. 138 (2017) 884–889. https://doi.org/10.1016/j.ejmech.2017.06.049

[35] Karaman, I., Gezegen, H., Gürdere, M.B., Dingil, A., Ceylan, M. Screening of Biological Activities of a Series of Chalcone Derivatives against Human Pathogenic Microorganisms. Chem. Biodivers.d 7 (2010) 400–408. https://doi.org/10.1002/cbdv.200900027

[36] Ullah, A., Ansari, F.L., Ihsan-ul-Haq, Nazir, S., Mirza, B. Combinatorial Synthesis, Lead Identification, and Antitumor Study of a Chalcone-Based Positional-Scanning Library. Chem. Biordivers. 4 (2007) 203–214. https://doi.org/10.1002/cbdv.200790025

[37] Tomar, V., Bhattacharjee, G., Kamaluddin, Rajakumar, S., Srivastava, K., Puri, S.K. Synthesis of new chalcone derivatives containing acridinyl moiety with potential antimalarial activity. Eur. J. Med. Chem.45 (2010) 745–751. https://doi.org/10.1016/j.ejmech.2009.11.022

[38] Abbass, F.A., Zimam, E.H. Synthesis, characterization and study biological activity of some new pyrimidine and 1,2,3,4-tetrazole derivatives based on sulfadiazine. Int. J. ChemTech Res. 9 (2018) 206–217.

[39] Nazir, S., Ansari, F.L., Hussain, T., Mazhar, K., Muazzam, A.G., Qasmi, Z.-H., Makhmoor, T., Noureen, H., Mirza, B. Brine shrimp lethality assay 'an effective prescreen': Microwave-assisted synthesis, BSL toxicity and 3DQSAR studies-based designing, docking and antitumor evaluation of potent chalcones. Pharm. Biol. 51 (2013) 1091–1103. https://doi.org/10.3109/13880209.2013.777930

[40] Simons, L.J., Caprathe, B.W., Callahan, M., Graham, J.M., Kimura, T., Lai, Y., LeVine, H., Lipinski, W., Sakkab, A.T., Tasaki, Y., Walker, L.C., Yasunaga, T., Ye, Y., Zhuang, N., Augelli-Szafran, C.E. The synthesis and structure–activity relationship of substituted *N*-phenyl anthranilicacid analogs as amyloid aggregation inhibitors. Bioorg. Med.Chem.Lett. 19 (2009) 654–657. https://doi.org/10.1016/j.bmcl.2008.12.049

[41] Jorge, S.D., Palace-Berl, F., Masunari, A., Cechinel, C.A., Ishii, M., Pasqualoto, K.F.M., Tavares, L.C. Novel benzofuroxan derivatives against multidrug-resistant *Staphylococcus aureus* strains: Design using Topliss' decision tree, synthesis and biological assay. Bioorg. Med. Chem. 19 (2011) 5031–5038. https://doi.org/10.1016/j.bmc.2011.06.034

[42] Xu, M., Wu, P., Shen, F., Ji, J., Rakesh, K.P. Chalcone derivatives and their antibacterial activities: Current development. Bioorg. Chem. 91 (2019) 103–133. https://doi.org/10.1016/j.bioorg.2019.103133

[43] Chen, Z.-H., Zheng, C.-J., Sun, L.-P., Piao, H.-R. Synthesis of new chalcone derivatives containing a rhodanine-3-acetic acid moiety with potential anti-bacterial activity. Eur.J.Med.Chem. 45 (2010) 5739–5743. https://doi.org/10.1016/j.ejmech.2010.09.031

[44] Marinho, D.S., Huf, G., Ferreira, B.L., Castro, H., Rodrigues, C.R., Sousa, V.P. de, Cabral, L.M. The study of vancomycin use and its adverse reactions associated to patients of a Brazilian university hospital. BMC Res. Notes 4 (2011) 236. https://doi.org/10.1186/1756-0500-4-236

[45] Aminov, R.I. A Brief History of the Antibiotic Era: Lessons Learned and Challenges for the Future. Front. Microbiol. 1 (2010). https://doi.org/10.3389/fmicb.2010.00134

[46] Brooks, B.D., Brooks, A.E. Therapeutic strategies to combat antibiotic resistance. Adv. Drug Deliv. Rev. 78 (2014) 14–27. https://doi.org/10.1016/j.addr.2014.10.027

[47] Tran, T.-D., Do, T.-H., Tran, N.-C., Ngo, T.-D., Huynh, T.-N.-P., Tran, C.-D., Thai, K.-M. Synthesis and anti-Methicillin resistant *Staphylococcus aureus* activity of substituted chalcones alone and in combination with non-beta-lactam antibiotics. Bioorg. Med.Chem.Lett. 22 (2012) 4555–4560. https://doi.org/10.1016/j.bmcl.2012.05.112

[48] Vásquez-Martínez, Y., Osorio, M., San Martín, D., Carvajal, M., Vergara, A., Sanchez, E., Raimondi, M., Zacchino, S., Mascayano, C., Torrent, C., Cabezas, F., Mejias, S., Montoya, M., Cortez-San Martín, M. Antimicrobial, Anti-Inflammatory and Antioxidant Activities of Polyoxygenated Chalcones. J. Braz. Chem. Soc. 30 (2019) https://doi.org/10.21577/0103-5053.20180177

[49] Wertheim, H.F., Melles, D.C., Vos, M.C., van Leeuwen, W., van Belkum, A., Verbrugh, H.A., Nouwen, J.L. The role of nasal carriage in *Staphylococcus aureus* infections. Lancet. Infect. Dis. 5 (2005) 751–762. https://doi.org/10.1016/S1473-3099(05)70295-4

[50] Weidenmaier, C., Kokai-Kun, J.F., Kristian, S.A., Chanturiya, T., Kalbacher, H., Gross, M., Nicholson, G., Neumeister, B., Mond, J.J., Peschel, A. Role of teichoicacids in *Staphylococcus aureus* nasal colonization, a major riskfactor in nosocomial infections. Nat. Med. 10 (2004) 243–245. https://doi.org/10.1038/nm991

[51] Burian, M., RautenFrontberg, M., Kohler, T., Fritz, M., Krismer, B., Unger, C., Hoffmann, W.H., Peschel, A., Wolz, C., Goerke, C. Temporal Expression of Adhesion Factors and Activity of Global Regulators during establishment of *Staphylococcus aureus* Nasal Colonization. J. Infect Dis. 201 (2010) 1414–1421. https://doi.org/10.1086/651619

[52] Mazmanian, S.K. *Staphylococcus aureus* Sortase, an Enzyme that Anchors Surface Proteins to the Cell Wall. Science. 285 (1999) 760–763. https://doi.org/10.1126/science.285.5428.760

[53] Clarke, S.R., Foster, S.J. Surface Adhesins of *Staphylococcus aureus*, in: Advances in Microbial Physiology. Adv. Microb. Physiol. 51 (2006) 187–224. https://doi.org/10.1016/S0065-2911(06)51004-5

[54] Chavakis, T., Wiechmann, K., Preissner, K.T., Herrmann, M. *Staphylococcus aureus* interactions with the endothelium: the role of bacterial "Secretable Expanded Repertoire Adhesive Molecules" (SERAM) in disturbing host defense systems. ThrombHaemost. 94 (2005) 278–285. https://doi.org/10.1160/TH05-05-0306

[55] Spaan, A.N., Surewaard, B.G.J., Nijland, R., van Strijp, J.A.G. Neutrophils Versus *Staphylococcus aureus*: A Biological Tugof War. Annu. Rev. Microbiol. 67 (2013) 629–650. https://doi.org/10.1146/annurev-micro-092412-155746

[56] Resch, A., Rosenstein, R., Nerz, C., Götz, F. Differential Gene Expression Profiling of *Staphylococcus aureus* Cultivated under Biofilm and Planktonic Conditions. Appl. Environ. Microbiol. 71 (2005) 2663–2676. https://doi.org/10.1128/AEM.71.5.2663-2676.2005

[57] Otto, M. Staphylococcal Biofilms. Microbiol. Spectr. 6 (2018). https://doi.org/10.1128/microbiolspec.GPP3-0023-2018

[58] Hansson, I.B. Microbiological Meat Quality in High- and Low-Capacity Slaughter houses in Sweden. J. Food Prot. 64 (2001) 820–825. https://doi.org/10.4315/0362-028X-64.6.820

[59] Alonzo, F., Torres, V.J., 2013. A Lesson in Survival: *S. aureus* versus the Skin. Cell Host & Microbe. 13 (2013) 3–5. https://doi.org/10.1016/j.chom.2013.01.001

[60] Whitchurch, C.B. Extracellular DNA Required for Bacterial Biofilm Formation. Science 295 (2002) 1487–1487. https://doi.org/10.1126/science.295.5559.1487

[61] de la Fuente-Núñez, C., Reffuveille, F., Fernández, L., Hancock, R.E. Bacterial biofilm development as a multicellular adaptation: antibiotic resistance and new therapeutic strategies. Curr. Opin. Microbiol. 16 (2013) 580–589. https://doi.org/10.1016/j.mib.2013.06.013

[62] Scherr, T.D., Heim, C.E., Morrison, J.M., Kielian, T. Hiding in Plain Sight: Interplay between Staphylococcal Biofilms and Host Immunity. Front. Immunol. 5 (2014). https://doi.org/10.3389/fimmu.2014.00037

[63] O'Toole, G., Kaplan, H.B., Kolter, R. Biofilm Formation as Microbial Development. Annu. Rev. Microbiol. 54 (2000) 49–79. https://doi.org/10.1146/annurev.micro.54.1.49

[64] Boles, B.R., Horswill, A.R. Staphylococcal biofilm disassembly. Trends in Microbiol. 19 (2011) 449–455. https://doi.org/10.1016/j.tim.2011.06.004

[65] Otto, M. Physical stress and bacterial colonization. FEMS Microbiol. 38 (2014) 1250–1270. https://doi.org/10.1111/1574-6976.12088

[66] Bassetti, M., Peghin, M., Trecarichi, E.M., Carnelutti, A., Righi, E., Del Giacomo, P., Ansaldi, F., Trucchi, C., Alicino, C., Cauda, R., Sartor, A., Spanu, T., Scarparo, C., Tumbarello, M. Characteristics of *Staphylococcus aureus* Bacteremia and Predictors of Early and Late Mortality. PLoS ONE 12 (2017) e0170236. https://doi.org/10.1371/journal.pone.0170236

[67] Singh, P., Anand, A., Kumar, V. Recent developments in biological activities of chalcones: a mini review. Eur.J.Med.Chem. 85 (2014) 758–777. https://doi.org/10.1016/j.ejmech.2014.08.033

[68] Mahapatra, D.K., Bharti, S.K., Asati, V. Chalcone scaffolds as anti-infective agents: structural and molecular target perspectives. Eur. J. Med.Chem. 101 (2015) 496–524. https://doi.org/10.1016/j.ejmech.2015.06.052

[69] Bozic, D.D., Milenkovic, M., Ivkovic, B., Cirkovic, I. Newly-synthesized chalcones-inhibition of adherence and biofilm formation of methicillin-resistant *Staphylococcus aureus*. Braz. J. Microbiol. 45 (2014) 263–270. https://doi.org/10.1590/S1517-83822014000100038

[70] Allegra, E., Titball, R.W., Carter, J., Champion, O.L. *Galleria mellonella* larvae allow the discrimination of toxic and non-toxic chemicals. Chemosphere. 198 (2018) 469–472. https://doi.org/10.1016/j.chemosphere.2018.01.175

[71] Cutuli, M.A., Petronio, G., Vergalito, F., Magnifico, I., Pietrangelo, L., Venditti, N., Di Marco, R. *Galleria mellonella* as a consolidated *in vivo* model hosts: New developments in

antibacterial strategies and novel drug testing. Virulence 10 (2019) 527–541. https://doi.org/10.1080/21505594.2019.1621649

[72] Wojda, I. Immunity of the greater wax moth *Galleria mellonella*: *Galleria mellonella* immunity. InsectS 24 (2017) 342–357. https://doi.org/10.1111/1744-7917.12325

[73] World Health Organization, WHO publishes list of bacteria for which new antibiotics are urgently needed. https://www.who.int/news/item/27-02-2017-who-publishes-list-of-bacteria-for-which-new-antibiotics-are-urgently-needed, 2017 (accessed 14 January 2021).

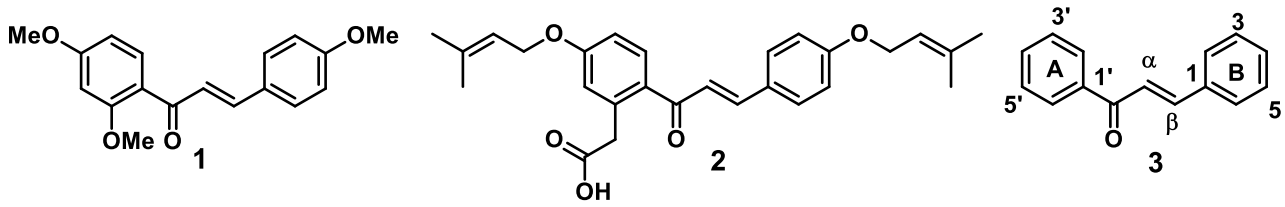

Figure 1. Structure of chalcone drugs (**1** and **2**) and chalcone with unsubstituted rings A and B (**3**)

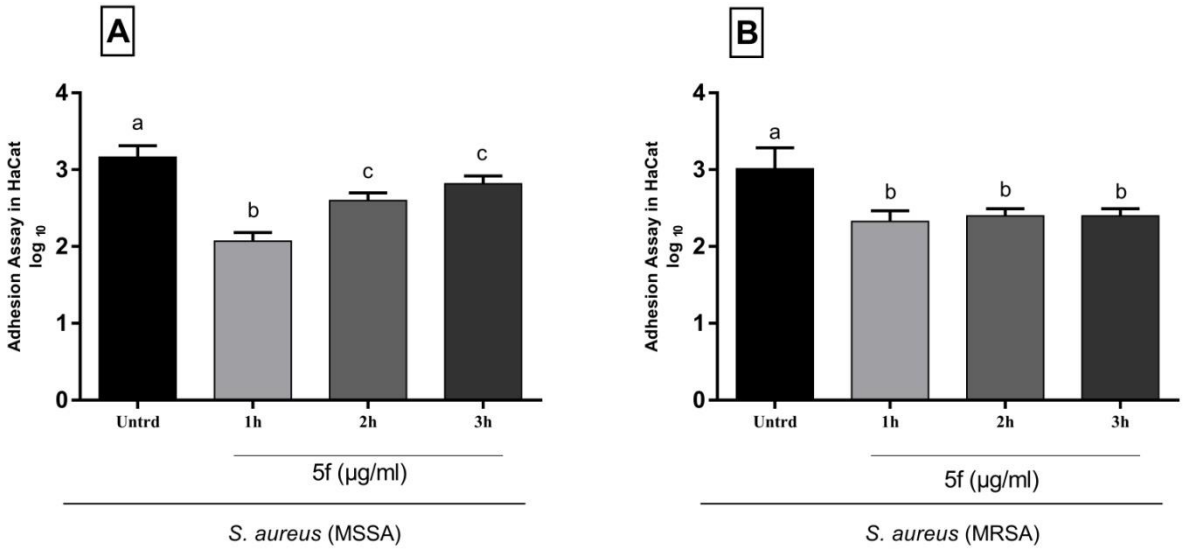

Figure 2. Anti-adhesion activity of **5f** on MSSA and MRSA adhesion to human HaCat. Different letters above the bar denote statistical difference when compared to each other. Data compared to vehicle where $P < 0.05$ - One-way ANOVA with Tukey Post test.

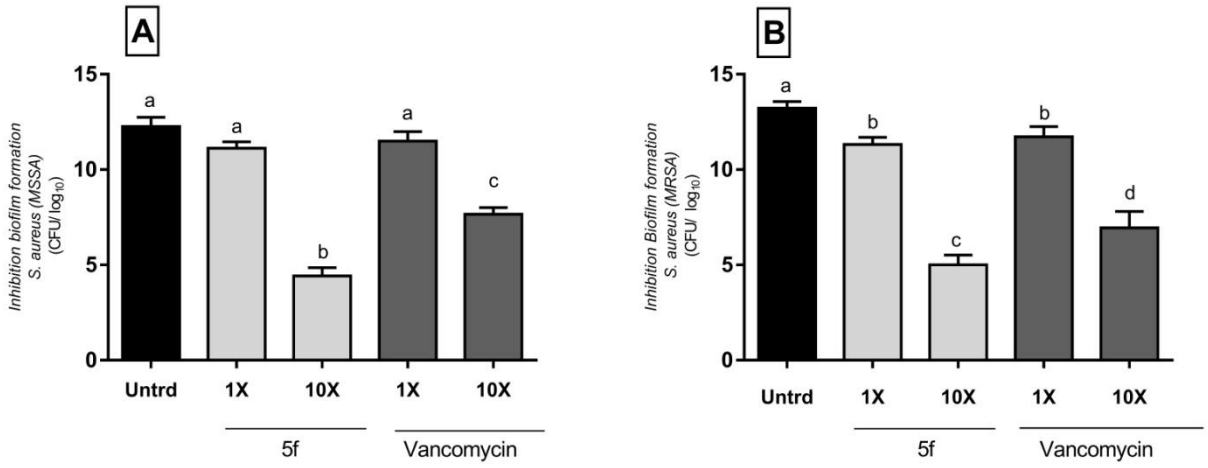

Figure 3. Effectof **5f** on MSSA and MRSA biofilm formation. Different letters above the bar denote statistical difference when compared to each other. Data compared to vehicle where $P < 0.05$ - One-way ANOVA with Tukey Post test.

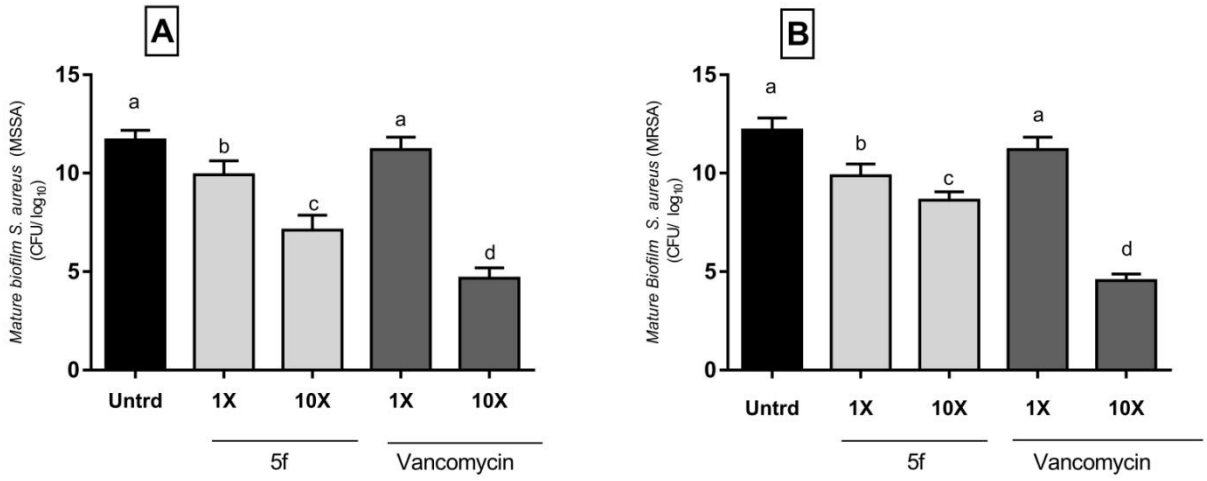

Figure 4. Effects of **5f** on MSSA and MRSA preformed biofilms. Different letters above the bar denote statistical difference when compared to each other. Data compared to vehicle where $P < 0.05$ - One-way ANOVA with Tukey Post test.

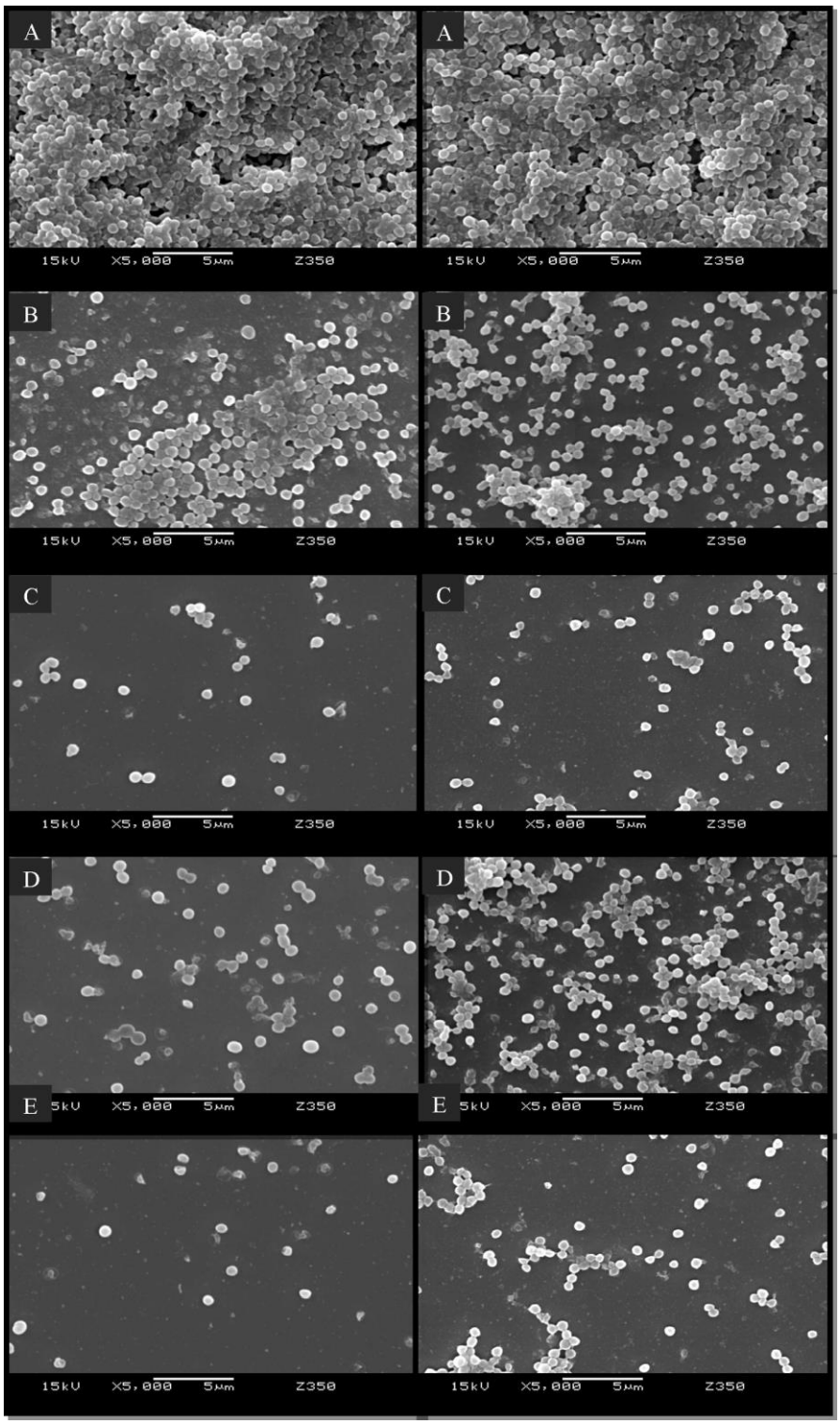

Figure 5. SEM photomicrographs (5,000 ×) showing MSSA biofilm (first column) and MRSA biofilm (second column) architecture biofilms **(A)** untreated; **(B)** biofilm treated with **5f** at MIC; **(C)** biofilm treated with **5f** at 10 × MIC; **(D)** biofilm treated with vancomycin at MIC; **(E)** biofilm treated with vancomycin at 10 × MIC. Bars: 5 μm.

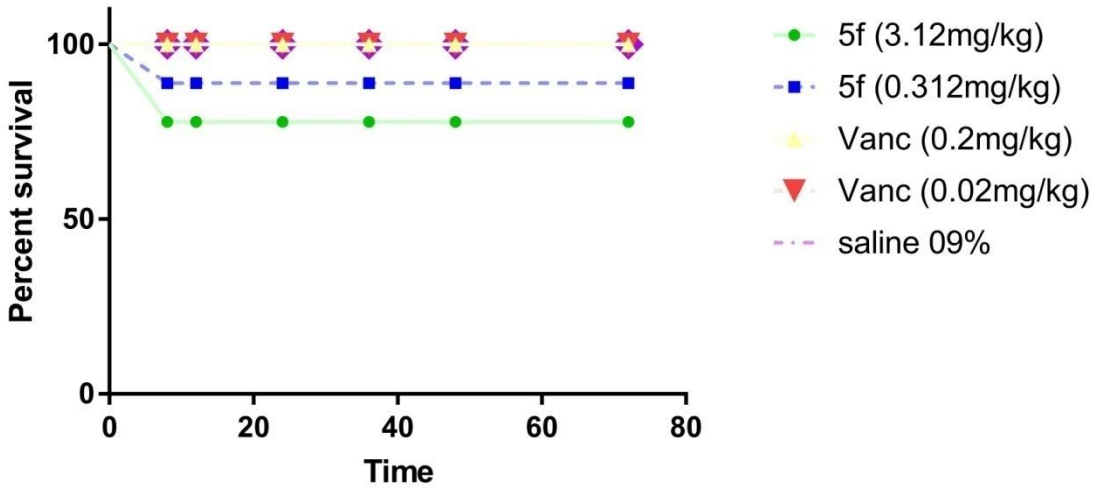

Figure 6. Percent survival over time of *G. mellonella*larvae injected with chalcone **5f** and vancomycin at respective MIC and 10 × MIC values ($P > 0.05$, log-rank test).

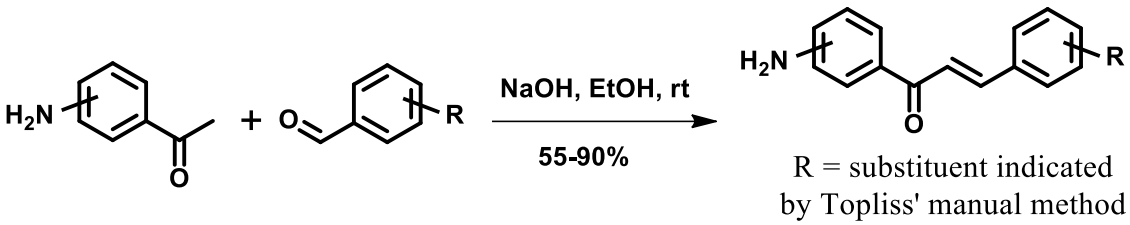

Scheme 1. Synthesis of chalcones

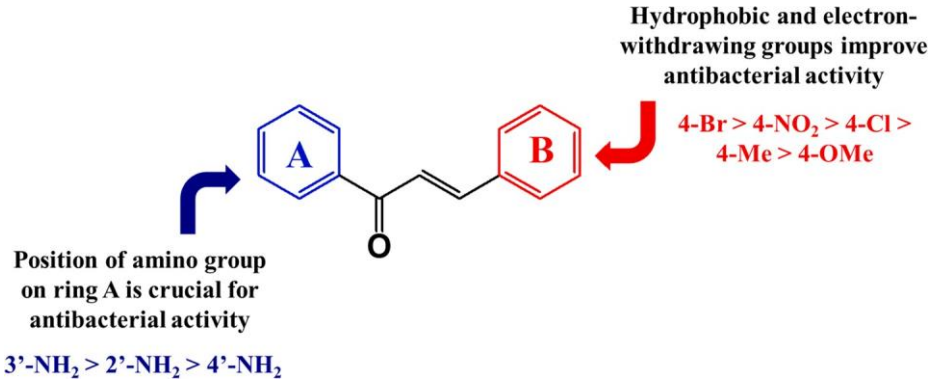

Scheme 2. SAR data assessed in this work, usign amino groups and substituents recommended by Topliss' manual method

Table 1. Antibacterial activity of chalcones against MSSA and MRSA expressed as MIC and MBC values in μg/mL

		MIC/MBC μg mL^{-1}	
Cpd.	R	MSSA	MRSA
4a	H	31.2/31.2	31.2/62.5
4b	4-Cl	15.6/31.2	7.8/15.6
4c	3,4-Cl_2	*	*
4d	4-CH_3	*	*
4e	4-OCH_3	62.5/ > 62.5	62.5/ > 62.5
5a	H	62.5/ > 62.5	62.5/> 62.5
5b	4-Cl	7.8/15.6	15.6/31.2
5c	3,4-Cl_2	1.9/7.8	15.6/31.2
5d	4-CH_3	31.2/31.2	*
5e	4-OCH_3	62.5/ > 62.5	*
5f	4-Br	1.9/3.9	7.8/7.8
5g	4-NO_2	3.9/7.8	7.8/31.2
6a	H	*	*
6b	4-Cl	*	*
6c	3,4-Cl_2	*	*
6d	4-CH_3	*	*
6e	4-OCH_3	*	*
methicillin		0.5/nd	2.0/nd
vancomycin		1.0/nd	2.0/nd

Cpd = compound. *MIC and MBC values were higher than 62.5 μg mL^{-1}. nd = not determined

Table 2. Antibacterial effect of combination between **5f** and vancomycin or methicillin against MSSA and MRSA

***S. aureus* strains**	**Combination**	**MIC (μg mL^{-1})**				**FICI**	**Type of combination**
		Alone		**Combined**			
		5f	**d**	**5f**	**d**	**$FIC_{5f}+FIC_d$**	
MSSA	**5f**+vancomycin (d)	1.9	1.0	0.4	0.1	0.3	Synergistic
	5f+ methicillin (d)	1.9	0.5	0.9	0.1	0.7	Additive
MRSA	**5f**+ vancomycin (d)	7.8	2.0	0.9	0.2	0.2	Synergistic
	5f+ methicillin (d)	7.8	2.0	3.9	1.0	1.0	Additive

d = drug (vancomycin or methicillin).

SUPPLEMENTARY MATERIAL

Design, synthesis and antibacterial activity of chalcones against MSSA and MRSA planktonic cells and biofilms

Mayara A. R. Garcia[a], Reinaldo S. Theodoro[a], Janaína de C. O. Sardi[b], Mariana B. Santos[a], Gabriela M. Ayusso[c], Fernando R. Pavan[c], Alan R. Costa[d], Lucas M. Santa Cruz[d], Pedro L. Rosalen[b], Luis O. Regasini[a,*]

[a]*Department of Chemistry and Environmental Sciences, Institute of Biosciences, Humanities and Exact Sciences, São Paulo State University, São José do Rio Preto, SP, Brazil.*

[b]*Department of Physiological Sciences, Piracicaba Dental School, University of Campinas, Piracicaba, SP, Brazil.*

[c]*Department of Biological Sciences, School of Pharmaceutical Sciences, São Paulo State University, Araraquara, SP, Brazil*

[d]*Núcleo de Contaminantes Orgânicos, Instituto Adolfo Lutz, São Paulo, SP, Brazil*

*** Corresponding author.**

E-mail addresses: luis.regasini@unesp.br (LO Regasini)

Figure SM1. ^{1}H NMR spectrum of compound **4a** (DMSO-d_6; 600 MHz)

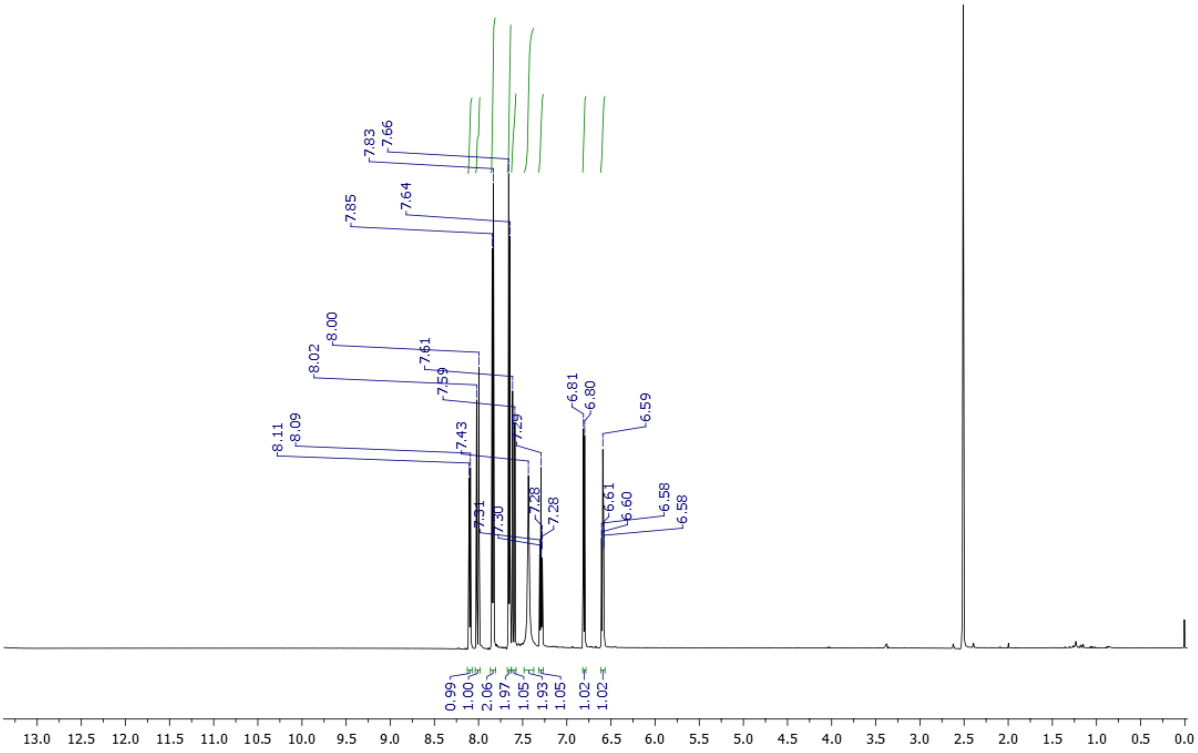

Figure SM2. ^{13}C NMR spectrum of compound **4a** (DMSO-d_6; 150 MHz)

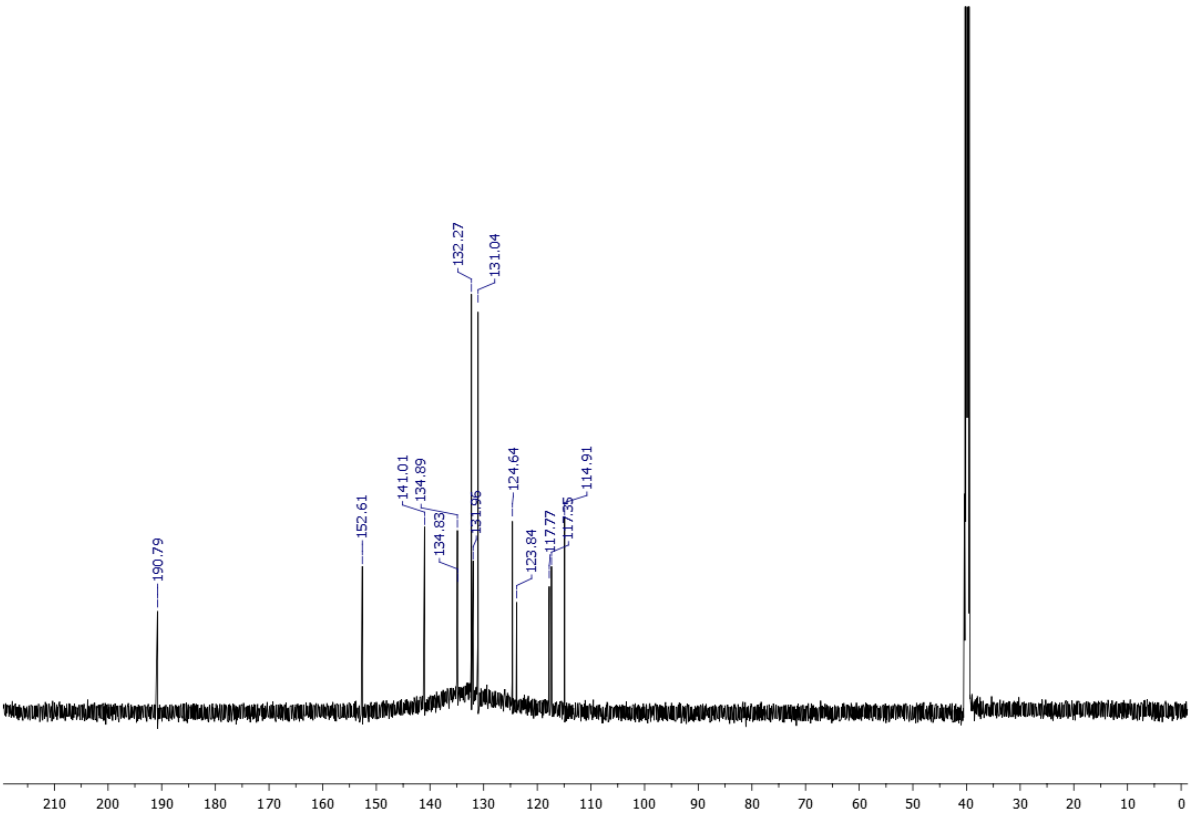

Figure SM3. Mass spectra (MS) of compound **4a**

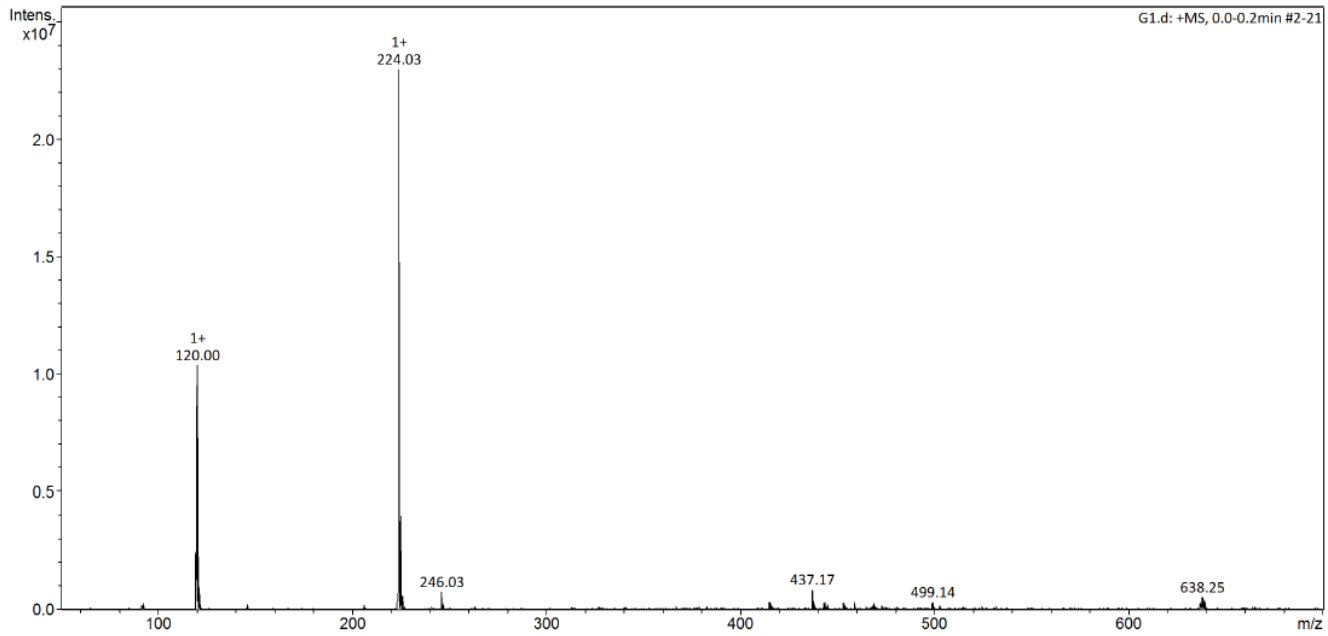

Figure SM4. UV-Vis spectra of compound **4a**

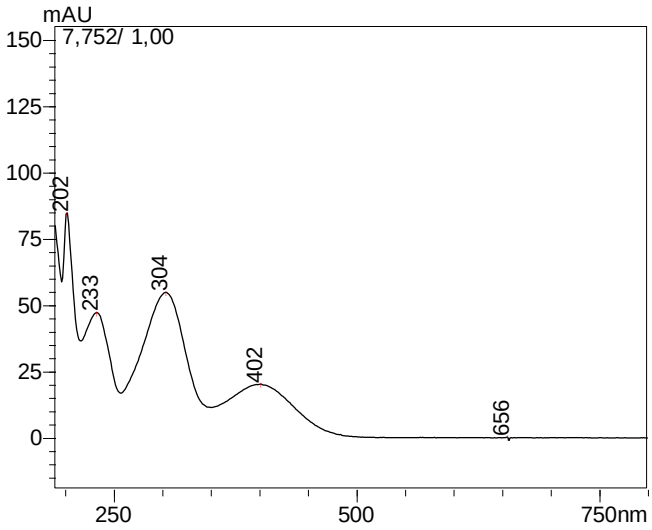

Figure SM5. HPLC cromatogram of compound **4a**

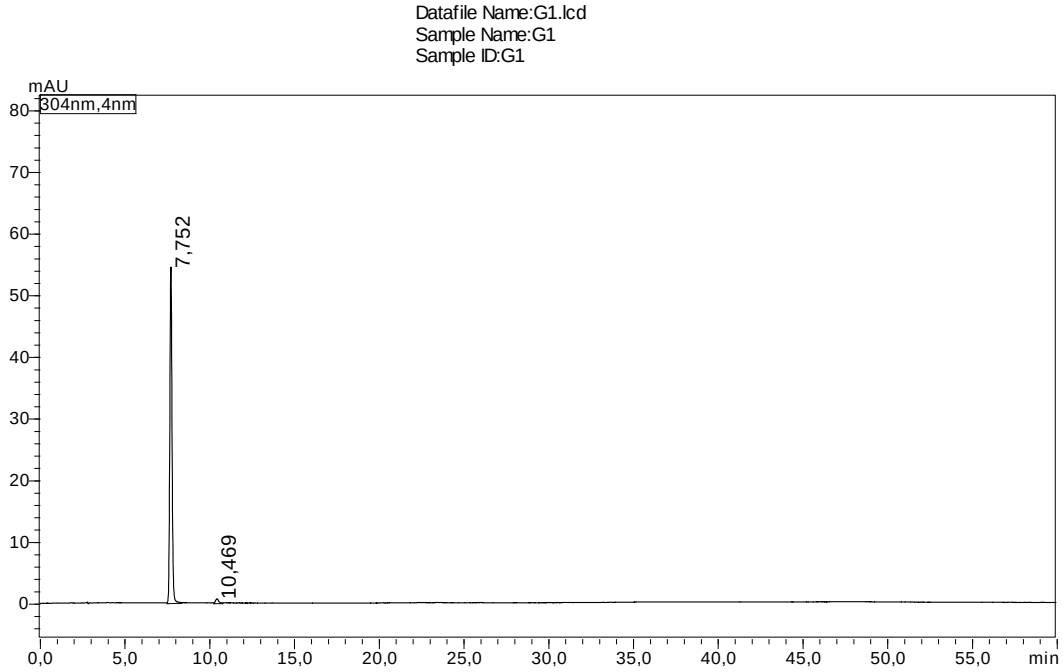

Figure SM6. ^{1}H NMR spectrum of compound **4b** (DMSO-d_6; 600 MHz)

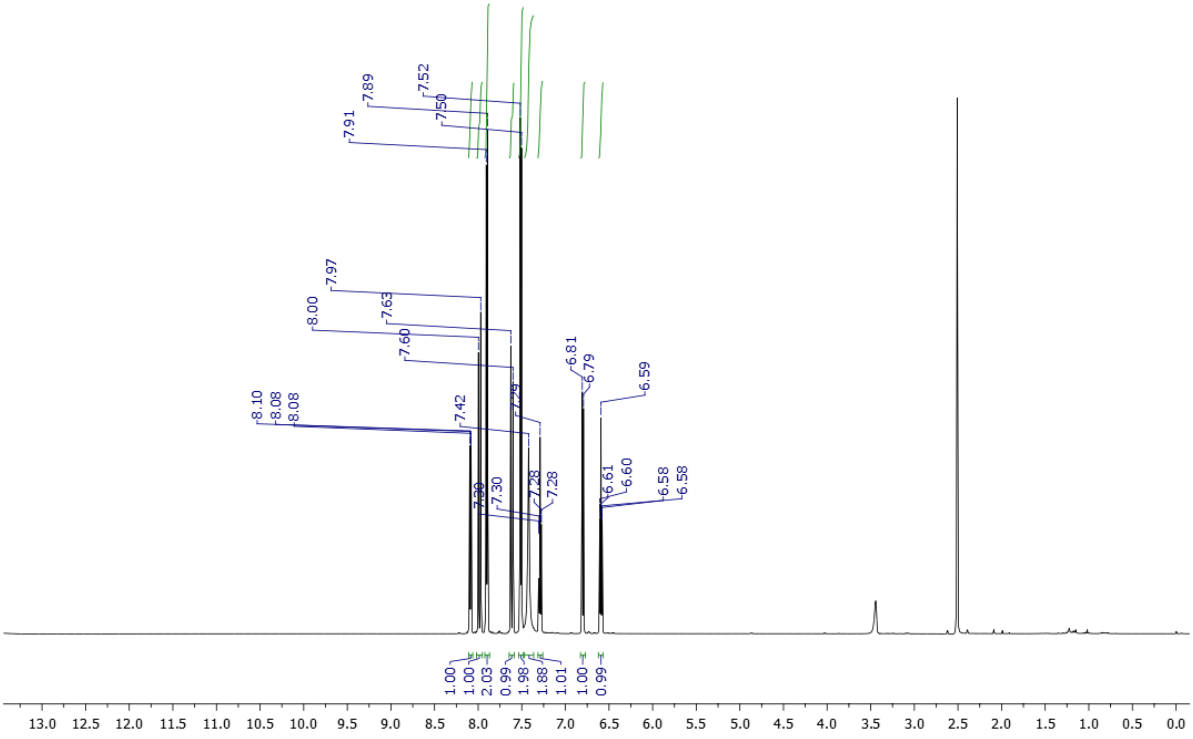

Figure SM 7. ^{13}C NMR spectrum of compound **4b** (DMSO-d_6; 150 MHz)

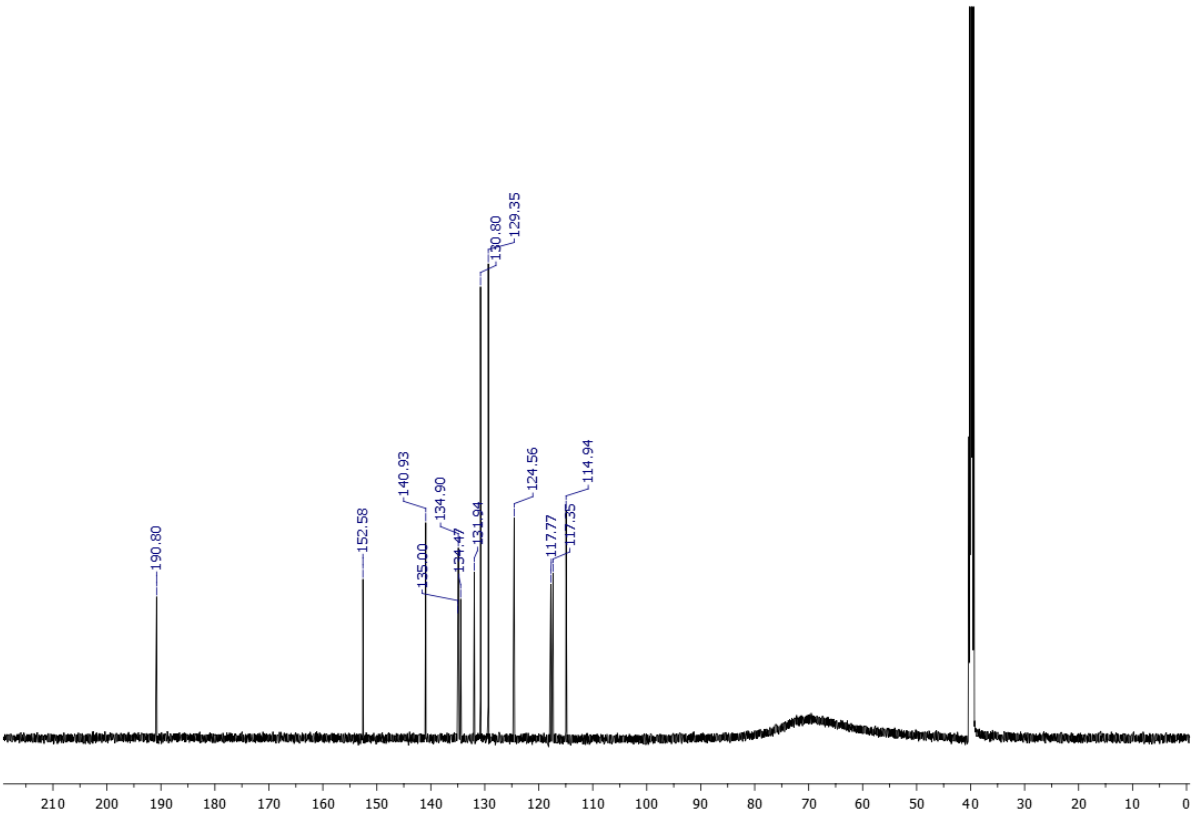

Figure SM8. Mass spectra (MS) of compound **4b**

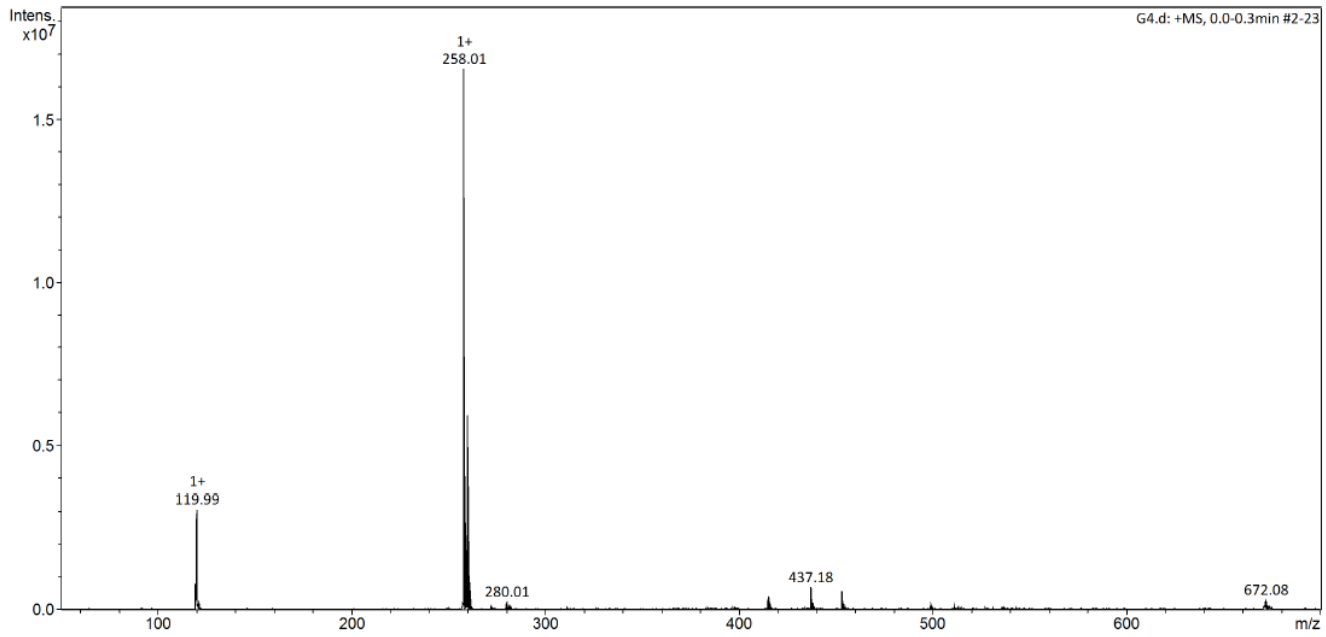

Figure SM9. UV-Vis spectra of compound **4b**

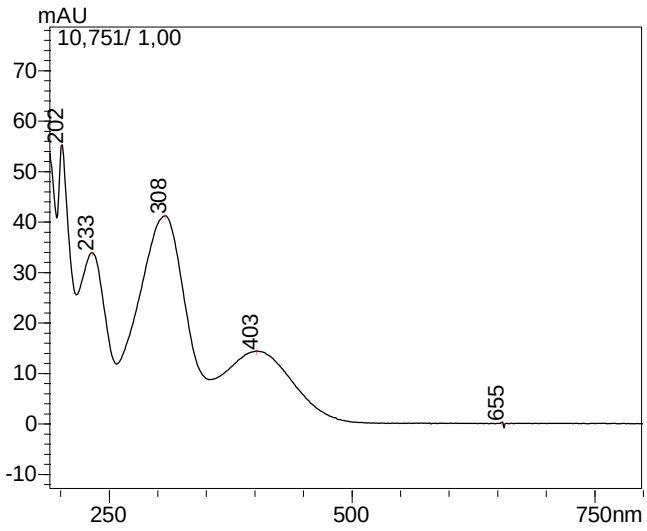

Figure SM 10. HPLC cromatogram of compound **4b**

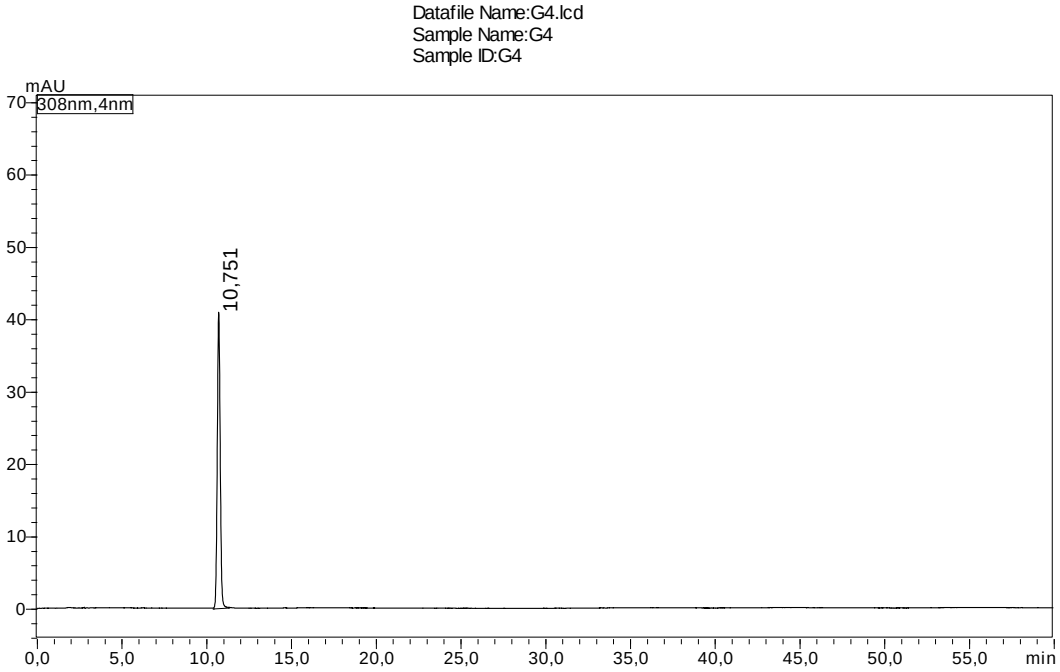

Figure SM11. ^{1}H NMR spectrum of compound **4c** (DMSO-d_6; 600 MHz)

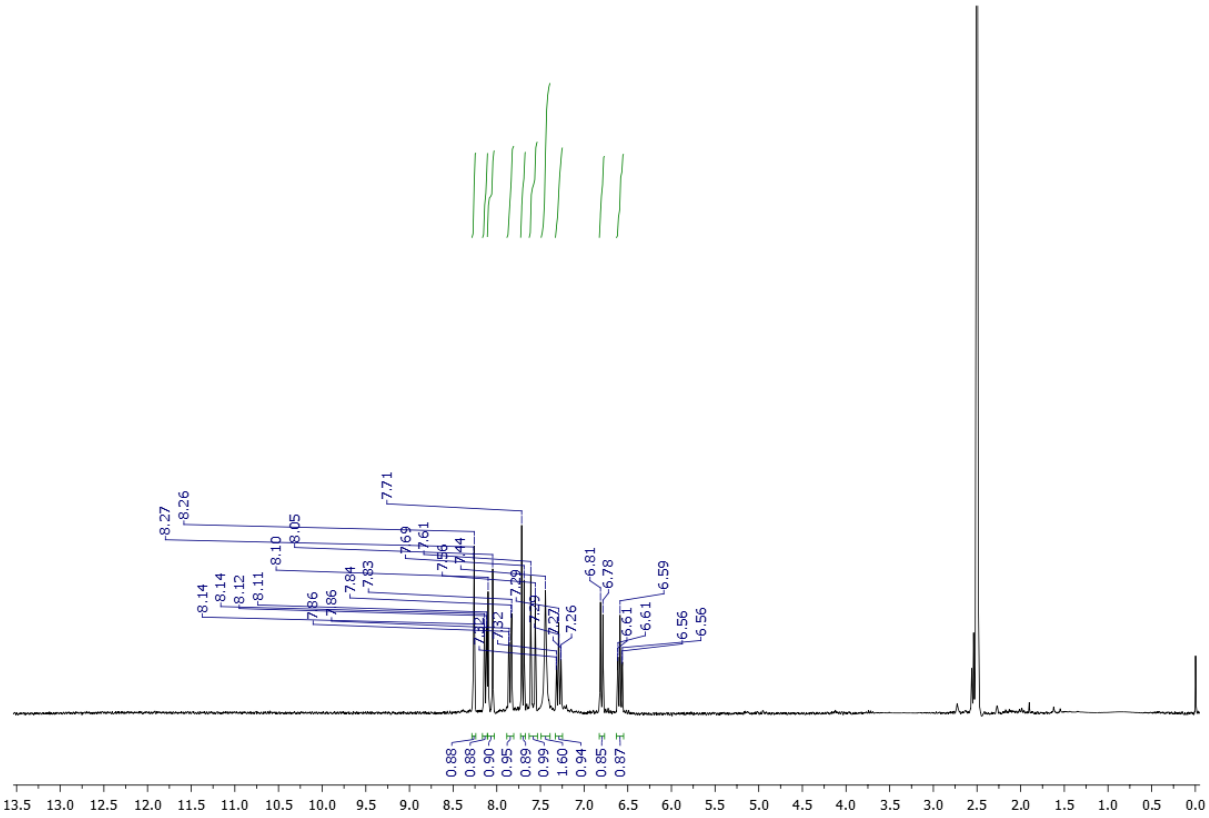

Figure SM12. ^{13}C NMR spectrum of compound **4c** (DMSO-d_6; 150 MHz)

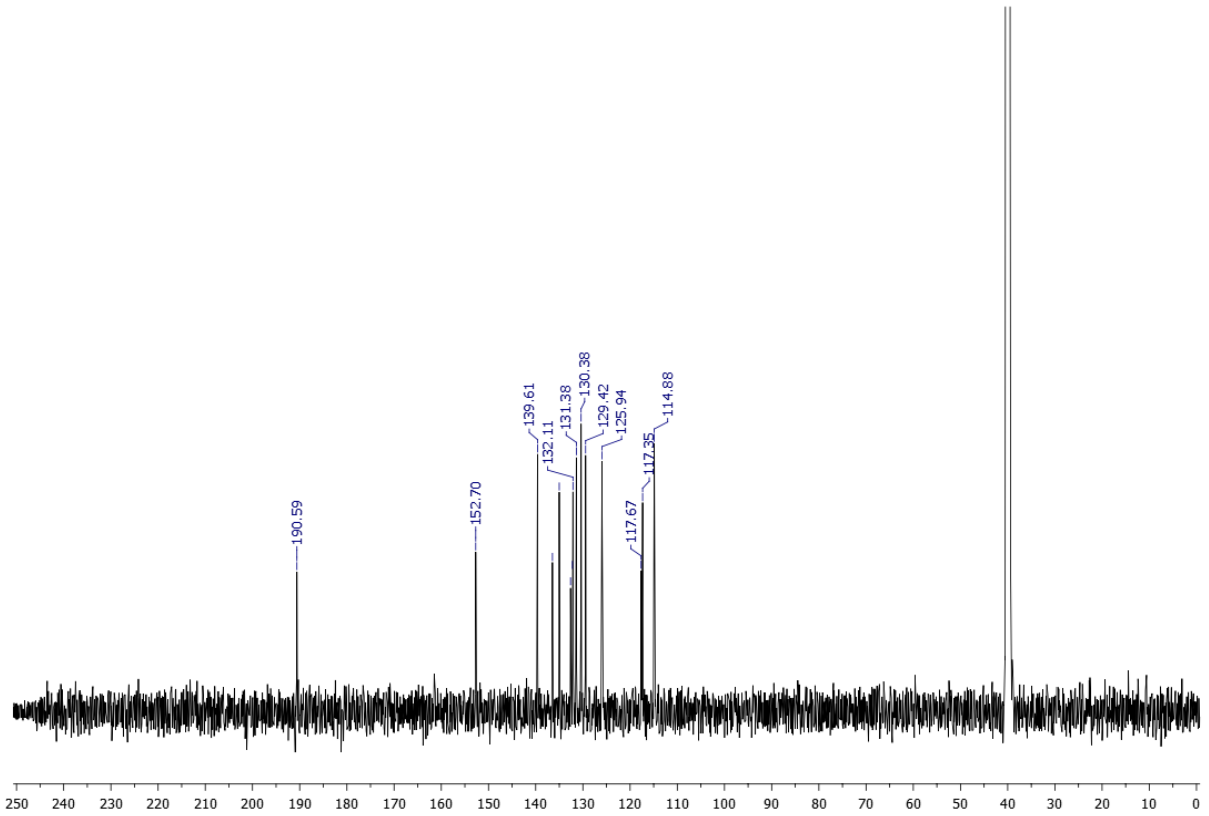

Figure SM13. Mass spectra (MS) of compound **4c**

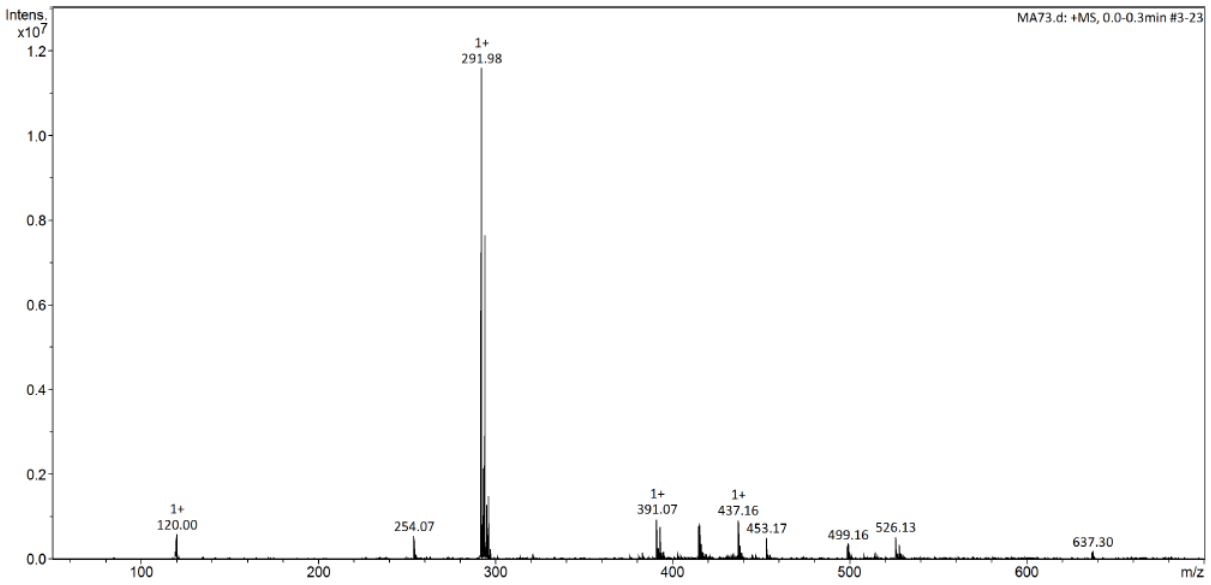

Figure SM14. UV-Vis spectra of compound **4c**

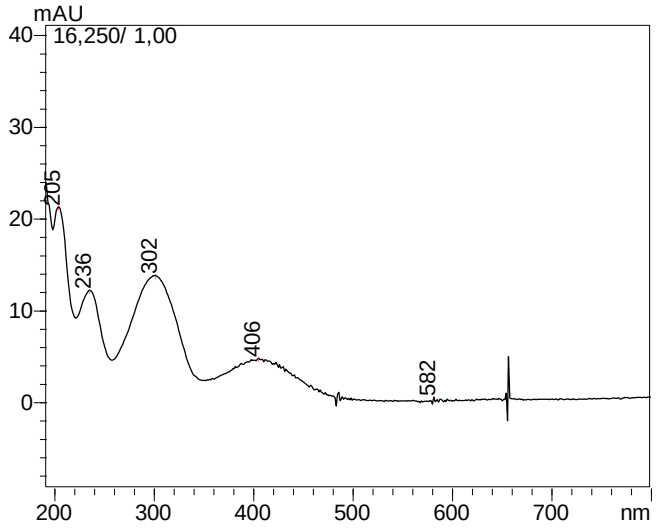

Figure SM15. HPLC cromatogram of compound **4c**

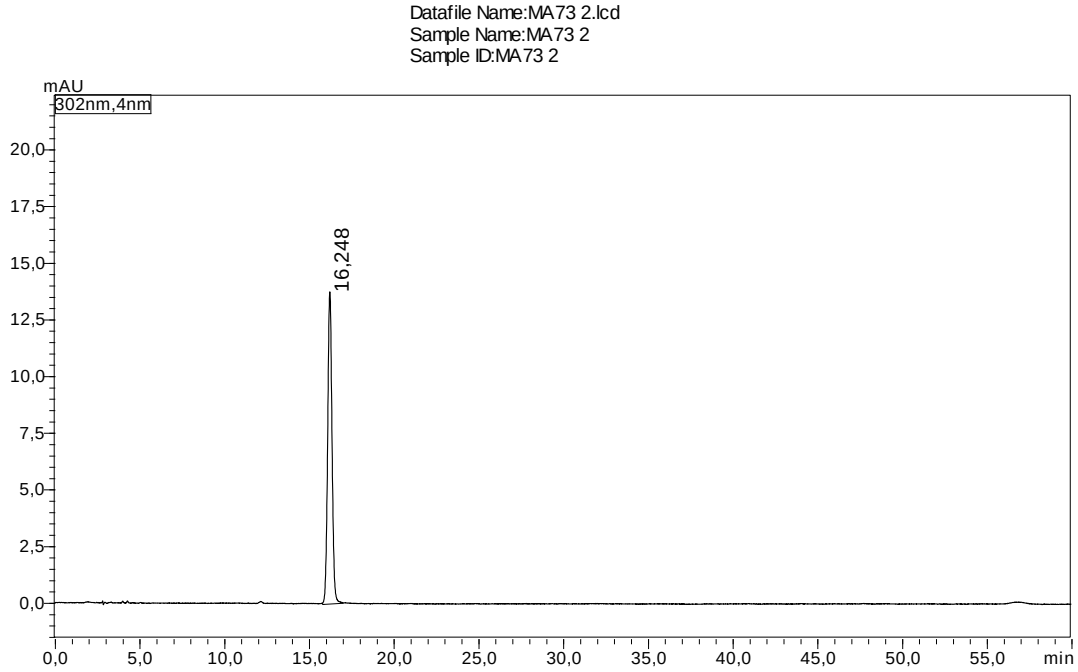

Figure SM16. ^{1}H NMR spectrum of compound **4d** (DMSO-d_6; 600 MHz)

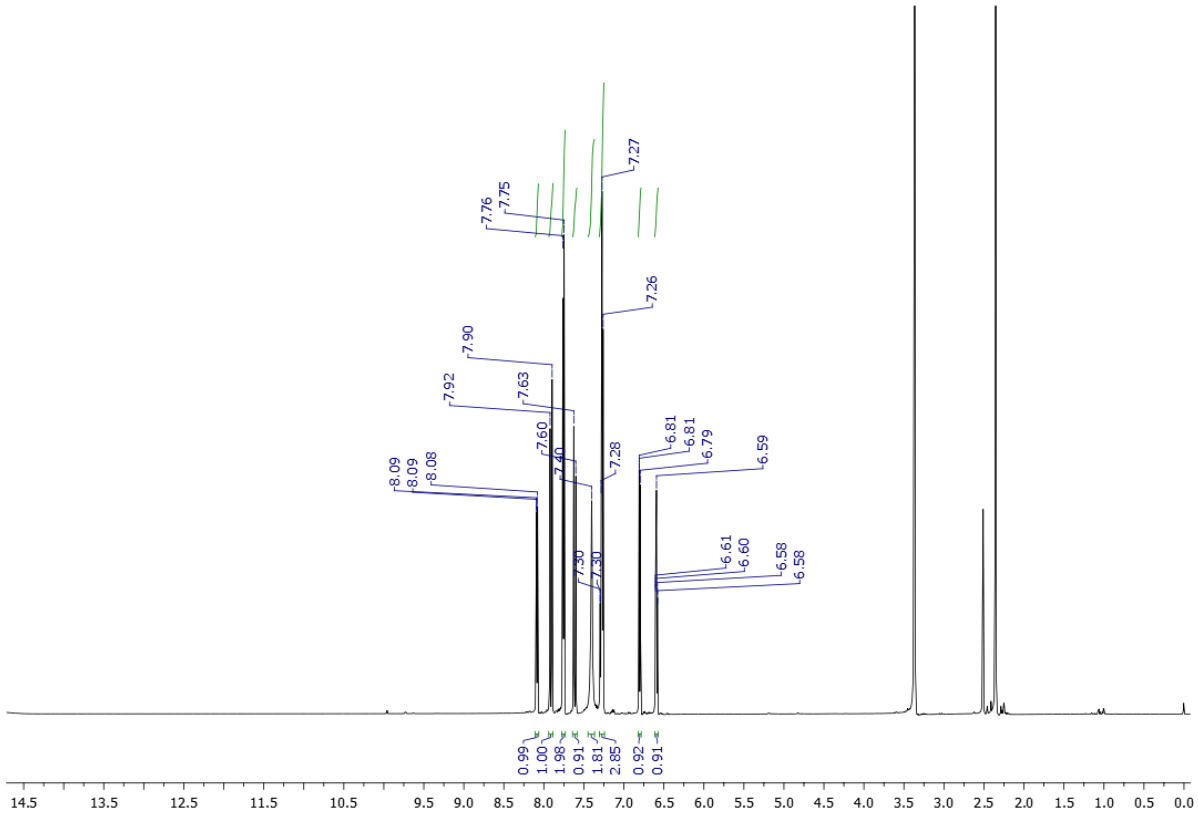

Figure SM17. ^{13}C NMR spectrum of compound **4d** (DMSO-d_6; 150 MHz)

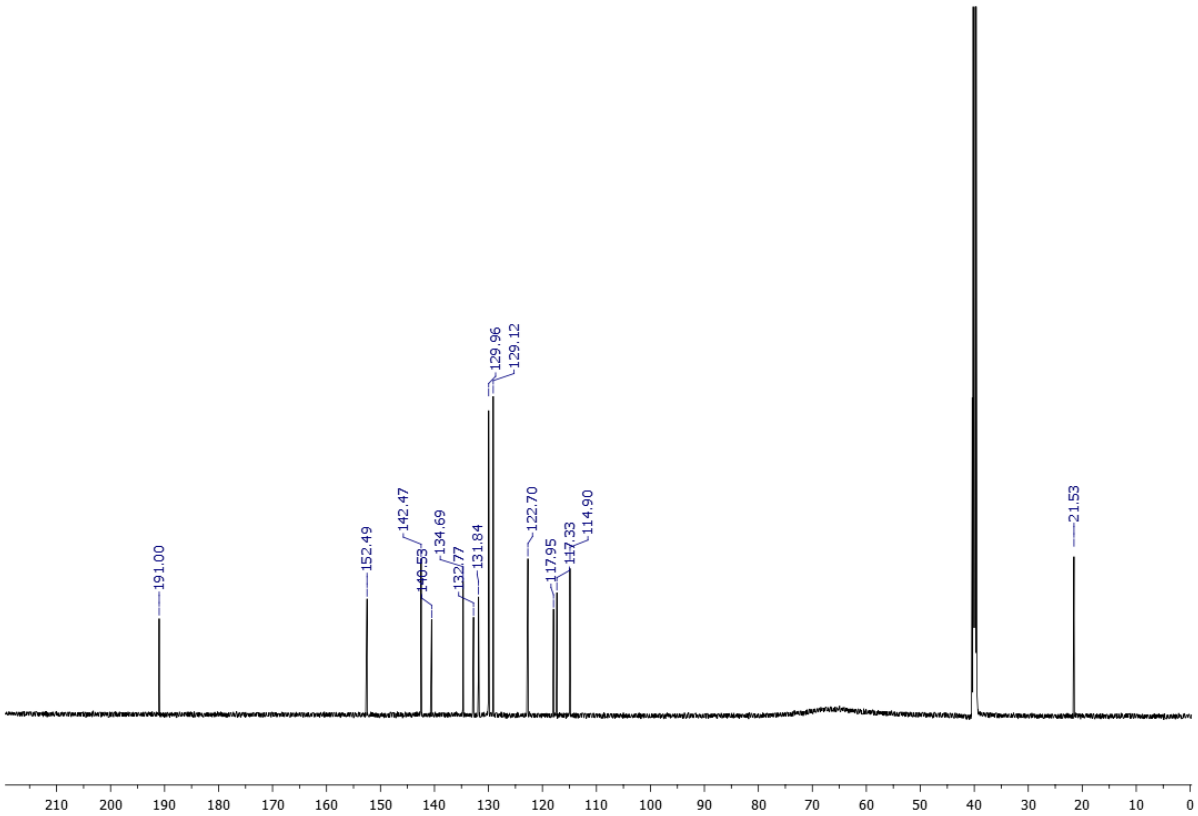

Figure SM18. Mass spectra (MS) of compound **4d**

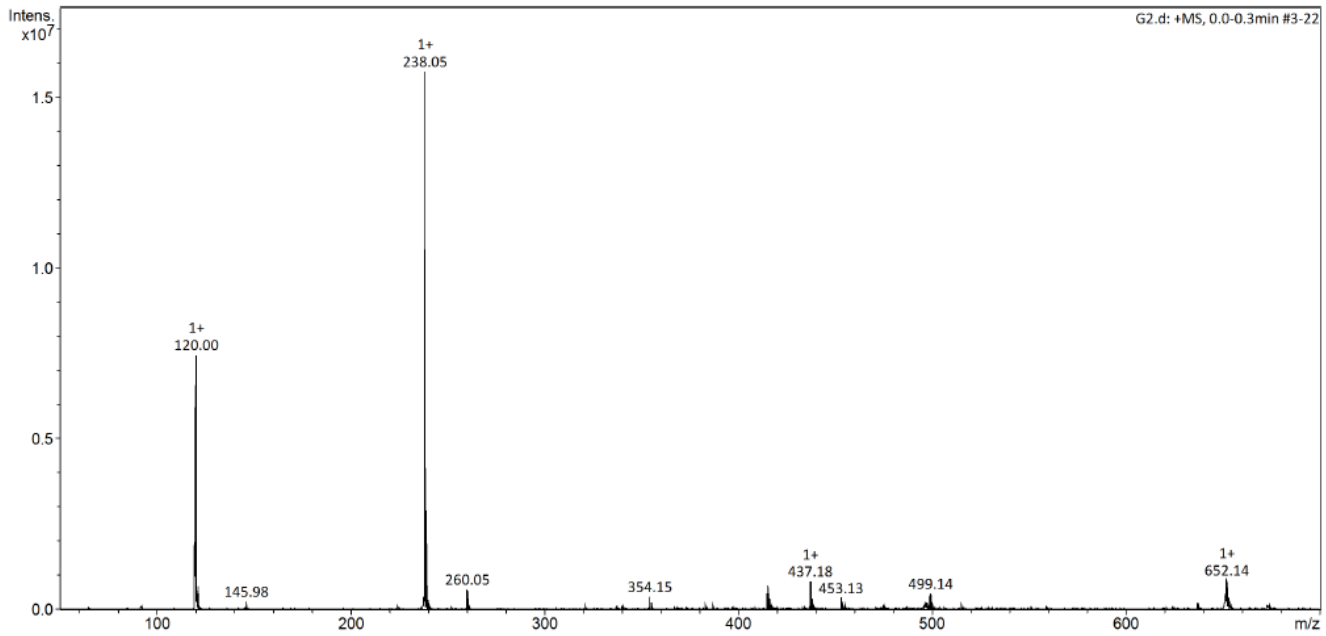

Figure SM19. UV-Vis spectra of compound **4d**

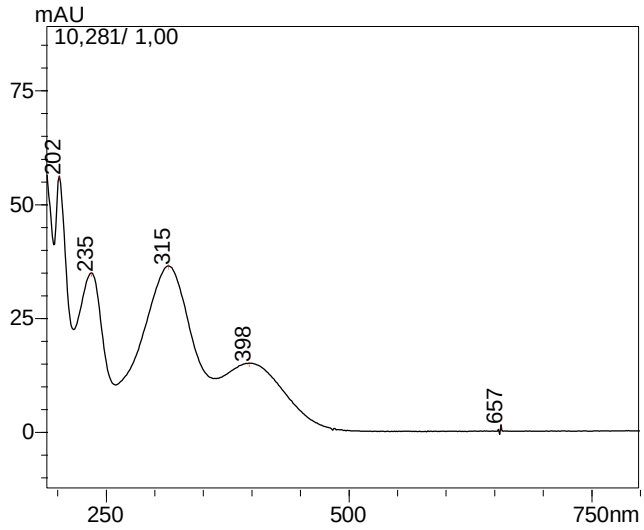

Figure SM20. HPLC cromatogram of compound **4d**

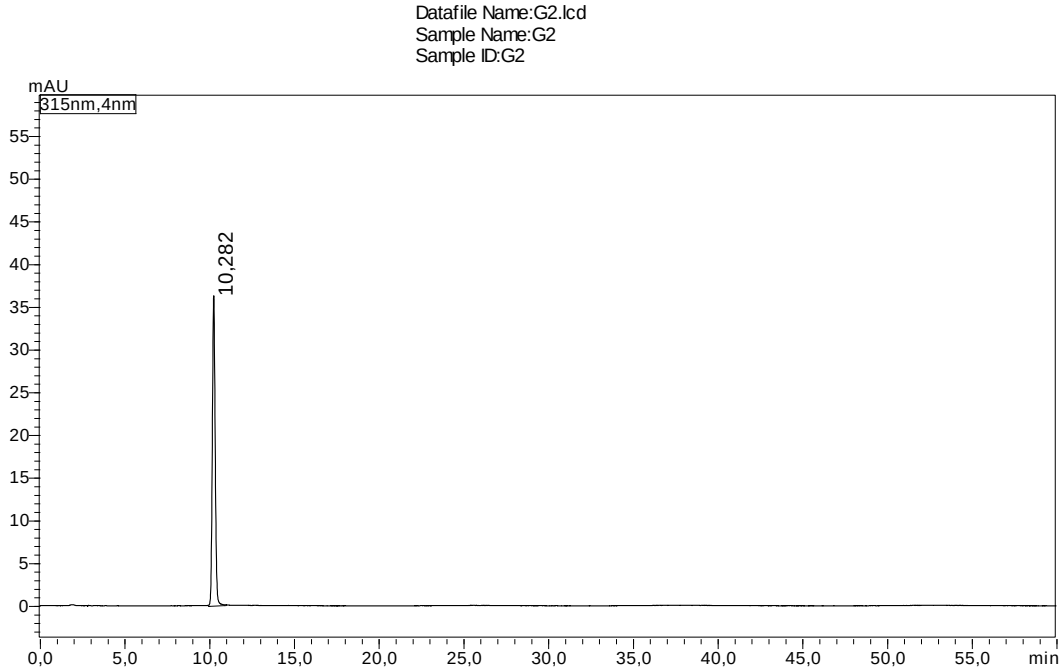

Figure SM21. ^{1}H NMR spectrum of compound **4e** (DMSO-d_6; 400 MHz)

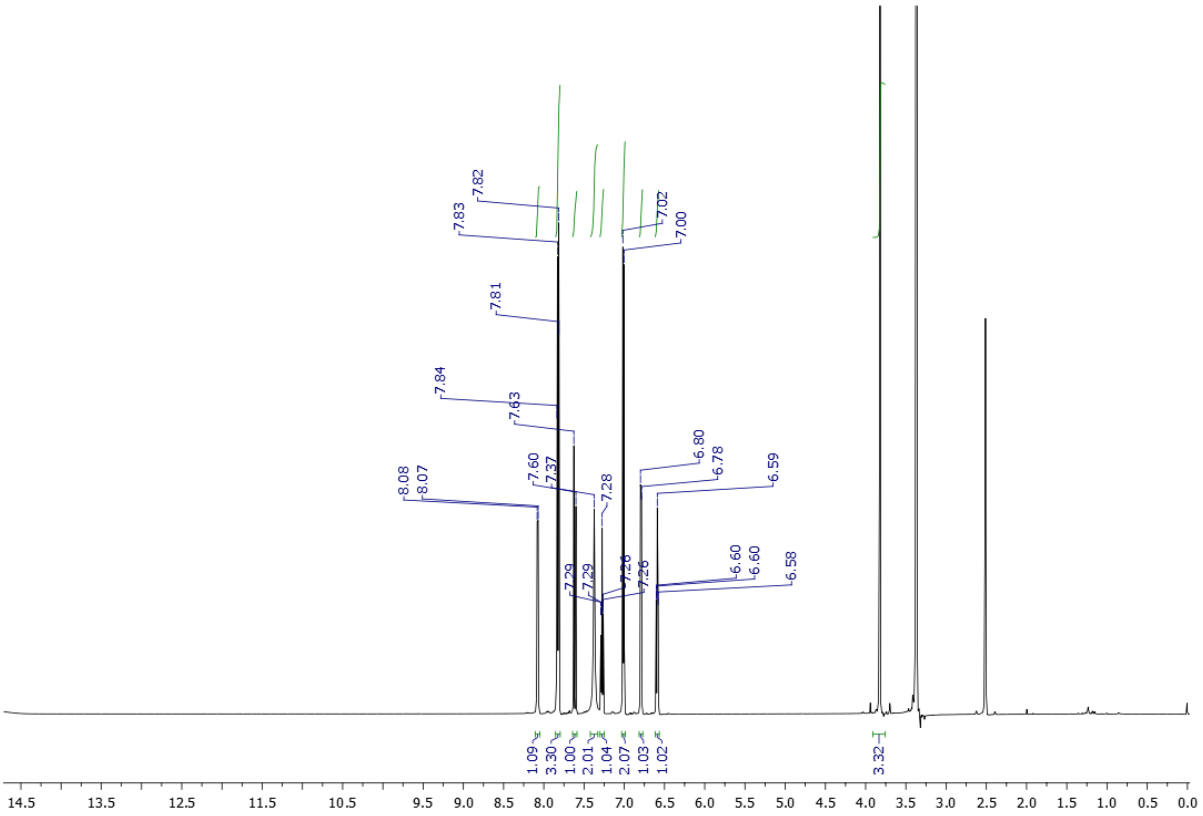

Figure SM22. ^{13}C NMR spectrum of compound **4e** (DMSO-d_6; 150 MHz)

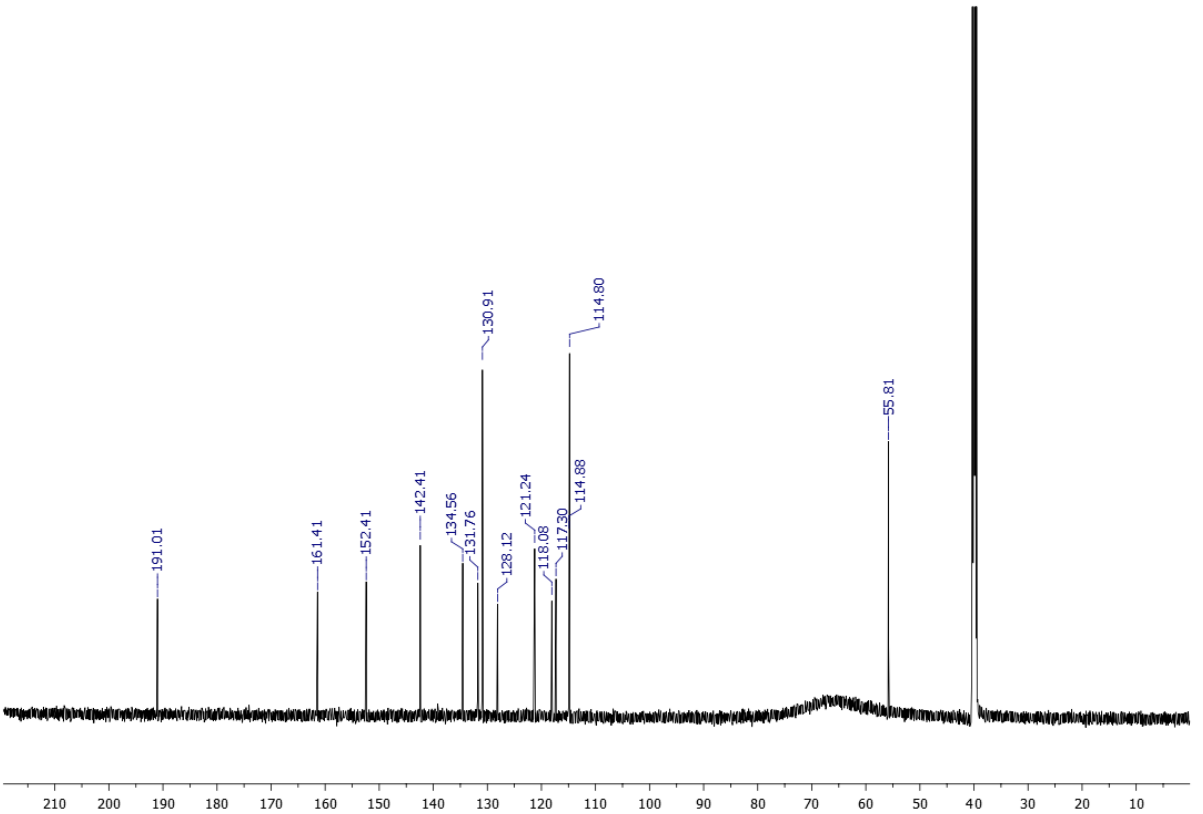

Figure SM23. Mass spectra (MS) of compound **4e**

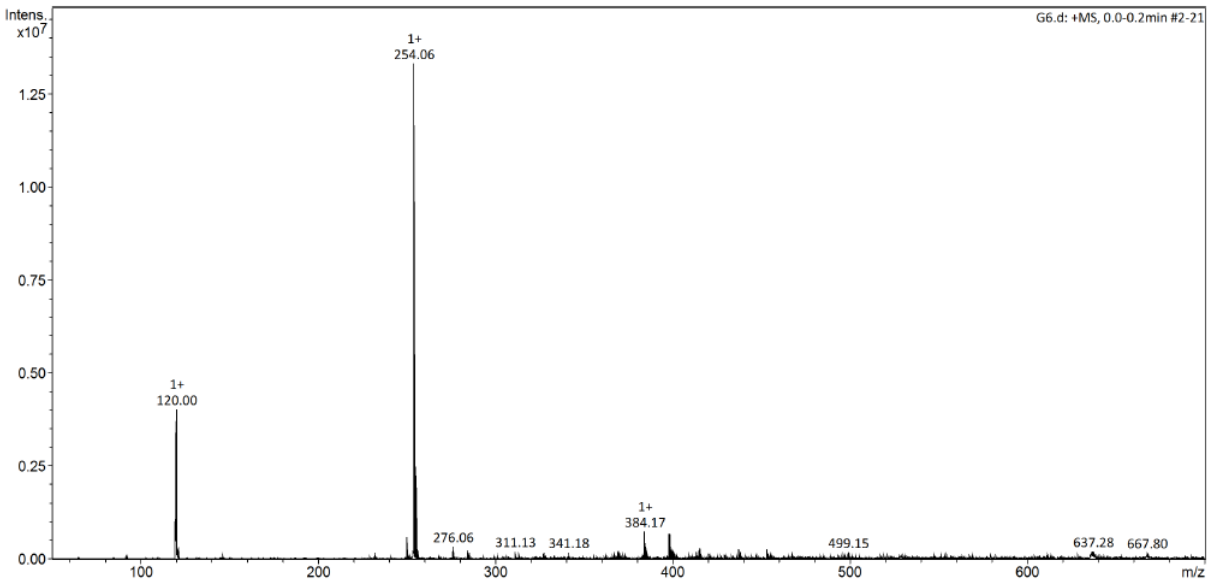

Figure SM24. UV-Vis spectra of compound **4e**

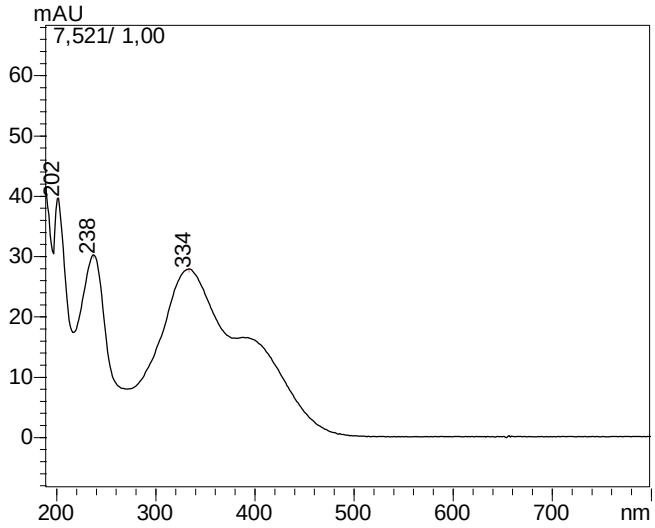

Figure SM25. HPLC cromatogram of compound **4e**

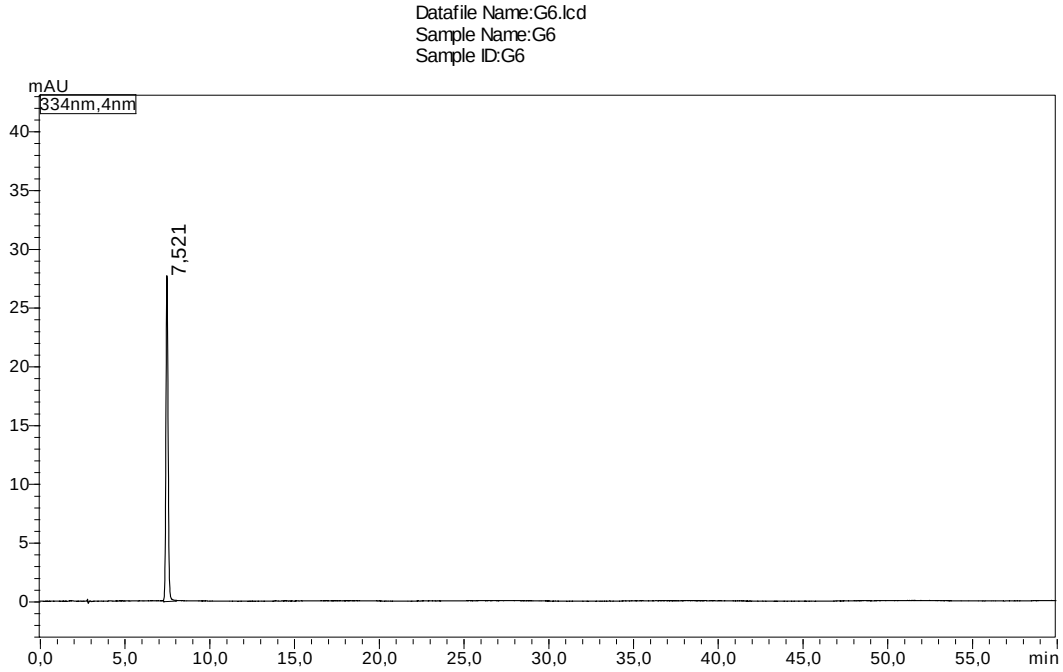

Figure SM 26. ^{1}H NMR spectrum of compound **5a** (DMSO-d_6; 600 MHz)

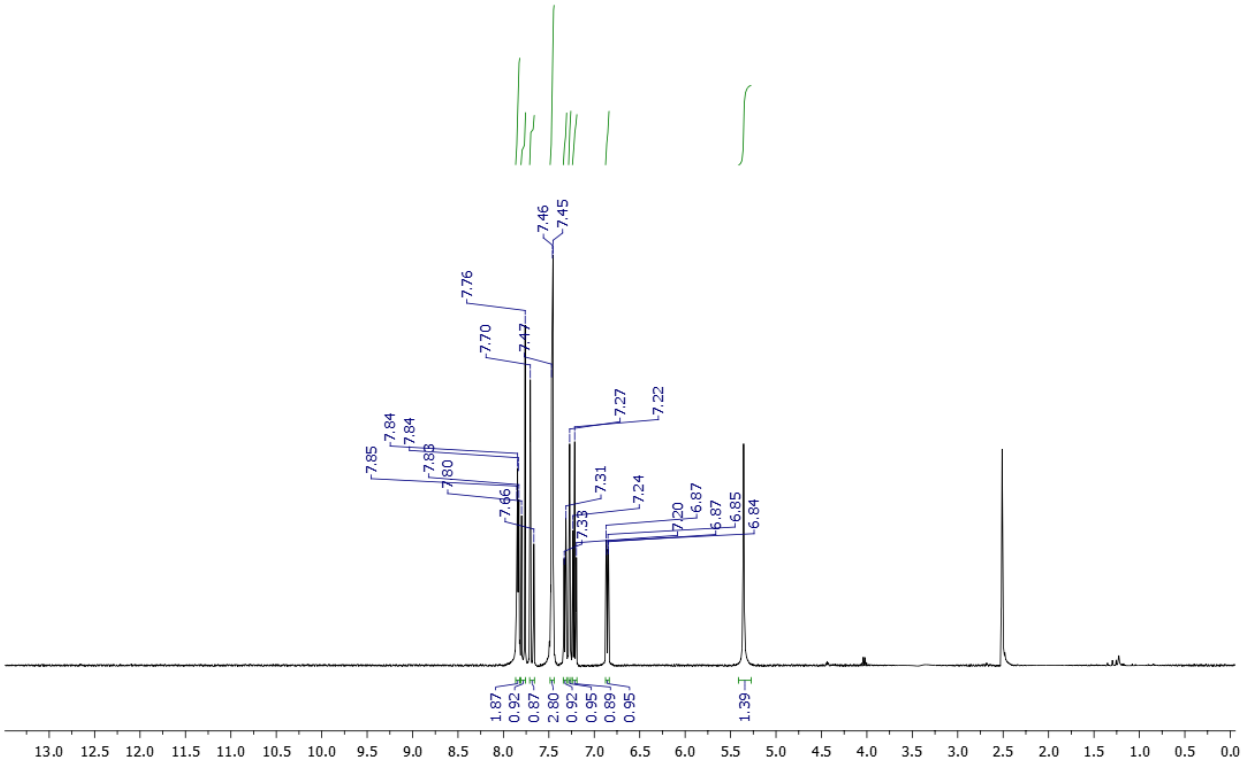

Figure SM 27.^{13}C NMR spectrum of compound **5a** (DMSO-d_6; 150 MHz)

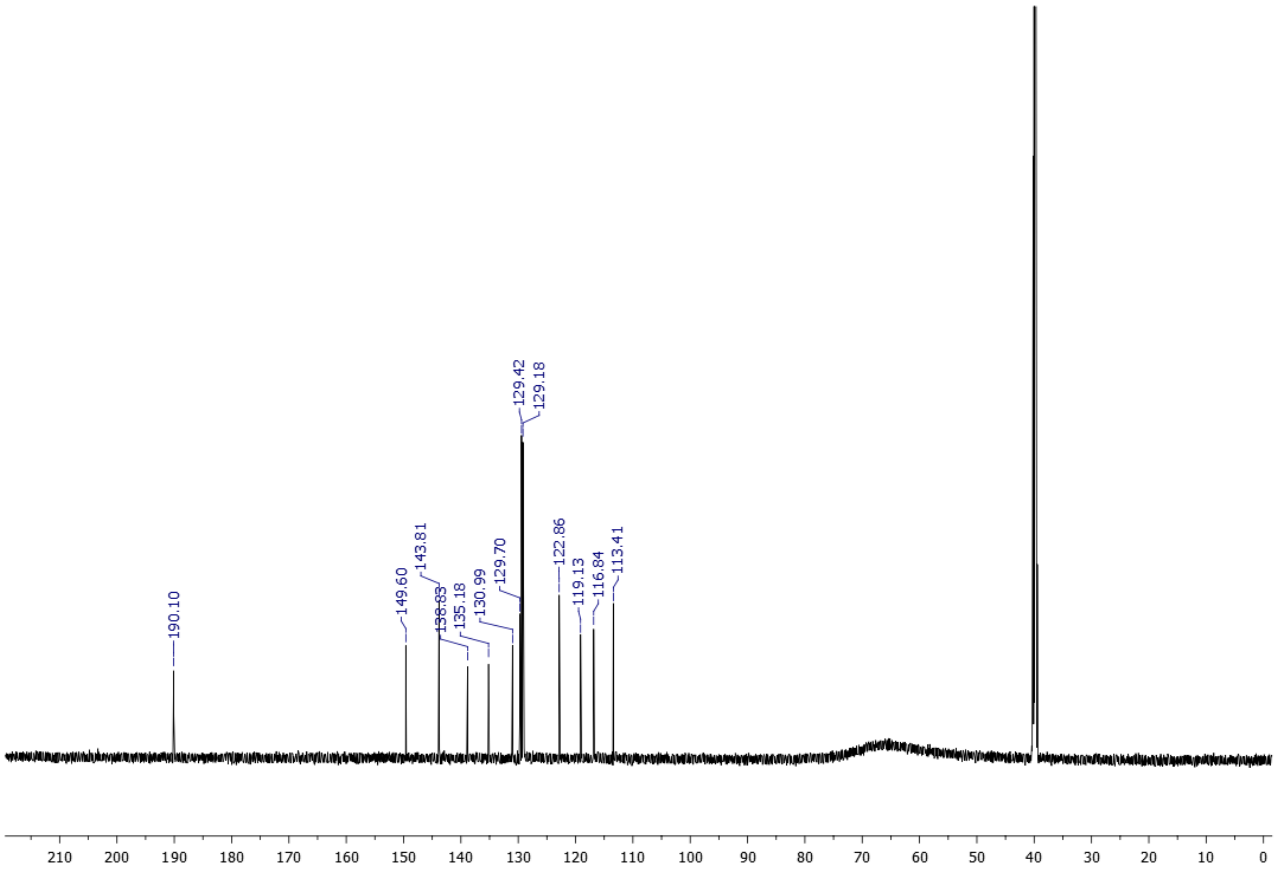

Figure SM28. Mass spectra (MS) of compound 5**a**

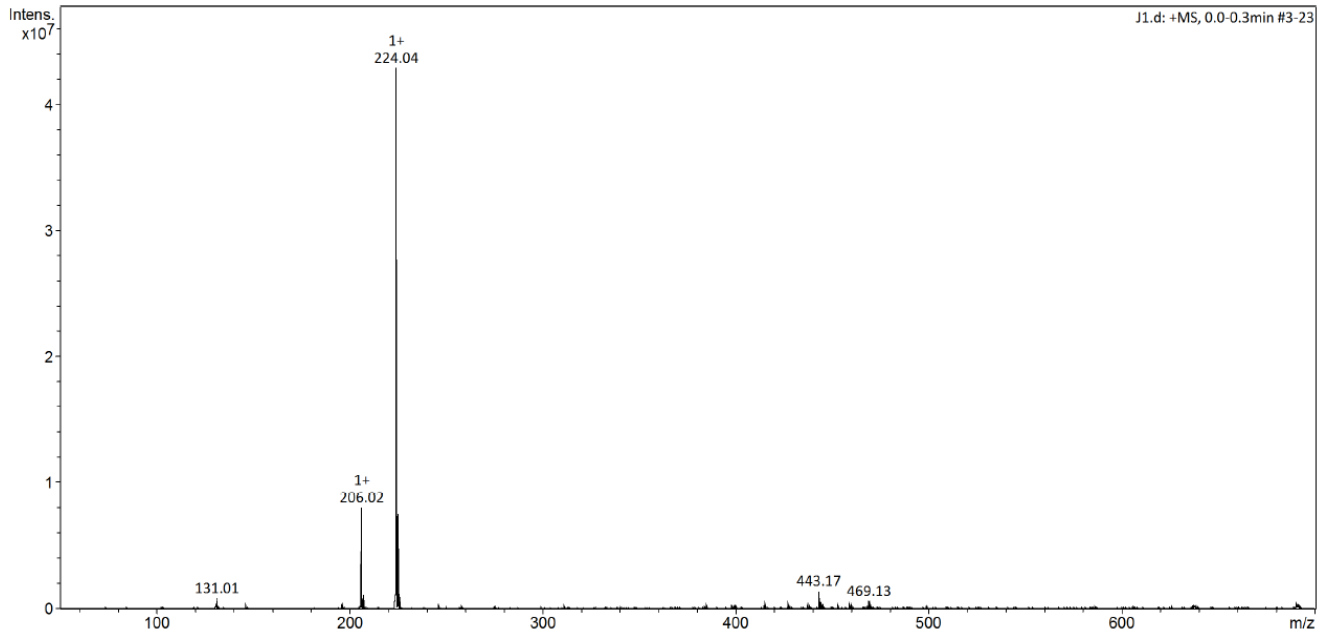

Figure SM29. UV-Vis spectra of compound **5a**

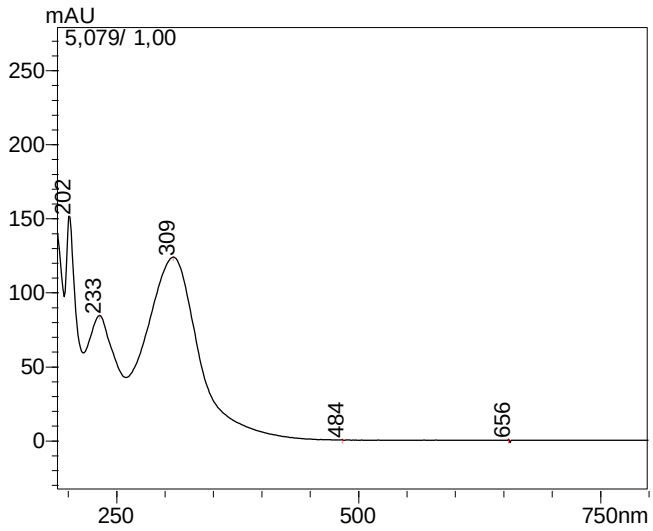

Figure SM30. HPLC cromatogram of compound **5a**

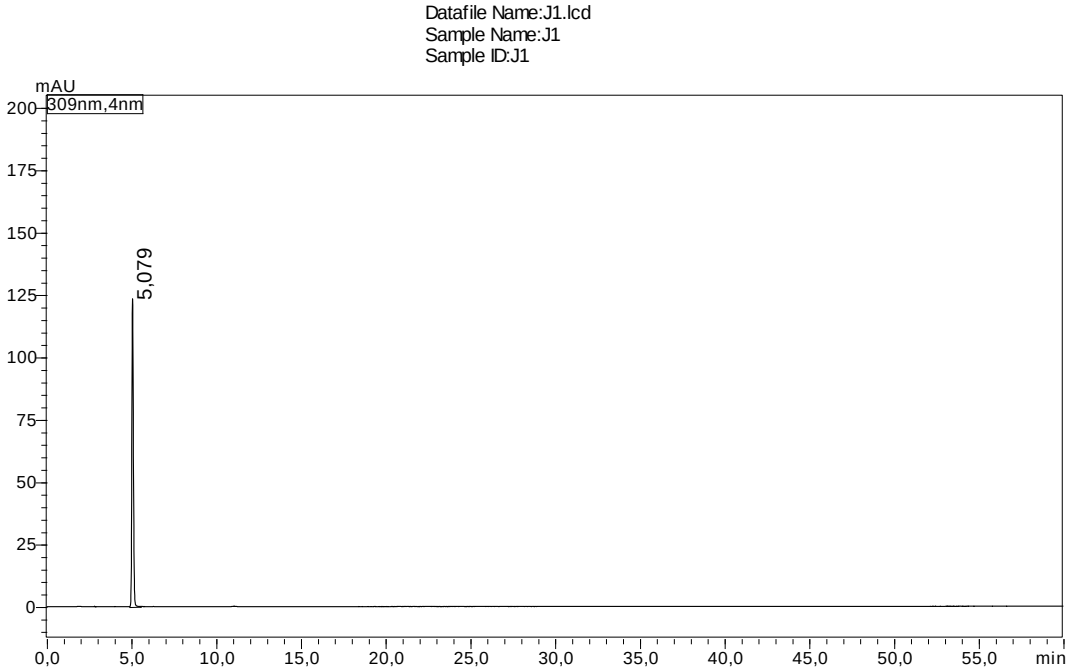

Figure SM31. ^{1}H NMR spectrum of compound **5b** (DMSO-d_6; 600 MHz)

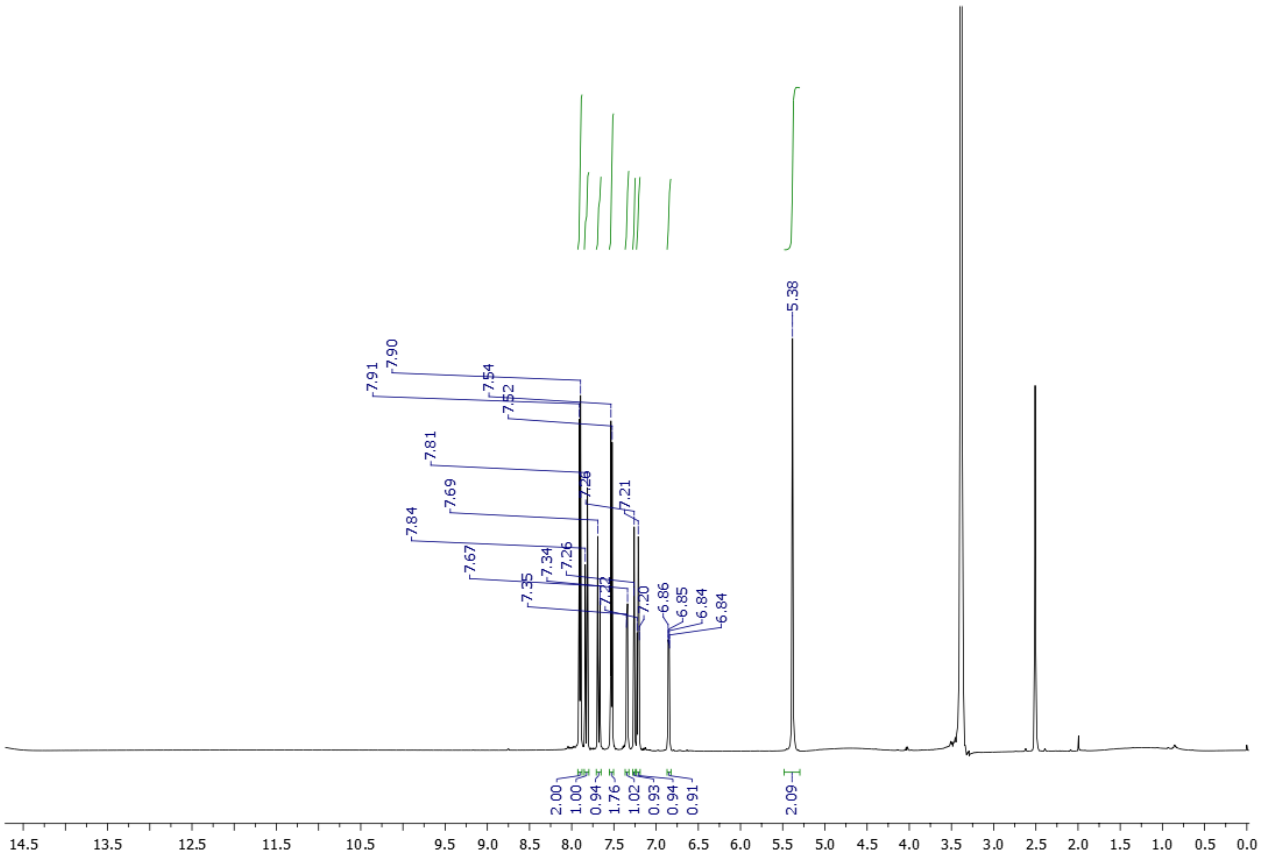

Figure SM32. ^{13}C NMR spectrum of compound **5b** (DMSO-d_6; 150 MHz)

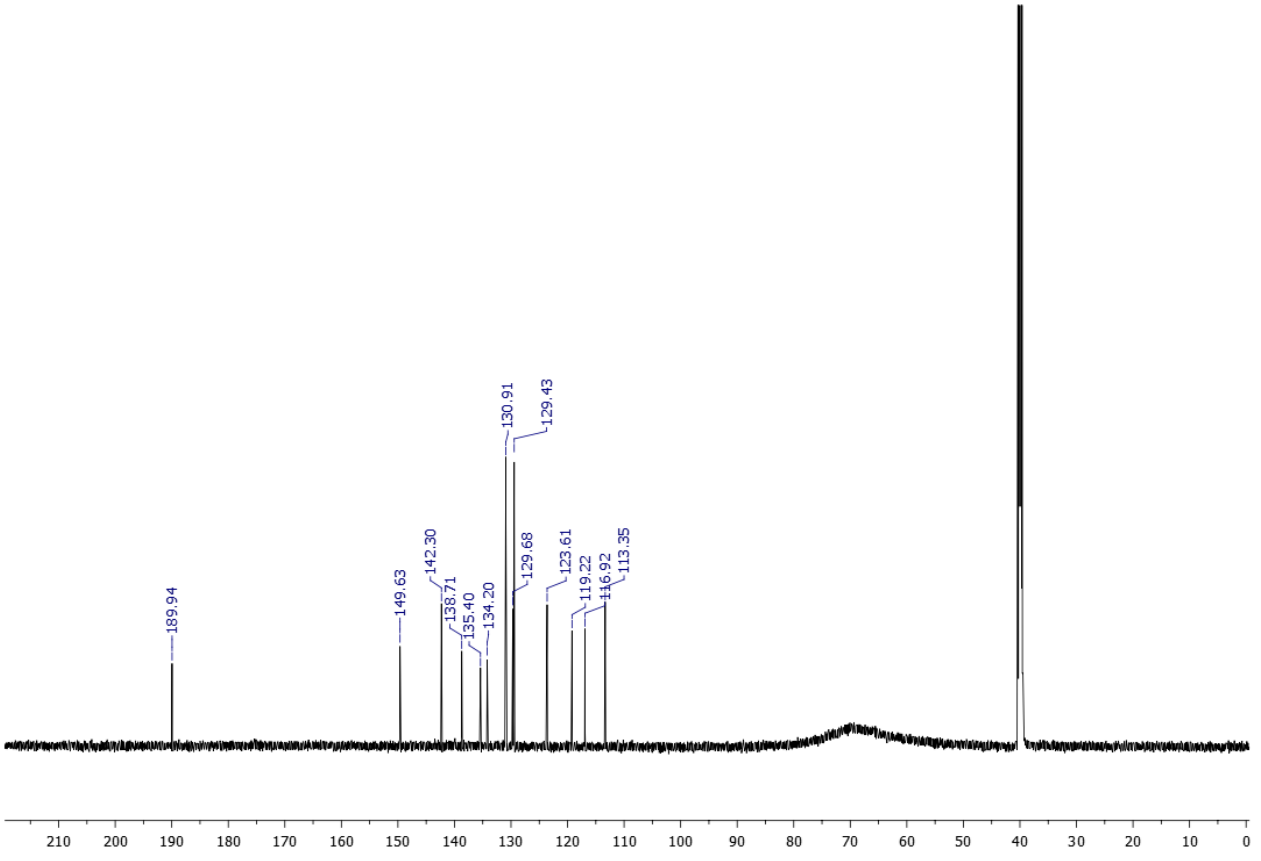

Figure SM33. Mass spectra (MS) of compound **5b**

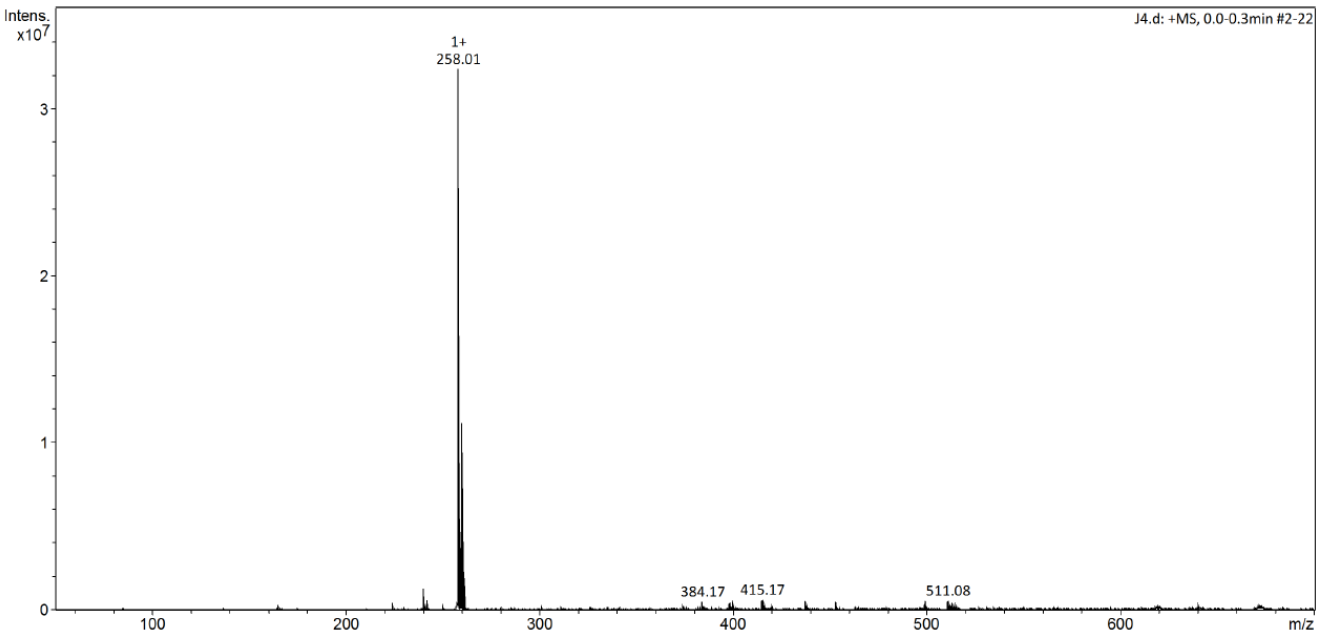

Figure SM34. UV-Vis spectra of compound **5b**

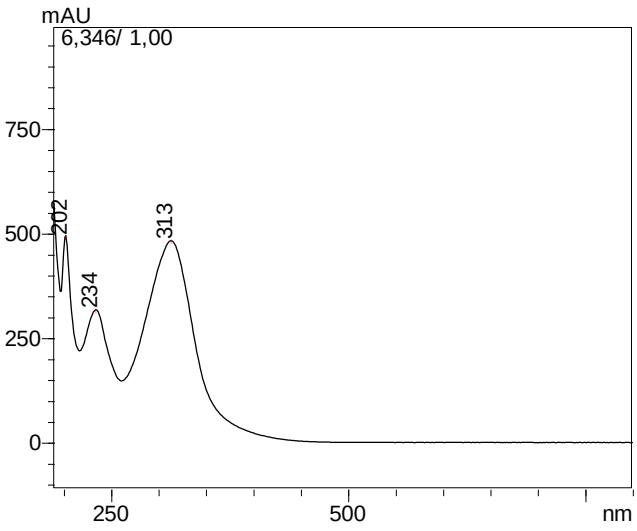

Figure SM35. HPLC cromatogram of compound **5b**

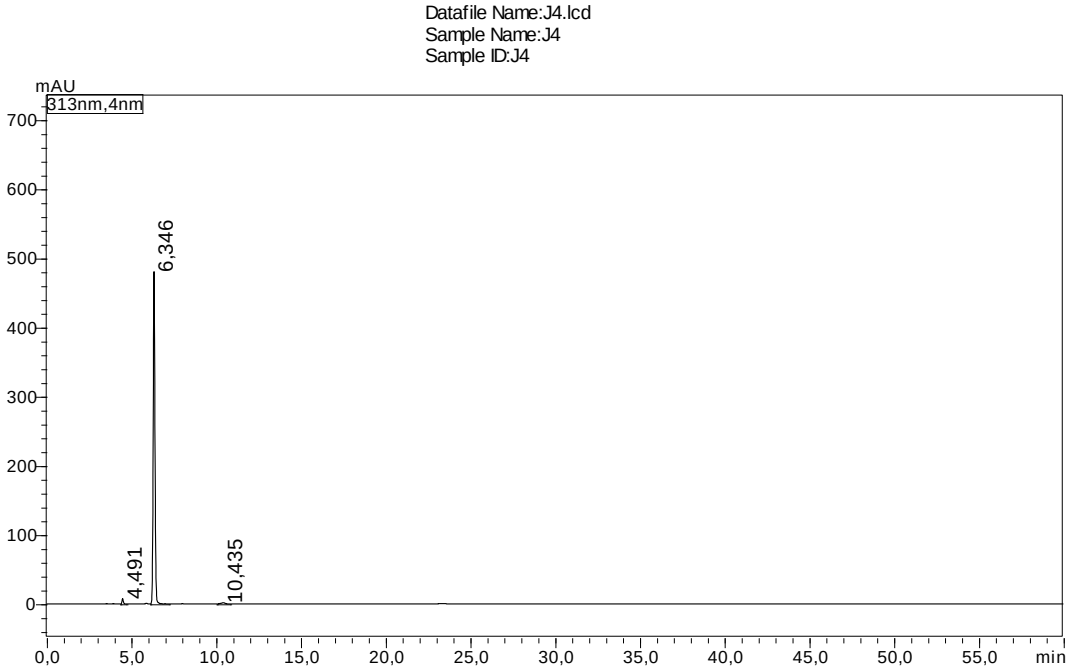

Figure SM36. ^{1}H NMR spectrum of compound **5c** ($CDCl_3$; 600 MHz)

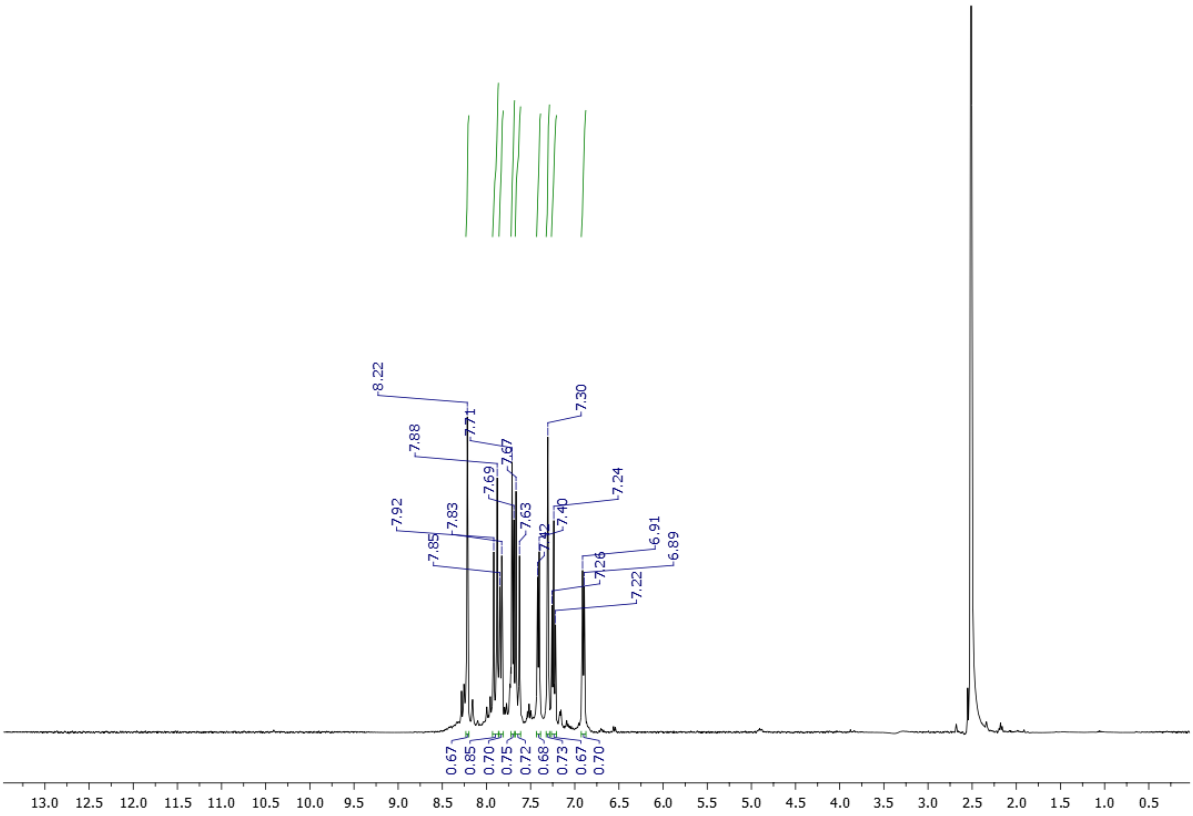

Figure SM37. ^{13}C NMR spectrum of compound **5c** ($CDCl_3$; 150 MHz)

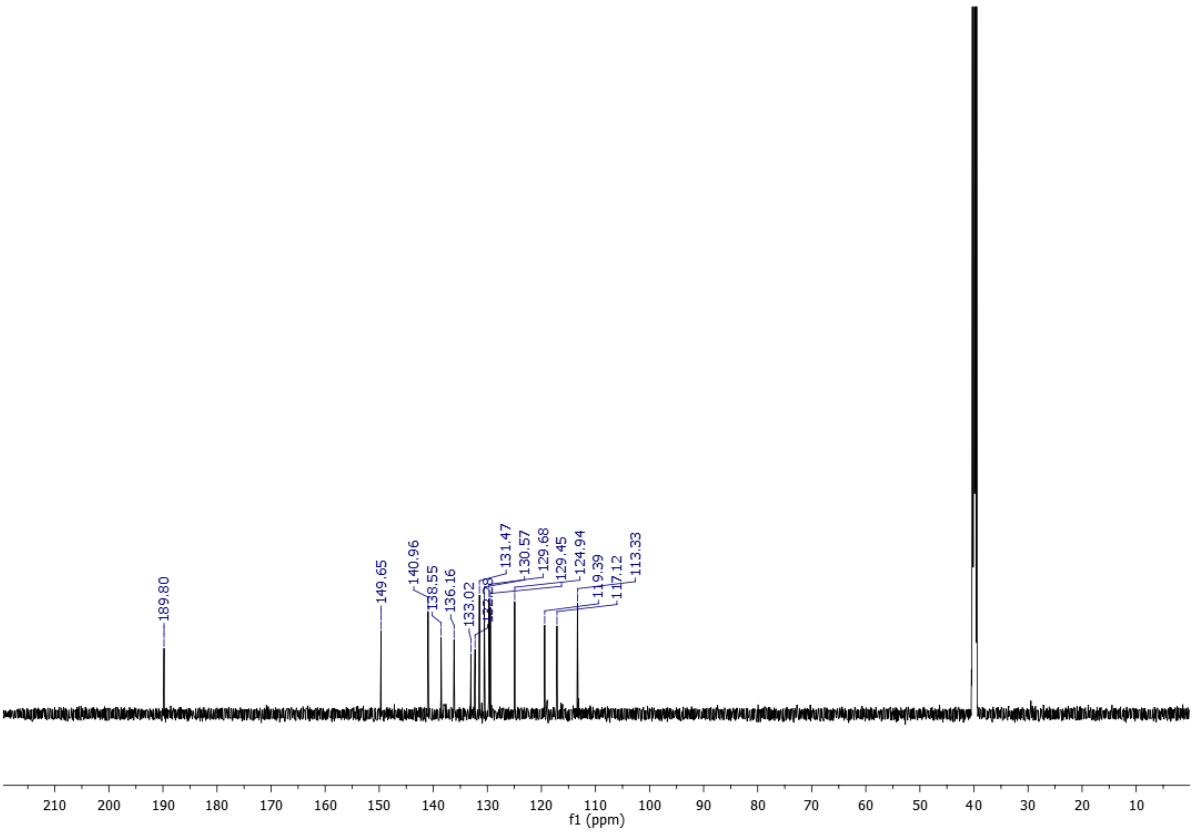

Figure SM38. Mass spectra (MS) of compound **5c**

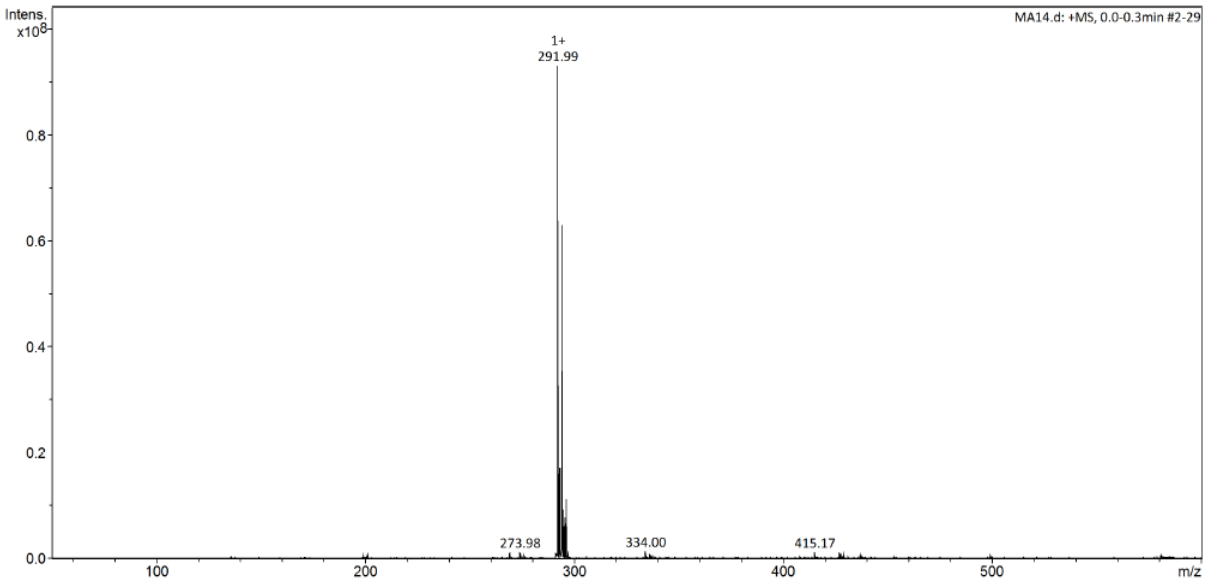

Figure SM 39. Mass spectra (MS/MS) precursor íon *m/s* 291.99 ([M + H^+])

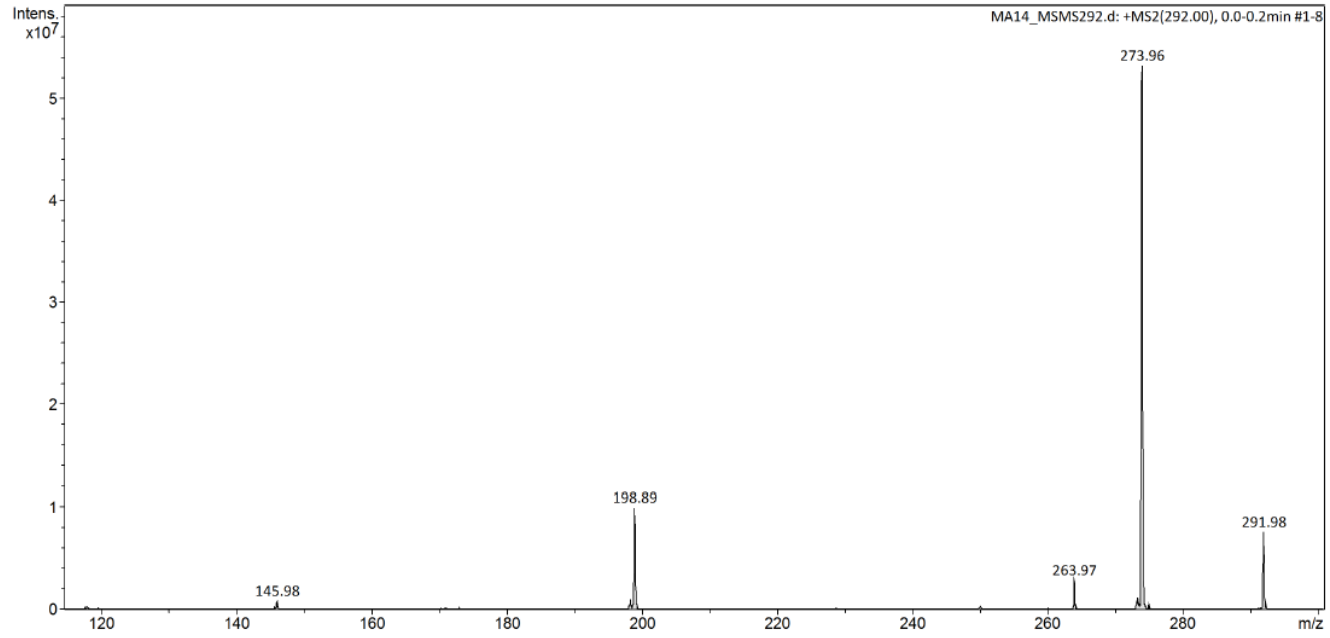

Figure SM40. UV-Vis spectra of compound **5c**

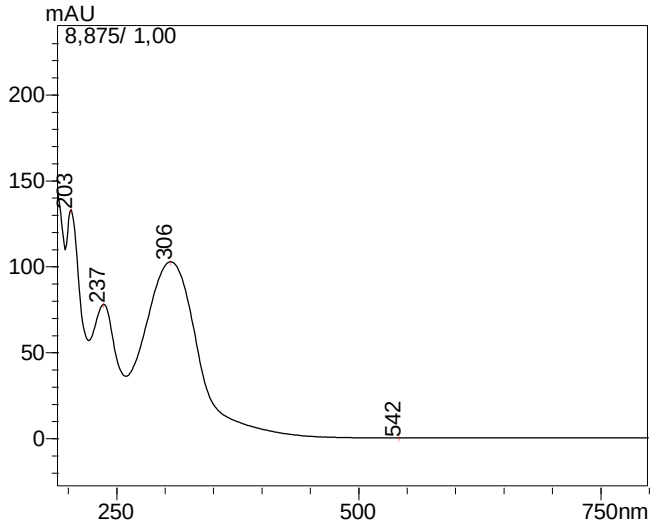

Figure SM41. HPLC cromatogram of compound **5c**

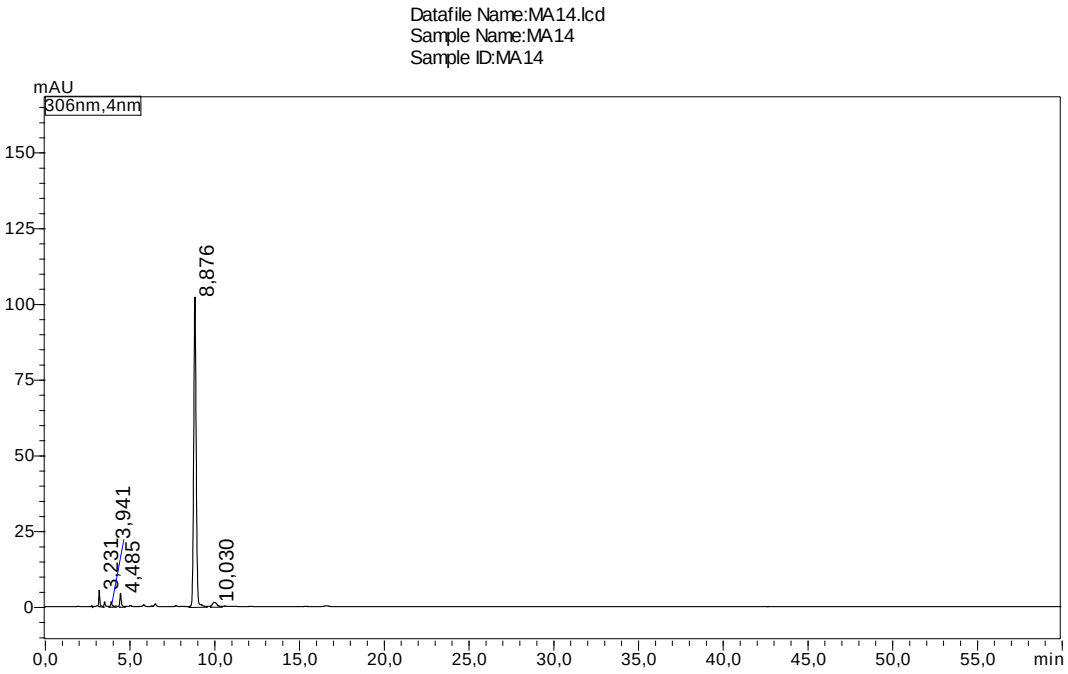

Figure SM42. ^{1}H NMR spectrum of compound **5d** (DMSO-d_6; 600 MHz)

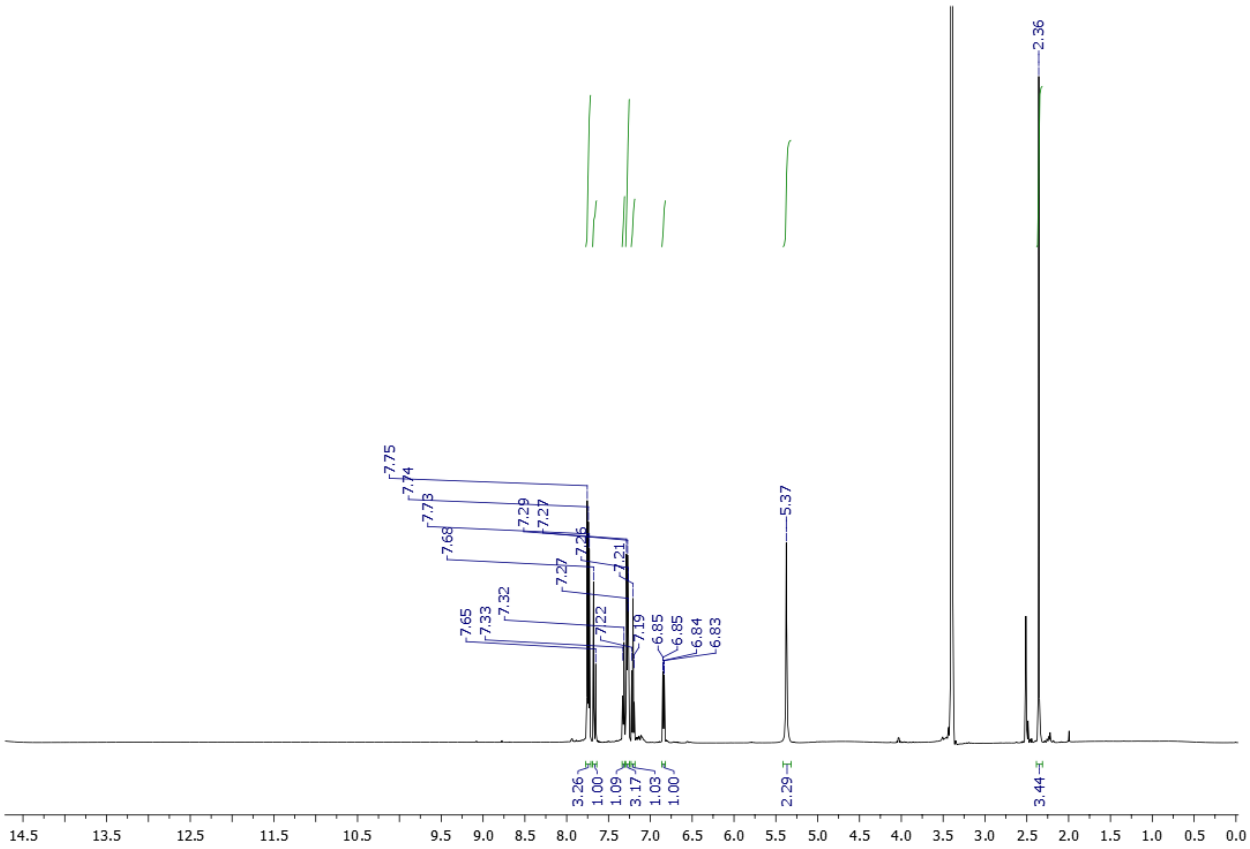

Figure SM43. ^{13}C NMR spectrum of compound **5d** (DMSO-d_6; 150 MHz)

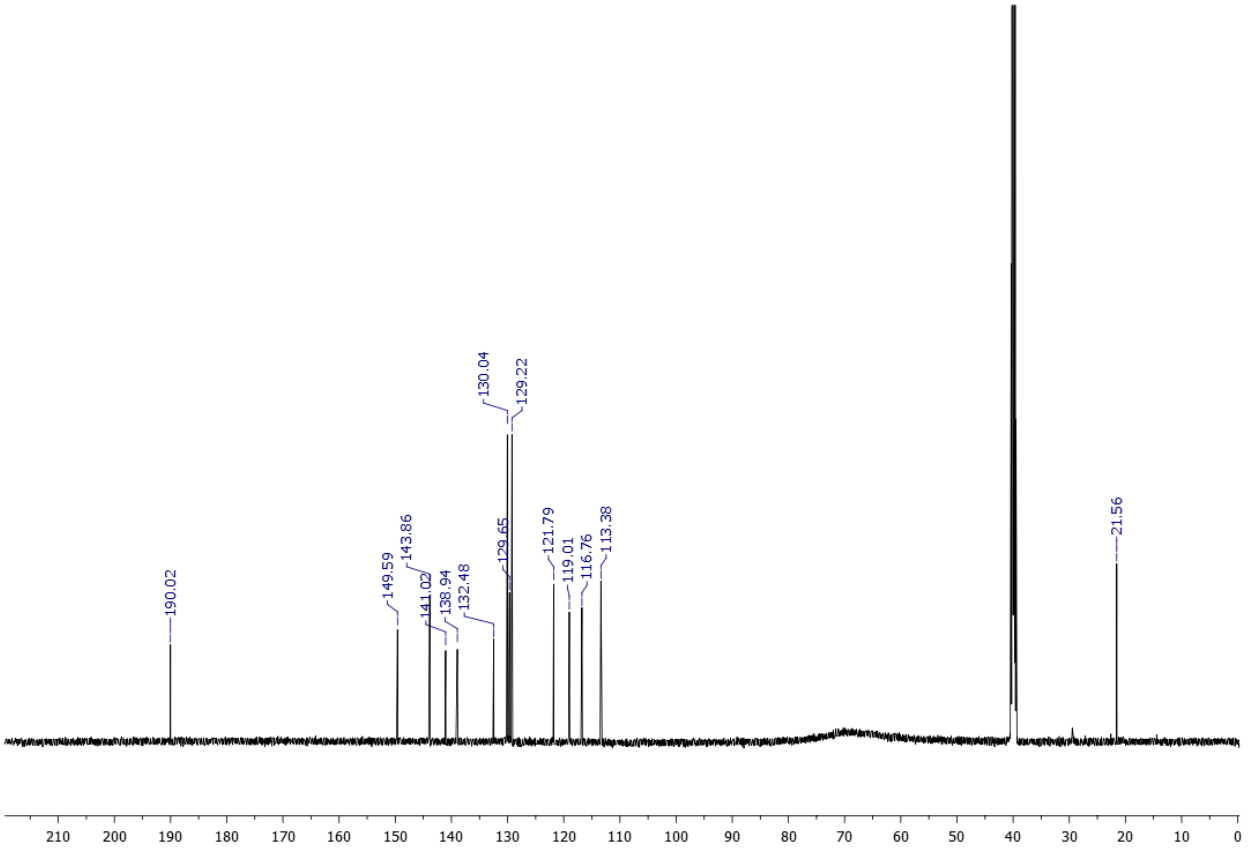

Figure SM44. Mass spectra (MS) of compound **5d**

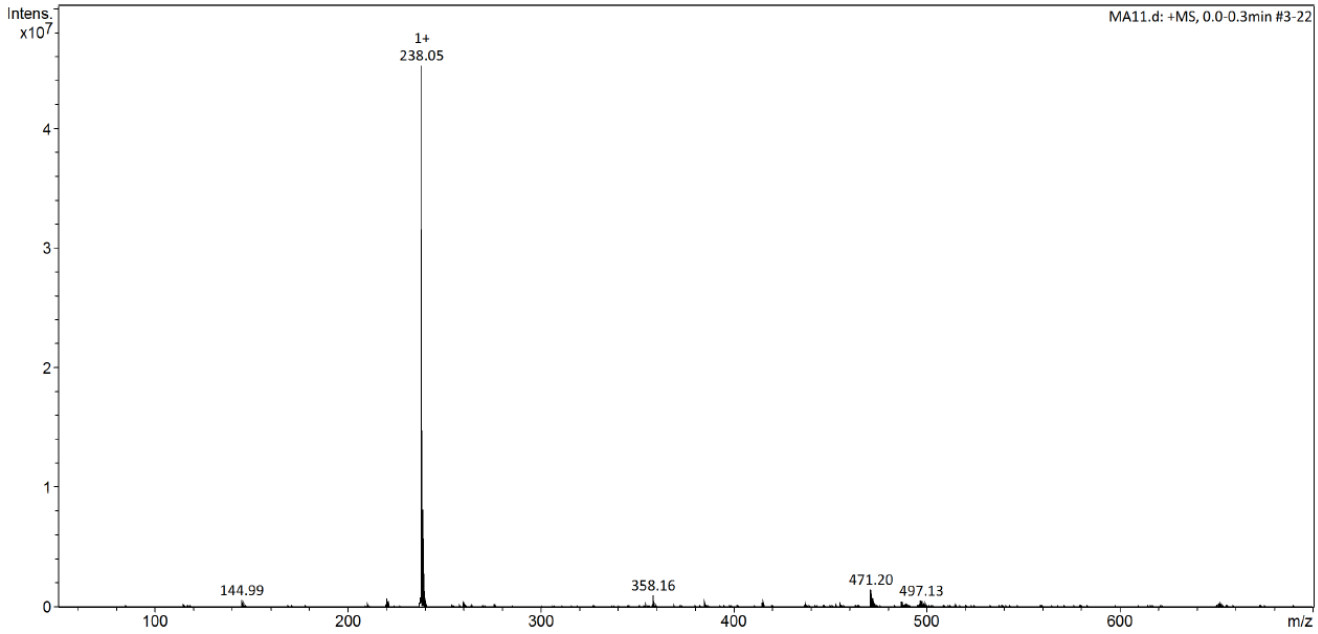

Figure SM45. UV-Vis spectra of compound **5d**

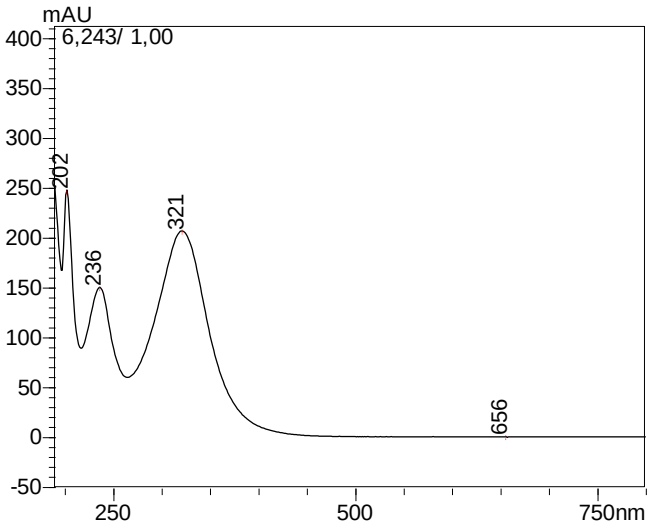

Figure SM46. HPLC cromatogram of compound **5d**

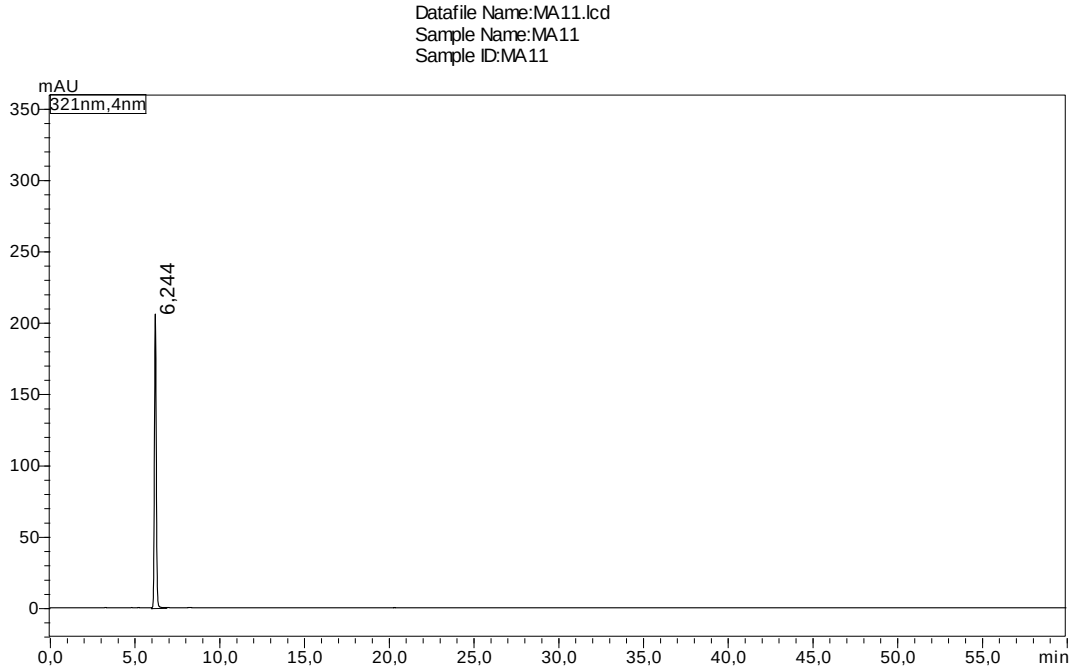

Figure SM47. ^{1}H NMR spectrum of compound **5e** (DMSO-d_6; 600 MHz)

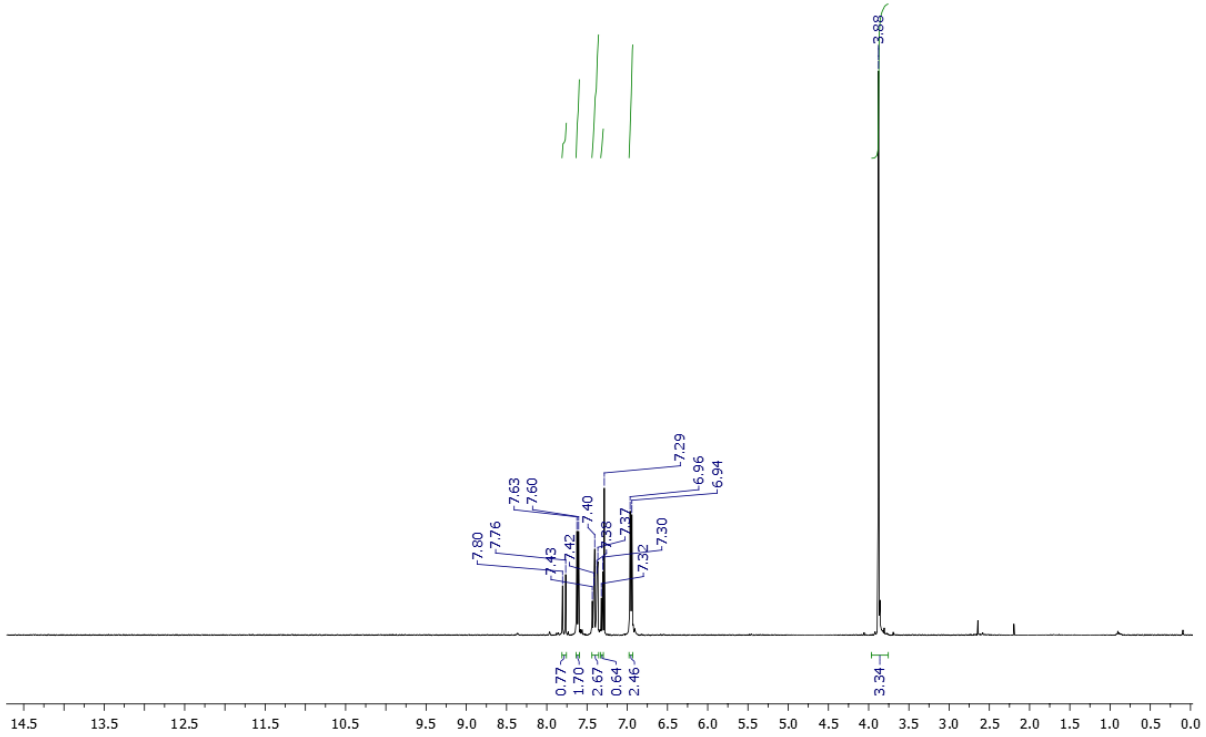

Figure SM48. ^{13}C NMR spectrum of compound **5e** (DMSO-d_6; 150 MHz)

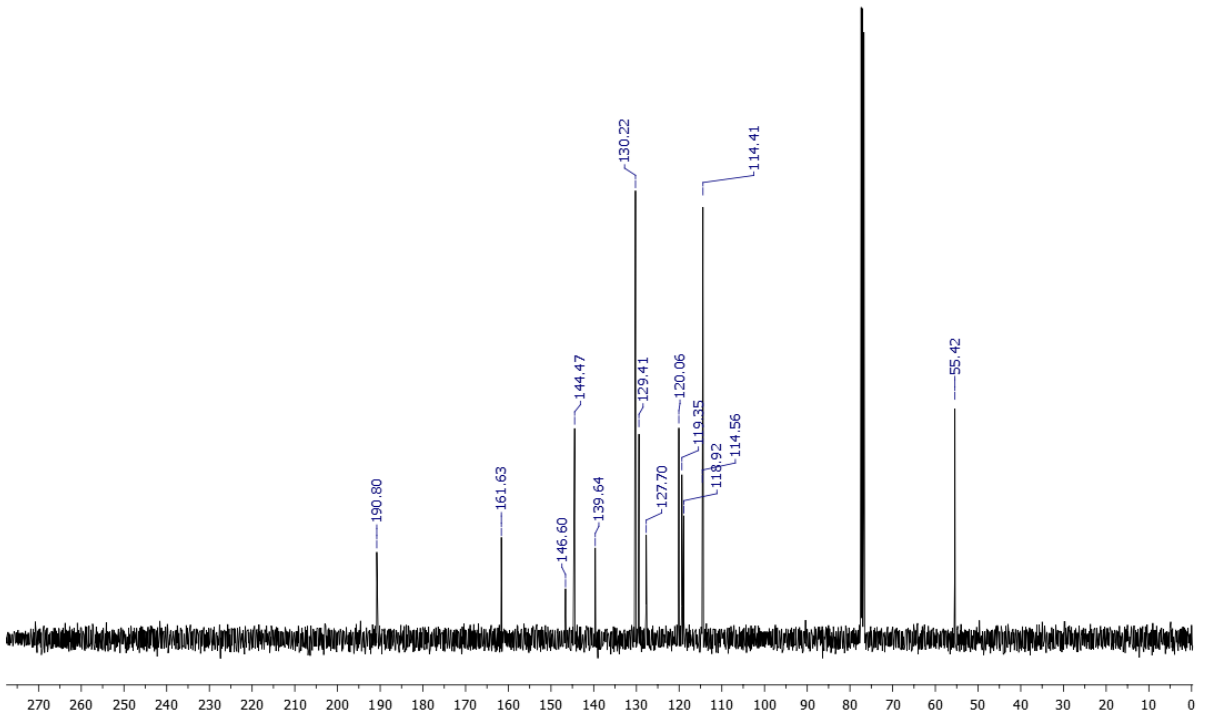

Figure SM49. Mass spectra (MS) of compound **5e**

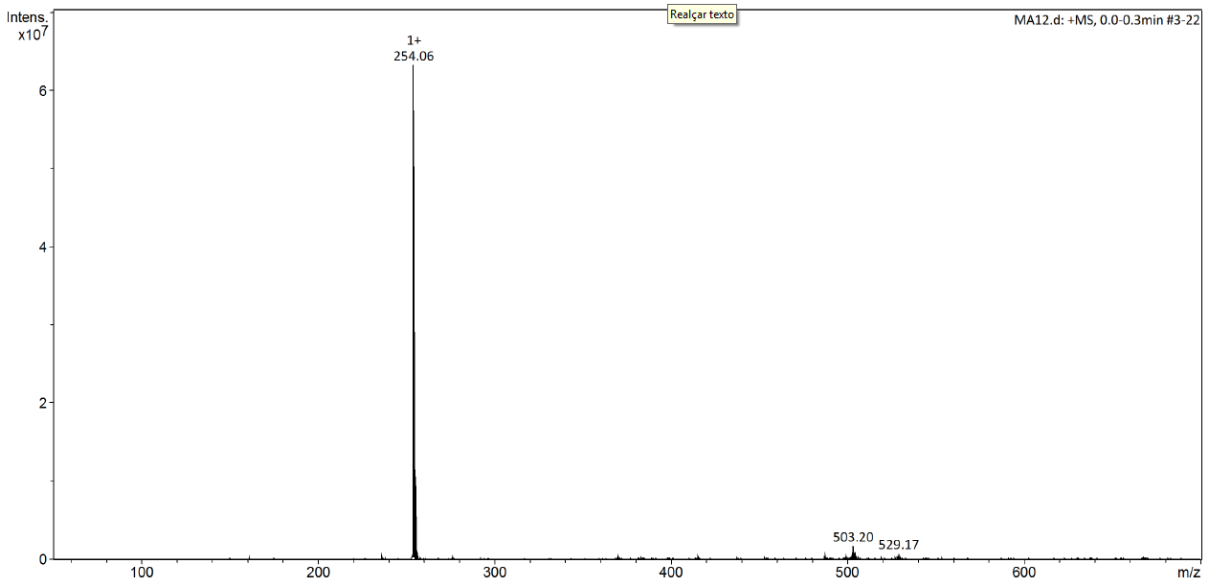

Figure SM50. UV-Vis spectra of compound **5e**

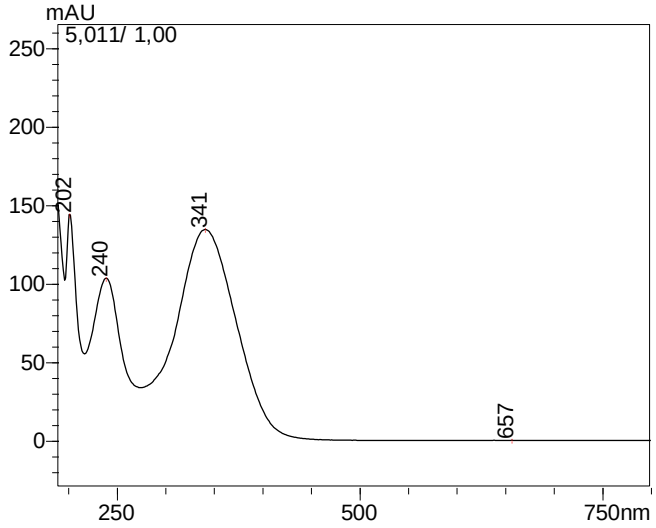

Figure SM51. HPLC cromatogram of compound **5e**

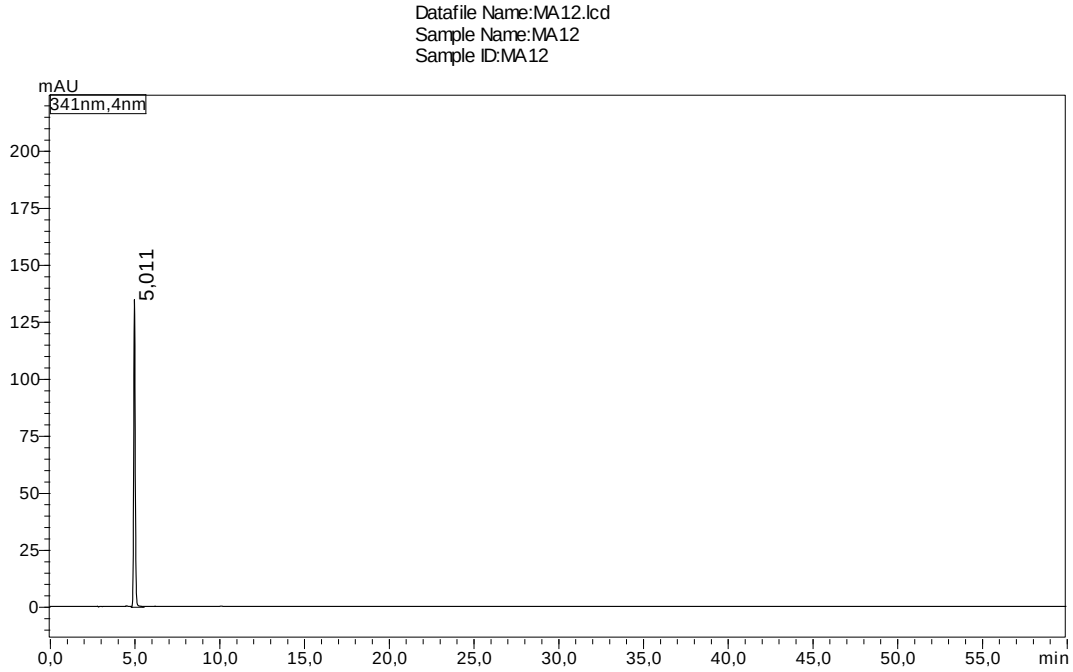

Figure SM52. ^{1}H NMR spectrum of compound **5f** (DMSO-d_6; 300 MHz)

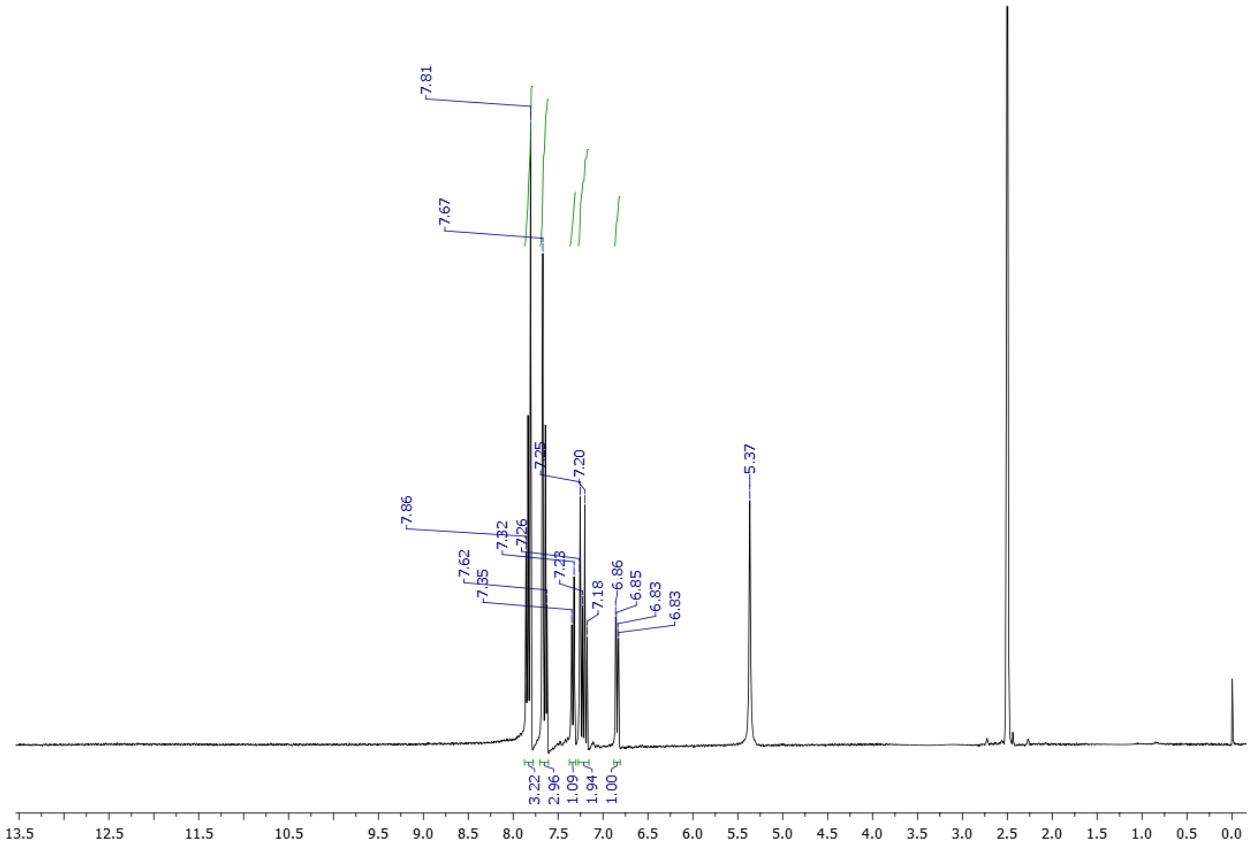

Figure SM53. ^{13}C NMR spectrum of compound **5f** (DMSO-d_6; 150 MHz)

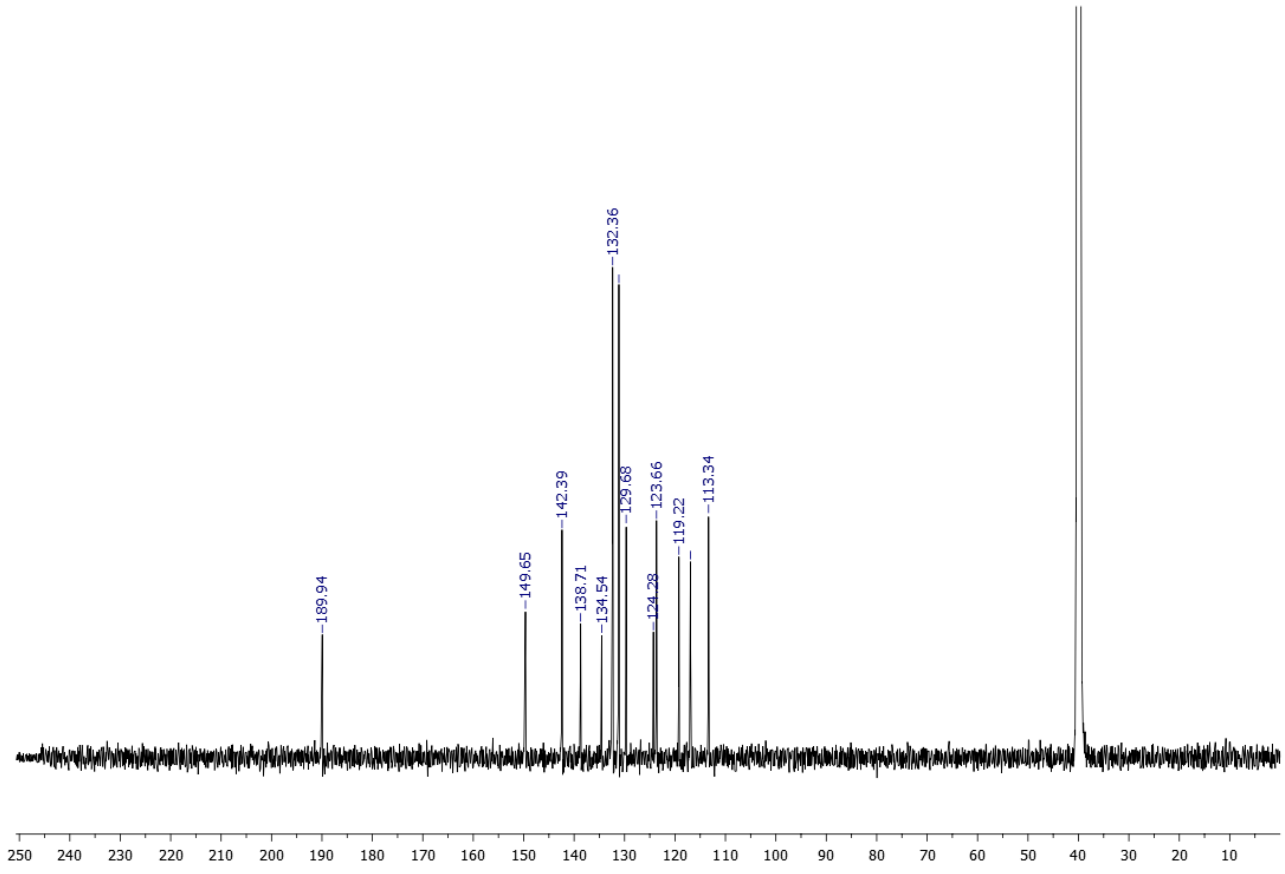

Figure SM54. Mass spectra (MS) of compound **5f**

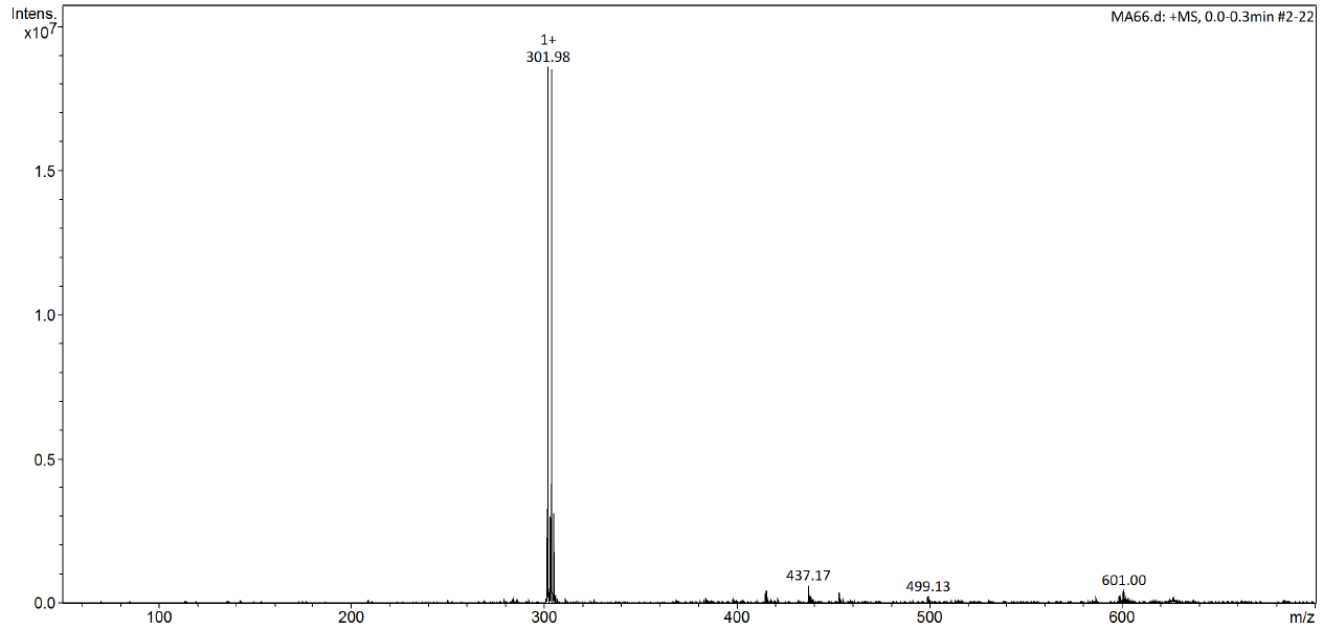

Figure SM55. Mass spectra (MS/MS) precursor íon *m/s* 301.98 ([M + H^+])

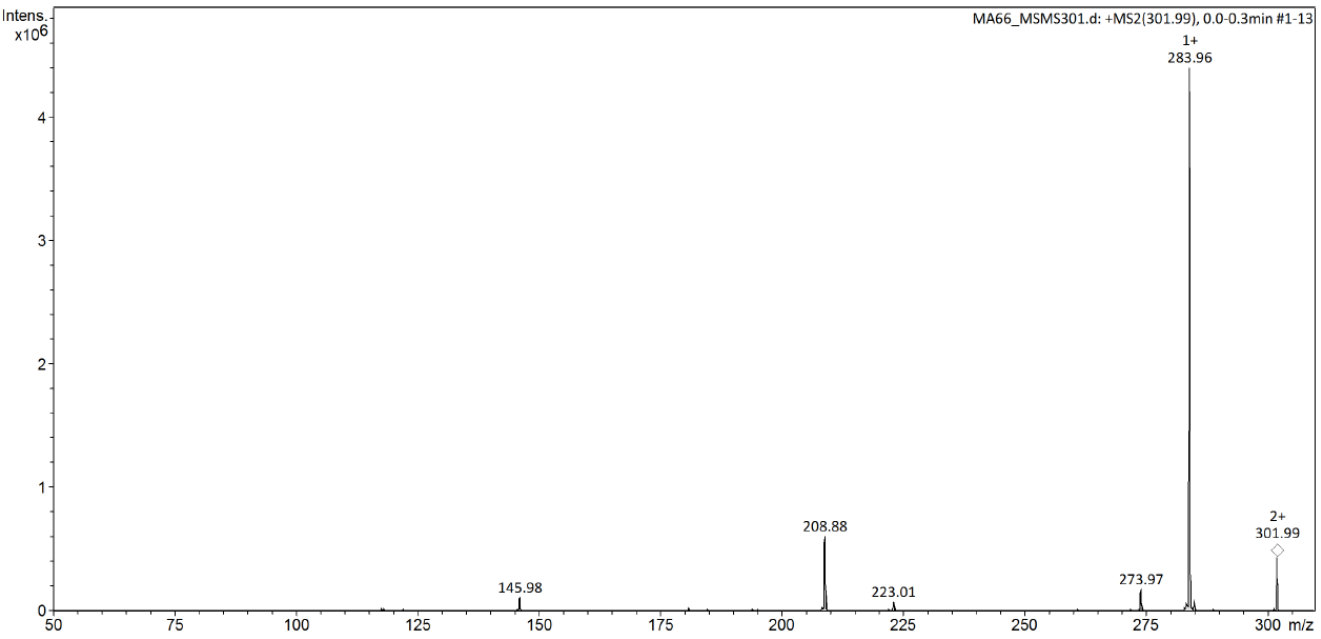

Figure SM56. UV-Vis spectra of compound **5f**

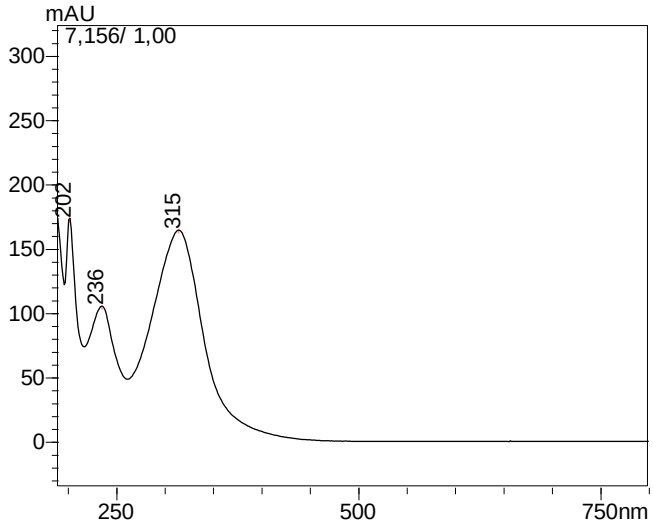

Figure SM57. HPLC cromatogram of compound **5f**

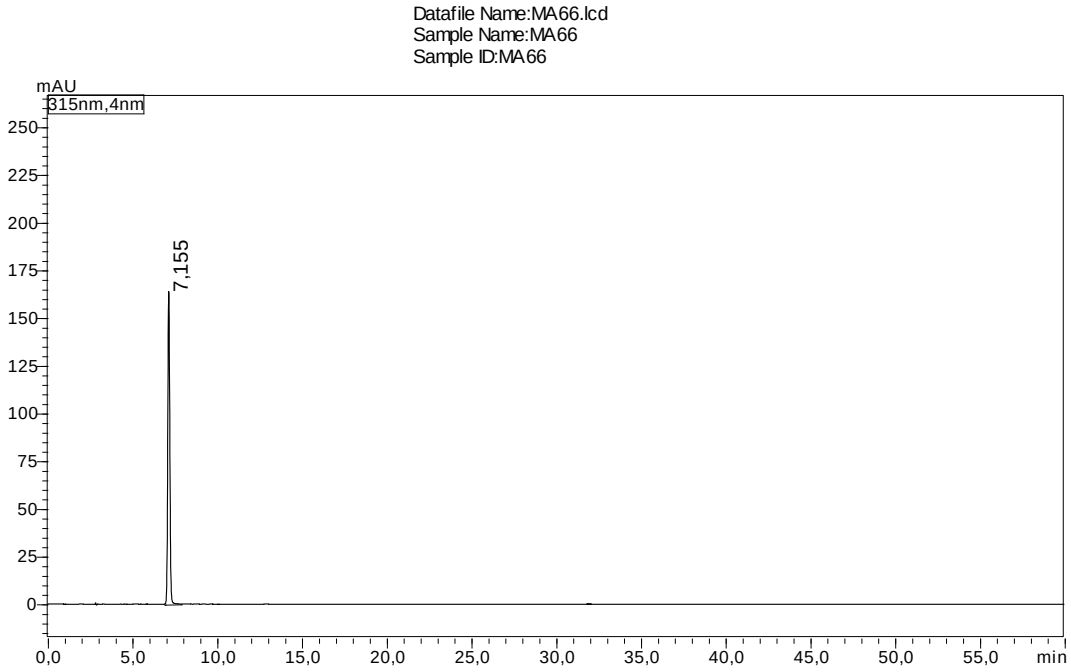

Figure SM58. ^{1}H NMR spectrum of compound **5g** (DMSO-d_6; 300 MHz)

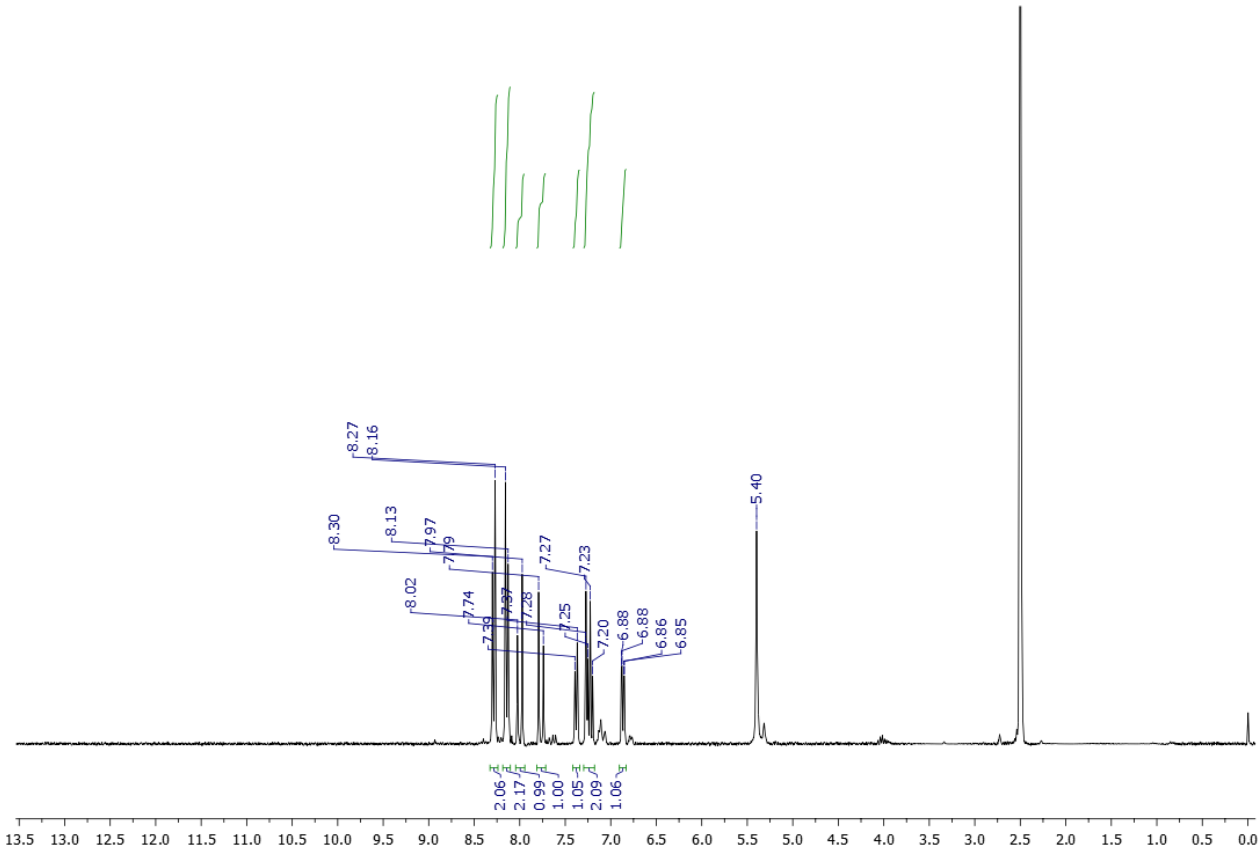

Figure SM59. ^{13}C NMR spectrum of compound **5g** (DMSO-d_6; 150 MHz)

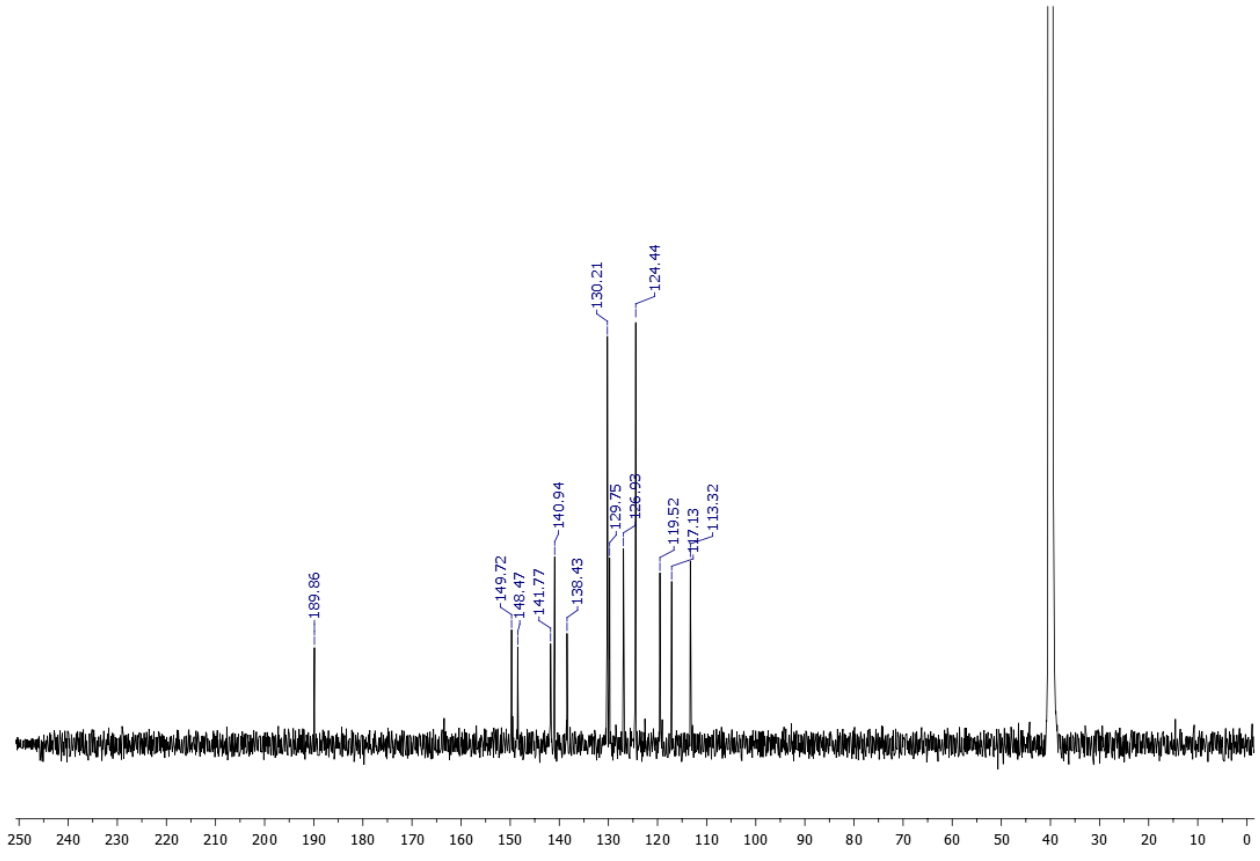

Figure SM60. Mass spectra (MS) of compound **5g**

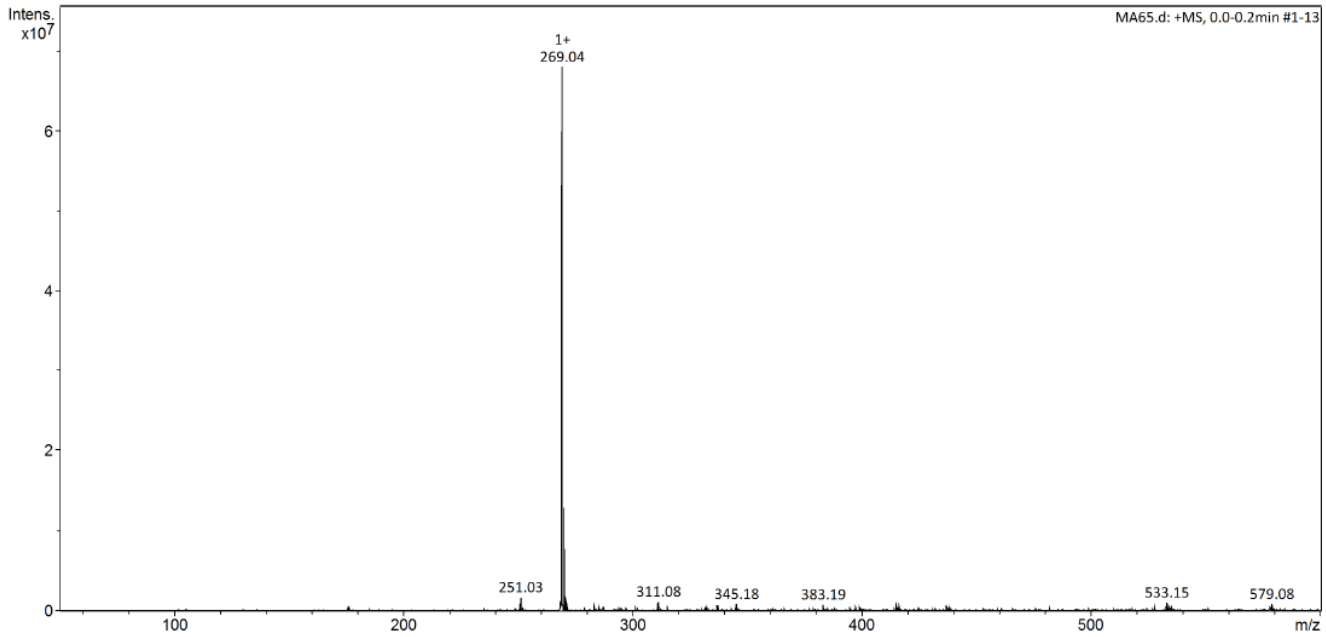

Figure SM61. Mass spectra (MS/MS) precursor íon *m/s* 269.04 ([M + H^+])

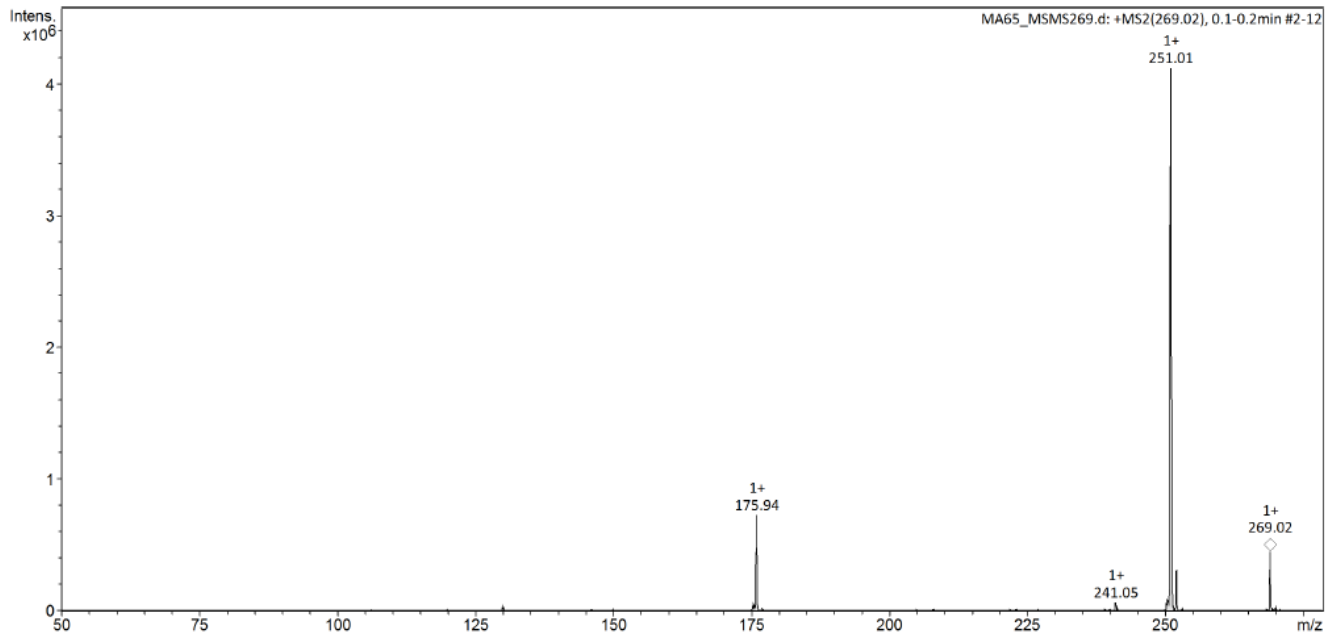

Figure SM62. UV-Vis spectra of compound **5g**

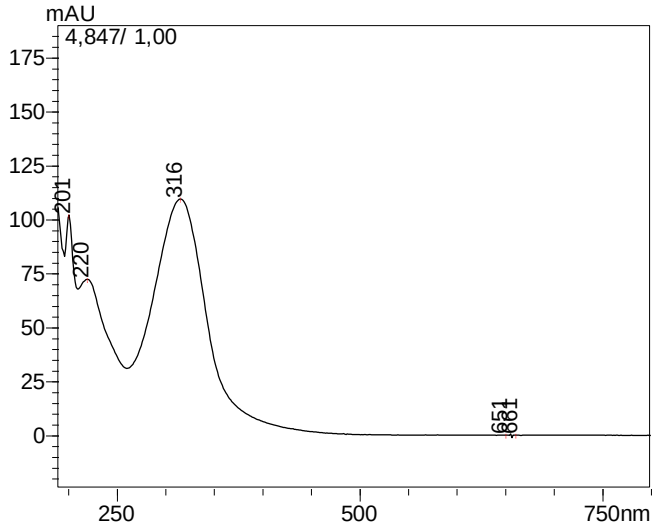

Figure SM63. HPLC cromatogram of compound **5g**

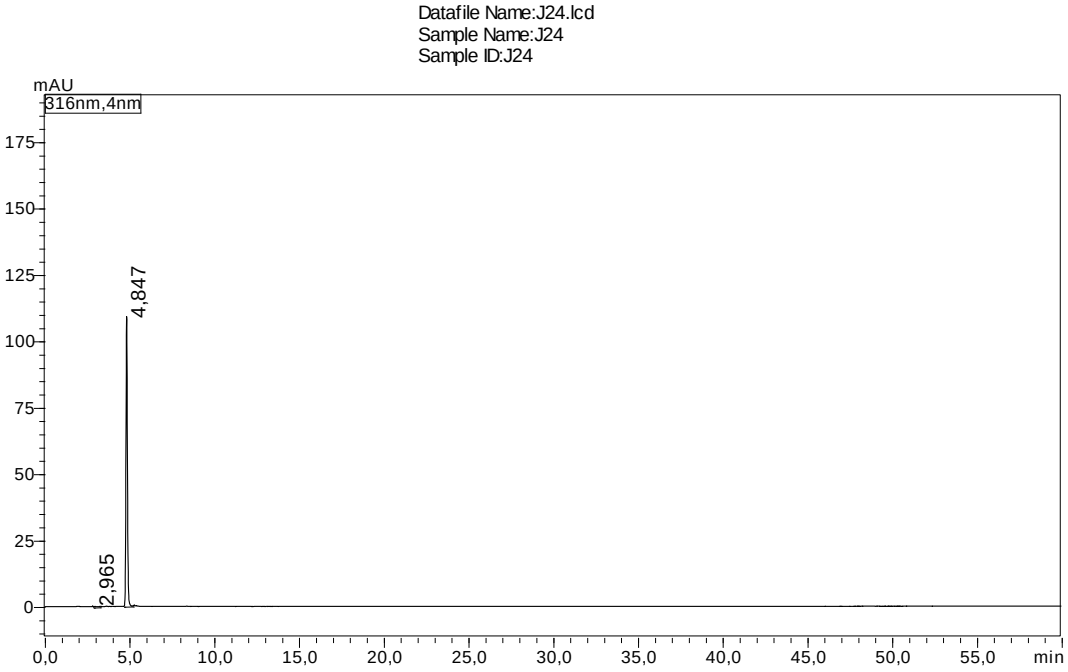

Figure SM64. ^{1}H NMR spectrum of compound **6a** (DMSO-d_6; 600 MHz)

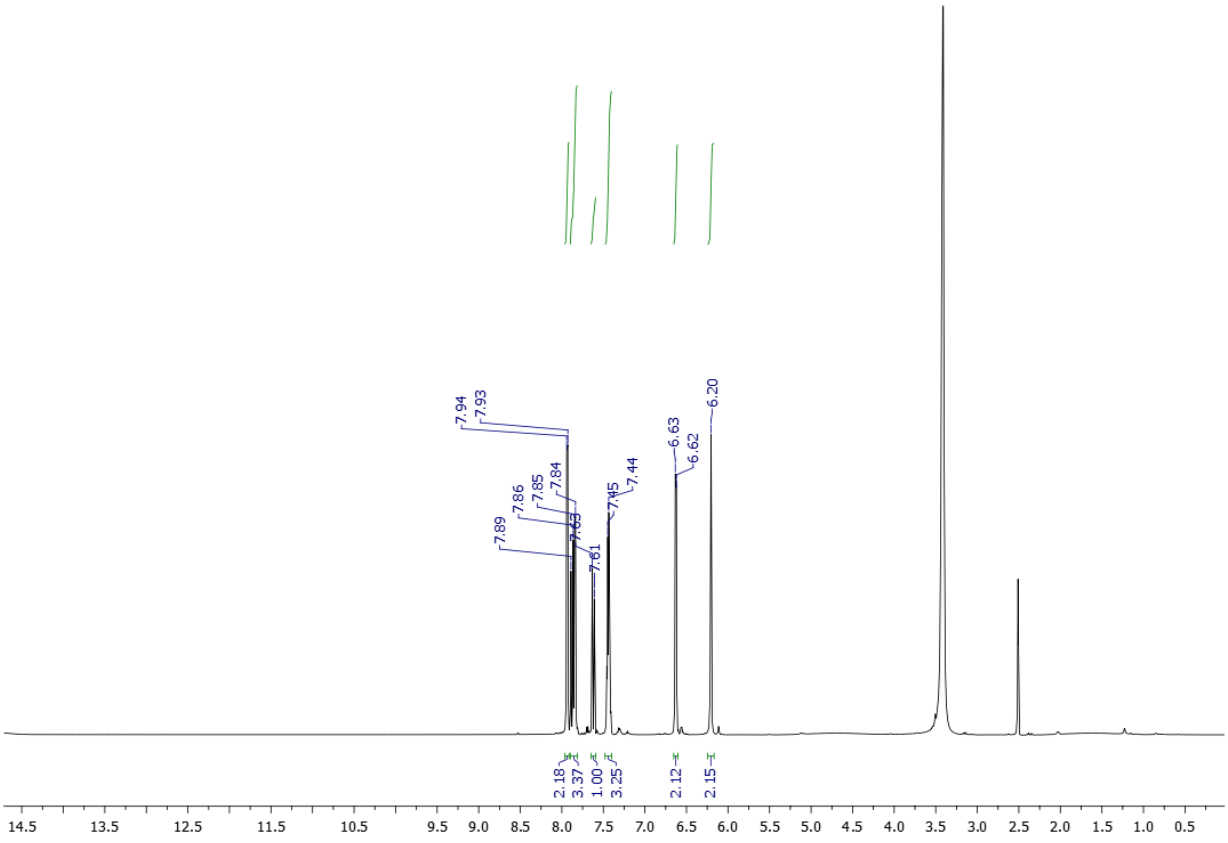

Figure SM65. ^{13}C NMR spectrum of compound **6a** (DMSO-d_6; 150 MHz)

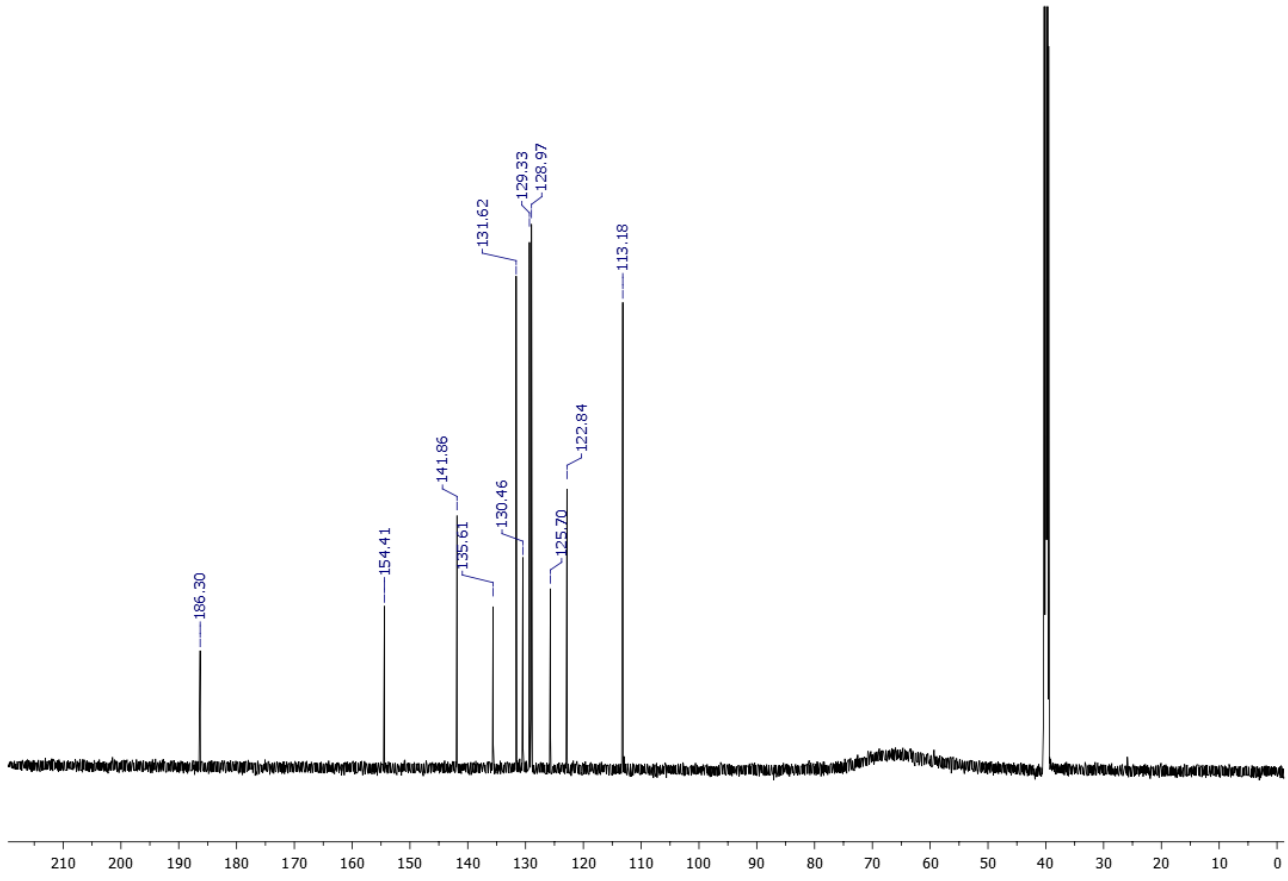

Figure SM66. Mass spectra (MS) of compound **6a**

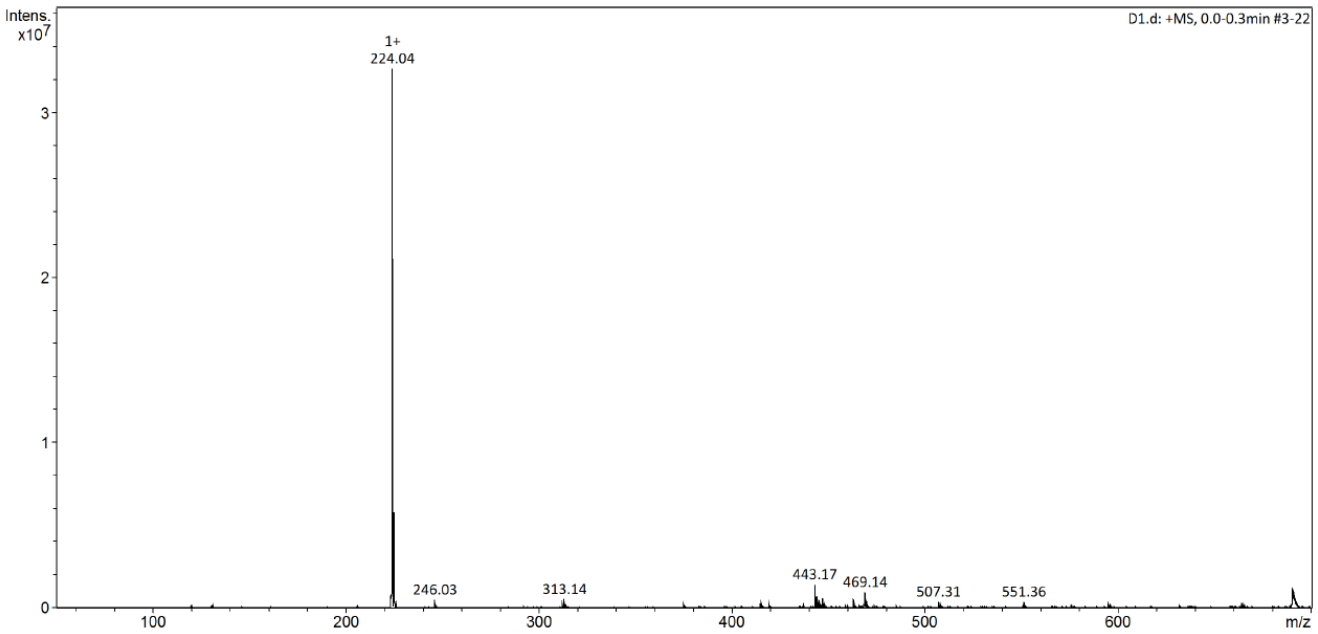

Figure SM67. UV-Vis spectra of compound **6a**

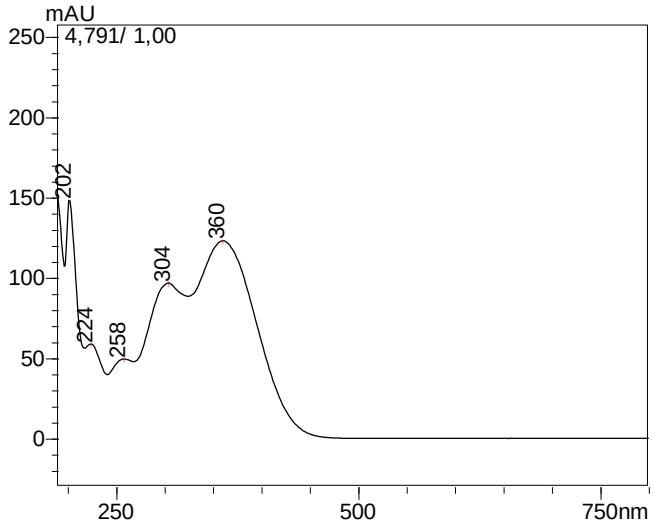

Figure SM68. HPLC cromatogram of compound **6a**

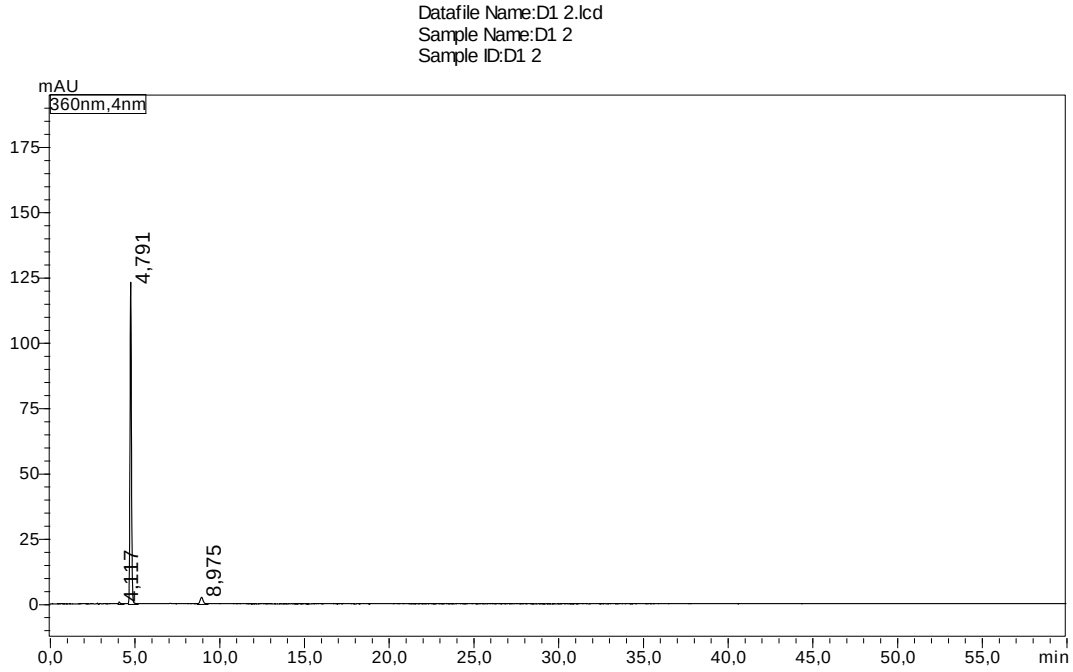

Figure SM69. ^{1}H NMR spectrum of compound **6b** (DMSO-d_6; 600 MHz)

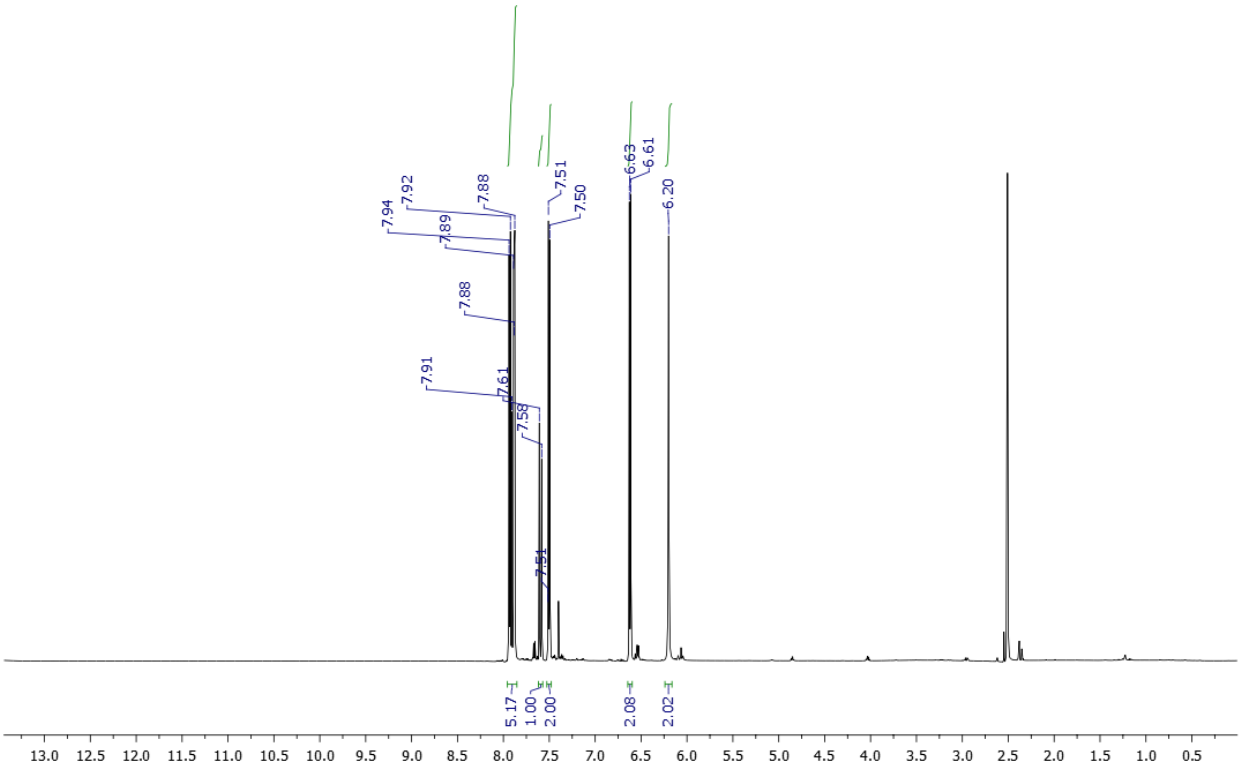

Figure SM70. ^{13}C NMR spectrum of compound **6b** (DMSO-d_6; 150 MHz)

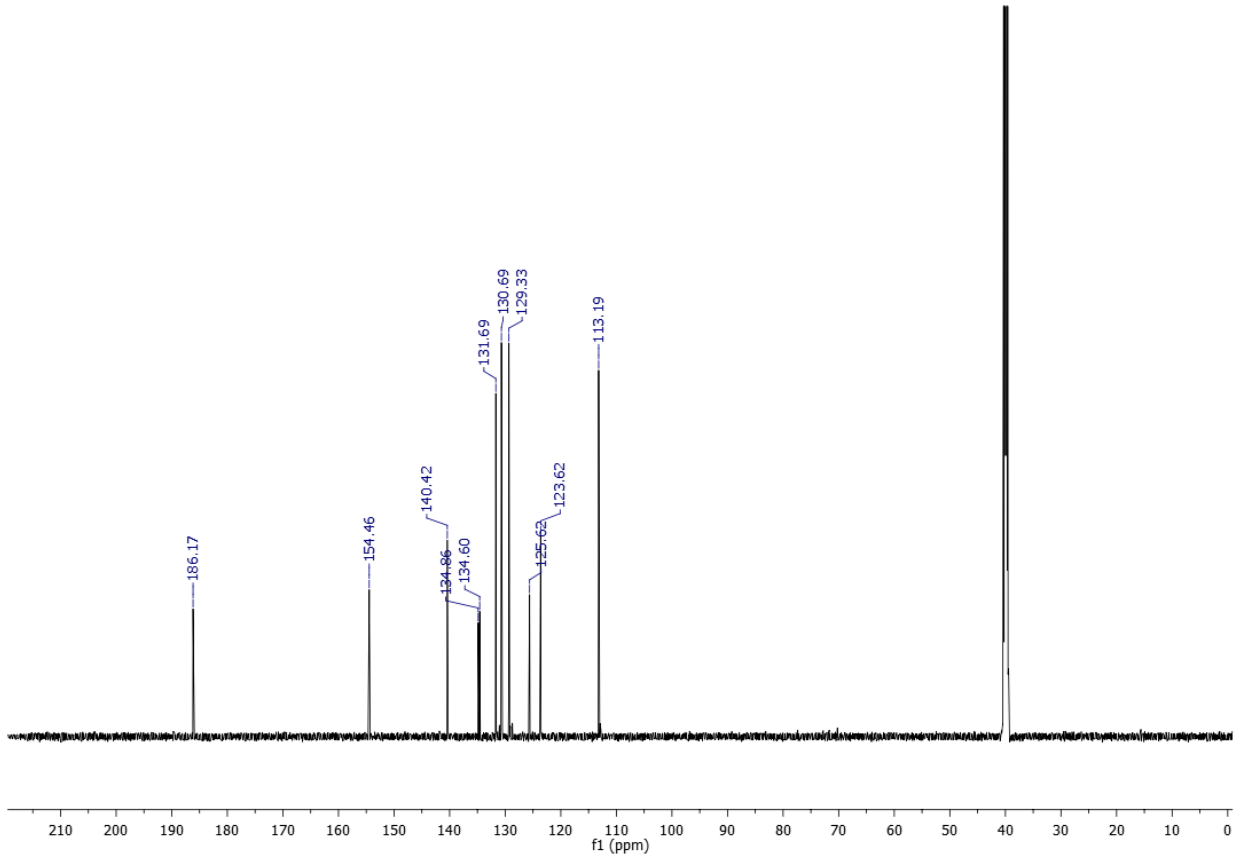

Figure SM71. Mass spectra (MS) of compound **6b**

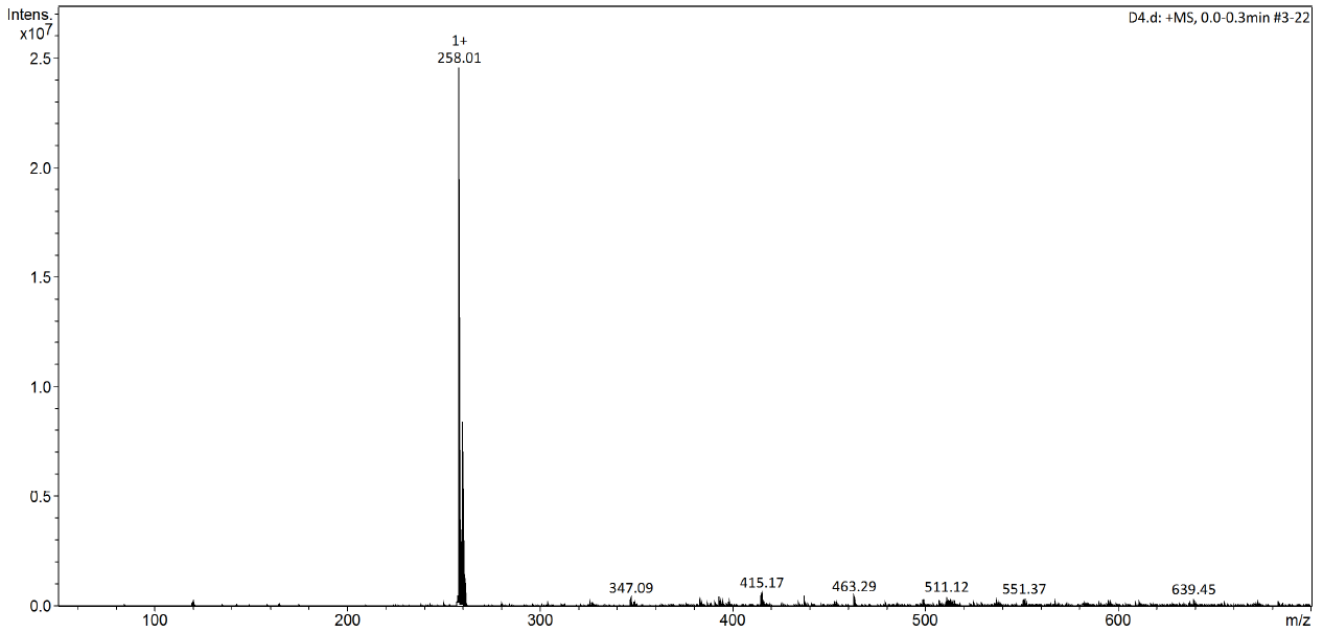

Figure SM72. UV-Vis spectra of compound **6b**

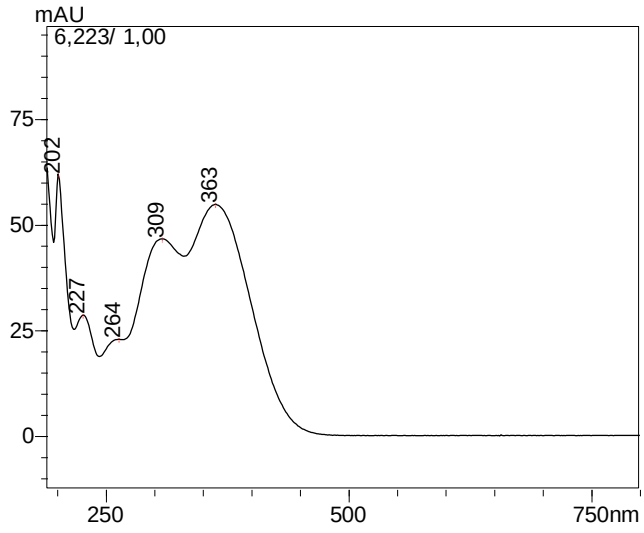

Figure SM73. HPLC cromatogram of compound **6b**

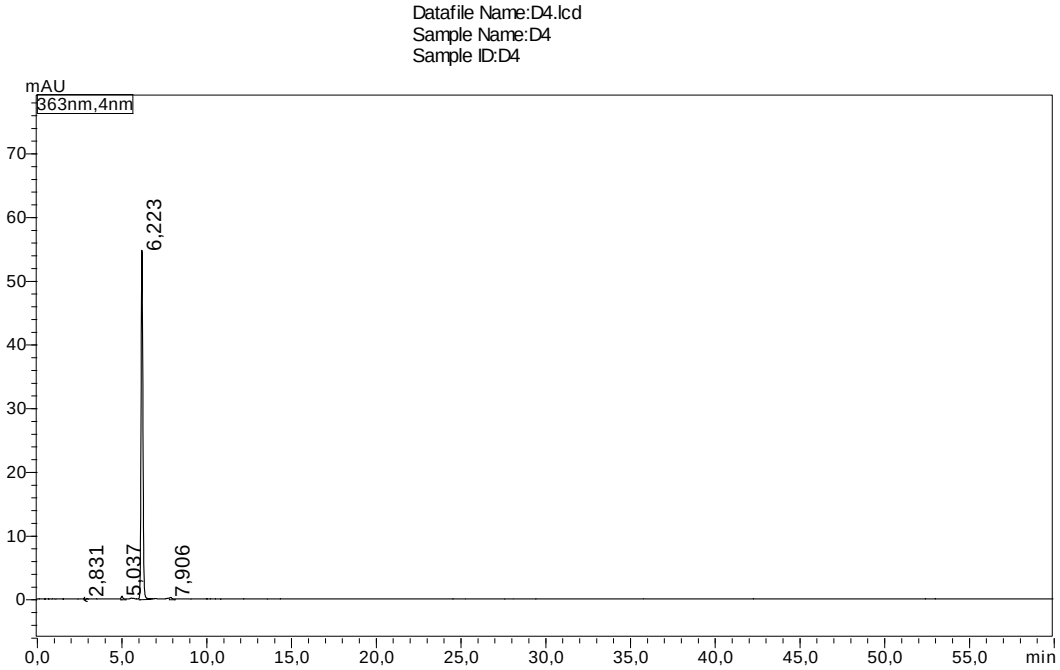

Figure SM74. ^{1}H NMR spectrum of compound **6c** (DMSO-d_6; 600 MHz)

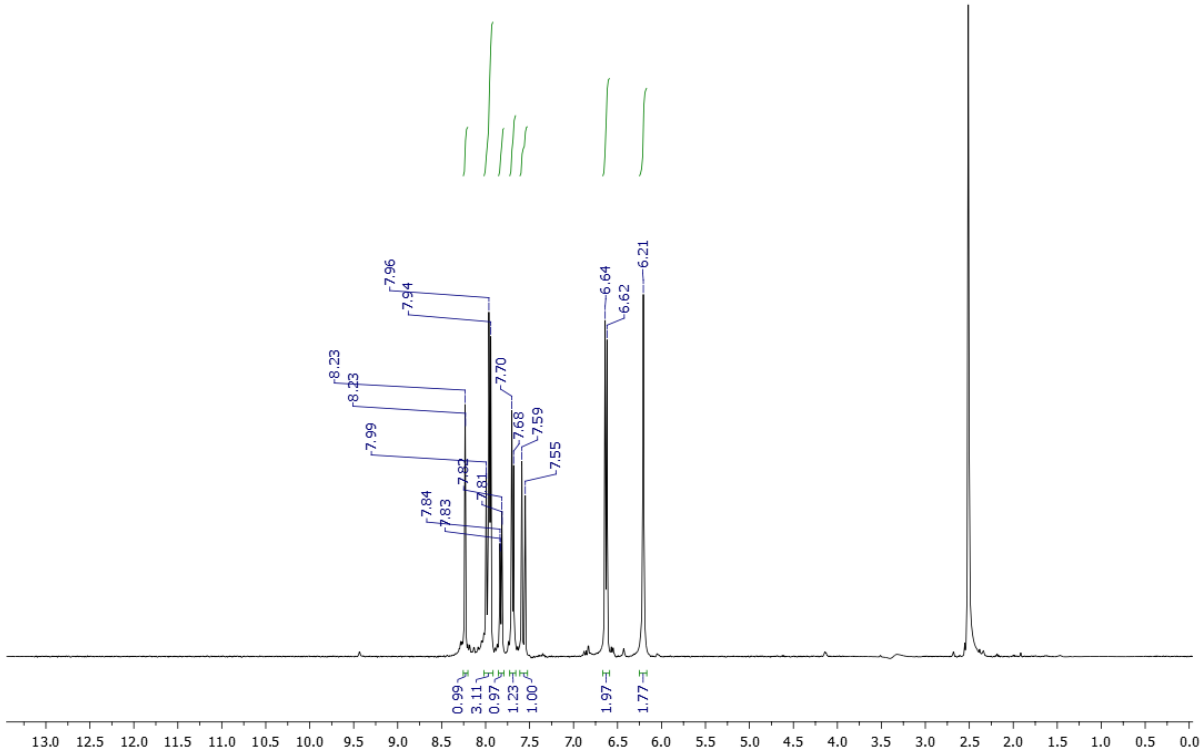

Figure SM75. ^{13}C NMR spectrum of compound **6c** (DMSO-d_6; 150 MHz)

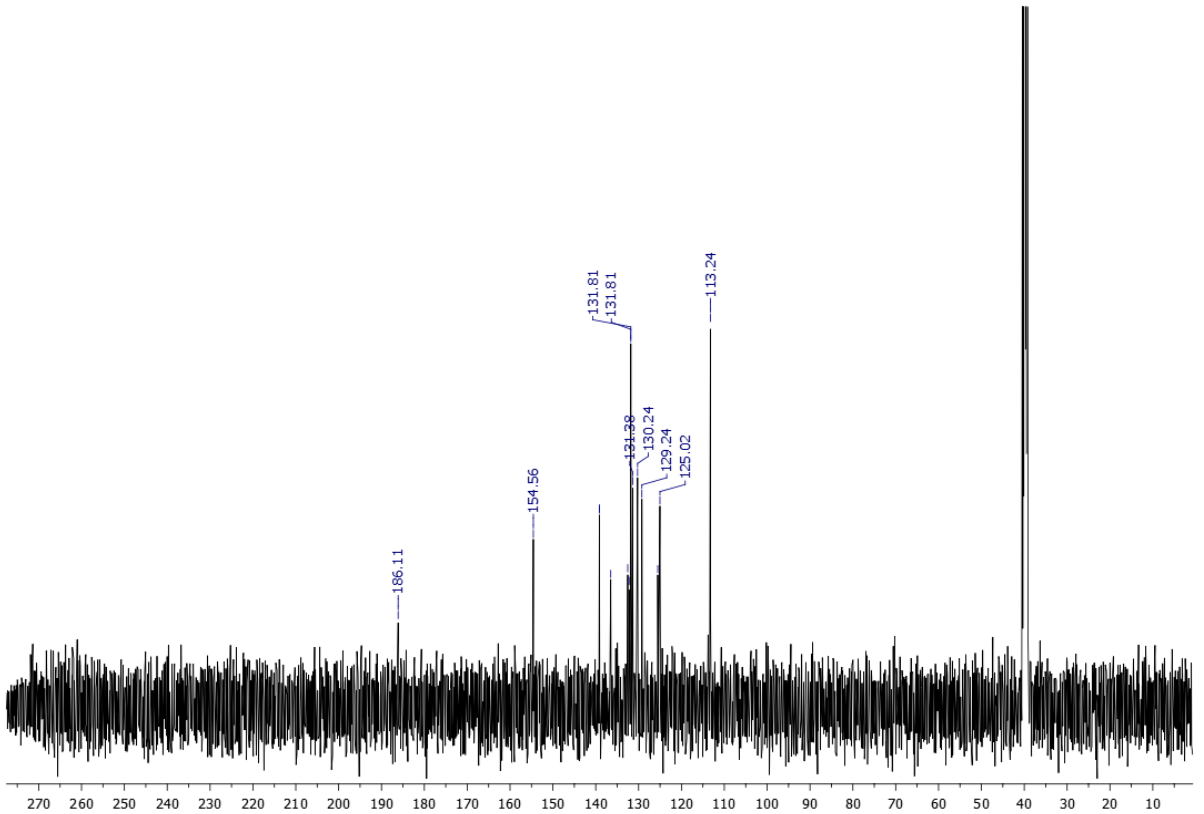

Figure SM76. Mass spectra (MS) of compound **6c**

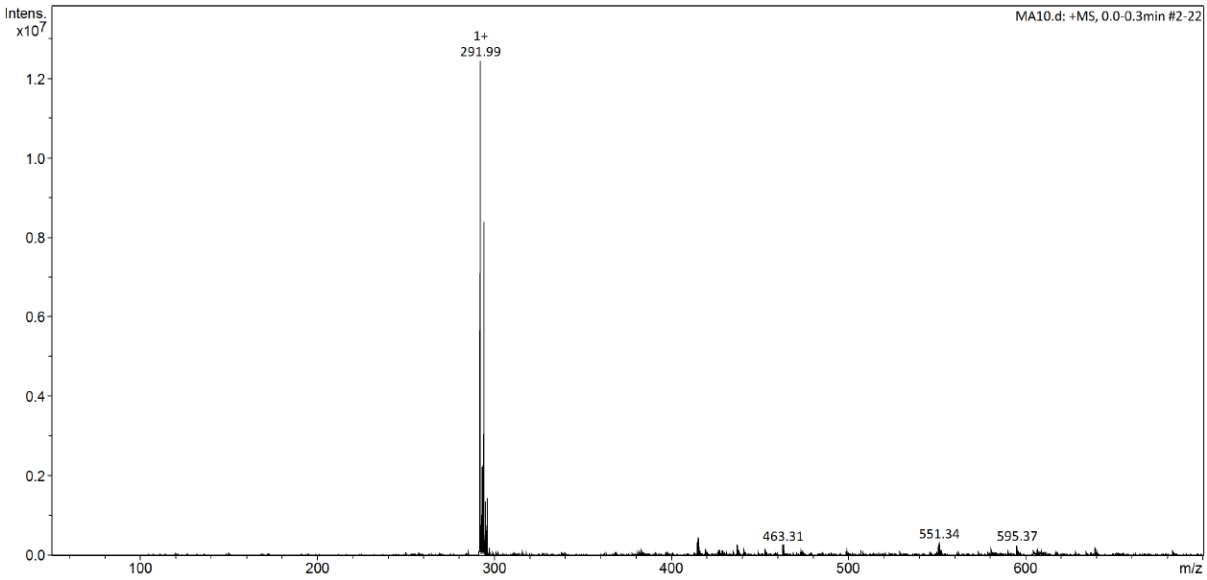

Figure SM77. UV-Vis spectra of compound **6c**

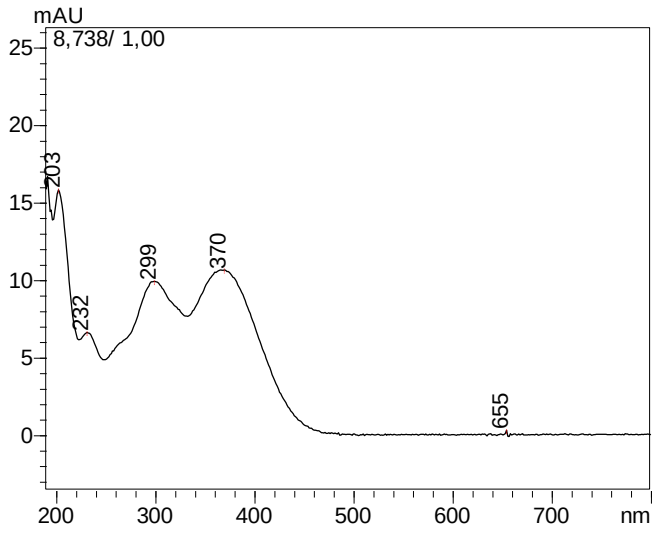

Figure SM78.HPLC cromatogram of compound **6c**

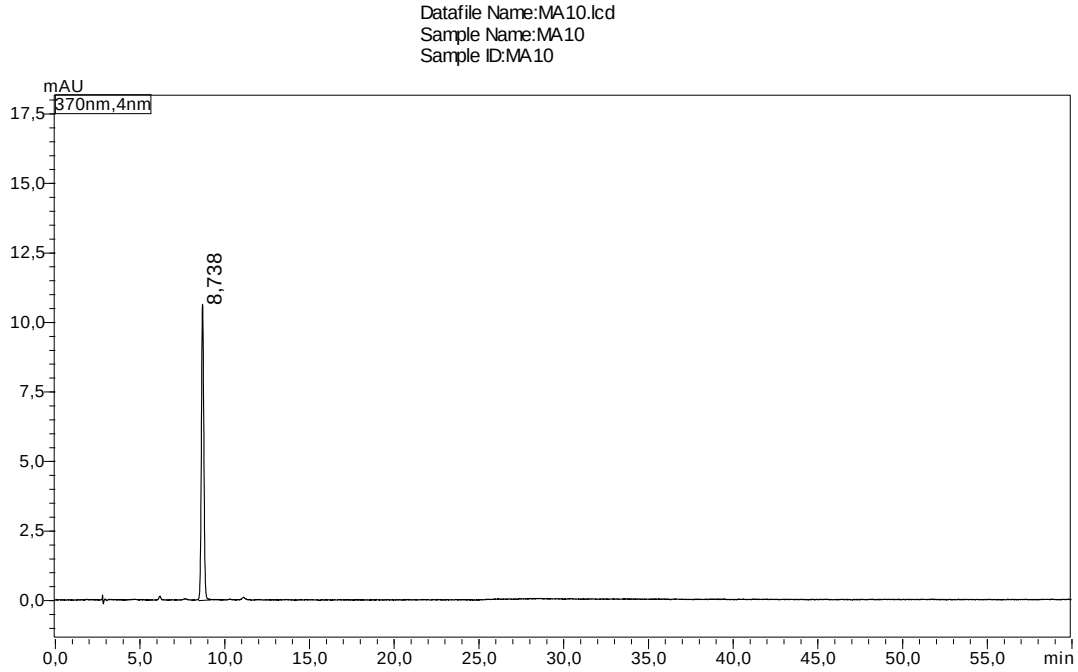

Figure SM79. ^{1}H NMR spectrum of compound **6d** (DMSO-d_6; 600 MHz)

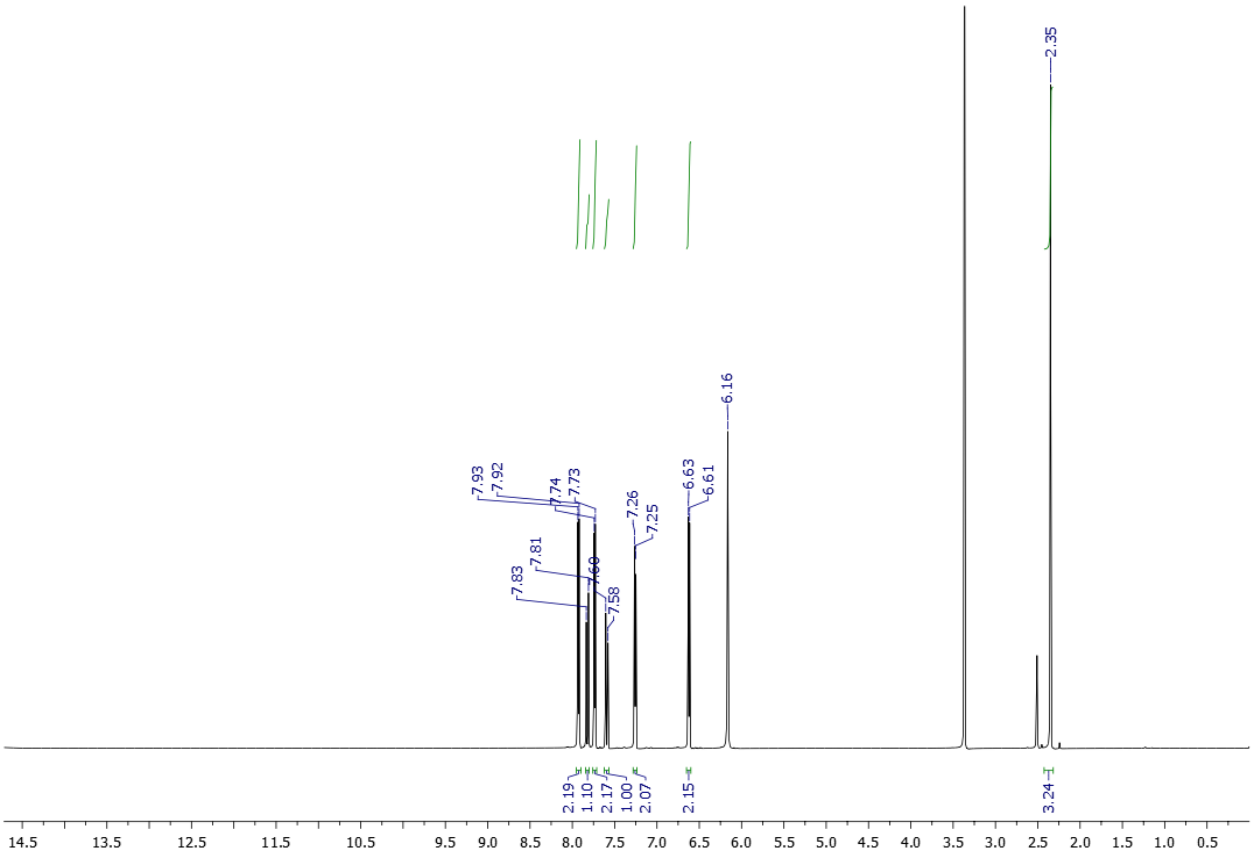

Figure SM80. ^{13}C NMR spectrum of compound **6d** (DMSO-d_6; 150 MHz)

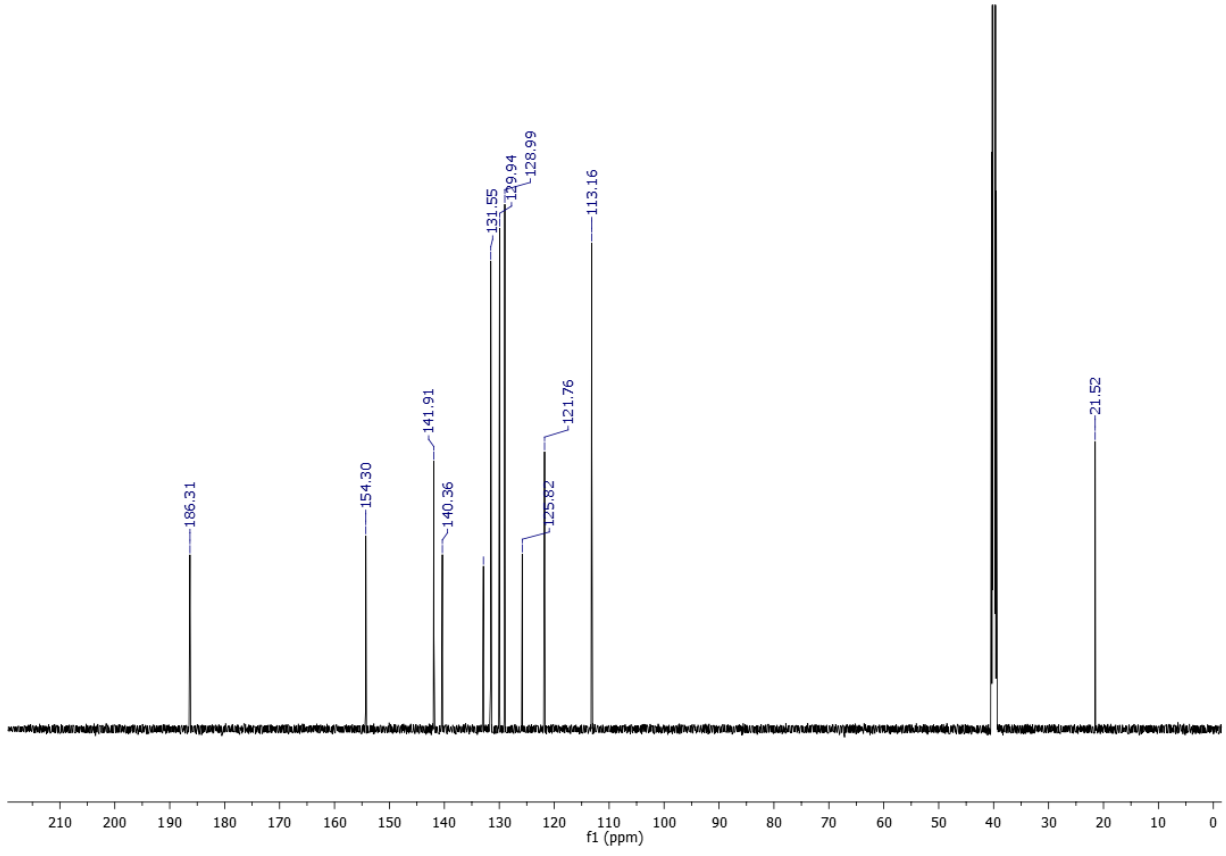

Figure SM81. Mass spectra (MS) of compound **6d**

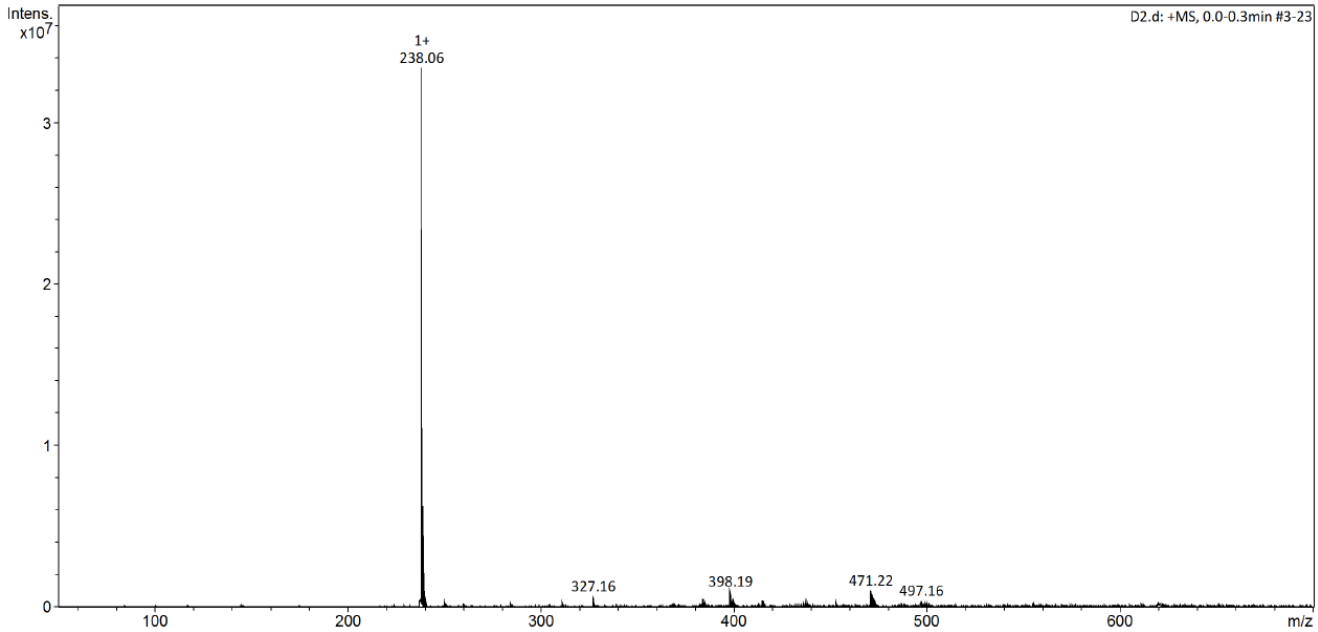

Figure SM82. UV-Vis spectra of compound **6d**

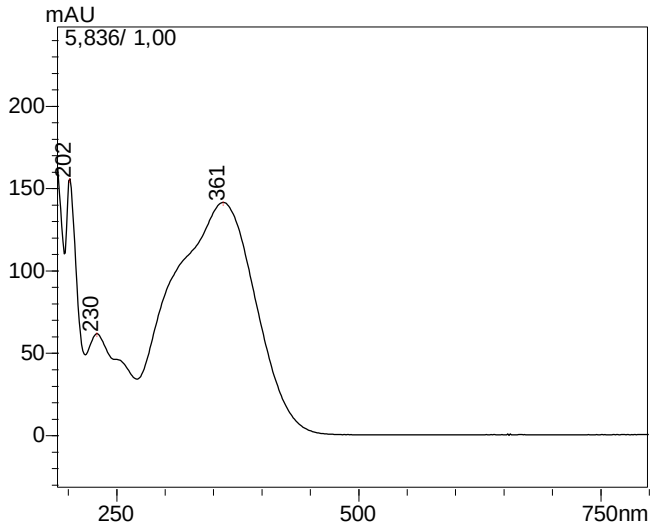

Figure SM83. HPLC cromatogram of compound **6d**

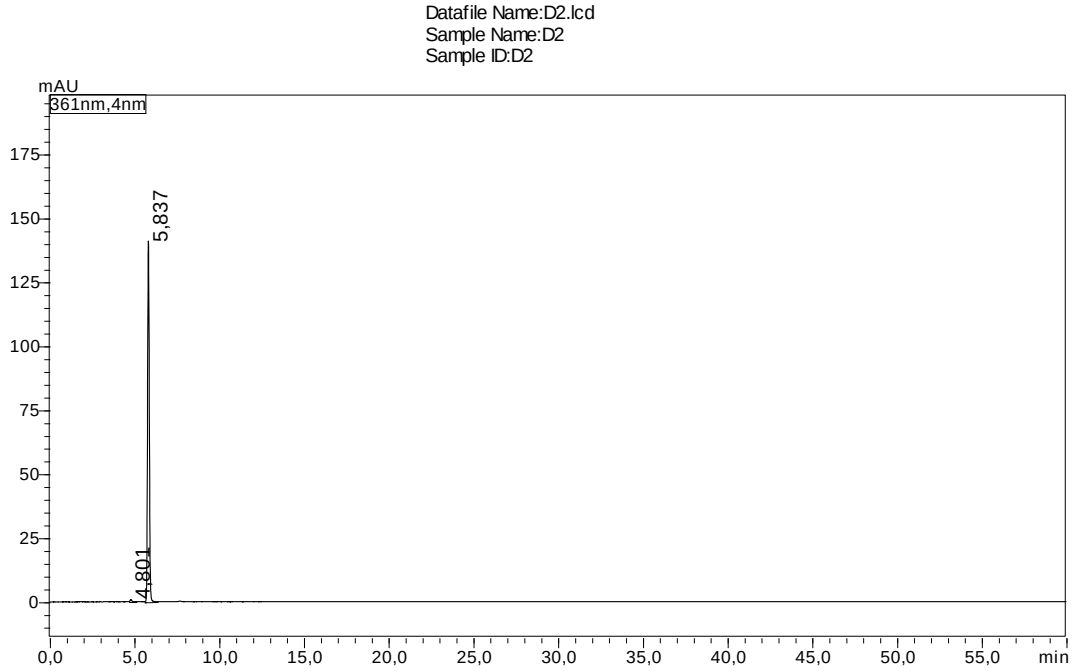

Figure SM84. ^{1}H NMR spectrum of compound **6e** (DMSO-d_6; 600 MHz)

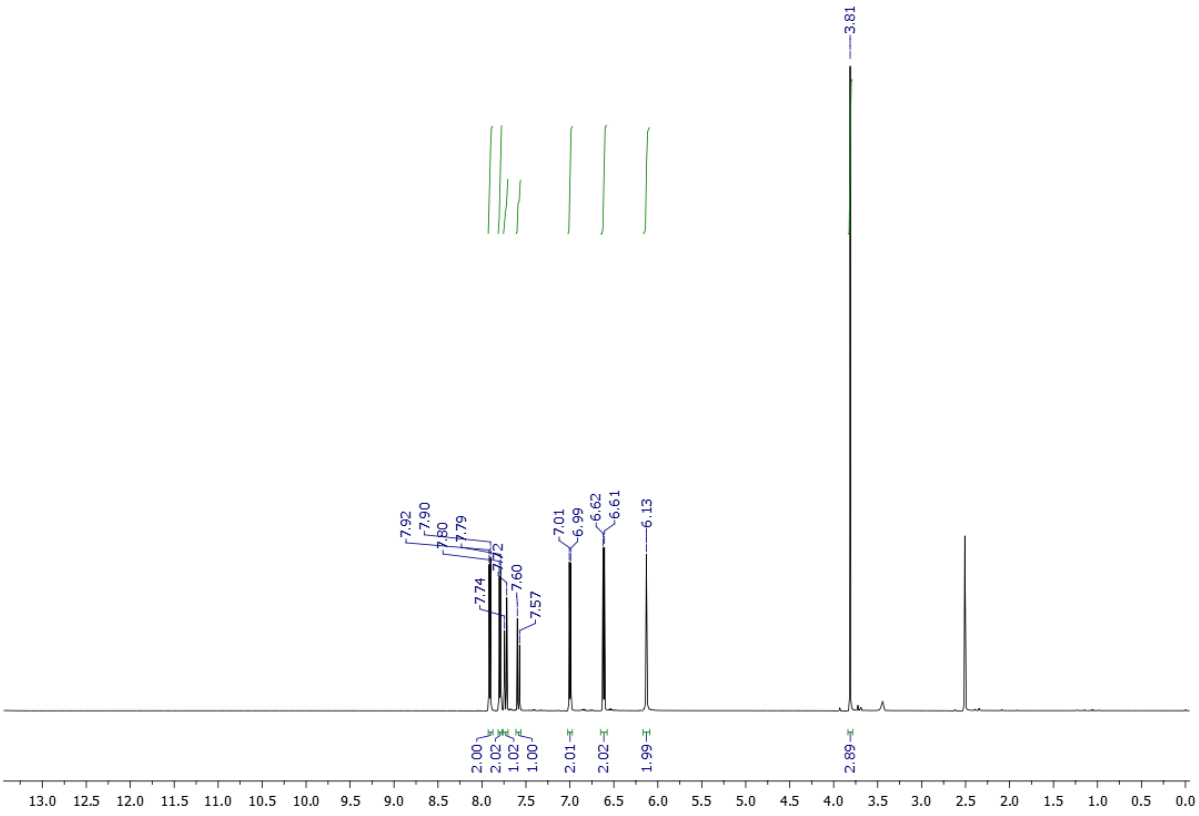

Figure SM85. ^{13}C NMR spectrum of compound **6e** (DMSO-d_6; 150 MHz)

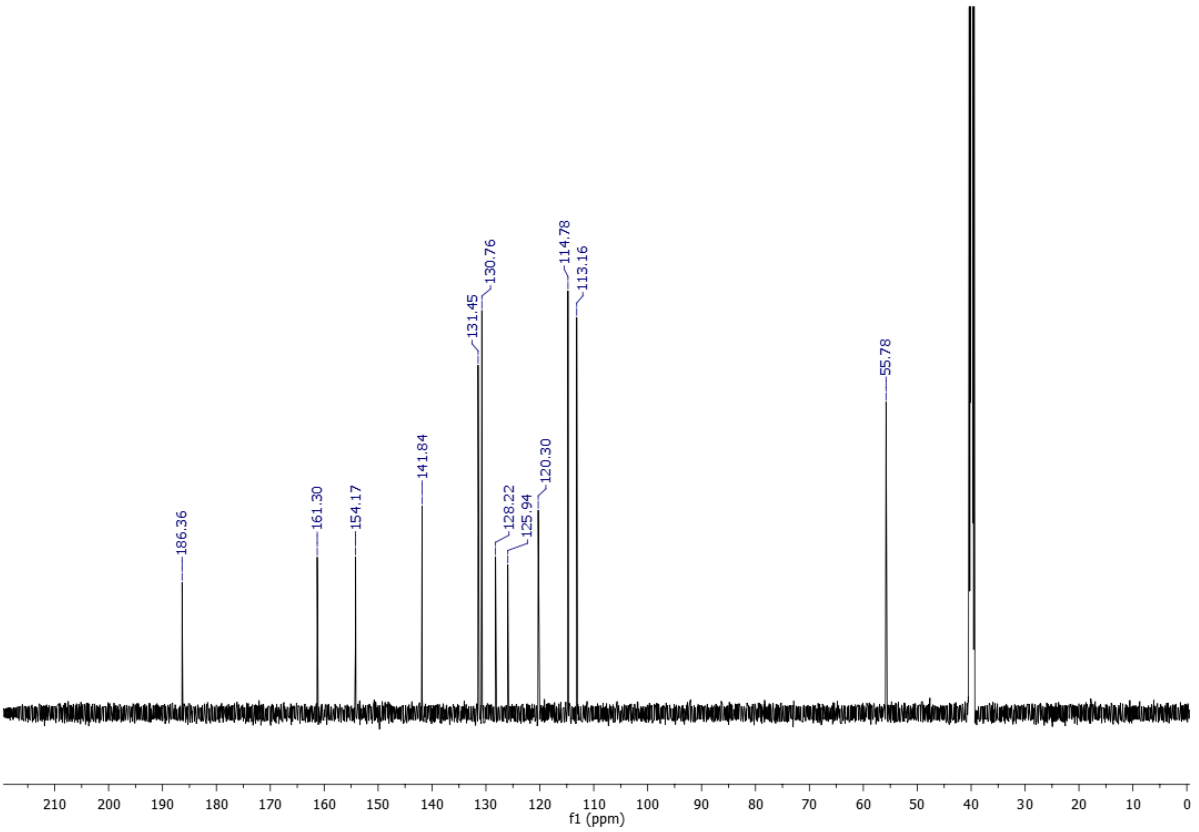

Figure SM86. Mass spectra (MS) of compound **6e**

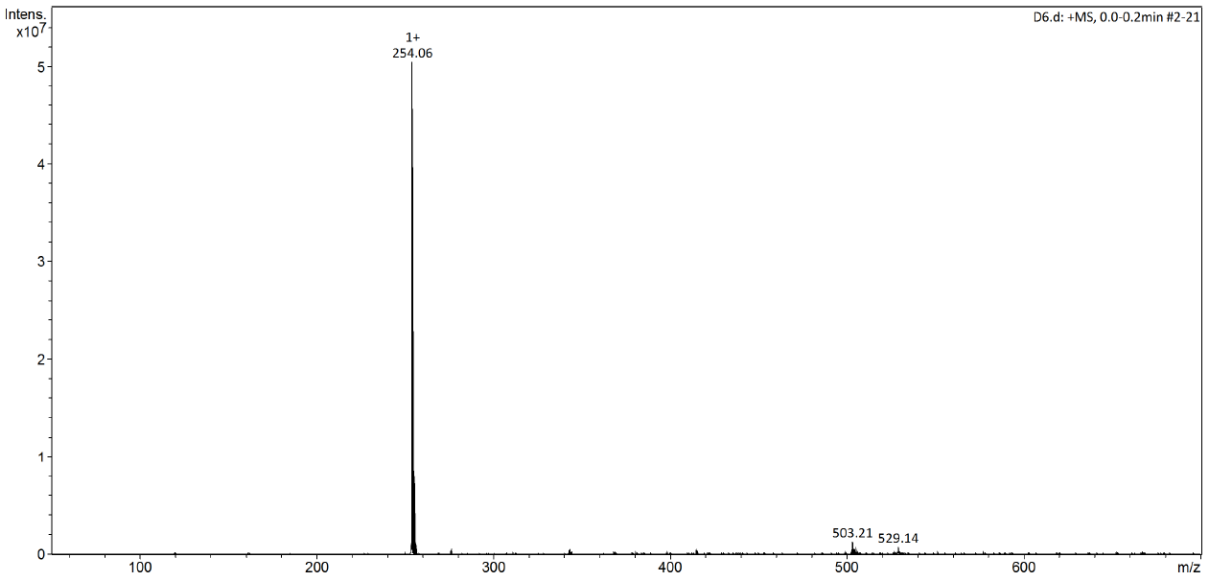

Figure SM87. UV-Vis spectra of compound **6e**

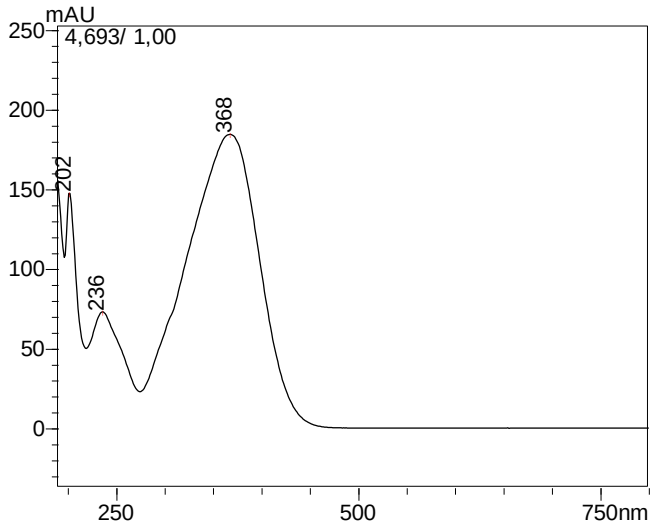

Figure SM88. HPLC cromatogram of compound **6e**

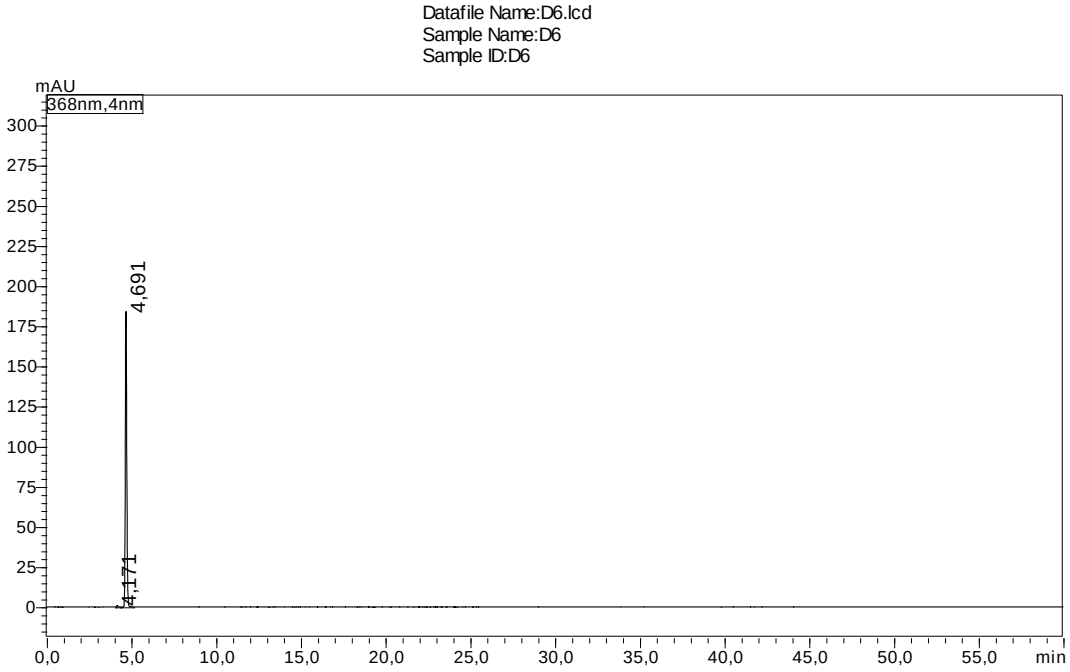

CAPÍTULO III

Bioorganic and Medicinal Chemistry

Synthesis and antifungal activity of chalcones against *Candida albicans* planktonic cells and biofilms

Mayara A. R. Garcia[a], Mariana B. Santos[a], Ricardo A. Z. Bertani[a], Janaína de C. O. Sardi[b], Pedro L. Rosalen[b], Luis O. Regasini[a,*]

[a]*Department of Chemistryand Environmental Sciences, Institute of Biosciences, Humanities and Exact Sciences, São Paulo State University Júlio de Mesquita Filho, São José do Rio Preto, SP, Brazil.*

[b]*Department of Physiological Sciences, Piracicaba Dental School, University of Campinas, Piracicaba, SP, brazil.*

*** Corresponding author.**

E-mail addresses: regasini@ibilce.unesp.br (LO Regasini)

ABSTRACT

Candida are opportunistic fungal that can become pathogenic when the patient has a compromised immune system. *Candida albicans* is the most important fungal opportunistic pathogen. *Candida* species can cause vaginits, cutaneous candidiais, candidemia and systemic infections. Also, fungal infections are considered a serious health problem and are a main cause of mortality worldwide. Thus, there a challenge in development of new compounds that act as antifungal. Herein, we designed and synthesized a serie of 40 chalcones, substituted by amino group on ring A, which were evaluated against five species of *Candida*. The antifungal potency was improved by substituents on ring B, which were designed according to Topliss' manual method and ring bioisosterism. 3-fluor-3'-aminochalcone (**3n**) was the most active, demonstrating minimum inhibitory concentration (MIC) values of 3.90 μg/mL against *C. albicans* and was selected for the subsequent tests in this strain. The association of **3n** with amphotericin B demonstrated synergistic effect against *C. albicans*, with Fractional Inhibiroty Concentration Index (FICI) value of 0.5. Subinhibitory concentration of **3n** inhibited the *C. albicans* adhesion to human keratinocytes. Chalcone **3n** was able to reduce *C. albicans* biofilm formation, as well as acts on preformed biofilm in concentration-dependent mode. Time-kill curve demonstrated that **3n** has fungicidal action after 12 hours of treatment. The mechanism of action assay indicated that **3n** interacts with membrane ergosterol, but not act on fungal cell wall of *C. albicans*. The acute toxicity assay, using *Galleria mellonella*, indicated low toxic effect of **3n**, after 72 h of treatment, displaying lethality to 20% larvae at 39 μg/mL and 390.0 μg/mL. These results demonstrate that **3n** is a potent anti-*Candida* agent with applications as an antifungal drug.

Keywords: Chalcone, Antifungal, Biofilm, Ergosterol

1. Introduction

Candida albicans is commonly found in the oral cavity, human intestine and vaginal microflora, but can become an opportunistic microorganism in immunocompromised individuals, being the main cause of nosocomial fungemia [1]. Infections caused by this species range from superficial mucosal lesions to systemic infections such as intra-abdominal abscess, peritonitis or osteomilitis. They have the ability to form biofilms on surfaces of medical devices, catheters and epithelial cells [2].

Resistance to antimicrobials is an obstacle that makes it difficult to treat various infectious diseases. One of the most common types of drug resistance is the ability of microorganisms to form biofilms on the surface of the skin and implanted medical devices [3–5]. When forming biofilm, *Candida* proliferates and forms a community of cells encased in a complex matrix, exhibiting resistance to several classes of drugs and is able to withstand concentrations of antifungals up to 1000 times higher than those that inhibit planktonic cells [6–8]. Many studies on biofilm, stem from *C. albicans*, however, other species are emerging that are capable of forming biofilm.

Amphotericin B has still been used as the drug of choice in treatment of systemic *Candida* infections. Although of *C. lusitaniae* and *C. guilliermondii*, demonstrate intrinsic resistance to amphotericin B, acquired resistance this drug is relatively rare [9]. Biofilms are approximately eight times more resistant to amphotericin B than their planktonic cells, depending on maturity of biofilm [10]. However, doses of amphotericin B necessary to reach the concentrations predicted to significantly reduce *Candida* biofilm cells are not safe to administer to patients.

Chalcones (or 1,3-diaryl-2-propen-1-ones) are recognized as privileged scaffolds by medicinal chemistry for drug discovery [11]. Some synthetic chalcones have show antifungal activity. Among them, naphthalene analogs demonstrated activity against *C. albicans* [12]. Messier and co-authors reported effect of chalcone 4-hydroxycordoin (1) against *C. albicans* biofilm. This chalcone was able to inhibit biofilm formation of *C. albicans* by 85% in concentration of 20 µg/mL. Also, concentrations ranging from 50 to 200 µg/mL caused a significant inhibition of yeast-hyphal transition [13].

In the search for new antifungal agents based in chalconic structures, we design and synthesized a series of 40 chalcones and evaluated their activity against five *Candida* species. The most active substance, 3-fluoro-3’-aminochalcone (**3n**) was selected for further bioassays including its effect associated with amphotericin B against *C. albicans* planktonic cells. Also,

we evaluated antifungal activity of **3n** against *C. albicans* biofilm formation and mature biofilms. We investigated the antifungal effect as a result of time, the ability of **3n** to prevent *C. albicans* adhesion to epithelial cells, the mode of action and determined *in vivo* acute toxicity using *Gallera mellonella* model.

2. Results and discussion

2.1. Compounds synthesis

We designed three series of 40 chalcones substituted by amino group at position 2', 3' and 4' (ring A) and benzene ring B substituted by withdrawing/donating electron groups. Also, were synthesized aryl analogues with benzene exchanged for furan, thiophene and pyridine rings. Chalcones were synthesized by Claisen-Schmidt reaction with isolated yields ranging from 50% to 95% after chromatographic purification over silica gel (Figure 1) [14].

Structure of chalcones was confirmed by ^{1}H NMR, ^{13}C NMR and UV spectral data analyses. Unprecedented substances in literature were analyzed by high resolution mass spectrometry (HRMS).

Figure 1

All NMR parameters, as hydrogen and carbon chemical shifts (δ_H and δc in ppm), integrations, multiplicities and coupling constants (*J* in Hz) corresponded to designed structures. Two typical aminochalcone signals in ^{1}H NMR spectra were diagnosed: (*i*) a pair of doublets with *J* values ranging from 15.2 Hz to 15.8 Hz, attributed to two hydrogens of carbon-carbon double bond with *E* configuration and (*ii*) broad singlets between ~7.4 ppm, ~5.4 ppm and ~6.2 ppm, related to two hydrogens of amino group at positions 2', 3' and 4', respectively. In ^{13}C NMR spectra, ketone signals were registered in 186.1 ppm $\leq \delta_C \leq$ 191.0 ppm, attributed to carbonyl carbon. HRMS spectra exhibited base peaks attributed to protonated molecule $[M+H]^+$. UV-Vis demonstrated λ_{max} values ranging from 286 nm to 370 nm, evidencing a chromophoricresoningπ-electrons system. HPLC-PAD data analyses of peak area indicated the chalcone purities, which ranging from 97% to 100%. All spectra and chromatograms are presented in supplemental material.

2.2. In vitro antifungal activity of aminochalcones

All chalcones were submitted to antifungal evaluations against *Candida albicans*, furnishing MIC and MFC values (Table 1). Series of compounds demonstrated active and inactive chalcones, suggesting that molecular variations were relevant for activity against *C. albicans*.

Table 1

In previous studies conducted by El-Din and co-authors, higher pH values were able to reduce *Candida albicans* adhesion to epithelial cells [15]. This encouraged us to investigate chalconic analogs with alkaline properties. Thus, we designed a series of chalcones substituted by amino group at *ortho*-, *meta*- and *para*-positions in ring A.

Firstly, we evaluated chalcones with amino positions 2' (**2a**, MIC = 62.5 μg/mL), 3' (**3a**, MIC = 15.6 μg/mL) and 4' (**4a**, MIC = 31.2 μg/mL) unsubstituted ring B, which were active against *C. albicans*. Those results encouraged us to prepare further analogues with substitutions on ring B.

Mohammed and co-authors described that organic compounds containing aromatic heterocyclic rings, such as thiophene and furan, are widely distributed in nature and generally of great importance in several biochemical processes, having a broad spectrum of biological activities [16]. Also, we imagine that analogues with rings containing six π electrons, similar to phenyl ring, could be bioactive [17]. 2-thiophenylchalcone was inactive in series 2' (**2b**) and 3' (**3b**), and 2-furanylchalcone was inactive in series 2' (**2c**). Pyridinylchacones were active in all series (2', 3' and 4'). Therefore, we concluded that six π electrons were not crucial to anticandidal activity. However, the bioactivity of pyridinylchalcones could be related to basicity of pyridine ring.

Amole and co-authors indicated that electronic density was crucial parameter to anticandidal activity of chalcones [18]. We assayed analogues substituted by electron-withdrawing groups (EWG), as chloro, and electron-donating groups (EDG), as methyl and methoxyl. However, substitutions by EDG in three series did not enhance the anticandidal effect, corroborating the negative effect of electron-donating groups for bioactivity. On the other hand, 3'-aminochalcones substituted by chloro (**3h**, MIC = 31.2 μg/mL) and dichloro (**3i**, MIC = 31.2 μg/mL) were active. The bioactivity comparison of the series **2**–**4** suggests 3'-aminochalcones (**3a**–**3i**) were more active than 2'-aminochalcones (**2a**–**2i**) and 4'-aminochalcones (**4a**–**4i**), evidencing the amino group position is essential to anticandidal activity. Based on results, we selected 3'-amino series to evaluate the effect of halogens (Cl,

Br and F) in different positions of ring B. Fryer and co-authors reported that steric effect caused by substitution of halogens in ortho position can impose certain conformations and alter biological functions, as in clonidine, an ortho-ortho replacement if chlorine, prevent free rotation and maintain the planes of aromatic rings perpendicular to each other [19, 20]. The substitution of 2,6-diCl (**3j**) increased the effect against *C. albicans* (MIC = 7.8 µg/mL), suggesting that ortho-ortho effect is an important antifungal parameter. Also, according to classification of potency of halogens in positions 2, 3 and 4 on ring B, fluorine led the most potent halogenated chalcones, followed by chloro and less potent bromine. Fluorine (position 3, **3n**) was the most active compound with MIC value of 3.90 µg/mL. In summary, smaller and more electronegative halogens corroborated to activity against *C. albicans*. Finally, we assayed analogues strongly EWG, as 4-trifluoromethoxyl (**3s**), 3-trifluoromethyl-4-chloro (**3t**) and nitro (**3u** and **3v**). However, substitutions by this groups did not enhance the anticandidal activity, suggesting electron-density on ring B is an important parameter to bioactive effect. The lowest MIC and MFC values displayed by **3n** encouraged us to select it for detailed anticandidal investigations in additional bioassays against *C. albicans*.

2.3. Checkerboard assay

We evaluated the effect of combination of **3n** with amphotericin B against *C. albicans* (Table 2). The combination with **3n** decreased MIC value of amphotericin B from 0.5 to 0.1 µg/mL. The 5-fold reduction of amphotericin B MIC values may be a therapeutic advantage, because leads to administrationof lower doses of amphotericin B and chalcone. Amphotericin B is an effective antifungal agent, however, its therapeutic use is hampered by its toxicity, including nausea, vomiting, rigors, fever hypertension and hypoxia [21]. The combination of **3n** and amphotericyn B evidencing synergic association, since FICI values was 0.4. In addition, resistance associated with planktonic cells and biofilms has already been studied *in vitro*, and there are reports that biofilms are resistant to amphotericin B [22]. The combination of antifungal agents may delay the onset of microbial resistance, resulting in synergistic effects that aid in the treatment of these infections [23]. Among these, clinical use of flucytosine is preffered in association of amphoterycin B [24, 25]. Also, the literature brings the association of chalcones with antifungals drugs, as Wang et al., that described the effect on the association of chalcones with fluconazole against *C. albicans*, resulting in 15 chalcones with a significant reduction in MIC values when combined with antifungal [26]. Our study

indicated that chalcones in association with amphotericyn B may have action against *Candida*.

Table 2

2.4. Time-kill

We evaluated the influence of exposure time and the concentration of chalcone **3n** on the fungal death process (Figure 2). Amphotericin B was also evaluated for comparison of antifungal action. Chalcone **3n** and amphotericin B showed similar reduction of viabilityuntil 4 hours. Fungicidal activity is usually determined by a decrease of 3 log10 units in the UFC/mL compared to the starting inoculum [27]. In 12 hours chalcone **3n** demonstrated fungicidal effect in both concentrations with a reducion of ≥3 log10 CFU/mL compared to starting inoculum. Amphotericin B demonstrated fungicidal effect in 8 hours and 12 hours for 10xMIC and MIC, respectively. In this context, fungicidal activity isclinically more importante than a fungistatic activity because the prophylactic use of fungistatic drugs has been associated with an increased frequency of drug resistance [28]. In addition, is pharmacologically important because the rapid elimination of microorganisms guaranteed therapeutic succes to prevent the spread of pathogens and disease progression [29]. Time-kill studies provide a more dynamic assessment of interaction between na antimicrobial agente and na organismo, such as pharmacodynamic characteristics or whether an agent produces dose or timedependent deaths [30].

Figure 2

Time-kill graph demonstrated that chalcone **3n** is dose and time dependent. Time-kill studies are not often used to guide therapy in a patient, however, they are useful for determining tolerance to lethal activity by antimicrobial agentes [31]. Similarly, Andrade and co-authors demonstrated the maximum fungicidal effect of 2,4-dihidroxichalcone at 2 × MIC in 6 hours.

2.5. Anti-adhesion to HaCat assay

Candida species are frequently colonizers of skin and mucosal surfaces, including urinary tract and oral cavity and infections involve cutaneous lesions [32]. In this context, we investigated the inhibition of **3n** on adhesion of *C. albicans* in human keratinocytes. The inhibitory effect of *C. albicans* adhesion to HaCat cells was tested in three different times and

concentration of ½ MIC value. The results indicated that 3n treatment at 1.9 µg/mL led to a small decrease in adhesion to HaCat cells (P<0.05) over time compared to untreated cells (Figure 3). The greatest inhibitory effect against *C. albicans* was at 1 hour. The chalcone showed anti-adherence effect similar to amphotericin B in the three times tested. In order to verify whether **3n** demonstrated toxicity agains HaCat cells, which could interferonanti-adhesion assay results, the cell viability was measured by MTT assay. At MIC/2 concentration, chalcone demonstrated 96% cell viability, indicating low toxicity. The anti-adhesion effect of **3n** on *C. albicans* is important to avoid the infection, once that microbial adhesion is the initial stage for biofilm formation, as it provides contact between microbial planktonic cells and a [33]. Initial adhesion is accomplished by superface adhesin proteins that are attached to the cell wall and interact with other cells or substrates [34].

Figure 3

2.6. Antibiofilm assays

Biofilm is defined as a complex polymeric structure of microorganisms, wrapped in an extracellular matrix, facilitating its virulence, besides exerting a barrier against drugs [35]. In this context, cells in biofilms and planktonic cells present notable differences with respect to their metabolism. Really, the development of biofilm begins when planktonic cells adhere to substrate and then grow and divide, creating a polymeric matrix including secreted exopolysaccharides (EPSs) [36]. *C. albicans* forms strongly structured biofilms composed of several types of cells (yeast, oval pseudo-hyphae or elongated hyphae) in an extracellular matrix [37]. Once formed on a surface, *C. albicans* biofilms acts as a reservoir for pathogenic cells, highly resistant to drugs and the host immune system, sowing infections in blood stream that can lead to systematic infections of tissues and organs [38]. Several classes of compounds are being studied to fight infections by biofilms, including azoles, polyenes and echinocandins [39]. Our group has been looking for molecules with antibiofilm activity of *C. albicans* including nitrochalcone and pentyl caffeate [40]. Herein, we evaluated the effects of **3n** on *C. albicans* biofilm formation and preformed biofilm. Chalcone **3n** and vancomycin was evaluated for their capacity to inhibit biofilm formation at respective MIC and 10 × MIC values (Figure 4). We performed a quantitative assay for determination of CFU/mL after initial biofilm formation. Treatment with **3n** and amphotericin B at MIC values did not inhibit the *C. albicans* biofilm formation. On the other hand, treatment with **3n** and amphotericin B at 10 × MIC values caused a significant decrease of *C. albicans* biofilm formation as

compared to the untreated groups ($P < 0.05$). At 10 × MIC the inhibitory effect against biofilm formation of **3n** was similar than amphotericin B, with a reduction of 3 $\log_{10}$ CFU/mL when compared to the untreated control. The activity of **3n** against *C. albicans* biofilm formation can cause damage in development of matrix.

Figure 4

We performed a quantitative assay for evaluated the effect of chalcone **3n** and amphotericin against biofilm pre-formed of *C. albicans*. The compounds were tested at their respective MIC and 10 × MIC values. Figure 5 shows that treatment with **3n** and amphotericin B at MIC values did not affect the survival of *C. albicans* biofilm. On the other hand, treatment with **3n** and amphotericin B at 10 × MIC values caused a smiller decrease of *C. albicans* preformed biofilm when compared to the untreated groups ($P < 0.05$). A characteristic of *C. albicans* biofilms is the presence of an extraceellular matrix formed during the maturation phase of the development of biofilms and encompasses a complex matrix of yeast, pseudohyphae and hyphal cells, providing protection against host immune defenses and antifungal drugs, and contributing to dimensional stability of biofilm [41].

Figure 5

Chalcone **3n** was able to decrease the survival of preformed biofilm, avoiding the complete maturation of biofilm. Antibiofilm activity of **3n** can be useful to combat preformed biofilm, preventing biofilm dispersion.

2.7. Mechanism of action assay

The fungal plasma membrane is formed by a double layer of phospholipids with intercalated proteins, in addition to also performing the function of selective transporto f substances from the extra and intracellular medium [42]. In this context, the main steroid present in fungal membrane is ergosterol which performs the same function as cholesterol in mammalian cell membranes [43].

With presence in fungal membrane and absent in human cells, ergosterol becomes an important molecular target, especially for drugs that interact with this sterol, forming pores and altering cellular permeability, such as amphotericin B [44].

Amphotericin B exerts its mechanism of action on the cell membrane by forming complexes with the ergosterol present in these membranes. As a consequence, occurs formation of channels that facilitate the exit of cytoplasmic content, leading to death of microorganism [45]. To assess whether chalcone **3n** act by this mechanism against *C.*

albicans, forming a complex with ergosterol, we determine MIC values in presence and absence of ergosterol. If fungal activity occurs thorugh the connection between chalcone and ergosterol, the exogenous ergosterol present in medium will prevent the binding to ergosterol the fungal cell membrane, since it is more available in medium, allowing fungal growth in the medium, a greater amount of chalcone would be needed to eliminate the fungus, leading to increased MIC [46].

MIC value of chalcone **3n** increased from 3.9 to 7.8 µg/mL in presence of ergosterol constaining *C. albicans* medium, suggesting that acts by this mechanism of action (Table 3). Amphotericin B exhibited increased of MIC from 0.5 to 16.0 µg/mL in presence of ergosterol, demonstrating the assay effectiveness.

Table 3

To investigate the action of chalcone **3n** on the cell wall of *C. albicans*, we performed the assay with sorbitol. Sorbitol is an osmotic protector used to establish protoplasts of fungi. Specific cell wall inhibitors have their antifungal effects inhibited in presence of sorbitol [47].

Cells are protected with sorbitol and grow even in presence of cell wall inhibitors, whereas in absence of sorbitol growth would be inhibited. This effect is detected by the change in MIC value in presence and absence of sorbitol [48]. If chalcone is an inhibitor of cell wall, it will cause fungal death in absence of a stabilizer, but in presence of sorbitol the preservation of microorganisms will occur, allowing their growth, which is evidenced by the increase in MIC value in sorbitol medium [46].

Chalcone **3n** showed no change in MIC (3.9 µg/mL) when added in *C. albicans* medium supplemented with 0.8 M sorbitol, suggesting that this compound does not inhibit fungal cell wall (Table 4). Caspofungin exhibited increased of MIC from 0.1 to 15.6 µg/mL in presence of sorbitol, confirming the assay effectiveness.

Table 4

Similarly, Andrade et al., reported the action of chalcones against *C. albicans*. Chalcone 2,4'-dihydroxychalcone exhibited binds to exogenous ergosterol but does not interfered with the synthesis of the fungal cell wall, corroborating our results [49].

2.8. Acute toxicity assay

In order to preliminarily evaluate toxicity of chalcone **3n** for clinical use, an alternative model of *Gallera mellonella* larvae was performed. Insect testing has ethical advantages and is economically viable over mammal testing, as well as providing rapid and

effective results on toxicity *in vivo*. Moreover, the results of *G. mellonella* models are comparable to those performed in mammals [50]. Their larvae have structural and functional similarities to mammal complexity, between them innate immune response, as well are well-accepted as an ethicalalternative for investigations [51]. Larva survival after vehicle treatment was 100% for 72 hours (Figure 6). In evaluated period, chalcone 3n did not demonstrate significant acute toxicity, exhibiting 10% and 20% larval mortality in values of 10 × MIC and 100 × MIC, respectively. Amphotericin B was not toxic to G. melonella larvae, showing a mortality of 5 to 10% in values of 10 × MIC and 100 × MIC, respectively.

Figure 6

These results motivate further toxicity studies in vertebrate animal models, as chalcone didn't show acute toxicity when tested at concentratin one hundred times highter than those used against *C. albicans* biofilms.

2.9. Additional anticandidal assay

In order to assess the anticandidal spectrum, chalcone **3n** was evaluated against another species of *Candida*. Chalcone **3n** was the most active against all strains tested, including *C. tropicallis*, *C. parapsilosis* and *C. glabrata* cells, exhibiting MIC values of 1.9, 3.9 and 1.9 μg/mL, respectively. Against these bacterial species, amphotericin B demonstrated MIC value of 0.5 μg/mL. *C. krusei* has been recongnized as a potentially multidrug-resistant (MDR) fungal pathogen, due to fluconazole resistance combined with reports of decreased susceptibility to both flucytosine and amphotericin B [30]. In this context, **3n** exhibited activity against *C. krusei* with MIC value of 7.8 μg/mL, demonstrating the importance of discovering new drug with antifungal action.

3. Conclusions

Our study reported that 3'-aminochalcones are potent agents against various *Candida* species and preliminary SAR investigations suggesting that halogens on ring B play a central role in anticandidal activity. In addtion, 3-fluor-3'-aminochalcone (**3n**) exhibited an inhibitory effect on mature and formation biofilm similar to amphotericin B, proving favorable in combating fungal resistance. Chalcone **3n** led to a decrease in *C. albicans* adhesion to

epithelial cells from the first hour of contact, proving to be effective in the first stage of biofilm formation. This compound demonstrated fungicidal effect against *C. albicans* after 12 hours of treatment. In addition, it is suggested that **3n** has a mechanism of action similar to amphotericin B, interacting with ergosterol, the main sterol of fungal plasma membrane, leading to alteration of membrane permeabilide. This assertion is reinforced with the resuult of combination of amphotericin B and sinergic effec **3n**, suggesting that two compounds act together by the same mechanism of action. Additionally, the sorbitol assay demonstrated that **3n** does not act on *C. albicans* cell wall synthesis. Finally, the in vivo model toxicity test showed that chalcone **3n** has less than 20% toxicity within 72 hours when administered at concentration of 100 × MIC.

4. Experimental section

4.1. General procedure for the synthesis of compounds

Reagents and solvents were purchased from Merck®. Series of chalcones was synthesized by Claisen-Schmidt aldol condensation, according Santos and co-authors [52]. Aldehyde derivatives (5 mmol) were added to a ethanolic solution of aminoacetophenone (5 mmol in 20 mL) in sodium hydroxide (1 mol/L) and the reaction mixture was kept at room temperature. Reagents conversion was monitored by thin layer chromatography. Products were poured onto ice from distilled water and filtered. All products were purified over sílica gel chromatography column eluted with mixtures of hexane and ethyl acetate. Melting points of the compounds were measured on open capillaries on Melt Temperature apparatus MS Tecnopon PFM-II. UV-Vis spectra and chromatograms were obtained in High Performance Liquid Chromatography with Diode Array Detector (HPLC-DAD) Agilent Tecnlogies® 1220 Infinity equipament, photodiodo array system (Agilent Tecnologies® Model 1260 Infinity) and Agilent Zorbax Eclipse Plus C-18® column (250 mm x 4.6 mm, 5 µL) using methanol:water (3:1) as mobile phase (1.0 mL/min). NMR spectra were obtained in a BrukerAvance III (14 T, 600 MHz) and BrukerAvance III (7 T, 400 MHz) spectrometer, using deuterated dimethyl sulfoxide (DMSO- d_6) as solvent. High Resolution Mass Spectra were obtained in ABSciex 5600 QTOF equipament (in positive mode) for unpublished chalcones.

(*E*)-1-(2'-aminophenyl)-3-phenylprop-2-en-1-one) (**2a**) Yellow solid, yield = 82%, mp = 61 – 63 ºC, purity: 99%, $\lambda_{máx}$ = 301 nm. ^{1}H NMR (600 MHz, DMSO) δ 6.59 (ddd, *J* = 1.0,

7.7 and 7.7; H-5'), 6.80 (d, *J* = 7.7; H-3'), 7.29 (ddd, *J* = 1.0, 7.7 and 7.7; H-4'), 7.43 (s, 2-NH_2), 7.60 (d, *J* = 15.5; H-α), 7.65 (d, *J* = 8.4; H-3, H-4 and H-5), 7.84 (d, *J* = 8.4; H-2 and H-6), 8.01 (d, *J* = 15.5; H-β), 8.10 (d, *J* = 7.7; H-6'). ^{13}C NMR (150 MHz) δ 114.9 (C-3'), 117.4 (C-5'), 117.8 (C-α), 123.8 (C-4), 124.6 (C-1'), 131.0 (C-2 and C-6), 132.0 (C-6'), 132.3 (C-3 and C-5), 134.8 (C-1), 134.9 (C-4'), 141.0 (C-β), 152.6 (C-2'), 190.8 (C-β') [53].

(*E*)-1-(2'-aminophenyl)-3-(2-thiophenyl)prop-2-en-1-one (**2b**) Yellow solid, yield = 93%, mp = 76 °C, purity: 99%, λ_{max} = 301 nm. ^{1}H NMR (600 MHz, DMSO-d_6) *δ* 6.59 (ddd, *J* = 1.0, 7.0 and 7.0; H-5'), 6.80 (dd, *J* = 1.0 and 7.0; H-3'), 7.18 (dd, *J* = 3.6 and 5.0; H-4), 7.28 (ddd, *J* = 1.0, 7.0 and 7.0; H-4'), 7.38 (s, 2'-NH_2), 7.60 (d, *J* = 15.2; H-α), 7.64 (d, *J* = 3.6; H-5), 7.74 (d, *J* = 5.0; H-3), 7.81 (d, *J* = 15.2; H-β), 7.96 (dd, *J* = 1.0 and 7.0; H-6'). ^{13}C NMR (150 MHz) *δ* 115.0 (C-3'), 117.3 (C-5'), 117.8 (C-3), 122.1 (C-α), 129.1 (C-4), 130.1 (C-1'), 131.5 (C-5), 132.3 (C-6'), 134.7 (C-β), 135.2 (C-4'), 140.5 (C-1), 152.5 (C-2'), 190.3 (C-β') [54].

(*E*)-1-(2'-aminophenyl)-3-(2-furanyl)prop-2-en-1-one (**2c**) Black oil, yield = 85%, purity: 99%, λ_{max} = 301 nm. ^{1}H NMR (600 MHz, DMSO-d_6) *δ* 6.59 (ddd, *J* = 1.0, 7.0 and 7.0; H-5'), 6.67 (dd, *J* = 1.0 and 7.0; H-3'), 6.80 (dd, *J* = 1.0 and 7.0; H-6'), 7.04 (d, *J* = 3.4; H-4), 7.27 (ddd, *J* = 1.0, 7.0 and 7.0; H-4'), 7.36 (s, 2'-NH_2), 7.47 (d, *J* = 15.3; H-α), 7.59 (d, *J* = 15.3; H-β), 7.88 (ddd, *J* = 3.4, 8.0 and 8.0; H-3 and H-5). ^{13}C NMR (150 MHz) *δ* 113.4 (C-3'), 115.1 (C-5'), 116.2 (C-3), 117.4 (C-α), 117.8 (C-4), 120.6 (C-1'), 129.2 (C-5), 131.3 (C-6'), 134.7 (C-β), 146.1 (C-4'), 151.9 (C-1), 152.4 (C-2'), 190.2 (C-β') [55].

(*E*)-1-(2'-aminophenyl)-3-(3-pyridinyl)prop-2-en-1-one (**2d**) Yellow solid, yield = 89%, mp = 71 – 72 °C, purity: 99%, λ_{max} = 301 nm. ^{1}H NMR (600 MHz, DMSO-d_6) *δ* 6.60 (ddd, *J* = 1.0, 7.4 and 7.4; H-5'), 6.82 (dd, *J* = 1.0 and 7.4; H-3'), 7.31 (ddd, *J* = 1.0, 7.4 and 7.4; H-4') 7.46 (s, 2'-NH_2), 7.48 (dd, *J* = 1.0 and 7.4; H-6'), 7.66 (d, *J* = 15.6; H-α), 8.11 (d, *J* = 15.6; H-β), 8.12 (d, *J* = 6.0; H-5), 8.34 (dd, *J* = 1.6 and 6.0; H-6), 8.60 (dd, *J* = 1.6 and 6.0; H-4), 9.00 (d, *J* = 1.6; H-2). ^{13}C NMR (150 MHz) *δ* 114.9 (C-3'), 117.4 (C-5'), 117.7 (C-5), 124.3 (C-α), 125.7 (C-1'), 131.3 (C-6'), 132.0 (C-1), 135.0 (C-6), 135.3 (C-4'), 138.9 (C-β), 150.6 (C-4), 151.0 (C-2), 152.7 (C-2'), 190.6 (C-β').

(*E*)-1-(2'-aminophenyl)-3-(4-pyridinyl)prop-2-en-1-one (**2e**) Yellow solid, yield = 86%, mp = 139 – 140 °C, purity: 99%, λ_{max} = 301 nm. ^{1}H NMR (600 MHz, DMSO-d_6) *δ* 6.60 (dd, *J* = 7.9 and 7.9; H-5'), 6.82 (d, *J* = 7.9; H-3'), 7.31 (dd, *J* = 7.9 and 7.9; H-4') 7.48 (s, 2'-NH_2), 7.57 (d, *J* = 15.5; H-α), 7.82 (d, *J* = 4.5; H-2 and H-6), 8.10 (d, *J* = 7.4; H-6'), 8.19 (d, *J* = 15.5; H-β), 8.65 (d, *J* = 4.5; H-3 and H-5). ^{13}C NMR (150 MHz) *δ* 114.9 (C-3'), 117.4 (C-

5'), 117.5 (C-5), 122.9 (C-2 and C-6), 128.3 (C-α), 132.1 (C-1'), 135.2 (C-6'), 139.4 (C-4'), 142.7 (C-β), 150.7 (C-3 and C-5), 152.8 (C-1), 152.7 (C-2'), 190.6 (C-β').

(*E*)-1-(2'-aminophenyl)-3-(4-methoxyphenyl)prop-2-en-1-one (**2f**) Yellow solid, yield = 93%, mp = 70 – 72 ºC, purity: 99%, λ_{max} = 301 nm. ^{1}H NMR (600 MHz, DMSO-d_6) δ 3.82 (s, 4-OCH_3), 6.59 (ddd, *J* = 1.0, 7.0 and 7.0; H-5'), 6.79 (d, *J* = 7.0; H-3'), 7.01 (d, *J* = 8.7; H-3 and H-5), 7.28 (ddd; *J* = 1.0, 7.0 and 7.0; H-4'), 7.37 (s, 2-NH_2), 7.61 (d, *J* = 15.5; H-α), 7.81 (d, *J* = 15.5; H-β), 7.82 (d, *J* = 8.7; H-2 and H-6), 8.08 (d, *J* = 7.0; H-6'). ^{13}C NMR (150 MHz) δ 55.8 (4-OCH_3), 114.8 (C-3 and C-5), 114.9 (C-3'), 117.3 (C-5'), 118.1 (C-α), 121.2 (C-1), 128.1 (C-1'), 130.9 (C-2 and C-6), 131.8 (C-6'), 134.6 (C-4'), 142.4 (C-β), 152.4 (C-2'), 161.4 (C-4), 191.0 (C-β') [53].

(*E*)-1-(2'-aminophenyl)-3-(4-methylphenyl)prop-2-en-1-one (**2g**) Yellow solid, yield = 85%, mp = 95 – 97 ºC, purity: 99%, λ_{max} = 302 nm. ^{1}H NMR (600 MHz, DMSO-d_6) δ 2.35 (s, 4-CH_3), 6.59 (ddd, *J* = 1.0, 8.0 and 8.0; H-5'), 6.80 (dd, *J* = 1.0 and 8.0; H-3'), 7.27 (d, *J* = 7.8; H-3 and H-5), 7.28 (ddd, *J* = 1.0, 8.0 and 8.0; H-4') 7.40 (s, 2'-NH_2), 7.61 (d, *J* = 15.5; H-α), 7.75 (d, *J* = 7.8; H-2 and H-6), 7.91 (d, *J* = 15.5; H-β), 8.09 (dd, *J* = 1.0 and 8.0; H-6'). ^{13}C NMR (150 MHz) δ 21.5 (4-CH_3), 114.9 (C-3'), 117.3 (C-5'), 118.0 (C-α), 122.7 (C-1'), 129.1 (C-2 and C-6), 130.0 (C-3 and C-5), 131.8 (C-6'), 132.8 (C-1), 134.7 (C-4'), 140.5 (C-4), 142.5 (C-β), 152.5 (C-2'), 191.0 (C-β') [53].

(*E*)-1-(2'-aminophenyl)-3-(4-chlorophenyl)prop-2-en-1-one (**2h**) Yellow solid, yield = 88%, mp = 93 – 95 ºC, purity: 98%, λ_{max} = 305 nm. ^{1}H NMR (600 MHz, DMSO-d_6) δ 6.59 (ddd, *J* = 1.2, 7.6 and 7.6; H-5'), 6.80 (d, *J* = 7.6; H-3'), 7.29 (ddd, *J* = 1.2, 7.6 and 7.6; H-4'), 7.42 (s, 2-NH_2), 7.51 (d, *J* = 8.5; H-2 and H-6), 7.61 (d, *J* = 15.5; H-α), 7.90 (d, *J* = 8.5; H-3 and H-5), 7.98 (d, *J* = 15.5; H-β), 8.09 (dd, *J* = 1.2 and 7.6; H-6'). ^{13}C NMR (150 MHz) δ 114.9 (C-3'), 117.4 (C-5'), 117.8 (C-α), 124.6 (C-1'), 129.4 (C-2 and C-6), 130.8 (C-3 and C-5), 131.9 (C-6'), 134.5 (C-1), 134.9 (C-4), 135.0 (C-4'), 140.9 (C-β), 152.6 (C-2'), 190.8 (C-β') [53].

(*E*)-1-(2'-aminophenyl)-3-(3,4-dichlorophenyl)prop-2-en-1-one (**2i**) Yellow solid, yield = 90%, mp = 95 – 97 ºC, purity: 97%, λ_{max} = 301 nm. ^{1}H NMR (300 MHz, DMSO-d_6) δ 6.60 (ddd, *J* = 1.1, 7.6 and 7.6; H-5'), 6.80 (dd, *J* = 1.1 and 7.6; H-3'), 7.31(ddd, *J* = 1.1, 7.6 and 7.6; H-4'), 7.44 (s, 2'-NH_2), 7.58 (d, *J* = 15.5; H-α), 7,70 (d, *J* = 8.3; H-2), 7.85 (dd, *J* = 1.5 and 8.3; H-6), 8.07 (d, *J* = 15.5; H-β), 8,13 (dd, *J* = 1.5 and 8.3; H-5), 8,26 (d, *J* = 1.1; H-6'). ^{13}C NMR (150 MHz) δ 114.9 (C-3'), 117.4 (C-5'), 117.7 (C-α), 125.9 (C-6), 129.4 (C-2), 130.4 (C-1'), 131.4 (C-5), 132.1 (C-6'), 132.2 (C-4), 132.6 (C-3), 135.0 (C-1), 136.5 (C-4'), 139.6 (C-β), 152.7 (C-2'), 190.6 (C-β') [53].

(*E*)-1-(3'-aminophenyl)-3-phenylprop-2-en-1-one) (**3a**) Yellow solid, yield = 55%, mp = 112 – 114 ºC, purity: 99%, λ_{max} = 309 nm. ^{1}H NMR (600 MHz, DMSO-d_6) δ 5.36 (s, 3'-NH_2), 6.86 (ddd, *J* = 1.0, 1.6 and 8.0; H-4'), 7.22 (dd, *J* = 8.0 and 8.0; H-5'), 7.27 (dd, *J* = 1.6 and 1.6; H-2'), 7.32 (ddd, *J* = 1.0, 1.6 and 8.0; H-6'), 7.46 (dd, *J* = 2.0 and 6.0; H-3, H-4 and H-5), 7.68 (d, *J* = 15.7; H-α), 7.78 (d, *J* = 15.7; H-β), 7.84 (dd, *J* = 2.0 and 6.0; H-2 e H-6). ^{13}C NMR (150 MHz) δ 113.4 (C-2'), 116.8 (C-6'), 119.1 (C-α), 122.9 (C-4'), 129.2 (C-2 and C-6), 129.4 (C-3 and C-5), 129.7 (C-4), 131.0 **(**C-5'), 135.2 (C-1), 138.8 (C-1'), 143.8 (C-β), 149.6 (C-3'), 190.1 (C-β') [53].

(*E*)-1-(3'-aminophenyl)-3-(2-thiophenyl)prop-2-en-1-one (**3b**) Yellow solid, yield = 91%, mp = 90 – 92 ºC, purity: 99%, λ_{max} = 340 nm. ^{1}H NMR (600 MHz, DMSO-d_6) δ 5.38 (3'-NH_2), 6.83 (ddd, *J* = 1.3, 2.5 and 7.2; H-4'), 7.20 (m, H-2', H-5', H-6' and H-4), 7.41 (d, *J* = 15.4; H-α), 7.66 (d, *J* = 3.5; H-3), 7.77 (d, *J* = 3.5; H-5), 7.86 (d, *J* = 15.4; H-β). ^{13}C NMR (150 MHz) δ 113.3 (C-2'), 116.5 (C-6'), 119.0 (C-4'), 121.1 (C-5), 129.2 (C-α), 129.7 (C-4), 130.6 (C-5'), 133.3 (C-3), 136.7 (C-β), 138.8 (C-1), 140.2 (C-1'), 149.6 (C-3'), 189.5 (C-β').

(*E*)-1-(3'-aminophenyl)-3-(2-furanyl)prop-2-en-1-one (**3c**) Yellow solid, yield = 94%, mp = 78 – 80 ºC, purity: 99%, λ_{max} = 340 nm. ^{1}H NMR (600 MHz, DMSO-d_6) δ 5.39 (3'-NH_2), 6.69 (dd, *J* = 2.5 and 6.0; H-4'), 6.82 (m, H-5'), 7.07 (d, *J* = 2.5; H-2'), 7.19 (d, *J* = 6.0; H-6' and H-4), 7.23 (d, *J* = 1.3; H-3), 7.40 (d, *J* = 15.4; H-α), 7.52 (d, *J* = 15.4; H-β), 7.91 (d, *J* = 1.3; H-5). ^{13}C NMR (150 MHz) δ 113.4 (C-2'), 113.6 (C-6'), 116.3 (C-4'), 117.3 (C-5), 118.9 (C-4), 119.4 (C-α), 129.7 (C-5'), 130.4 (C-β), 138.8 (C-1'), 146.5 (C-3), 149.7 (C-3'), 151.6 (C-1), 189.4 (C-β').

(*E*)-1-(3'-aminophenyl)-3-(3-pyridinyl)prop-2-en-1-one (**3d**) Yellow solid, yield = 80%, mp = 122 – 124 ºC, purity: 99%, λ_{max} = 300 nm. ^{1}H NMR (600 MHz, DMSO-d_6) δ 5.38 (3'-NH_2), 6.69 (ddd, *J* = 1.0, 2.0 and 8.0; H-4'), 7.22 (dd, *J* = 8.0 and 8.0; H-5'), 7.27 (dd, *J* = 2.0 and 2.0; H-2'), 7.36 (d, *J* = 8.0; H-6'), 7.49 (dd, *J* = 4.7 and 8.0; H-5), 7.71 (d, *J* = 15.8; H-α), 7.93 (d, *J* = 15.8; H-β), 8.32 (dd, *J* = 1.7 and 8.0; H-6), 8.61 (dd, *J* = 1.7 and 4.7; H-4), 8.99 (d, *J* = 1.7; H-2). ^{13}C NMR (150 MHz) δ 113.4 (C-2'), 117.0 (C-6'), 119.4 (C-4'), 124.4 (C-5), 124.8 (C-α), 129.7 (C-5'), 131.1 (C-1), 135.4 (C-6), 138.6 (C-1'), 140.3 (C-β), 149.6 (C-4), 150.7 (C-2), 151.4 (C-3'), 189.9 (C-β').

(*E*)-1-(3'-aminophenyl)-3-(4-pyridinyl)prop-2-en-1-one (**3e**) Yellow solid, yield = 80%, mp = 137 – 139 ºC, purity: 99%, λ_{max} = 288 nm. ^{1}H NMR (600 MHz, DMSO-d_6) δ 5.40 (3'-NH_2), 6.69 (dd, *J* = 2.0 and 7.3; H-4'), 7.23 (dd, *J* = 7.3 and 7.3; H-5'), 7.27 (dd, *J* = 2.0 and 2.0; H-2'), 7.36 (d, *J* = 7.3; H-6'), 7.63 (d, *J* = 15.8; H-α), 7.81 (d, *J* = 6.0; H-2 and H-6), 8.01 (d, *J* = 15.8; H-β), 8.66 (d, *J* = 6.0; H-3 and H-5). ^{13}C NMR (150 MHz) δ 113.4 (C-2'),

117.1 (C-6'), 119.5 (C-4'), 122.9 (C-2 and C-6), 127.2 (C-α), 129.8 (C-5'), 138.3 (C-1'), 140.8 (C-1), 142.4 (C-β), 149.7 (C-3'), 150.8 (C-3 and C-5), 190.0 (C-β').

(*E*)-1-(3'-aminophenyl)-3-(4- methoxyphenyl)prop-2-en-1-one) (**3f**) Yellow solid, yield = 62%, mp = 122 – 124 ºC, purity: 99%, λ_{max} = 307 nm. ^{1}H NMR (600 MHz, DMSO-d_6) δ 3.88 (s, 4-OCH_3), 6.95 (d, *J* = 8.8; H-3 and H-5), 7.31 (d, *J* = 7.7; H-4'), 7.37 (d, *J* = 2.0; H-2'), 7.38 (d, *J* = 15.6; H-α), 7.41 (d, *J* = 2.0; H-6'), 7.42 (d, *J* = 7.7; H-5'), 7.61 (d, *J* = 8.8; H-2 and H-6), 7.78 (d, *J* = 15.6; H-β). ^{13}C NMR (150 MHz) δ 55.4 (4-OCH_3), 114.4 (C-3 and C-5), 114.6 (C-2'), 118.9 (C-6'), 119.4 (C-α), 120.1 (C-4'), 127.7 (C-1), 129.4 (C-5'), 130.2 (C-2 and C-6), 139.6 (C-1'), 144.5 (C-β), 146.6 (C-3'), 161.6 (C-4), 190.5 (C-β') [53].

(*E*)-1-(3'-aminophenyl)-3-(4-methylphenyl)prop-2-en-1-one (**3g**) Yellow solid, yield = 71%, mp = 103 – 105 ºC, purity: 99%, λ_{max} = 306 nm. ^{1}H NMR (600 MHz, DMSO-d_6) δ 2.36 (s, 4-CH_3), 5.37 (s, 3'-NH_2), 6.84 (dd, *J* = 1.8 and 7.8; H-4'), 7.21 (dd, *J* = 7.8 and 7.8; H-5'), 7.27 (d, *J* = 1.8; H-2'), 7.28 (d, *J* = 8.1; H-3 and H-5), 7.32 (d, *J* = 7.8; H-6'), 7.67 (d, *J* = 15.3; H-α), 7.74 (d, *J* = 15.3; H-β), 7.75 (d, *J* = 8.1; H-2 and H-6). ^{13}C NMR (150 MHz) δ 21.6 (4-CH_3), 113.4 (C-2'), 116.8 (C-6'), 119.0 (C-α), 121.8 (C-4'), 129.2 (C-2 and C-6), 129.7 (C-5'),130.0 (C-3 and C-5), 132.5 (C-1), 138.9 (C-4), 141.0 (C-1'), 143.9 (C-β), 149.6 (C-3'), 190.0 (C-β') [53].

(*E*)-1-(3'-aminophenyl)-3-(4-chlorophenyl)prop-2-en-1-one) (**3h**) Yellow solid, yield = 75% yield, mp = 110 – 112 ºC, purity: 99%, λ_{max} = 311 nm. ^{1}H NMR (600 MHz, DMSO-d_6) δ 5.38 (3'-NH_2), 6.85 (dd, *J* = 1.8 and 7.8; H-4'), 7.21 (dd, *J* = 7.8 and 7.8; H-5'), 7.26 (d, *J* = 1.8; H-2'), 7.34 (d, *J* = 7.8; H-6'), 7.53 (d, *J* = 8.5; H-2 and H-6),7.68 (d, *J* = 15.7; H-α), 7.83 (d, *J* = 15.7; H-β), 7.90 (d, *J* = 8.5; H-3 and H-5). ^{13}C NMR (150 MHz) δ 113.4 (C-2'), 116.9 (C-6'), 119.2 (C-α), 123.6 (C-4'), 129.4 (C-2 and C-6), 129.7 (C-5'), 130.9 (C-3 and C-5), 134.2 (C-1), 135.4 (C-4), 138.7 (C-1'), 142.3 (C-β), 149.6 (C-3'), 189.9 (C-β') [53].

(*E*)-1-(3'-aminophenyl)-3-(3,4-dichlorophenyl)prop-2-en-1-one (**3i**) Yellow solid, yield = 80%, mp = 120 – 122 ºC, purity: 96%, λ_{max} = 304 nm. ^{1}H NMR (600 MHz, DMSO-d_6) δ 6.90 (d, *J* = 7.7; H-4'), 7.24 (dd, *J* = 7.7 and 7.7; H-5'), 7.30 (d, *J* = 1.0; H-2'), 7.41(d, *J* = 7.7; H-6'), 7.65 (d, *J* = 15.7; H-α), 7.70 (d, *J* = 8.4; H-6), 7.84 (d, *J* = 8.4; H-5), 7.90 (d, *J* = 15.7; H-β), 8.22 (d, *J* = 1.1; H-2). ^{13}C NMR (150 MHz) δ 113.3 (C-2'), 117.1 (C-6'), 119.4 (C-α), 124.9 (C-4'), 129.5 (C-6), 129.7 (C-2), 130.6 (C-5'), 131.5 (C-5), 132.3 (C-4), 133.0 (C-3), 136.2 (C-1), 138.6 (C-1'), 141.0 (C-β), 149.7 (C-3'), 189.8 (C-β'). HRMS $C_{15}H_{11}Cl_2NO_2$ $[M + H]^+$: calculated 292.0290, observed 292.0282, error 2.74 ppm [53].

(*E*)-1-(3'-aminophenyl)-3-(2,6-dichlorophenyl)prop-2-en-1-one (**3j**) Yellow solid, yield = 73%, mp = 101 – 102 ºC, purity: 97%, λ_{max} = 286 nm. ^{1}H NMR (600 MHz, DMSO-

d_6) δ 5.44 (3'-NH_2), 6.86 (dd, J = 2.3 and 7.0; H-4'), 7.22 (m, H-2', H-5' and H-6'), 7.45 (dd, J = 8.1 and 8.1; H-4), 7.61 (d, J = 8.1; H-3 and H-5), 7.66 (d, J = 16.0; H-α), 7.69 (d, J = 16.0; H-β). ^{13}C NMR (150 MHz) δ 113.3 (C-2'), 116.7 (C-6'), 119.5 (C-α), 129.6 (C-3 and C-5), 129.9 (C-4'), 131.3 (C-5'), 131.5 (C-4), 132.6 (C-1), 134.6 (C-2 and C-6), 136.7 (C-1'), 138.2 (C-β), 149.8 (C-3'), 189.8 (C-β'). HRMS $C_{15}H_{11}Cl_2NO_2$ $[M + H]^+$: calculated 292.0290, observed 292.0282, error 2.74 ppm.

(*E*)-1-(3'-aminophenyl)-3-(3-chlorophenyl)prop-2-en-1-one (**3k**) Yellow solid, yield = 65%, mp = 73 – 75 ºC, purity: 95%, λ_{max} = 299 nm. ^{1}H NMR (600 MHz, DMSO-d_6) δ 5.38 (3'-NH_2), 6.86 (ddd, J = 1.0, 2.2 and 7.8; H-4'), 7.22 (dd, J = 7.8 and 7.8; H-5'), 7.28 (d, J = 2.2 and 2.2; H-2'), 7.38 (d, J = 7.8; H-6'), 7.47 (d, J = 7.5; H-5), 7.50 (d, J = 3.0; H-4), 7.66 (d, J = 15.7; H-α), 7.80 (d, J = 7.5; H-6), 7.89 (d, J = 15.7; H-β), 8.03 (s, H-2). ^{13}C NMR (150 MHz) δ 113.4 (C-2'), 117.1 (C-6'), 119.3 (C-α), 124.4 (C-4'), 128.1 (C-6), 128.3 (C-2), 129.7 (C-4), 130.5 (C-5'), 131.2 (C-5), 134.3 (C-3), 137.5 (C-1), 138.6 (C-1'), 142.0 (C-β), 149.6 (C-3'), 189.9 (C-β').

(*E*)-1-(3'-aminophenyl)-3-(2-chlorophenyl)prop-2-en-1-one (**3l**) Yellow solid, yield = 59%, mp = 82 – 83 ºC, purity: 99%, λ_{max} = 299 nm. ^{1}H NMR (600 MHz, DMSO-d_6) δ 5.39 (3'-NH_2), 6.86 (ddd, J = 1.0, 2.3 and 7.8; H-4'), 7.22 (dd, J = 7.8 and 7.8; H-5'), 7.27 (dd, J = 2.3 and 2.3; H-2'), 7.35 (d, J = 7.8; H-6'), 7.47 (m, H-4 and H-5), 7.58 (dd, J = 1.5 and 7.7; H-3), 7.84 (d, J = 15.6; H-α), 7.98 (d, J = 15.6; H-β), 8.16 (dd, J = 1.5 and 7.7; H-6). ^{13}C NMR (150 MHz) δ 113.4 (C-2'), 117.0 (C-6'), 119.4 (C-α), 125.7 (C-4'), 128.2 (C-6), 128.9 (C-5), 129.7 (C-3), 130.5 (C-4), 132.4 (C-5'), 132.8 (C-2), 134.7 (C-1), 138.4 (C-1'), 138.5 (C-β), 149.7 (C-3'), 189.9 (C-β').

(*E*)-1-(3'-aminophenyl)-3-(4-fluorophenyl)prop-2-en-1-one (**3m**) Yellow solid, yield = 77%, mp = 70 – 71 ºC, purity: 99%, λ_{max} = 308 nm. ^{1}H NMR (600 MHz, DMSO-d_6) δ 5.37 (3'-NH_2), 6.85 (dd, J = 1.9 and 7.7; H-4'), 7.21 (dd, J = 7.7 and 7.7; H-5'), 7.26 (dd, J = 1.9 and 1.9; H-2'), 7.32 (m, H-3, H-5 and H-6'), 7.69 (d, J = 15.7; H-α), 7.76 (d, J = 15.7; H-β), 7.94 (dd, J = 3.0 and 8.6; H-2 and H-6). ^{13}C NMR (150 MHz) δ 113.4 (C-2'), 116.4 (d, $J_{C,F}$ = 21.7; C-3 and C-5), 116.8 (C-6), 119.1 (C-α), 122.8 (C-4'), 129.6 (C-5'), 131.5 (d, $J_{C,F}$ = 8.4; C-2 and C-6), 131.9 (C-1), 138.8 (C-1'), 142.5 (C-β), 149.6 (C-3'), 163.8 (d, $J_{C,F}$ = 248.8; C-4), 190.0 (C-β').

(*E*)-1-(3'-aminophenyl)-3-(3-fluorophenyl)prop-2-en-1-one (**3n**) Yellow solid, yield = 68%, mp = 81 – 83 ºC, purity: 99%, λ_{max} = 303 nm. ^{1}H NMR (600 MHz, DMSO-d_6) δ 5.36 (3'-NH_2), 6.86 (dd, J = 2.0 and 7.7; H-4'), 7.22 (dd, J = 7.7 and 7.7; H-5'), 7.28 (dd, J = 2.0 and 2.0; H-2'), 7.29 (dd, J = 2.5 and 8.8; H-4), 7.36 (d, J = 7.7; H-6'), 7.49 (m; H-2), 7.67 (m,

H-6 and H-α), 7.81 (d, *J* = 8.8; H-5), 7.86 (d, *J* = 15.7; H-β). ^{13}C NMR (150 MHz) *δ* 113.4 (C-2'), 115.1 (d, $J_{C,F}$ = 21.5; C-2), 117.0 (C-6), 117.6 (d, $J_{C,F}$ = 21.5; C-4), 119.3 (C-α), 124.4 (C-6), 125.8 (C-4'), 129.7 (C-5'), 131.3 (d, $J_{C,F}$ = 8.4; C-5), 137.8 (d, $J_{C,F}$ = 8.4; C-1), 138.7 (C-1'), 142.3 (C-β), 149.6 (C-3'), 162.9 (d, $J_{C,F}$ = 243.8; C-4), 190.0 (C-β').

(*E*)-1-(3'-aminophenyl)-3-(2-fluorophenyl)prop-2-en-1-one (**3o**) Yellow solid, yield = 61%, mp = 65 – 66 ºC, purity: 99%, λ_{max} = 303 nm. ^{1}H NMR (600 MHz, DMSO-d_6) *δ* 5.40 (3'-NH_2), 6.86 (ddd, *J* = 1.0, 2.3 and 7.6; H-4'), 7.22 (dd, *J* = 7.6 and 7.6; H-5'), 7.26 (dd, *J* = 2.3 and 2.3; H-2'), 7.31 (d, *J* = 7.6; H-6'), 7.34 (m, H-3 and H-6), 7.52 (tdd, *J* = 1.5, 5.5 and 7.3; H-4), 7.77 (d, *J* = 15.8; H-α), 7.84 (d, *J* = 15.8; H-β), 8.16 (ddd, *J* = 1.6, 7.3 and 7.3; H-5). ^{13}C NMR (150 MHz) *δ* 113.4 (C-2'), 116.7 (d, $J_{C,F}$ = 21.9; C-3), 116.8 (C-6'), 119.3 (C-α), 122.9 (C-4), 125.1 (C-1), 125.5 (C-5), 129.7 (C-5' and C-6), 132.9 (d, $J_{C,F}$ = 9.3; C-4), 135.1 (C-1'), 138.6 (C-β), 149.7 (C-3'), 161.4 (d, $J_{C,F}$ = 251.4; C-4), 189.9 (C-β'). HRMS $C_{15}H_{12}FNO$ $[M + H]^+$: calculated 242.0976, observed 241.0975, error 0.41 ppm.

(*E*)-1-(3'-aminophenyl)-3-(4-bromophenyl)prop-2-en-1-one (**3p**) Yellow solid, yield = 75%, mp = 115 – 117 ºC, purity: 98%, λ_{max} = 298 nm. ^{1}H NMR (300 MHz, DMSO-d_6) *δ* 5.37 (s, 3'-NH_2), 6.84 (dd, *J* = 2.0 and 7.7; H-4'), 7.20 (dd, *J* = 7.7 and 7.7; H-5'), 7.26 (dd, *J* = 2.0 and 2.0; H-2'), 7.34 (d, *J* = 7.7; H-6'), 7.65 (d, *J* = 15.0; H-α), 7.66 (d, *J* = 8.7; H-2 and H-6), 7.83 (d, *J* = 15.0; H-β), 7.82 (d, *J* = 8.7; H-3 and H-5). ^{13}C NMR (150 MHz) *δ* 113.3 (C-2'), 116.9 (C-6'), 119.2 (C-α), 123.7 (C-4'), 124.3 (C-4), 129.7 (C-5'), 131.1 (C-2 and C-6), 132.4 (C-3 and C-5), 134.5 (C-1), 138.7 (C-1'), 142.4 (C-β), 149.7 (C-3'), 189.9 (C-β') [53].

(*E*)-1-(3'-aminophenyl)-3-(3-bromophenyl)prop-2-en-1-one (**3q**) Yellow solid, yield = 68%, mp = 69 – 71 ºC, purity: 98%, λ_{max} = 298 nm. ^{1}H NMR (600 MHz, DMSO-d_6) *δ* 5.37 (3'-NH_2), 6.86 (ddd, *J* = 1.0, 2.0 and 7.9; H-4'), 7.22 (dd, *J* = 7.9 and 7.9; H-5'), 7.28 (dd, *J* = 2.0 and 2.0; H-2'), 7.37 (d, *J* = 7.9; H-6'), 7.41 (dd, *J* = 7.8 and 7.8; H-5), 7.62 (d, *J* = 1.6; H-4), 7.64 (d, *J* = 15.7; H-α), 7.83 (d, *J* = 7.8; H-6), 7.87 (d, *J* = 15.7; H-β), 8.16 (d, *J* = 1.6; H-2). ^{13}C NMR (150 MHz) *δ* 113.4 (C-2'), 117.1 (C-6'), 119.3 (C-α), 122.9 (C-4'), 124.4 (C-3), 128.5 (C-6), 129.7 (C-2), 131.2 (C-5'), 131.4 (C-5), 133.4 (C-4), 137.7 (C-1), 138.6 (C-1'), 142.0 (C-β), 149.6 (C-3'), 189.9 (C-β').

(*E*)-1-(3'-aminophenyl)-3-(2-bromophenyl)prop-2-en-1-one (**3r**) Yellow solid, yield = 59%, mp = 60 – 62 ºC, purity: 97%, λ_{max} = 297 nm. ^{1}H NMR (600 MHz, DMSO-d_6) *δ* 5.39 (3'-NH_2), 6.87 (dd, *J* = 1.6 and 7.7; H-4'), 7.22 (dd, *J* = 7.7 and 7.7; H-5'), 7.27 (s, H-2'), 7.35 (d, *J* = 7.7; H-6'), 7.39 (ddd, *J* = 1.1, 7.4 and 7.4; H-5), 7.49 (dd, *J* = 7.4 and 7.4; H-4), 7.74 (d, *J* = 7.4; H-6), 7.80 (d, *J* = 15.6; H-α), 7.94 (d, *J* = 15.6; H-β), 8.13 (d, *J* = 7.4; H-3). ^{13}C NMR (150 MHz) *δ* 113.4 (C-2'), 117.0 (C-2), 119.4 (C-6'), 125.7 (C-α), 125.8 (C-4'),

128.7 (C-5), 129.1 (C-6), 129.7 (C-5'), 132.5 (C-4), 133.8 (C-3), 134.5 (C-1), 138.5 (C-1'), 141.1 (C-β), 149.7 (C-3'), 189.9 (C-β'). HRMS $C_{15}H_{12}BrNO$ $[M + H]^+$: calculated 302.0175, observed 302.0178, error 0.99 ppm.

(*E*)-1-(3'-aminophenyl)-3-(4-(trifluoromethoxy)phenyl)prop-2-en-1-one (**3s**) Yellow solid, yield = 80%, mp = 103 – 104 ºC, purity: 99%, λ_{max} = 301 nm. ^{1}H NMR (600 MHz, DMSO-d_6) δ 6.99 (dd, *J* = 1.0, 2.3 and 7.8; H-4'), 7.28 (dd, *J* = 7.8 and 7.8; H-5'), 7.37 (d, *J* = 8.4; H-2 and H-6), 7.40 (m, H-2' and H-6'), 7.72 (d, *J* = 15.7; H-α), 7.77 (d, *J* = 15.7; H-β), 7.88 (d, *J* = 8.2; H-3 and H-5). ^{13}C NMR (150 MHz) δ 114.1 (C-2'), 117.8 (C-6'), 119.7 (C-α), 120.9 (C-2 and C-6), 123.1 (C-4'), 129.1 (C-5'), 129.9 (C-3, C-5 and 4-CF_3), 134.0 (C-1), 138.6 (C-1'), 142.4 (C-β), 148.4 (C-3'), 150.4 (C-4), 191.2 (C-β'). HRMS $C_{16}H_{12}F_3NO_2$ $[M + H]^+$: calculated 308.0893, observed 308.0894, error 0.32 ppm.

(*E*)-1-(3'-aminophenyl)-3-(4-chloro-3-(trifluoromethyl)phenyl)prop-2-en-1-one (**3t**) Yellow solid, yield = 50%, mp = 123 – 124 ºC, purity: 96%, λ_{max} = 312 nm. ^{1}H NMR (600 MHz, DMSO-d_6) δ 6.16 (ddd, *J* = 1.0, 2.3 and 7.9; H-4'), 6.45 (dd, *J* = 7.9 and 7.9; H-5'), 6.58 (dd, *J* = 2.3 and 2.3; H-2'), 6.59 (dd, *J* = 1.0 and 7.9; H-6'), 6.87 (d, *J* = 7.8; H-5), 6.93 (d, *J* = 15.7; H-α), 6.99 (d, *J* = 15.7; H-β), 7.19 (dd, *J* = 1.8 and 8.3; H-6), 7.30 (d, *J* = 1.8; H-2). ^{13}C NMR (150 MHz) δ 114.1 (C-2'), 117.8 (4-CF_3), 119.8 (C-6'), 123.7 (C-α), 124.5 (C-4'), 127.4 (C-2), 129.1 (C-3 and C-5), 131.9 (C-4), 132.4 (C-5'), 133.0 (C-6), 134.6 (C-1), 138.4 (C-1'), 140.9 (C-β), 148.4 (C-3'), 190.8 (C-β').

(*E*)-1-(3'-aminophenyl)-3-(4-nitrophenyl)prop-2-en-1-one (**3u**) Orange solid, yield = 70%, mp = 143 – 145 ºC, purity: 98%, λ_{max} = 313 nm. ^{1}H NMR (300 MHz, DMSO-d_6) δ 5.40 (s, 3'-NH_2), 6.88 (dd, *J* = 2.0 and 7.8; H-4'), 7.23 (dd, *J* = 7.8 and 7.8; H-5'), 7.28 (dd, *J* = 2.0 and 2.0; H-2'), 7.38 (d, *J* = 7.8; H-6'), 7.77 (d, *J* = 15.7; H-α), 8.00 (d, *J* = 15.7; H-β), 8.14 (d, *J* = 8.3; H-2 and H-6), 8.22 (d, *J* = 8.3; H-3 and H-5). ^{13}C NMR (150 MHz) δ 113.3 (C-2'), 117.1 (C-6'), 119.5 (C-α), 124.4 (C-3 and C-5), 126.9 (C-4'), 129.8 (C-5'), 130.2 (C-2 and C-6), 138.4 (C-1'), 140.9 (C-1), 141.8 (C-β), 148.5 (C-4), 149.7 (C-3'), 189.9 (C-β') [53].

(*E*)-1-(3'-aminophenyl)-3-(3-nitrophenyl)prop-2-en-1-one (**3v**) Orange solid, yield = 66%, mp = 152 – 154 ºC, purity: 99%, λ_{max} = 288 nm. ^{1}H NMR (600 MHz, DMSO-d_6) δ 5.39 (3'-NH_2), 6.87 (ddd, *J* = 1.0, 2.3 and 7.9; H-4'), 7.23 (dd, *J* = 7.9 and 7.9; H-5'), 7.29 (dd, *J* = 2.3 and 2.3; H-2'), 7.41 (dd, *J* = 1.0 and 7.9; H-6'), 7.75 (dd, *J* = 8.0 and 8.0; H-5), 7.81 (d, *J* = 15.7; H-α), 8.02 (d, *J* = 15.7; H-β), 8.27 (ddd, *J* = 1.7, 1.7 and 8.0; H-4), 8.32 (d, *J* = 8.0; H-6), 8.74 (d, *J* = 1.7; H-2). ^{13}C NMR (150 MHz) δ 113.4 (C-2'), 117.2 (C-6'), 119.4 (C-4), 123.4 (C-2), 125.0 (C-α), 125.7 (C-4'), 129.7 (C-5), 130.8 (C-5'), 135.4 (C-6), 137.2 (C-1), 138.5 (C-1'), 141.2 (C-β), 148.9 (C-3), 149.7 (C-3'), 189.9 (C-β').

(*E*)-1-(4'-aminophenyl)-3-phenylprop-2-en-1-one) (**4a**) Yellow solid, yield = 60%, mp = 89 – 90 °C, purity: 99%, λ_{max} = 358 nm. ^{1}H NMR (600 MHz, DMSO-d_6) δ 6.20 (s, 4'-NH_2), 6.63 (d, *J* = 8.6; H-3' and H-5'), 7.44 (d, *J* = 7.4; H-3, H-4 and H-5), 7.62 (d, *J* = 15.6; H-α), 7.84 (d, *J* = 7.4; H-2 and H-6), 7.88 (d, *J* = 15.6; H-β), 7.93 (d, *J* = 8.6; H-2' and H-6'). ^{13}C NMR (150 MHz) δ 113.2 (C-3' and C-5'), 122.8 (C-α), 125.7 (C-1'), 129.0 (C-2 and C-6), 129.3 (C-3 and C-5), 130.5 (C-4), 131.6 (C-2' and C-6'), 135.6 (C-1), 141.9 (C-β), 154.4 (C-4'), 186.3 (C-β') [53].

(*E*)-1-(4'-aminophenyl)-3-(2-thiophenyl)prop-2-en-1-one (**4b**) Yellow solid, yield = 80%, mp = 119 – 120 °C, purity: 99%, λ_{max} = 368 nm. ^{1}H NMR (600 MHz, DMSO-d_6) δ 6.17 (s, 4-NH_2), 6.62 (d, *J* = 8.7; H-3' and H-5'), 7.17 (dd, *J* = 3.5 and 5.0; H-4), 7.50 (d, *J* = 15.3; H-α), 7.60 (d, *J* = 3.5; H-3), 7.72 (d, *J* = 5.0; H-5), 7.78 (d, *J* = 15.3; H-β), 7.86 (d, *J* = 8.7; H-2' and H-6'). ^{13}C NMR (150 MHz) δ 113.2 (C-3' and C-5'), 121.3 (C-3), 125.6 (C-α), 129.0 (C-1'), 129.7 (C-4), 131.4 (C-2' and C-6'), 132.1 (C-5), 134.7 (C-β), 140.7 (C-2), 154.4 (C-4'), 185.7 (C-β') [56].

(*E*)-1-(4'-aminophenyl)-3-(2-furanyl)prop-2-en-1-one (**4c**) Yellow solid, yield = 87%, mp = 114 – 116 °C, purity: 99%, λ_{max} = 370 nm. ^{1}H NMR (600 MHz, DMSO-d_6) δ 6.17 (s, 4-NH_2), 6.62 (d, *J* = 8.7; H-3' and H-5'), 6.66 (dd, *J* = 1.6 and 3.4; H-4), 7.01 (d, *J* = 3.4; H-3), 7.45 (d, *J* = 15.4; H-α), 7.51 (d, *J* = 15.4; H-β), 7.83 (d, *J* = 8.7; H-2' and H-6'), 7.86 (d, *J* = 1.6; H-5). ^{13}C NMR (150 MHz) δ 113.2 (C-3' and C-5'), 113.3 (C-3), 115.9 (C-α), 119.7 (C-1'), 125.6 (C-4), 128.7 (C-5), 131.4 (C-2' and C-6'), 145.9 (C-β), 152.0 (C-2), 154.4 (C-4'), 185.7 (C-β') [56].

(*E*)-1-(4'-aminophenyl)-3-(3-pyridinyl)prop-2-en-1-one (**4d**) Yellow solid, yield = 85%, mp = 166 – 167 °C, purity: 99%, λ_{max} = 362 nm. ^{1}H NMR (600 MHz, DMSO-d_6) δ 6.21 (s, 4-NH_2), 6.63 (d, *J* = 8.6; H-3' and H-5'), 7.47 (dd, *J* = 4.2 and 7.9; H-5), 7.64 (d, *J* = 15.6; H-α), 7.96 (d, *J* = 8.6; H-2' and H-6'), 8.02 (d, *J* = 15.6; H-β), 8.32 (d, *J* = 7.9; H-6), 8.58 (dd, *J* = 1.1 and 4.2; H-4), 8.98 (d, *J* = 1.1; H-2). ^{13}C NMR (150 MHz) δ 113.2 (C-3' and C-5'), 124.3 (C-5), 124.8 (C-α), 125.5 (C-1'), 131.4 (C-1), 131.8 (C-2' and C-6'), 135.2 (C-6), 138.4 (C-β), 150.5 (C-4), 150.9 (C-2), 154.6 (C-4'), 185.9 (C-β') [56].

(*E*)-1-(4'-aminophenyl)-3-(4-pyridinyl)prop-2-en-1-one (**4e**) Yellow solid, yield = 78%, mp = 178 – 180 °C, purity: 99%, λ_{max} = 362 nm. ^{1}H NMR (600 MHz, DMSO-d_6) δ 6.27 (s, 4-NH_2), 6.63 (d, *J* = 8.8; H-3' and H-5'), 7.56 (d, *J* = 15.6; H-α), 7.80 (d, *J* = 6.1; H-2 and H-6), 7.95 (d, *J* = 8.8; H-2' and H-6'), 8.10 (d, *J* = 15.6; H-β), 8.64 (d, *J* = 6.1; H-3 and H-5). ^{13}C NMR (150 MHz) δ 113.2 (C-3' and C-5'), 122.8 (C-2 and C-6), 125.3 (C-1'), 127.3 (C-

α), 131.9 (C-2’ and C-6’), 138.9 (C-1), 142.8 (C-β), 150.7 (C-3 and C-5), 154.7 (C-4’), 185.9 (C-β’) [56].

(*E*)-1-(4'-aminophenyl)-3-(4-methoxyphenyl)prop-2-en-1-one (4f) Yellow solid, yield = 66%, mp = 109 – 111 °C, purity: 99%, λ_{max} = 364 nm. ^{1}H NMR (600 MHz, DMSO-d_6) δ 3.81 (s, 4-OCH_3), 6.13 (s, 4’-NH_2), 6.61 (d, *J* = 8.7; H-3’ and H-5’), 7.00 (d, *J* = 8.8; H-3 and H-5), 7.58 (d, *J* = 15.5; H-α), 7.73 (d, *J* = 15.5; H-β), 7.80 (d, *J* = 8.8; H-2 and H-6), 7.91(d, *J* = 8.7; H-2’ and H-6’). ^{13}C NMR (150 MHz) δ 55.8 (4-OCH_3), 113.2 (C-3 and C-5), 114.8 (C-3’ and C-5’), 120.3 (C-α), 125.9 (C-1), 128.2 (C-1’), 130.8 (C-2 and C-6), 131.5 (C-2’ and C-6’), 141.8 (C-β), 154.2 (C-4’), 161.3 (C-4), 186.4 (C-β’) [53].

(*E*)-1-(4'-aminophenyl)-3-(4-methylphenyl)prop-2-en-1-one (**4g**) Yellow solid, yield = 73%, mp = 130 – 132 °C, purity: 98%, λ_{max} = 356 nm. ^{1}H NMR (600 MHz, DMSO-d_6) δ 2.34 (s, 4-CH_3), 6.16 (s, 4’-NH_2), 6.62 (d, *J* = 8.5; H-3’ and H-5’), 7.26 (d, *J* = 7.9; H-3 and H-5), 7.59 (d, *J* = 15.5; H-α), 7.73 (d, *J* = 7.9; H-2 and H-6), 7.82 (d, *J* = 15.5; H-β), 7.93 (d, *J* = 8.5; H-2’ and H-6’). ^{13}C NMR (150 MHz) δ 21.5 (4-CH_3), 113.2 (C-3’ and C-5’), 121.8 (C-α), 125.8 (C-1’), 129.0 (C-2 and C-6), 129.9 (C-3 and C-5), 131.6 (C-1), 132.9 (C-2’ and C-6’), 140.4 (C-4), 141.9 (C-β), 154.3 (C-4’), 186.3 (C-β’) [53].

(*E*)-1-(4'-aminophenyl)-3-(4-chlorophenyl)prop-2-en-1-one (**4h**) Yellow solid, yield = 79%, mp = 154 – 156 °C, purity: 99%, λ_{max} = 362 nm. ^{1}H NMR (600 MHz, DMSO-d_6) δ 6.20 (s, 4’-NH_2), 6.62 (d, *J* = 8.8; H-3’ and H-5’), 7.50 (d, *J* = 7.4; H-2 and H-6), 7.60 (d, *J* = 15.6; H-α), 7.88 (d, *J* = 7.4; H-3 and H-5), 7.90 (d, *J* = 15.6; H-β), 7.93 (d, *J* = 8.8; H-2’ and H-6’). ^{13}C NMR (150 MHz) δ 113.2 (C-3’ and C-5’), 123.6 (C-α), 125.6 (C-1’), 129.3 (C-2 and C-6), 130.7 (C-3 and C-5), 131.7 (C-2’ and C-6’), 134.6 (C-1), 134.9 (C-4), 140.4 (C-β), 154.5 (C-4’), 186.2 (C-β’) [53].

(*E*)-1-(4'-aminophenyl)-3-(3,4-dichlorophenyl)prop-2-en-1-one (**4i**) Yellow solid, yield = 82%, mp = 181 – 183 °C, purity: 99%, λ_{max} = 364 nm. ^{1}H NMR (600 MHz, DMSO-d_6) δ 6,21 (s, 4’-NH_2), 6.63 (d, *J* = 8.5; H-3’ and H-5’), 7.57 (d, *J* = 15.5; H-α), 7.69 (d, *J* = 8.3; H-5), 7.82 (dd, *J* = 1.5 and 8.3; H-6), 7.95 (d; *J* = 8.5; H-2’ and H-6’), 7.97 (d, *J* = 15.5; H-β), 8.23 (d; *J* = 1.5; H-2). ^{13}C NMR (150 MHz) δ 113.2 (C-3’ and C-5’), 125.0 (C-α), 125.5 (C-1’), 129.2 (C-5), 130.2 (C-2), 131.4 (C-6), 131.8 (C-2’ and C-6’), 132.2 (C-4), 132.5 (C-3), 136.5 (C-1), 139.2 (C-β), 154.6 (C-4’), 186.1 (C-β’) [53].

4.2. Determination of Minimum Inhibitory and Fungicidal Concentrations (MIC/MFC)

The strain used in this assay, including *C. albicans* ATCC 90028. Strain was maintained as frozen stocks at –80 ºC until use. The minimum inhibitory concentration (MIC) was determined according to the document M27 A2-S3 (2008) of Clinical and Laboratory Standards Institute (CLSI) with some adaptations [57]. For the assays, the strain was seeded on Sabouraud dextrose agar (SDA) at 37°C for 24 hours. From this culture, the inoculum was obtained and diluted in RPMI-1640 (Sigma-Aldrich) with L-glutamine without sodium bicarbonate, supplemented with 2% glucose, buffered at pH 7.0 using MOPS buffer (0.165 mol/L) (sigma-Aldrich), with the concentration between 2.5 and 5.10^4 CFU/mL, which was distributed in 96-well plates. Inoculum absorbance was confirmed by Spectrophotometer Unico 1100RS. The substances were diluted in DMSO and added to the plates at concentrations ranging from 62.5 to 0.48 μg/mL. Plates were incubated at 37 ° C and MIC values were established as the concentration capable of of inhibition of fungal growth after visual readings. Amphotericin B (Merck®) was used as reference antifungal drug. Minimum fungicidal concentration (MFC) was determined by transferring each 96-well microplates concentration to plate with SDA and subsequent incubation at 37 ° C for 24 hours. MFC was defined as the lowest concentration that did not allow fungal growth visible in the solid medium.

4.3. Checkboard assay

Interaction effect of chalcone **3n** with amphotericin B was evaluated by the microdilution broth checkerboard method [58, 59]. Amphotericin B (4 to 0.0062 μg/mL) was tested along with chalcone **3n** (62.5 to 0.12 μg/mL). The medium was diluted in RPMI-1640 (Sigma-Aldrich) with L-glutamine without sodium bicarbonate, supplemented with 2% glucose, buffered at pH 7.0 using MOPS buffer (0.165 mol/L) with the concentration between 2.5 and 5.10^4 CFU/mL and distributed in 96-well plates. The plates were incubated at 37 °C with microplate readings at 490 nm after 24 hours. The compounds were also tested alone. The combinatorial test result was the lowest concentration of eachcombination that completely inhibited sample growth after visual readings. The fractional inhibitory concentrationindex (FICI) was calculated using formula $FICI = FIC_A + FIC_B$, where FIC is the ratio of MIC of the drug in combination with MIC alone. The combination is synergistic when $FICI \leq 0.5$, additive when $0.5 < FICI < 1.0$, indifferent if $1.0 < FICI < 4.0$and antagonistic if $FICI > 4$ [59].

4.4. Time-kill assay

Assay of time-kill was performed as described by Li and co-authors with minor modifications [60]. To investigate the effect of **3n** and amphotericin B in time of dead of *C. albicans*, the inoculum was diluted in YNB until concentration final of 1.10^5 CFU/mL and distributed in five Falcon tubes: untreated, **3n** (MIC), **3n** (10MIC), amphotericin B (MIC) and amphotericin B (10 × MIC). Tubes were incubed at 37°C and a curve (0, 2, 4, 8 and 12 hours) was plotted in different times. After determined time, an aliquot was colleted and serial dilutions perfomed. 50 µL of each suspension were added in SDA plates and incubated at 37° C for 24 hours. Time-kill curve was determined in comparison to the untreated cells [27].

4.5. Anti-adhesion assay

In order to determine the anti-adhesion activity of **3n**, immortalized human keratinocytes (HaCat cells) were obtained from the Bank of Cells of Rio de Janeiro (RJ, Brazil). Cell culture and anti-adhesion assay were performed as described by Emeri and co-authors, with minor modifications [40]. Cells were maintained in DMEM medium supplemented with 10% fetal bovine serum plus 100 U/mL penicillin, streptomycin sulfate and L-glutamine at 37 °C in 5% CO_2 atmosphere. A curve (1, 2 and 3 hours) was plotted to establish *C. albicans* adhesion to HaCat cells. The concentration of 1.10^5 cells/well was distributed in 24-well plates [61]. After formation of the cell monolayers, aliquots of 500 µL of candidal inoculums were added the wells (1.10^3 CFU/mL) together with chalcone or amphotericin B in MIC/2 values, 0.25 and 1.9 µg/mL, respectively. The plate was incubated at 37° C in 5% CO_2 at the times determined for adhesion. After the incubation time, the cells were washed three times with sterile PBS and trypsinized. Aliquots 50 µL were added in SDA plates and incubated at 37° C for 24 hours. The subinhibitory concentration was selected as it ensures candidal growth and survival were not severely affected by **3n**. Inhibition of adhesion was determined based on the final number of adhered fungal in comparison to an untreated group (fungal + cells + DMEM) indicating 100% fungal adhesion. In order to check if **3n** directly acts on adhesion bacterial to HaCaTcells instead of causes HaCaT viability reduction, we included a test with HaCaT cells treated **3n** at its MIC/2 value. The percentage of

inhibition of adhesion was calculed based on final number of adhered *candida* cells in comparison to an untreated control considered 100% adhesion.

4.6. Biofilm formation inhibition assay

Inhibitory effect on *C. albicans* biofilm formation was evaluted by to protocol described by Pitangui and co-authors [62] with some modifications. To investigate the effect of **3n** and amphotericin B towards *C. albicans* biofilm formation, aliquot 100 µL of fungal suspension (1.10^8 CFU/mL) was added to Yeast Nitrogen Base (YNB), distributed in 96-well plates and incubated at 37° C for 2 hours. After initial formation of the biofilms, plates were washed three times with PBS to remove dead and non-adherent cells. An aliquot of 100 µL YNB containing **3n** or amphotericin B at their MIC and 10 × MIC values were added to the wells. The plates were incubated at 37 °C for 24 hours. After this time, the plates were washed three times with PBS and 100 µL transferred to a tube with 900 µL of PBS and serial dilutions were performed.20 µL of each suspension were added in SDA plates and incubated at 37° C for 24 hours [63]. The percentage of CFU was determined in comparison to the untreated *C. albicans* biofilms.

4.7. Preformed biofilm inhibition assay

Assay of preformed biofilm inhibition of *C. albicans* was carried out according to protocol described by Pitangui and collaborators, with minor modifications [62]. Aliquot of 100 µL of fungal suspension (1.10^8 CFU/mL) was added to Yeast Nitrogen Base (YNB), distributed in 96-well plates and incubated at 37° C for 24 hours, allowing biofilm formation [60]. Following preformed biofilms, the wells were washed three times with sterile saline (0.85%) to remove dead and non-adherent cells. An aliquot of 100 µL YNB containing **3n** and amphotericin B at their MIC and 10 × MIC values were added to the wells. The plates were incubated at 37 °C for 24 hours. After this time, the plates were washed three times with PBS and 100 µL transferred to a tube with 900 µL of PBS and serial dilutions were performed.20 µL of each suspension were added in SDA plates and incubated at 37° C for 24 hours. The percentage of CFU was determined in comparison to the untreated *C. albicans* biofilms.

4.8. Mechanism of action assay

4.8.1. Ergosterol assay

Assay of interaction between **3n** and ergosterol of *C. albicans* was carried out according to protocol described by Escalante and collaborators [46]. For the assays, the strain was seeded on Sabouraud dextrose agar (SDA) at 37°C for 24 hours. From this culture, the inoculum was obtained and diluted in medium RPMI-1640 supplemented with 400 µL of ergosterol, 96% ethanol and Tween 80, with the concentration between 2.5 and 5.10^4 CFU/mL, which was distributed in 96-well plates. Chalcone **3n** was diluted in DMSO and added to the plates at concentrations ranging from 62.5 to 0.48 µg/mL. Amphotericin B was used as reference antifungal drug. Plates were incubated at 37 ° C. MIC value was established as the concentration capable of of inhibition of fungal growth after visual readings.

4.8.2. Sorbitol assay

Action of chalcone 3n on the cell wall of *C. albicans* was evaluted by to protocol described by Frost and co-authors [64]. The strain was seeded on Sabouraud dextrose agar (SDA) at 37°C for 24 hours. Inoculum was obtained and diluted in medium RPMI-1640 supplemented with 0.8 M of sorbitol, with the concentration between 2.5 and 5.10^4 CFU/mL, which was distributed in 96-well plates. Chalcone **3n** was diluted in DMSO and added to the well at concentrations ranging from 62.5 to 0.48 µg/mL. Caspofungin was used as reference antifungal drug. Plates were incubated at 37 ° C. MIC value was established as the concentration capable of of inhibition of fungal growth after visual readings.

4.9. Acute toxicity assay

In vivo assay was performed to test the acute toxicity of **3n** and amphotericin B as described by Megaw and collaborators with minor modifications [65]. A total of 50 healthy larvae weighing between 0.2 and 0.3 g were selected and separated in five groups: **3n** (10 × MIC, 39.0µg/mL or 1.56 mg/kg/larvae), **3n** (100 × MIC, 390 µg/mLor 15.6 mg/kg/larvae), amphotericin B (10 ×MIC, 5.0µg/mL or 0.2 mg/kg/larvae), amphotericin B (100 ×MIC, 50.0µg/mL or 2.0 mg/kg/larvae), and vehicle control (DMSO). The larvae were chilled on ice for 20 minutes and had their prolegs cleaned with 70% ethanol. Five-microliters of chalcone**3n**solutions in DMSO, amphotericin B solutions in DMSO and vehicle were injected into the hemocoel of each larva through the last left proleg using a 10 µL Hamilton syringe

(Hamilton, Reno, NV). After injection, the larvae were incubated at 37° C and survival monitored at time intervals of 8 hoursduring 72 hours. The larvae that did not move when touched and containing high levels of melanization were counted as dead [65].

4.10. Additional antifungal assay

In order to investigate the antibacterial spectrum, chalcone **3n** was evaluated against *C. tropicalis* ATCC 750, *C. parapsilosis* ATCC 22019, *C. glabrata* ATCC 90030 and *C. krusei* ATCC 6258. MIC values were determined according to the document M27 A2-S3 (2008) of Clinical and Laboratory Standards Institute (CLSI) with some adaptations [57]. For the assays, the strain was seeded on Sabouraud dextrose agar (SDA) at 37°C for 24 hours. From this culture, the inoculum was obtained and diluted in RPMI-1640 (Sigma-Aldrich) with L-glutamine without sodium bicarbonate, supplemented with 2% glucose, buffered at pH 7.0 using MOPS buffer (0.165 mol/L), with the concentration between 2.5 and 5.10^4 CFU/mL, which was distributed in 96-well plates. Chalcone was diluted in DMSO and added to the plates at concentrations ranging from 62.5 to 0.48 μg/mL. Plates were incubated at 37 ° C and MIC values were established as the concentration capable of of inhibition of fungal growth after visual readings. MFC was determined by transferring each 96-well microplates concentration to plate with SDA and subsequent incubation at 37 ° C for 24 hours. MFC was defined as the lowest concentration that did not allow fungal growth visible in the solid medium.

4.11. Statistical analises

All assays were performed in triplicate for three independent experiments using the GraphPad Prism version 5.0 (GraphPad Software Inc.). The data concerning the biofilm assays were analyzed by one-way analysis of variance (ANOVA) with Tukey's multiple comparison test, with a significance level of 5%. For the *G. mellonella* toxicity model, Kaplan-Meier killing curves were plotted on GraphPad Prism version 5.0 and estimations of differences in survival were compared using log-rank test.

References

1. Tong Y, Tang J. *Candida albicans* infection and intestinal immunity. *Microbiological Research*. 2017;198:27-35.

2. Blot S, De Waele JJ. Critical issues in the clinical management of complicated intra-abdominal infections: *Drugs*. 2005;65:1611-1620.

3. Mah T-F. Biofilm-specific antibiotic resistance. *Future Microbiology*. 2012;7:1061-1072.

4. Römling U, Balsalobre C. Biofilm infections, their resilience to therapy and innovative treatment strategies. *J Intern Med*. 2012;272:541-561.

5. Fanning S, Mitchell AP. Fungal biofilms. Heitman J, ed. *PLoS Pathog*. 2012;8:e1002585.

6. Chandra J, Kuhn DM, Mukherjee PK, Hoyer LL, McCormick T, Ghannoum MA. Biofilm formation by the fungal pathogen *Candida albicans*: development, architecture, and drug resistance. *J Bacteriol*. 2001;183:5385-5394.

7. Douglas LJ. Candida biofilms and their role in infection. *Trends in Microbiology*. 2003;11:30-36.

8. Donlan RM, Costerton JW. Biofilms: survival mechanisms of clinically relevant microorganisms. *CMR*. 2002;15:167-193.

9. White TC, Marr KA, Bowden RA. Clinical, cellular, and molecular factors that contribute to antifungal drug resistance. *Clin Microbiol Rev*. 1998;11:382-402.

10. Tobudic S, Kratzer C, Lassnigg A, Graninger W, Presterl E. In vitro activity of antifungal combinations against *Candida albicans* biofilms. *Journal of Antimicrobial Chemotherapy*. 2010;65:271-274.

11. Zhuang C, Zhang W, Sheng C, Zhang W, Xing C, Miao Z. Chalcone: a privileged structure in medicinal chemistry. *Chem Rev*. 2017;117:7762-7810.

12. Gupta D, Jain D. Chalcone derivatives as potential antifungal agents: Synthesis, and antifungal activity. *J Adv Pharm Technol Res*. 2015;6:114.

13. Messier C, Epifano F, Genovese S, Grenier D. Inhibition of *Candida albicans* biofilm formation and yeast-hyphal transition by 4-hydroxycordoin. *Phytomedicine*. 2011;18:380-383.

14. Bahekar SP, Hande SV, Agrawal NR, et al. Sulfonamide chalcones: Synthesis and in vitro exploration for therapeutic potential against Brugia malayi. *European Journal of Medicinal Chemistry*. 2016;124:262-269.

15. Karam El-Din A-ZA, Al-Basri HM, El-Naggar MY. Critical factors affecting the adherence of *Candida albicans* to the vaginal epithelium. *Journal of Taibah University for Science*. 2012;6:10-18.

16. Youssef MSK, Abeed AAO. Synthesis and antimicrobial activity of some novel 2-thienyl substituted heterocycles. *Heterocyclic Communications*. 2014;20.

17. Brown N. Bioisosteres and scaffold hopping in medicinal chemistry. *Mol Inf*. 2014;33:458-462.

18. Amole KL, Bello IA, Oyewale AO. Synthesis, characterization and antifungal study of five new derivatives of e-1-(2-hydroxyphenyl)chalcone. *Chemistry Africa*. 2019;2:1-14.

19. Fryer RI, Zhang P, Rios R, Gu ZQ, Basile AS, Skolnick P. Structure-activity relationship studies at benzodiazepine receptor (BZR): a comparison of the substituent effects of pyrazoloquinolinone analogs. *Journal Medicinal Chemistry*. 1993;36:1669-1673.

20. Strebel S, Gurzeler JA, Schneider MC, Aeschbach A, Kindler CH. Small-dose intrathecal clonidine and isobaric bupivacaine for orthopedic surgery: a dose-response study: *Anesthesia & Analgesia*. 2004;99:1231-1238.

21. Laniado-Laborín R, Cabrales-Vargas MN. Amphotericin B: side effects and toxicity. *Revista Iberoamericana de Micología*. 2009;26:223-227.

22. Khot PD, Suci PA, Miller RL, Nelson RD, Tyler BJ. A small subpopulation of blastospores in *Candida albicans* biofilms exhibit resistance to amphotericin b associated with differential regulation of ergosterol and β-1,6-glucan pathway genes. *AAC*. 2006;50:3708-3716.

23. Eldesouky HE, Li X, Abutaleb NS, Mohammad H, Seleem MN. Synergistic interactions of sulfamethoxazole and azole antifungal drugs against emerging multidrug-resistant Candida auris. *International Journal of Antimicrobial Agents*. 2018;52:754-761.

24. Nett JE, Andes DR. Antifungal agents. *Infectious Disease Clinics of North America*. 2016;30:51-83.

25. Prasad R, Shah AH, Rawal MK. Antifungals: mechanism of action and drug resistance. In: Ramos J, Sychrová H, Kschischo M, eds. *Yeast Membrane Transport*. Vol 892. Springer International Publishing; 2016:327-349.

26. Wang Y-H, Dong H-H, Zhao F, et al. The synthesis and synergistic antifungal effects of chalcones against drug resistant *Candida albicans*. *Bioorganic & Medicinal Chemistry Letters*. 2016;26:3098-3102.

27. Klepser M. Multi-center evaluation of antifungal time-kill methods: *Journal of Infectious Disease Pharmacotherapy*. 2001;5:29-41.

28. Monk BC, Goffeau A. Outwitting multidrug resistance to antifungals. *Science*. 2008;321:367-369.

29. Ling LL, Schneider T, Peoples AJ, et al. Erratum: A new antibiotic kills pathogens without detectable resistance. *Nature*. 2015;520:388-388.

30. Pfaller MA, Sheehan DJ, Rex JH. Determination of fungicidal activities against yeasts and molds: lessons learned from bactericidal testing and the need for standardization. *CMR*. 2004;17:268-280.

31. Ernst EJ, Roling EE, Petzold CR, Keele DJ, Klepser ME. In vitro activity of micafungin (FK-463) against candida spp. : microdilution, time-kill, and postantifungal-effect studies. *AAC*. 2002;46:3846-3853.

32. Kashem SW, Kaplan DH. Skin immunity to *Candida albicans*. *Trends in Immunology*. 2016;37:440-450.

33. Mathé L, Van Dijck P. Recent insights into *Candida albicans* biofilm resistance mechanisms. *Curr Genet*. 2013;59(4):251-264. doi:10.1007/s00294-013-0400-3

34. Liu Y, Filler SG. *Candida albicans* als3, a multifunctional adhesin and invasin. *Eukaryotic Cell*. 2011;10:168-173.

35. Costerton JW, Lewandowski Z, Caldwell DE, Korber DR, Lappin-Scott HM. Microbial biofilms. *Annu Rev Microbiol*. 1995;49:711-745.

36. Shchepin R, Hornby JM, Burger E, Niessen T, Dussault P, Nickerson KW. Quorum sensing in *Candida albicans*. *Chemistry & Biology*. 2003;10:743-750.

37. Chandra J, Kuhn DM, Mukherjee PK, Hoyer LL, McCormick T, Ghannoum MA. Biofilm formation by the fungal pathogen *Candida albicans*: development, architecture, and drug resistance. *J Bacteriol*. 2001;183:5385-5394.

38. Dietrich LA, Friedmann TS, eds. *Candida Albicans: Symptoms, Causes and Treatment Options*. *Nova Biomedical*; 2013.

39. Bink A. Anti-biofilm strategies: how to eradicate candida biofilms? *TOMYCJ*. 2011;5:29-38.

40. Emeri FT de AS, Rosalen PL, Paganini ÉR, et al. Antimicrobial activity of nitrochalcone and pentyl caffeate against hospital pathogens results in decreased microbial adhesion and biofilm formation. *Biofouling*. 2019;35:129-142.

41. Nett JE, Zarnowski R, Cabezas-Olcoz J, et al. Host contributions to construction of three device-associated *Candida albicans* biofilms. Deepe GS, ed. *Infect Immun*. 2015;83:4630-4638.

42. Cabezón V, Llama-Palacios A, Nombela C, Monteoliva L, Gil C. Analysis of *Candida albicans* plasma membrane proteome. *Proteomics*. 2009;9:4770-4786.

43. Bowman SM, Free SJ. The structure and synthesis of the fungal cell wall. *Bioessays*. 2006;28:799-808.

44. Minnebruggen GV, Francois IEJA, Cammue BPA, et al. A General Overview on Past, Present and Future Antimycotics. *TOMYCJ*. 2010;4:22-32.

45. Mouri R, Konoki K, Matsumori N, Oishi T, Murata M. Complex formation of amphotericin b in sterol-containing membranes as evidenced by surface plasmon resonance †. *Biochemistry*. 2008;47:7807-7815.

46. Escalante A, Gattuso M, Pérez P, Zacchino S. Evidence for the mechanism of action of the antifungal phytolaccoside b isolated from *phytolacca tetramera* hauman. *J Nat Prod*. 2008;71:1720-1725.

47. Frost DJ, Brandt KD, Cugier D, Goldman R. A whole-cell *Candida albicans* assay for the detection of inhibitors towards fungal cell wall synthesis and assembly. *J Antibiot*. 1995;48:306-310.

48. Svetaz L, Agüero M, Alvarez S, et al. Antifungal activity of *zuccagnia punctata* cav. : evidence for the mechanism of action. *Planta Med*. 2007;73:1074-1080.

49. Andrade JT, Santos FRS, Lima WG, et al. Design, synthesis, biological activity and structure-activity relationship studies of chalcone derivatives as potential anti-*Candida* agents. *J Antibiot*. 2018;71:702-712.

50. Champion OL, Wagley S, Titball RW. *Galleria mellonella* as a model host for microbiological and toxin research. *Virulence*. 2016;7:840-845.

51. Wojda I. Immunity of the greater wax moth *Galleria mellonella*: Galleria mellonella immunity. *Insect Science*. 2017;24:342-357.

52. dos Santos MB, Pinhanelli VC, Garcia MAR, et al. Antiproliferative and pro-apoptotic activities of 2'- and 4'-aminochalcones against tumor canine cells. *European Journal of Medicinal Chemistry*. 2017;138:884-889.

53. Garcia MAR, Theodoro RS, Sardi JCO, et al. Design, synthesis and antibacterial activity of chalcomes against MSSA and MRSA planktonic cells and biofilms. *Bioorganic Chemistry.* 2021;116:105279.

54. Ruanwas P, Chantrapromma S, Fun HK. Synthesis, characterization, antioxidant, and antibacterial activities of 2-aminochalcones and crystal structure of (2*E*)-1-(2-aminophenyl)-3-(4-ethoxyphenyl)-2-propen-1-one. *Mol. Cryst. Liq. Cryst.* 2015;609:126-139.

55. Zhao F, Zhao QJ, Zhao JX, Zhang DZ, Wu QY, Jin YS. Synthesis and cdc25B inhibitory activity evaluation of chalcones. *Chem. Nat. Compd*. 2013;49:206-214.

56. dos Santos MB, Bertholin Anselmo D, de Oliveira JG, et al. Antiproliferative activity and p53 upregulation effects of chalcones on human breast cancer cells. *Journal of Enzyme Inhibition and Medicinal Chemistry*. 2019;34:1093-1099.

57. Rex JH, Clinical and Laboratory Standards Institute, eds. *Reference Method for Broth Dilution Antifungal Susceptibility Testing of Yeasts: Approved Standard*. 3rd ed. National Committee for Clinical Laboratory Standards; 2008.

58. Odds FC. Synergy, antagonism, and what the chequerboard puts between them. *Journal of Antimicrobial Chemotherapy*. 2003;52:1-1.

59. Sangalli-Leite F, Scorzoni L, Alves de Paula e Silva AC, et al. Synergistic effect of pedalitin and amphotericin B against *Cryptococcus neoformans* by *in vitro* and *in vivo* evaluation. *International Journal of Antimicrobial Agents*. 2016;48:504-511.

60. Li D-D, Zhao L-X, Mylonakis E, et al. *In vitro* and *in vivo* activities of pterostilbene against *Candida albicans* biofilms. *Antimicrob Agents Chemother*. 2014;58:2344-2355.

61. Sardi JCO, Duque C, Mariano FS, Marques MR, Höfling JF, Gonçalves RB. Adhesion and invasion of *Candida albicans* from periodontal pockets of patients with chronic periodontitis and diabetes to gingival human fibroblasts. *Med Mycol*. 2012;50:43-49.

62. Pitangui NS, Sardi JCO, Silva JF, et al. Adhesion of *Histoplasma capsulatum* to pneumocytes and biofilm formation on an abiotic surface. *Biofouling*. 2012;28:711-718.

63. Ibarra-Trujillo C, Villar-Vidal M, Gaitán-Cepeda LA, Pozos-Guillen A, Mendoza-de Elias R, Sánchez-Vargas LO. Ensayo de formación y cuantificación de biopelículas mixtas de *Candida albicans* y *Staphylococcus aureus*. *Revista Iberoamericana de Micología*. 2012;29:214-222.

64. Frost DJ, Brandt KD, Cugier D, Goldman R. A whole-cell *Candida albicans* assay for the detection of inhibitors towards fungal cell wall synthesis and assembly. *J Antibiot*. 1995;48:306-310.

65. Megaw J, Thompson TP, Lafferty RA, Gilmore BF. Galleria mellonella as a novel in vivo model for assessment of the toxicity of 1-alkyl-3-methylimidazolium chloride ionic liquids. *Chemosphere*. 2015;139:197-201.

Fig 1. Synthesis of chalcones

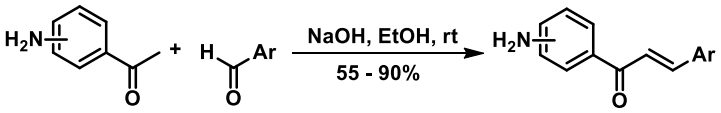

Ar = ring B

Fig 2. Time-kill curve of **3n** on *C. albicans*.

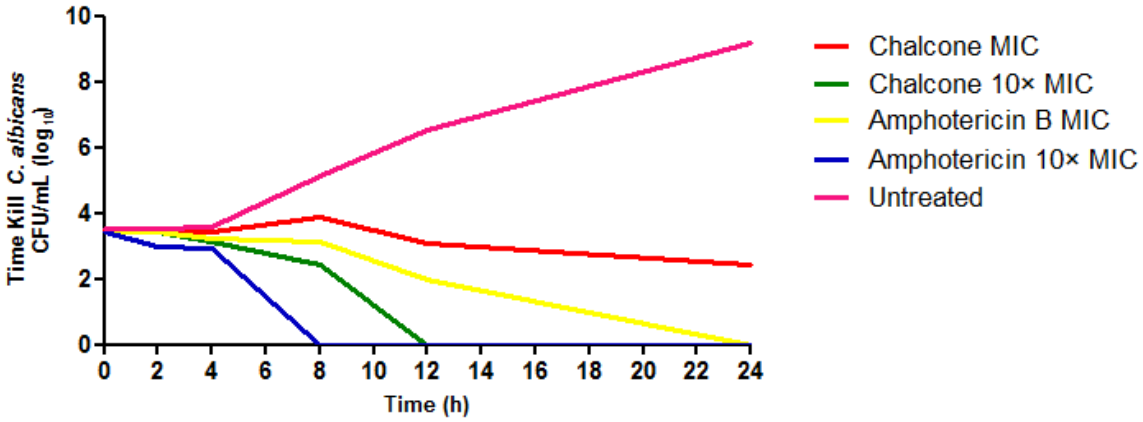

Fig 3. Anti-adhesion activity of **3n** on *C. albicans* adhesion to human HaCat. Different letters above the bar denote statistical difference when compared to each other. Data compared to vehicle where $P < 0.05$ - One-way ANOVA with Tukey Post test.

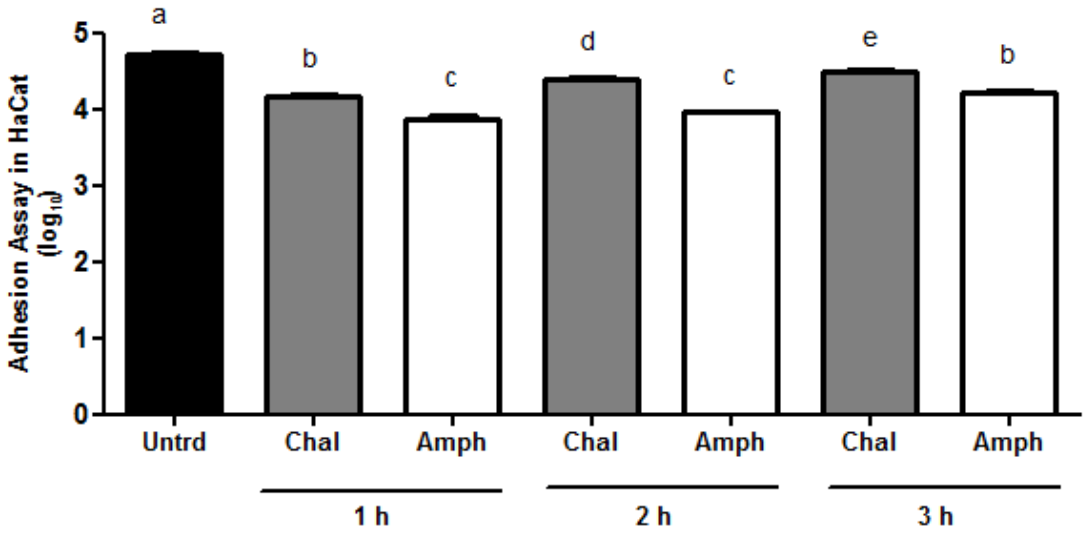

Fig 4. Effect of **3n** on *C. albicans* biofilm formation. Different letters above the bar denote statistical difference when compared to each other. Data compared to vehicle where $P < 0.05$ - One-way ANOVA with Tukey Post test.

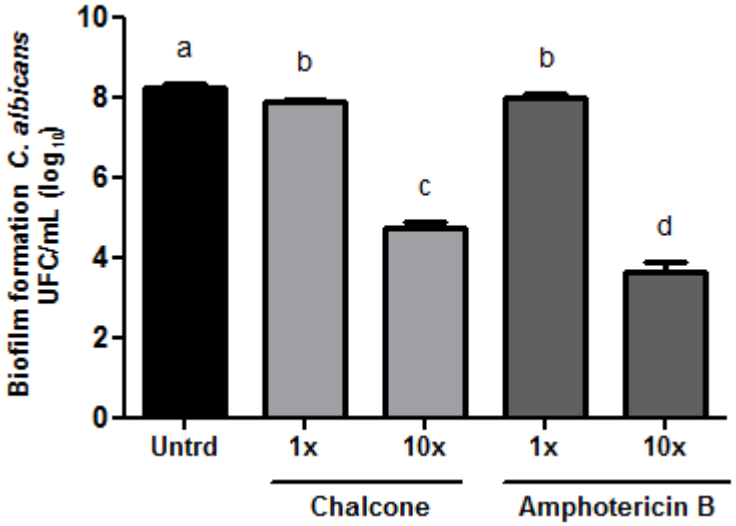

Fig 5. Effect of **3n** on *C. albicans* preformed biofilms. Different letters above the bar denote statistical difference when compared to each other. Data compared to vehicle where $P < 0.05$ - One-way ANOVA with Tukey Post test.

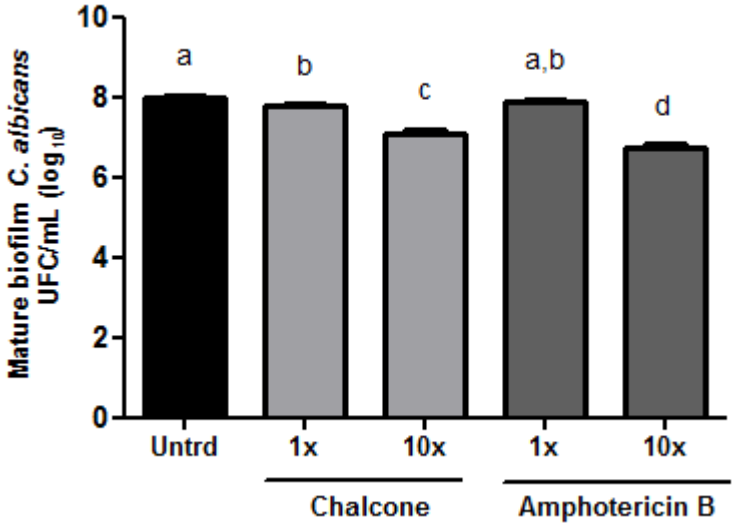

Fig 6. Percent survival over time of *G. mellonella* larvae injected with chalcone **3n** and amphotericin B respective MIC and 10 × MIC values ($P > 0.05$, log-rank test).

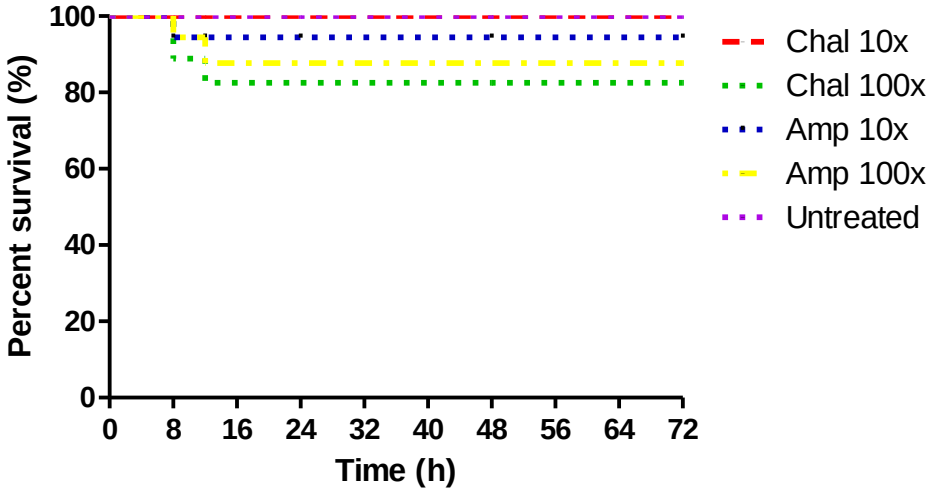

Table 1. Antifungal activity of chalcones against *C. albicans* expressed as MIC and MFC values in μg/mL

Chalcone	Ar	MIC/MFC (μg/mL)
		C. albicans
2a	phenyl	62.5/ > 62.5
2b	2-thiophenyl	*
2c	2-furanyl	*
2d	3-pyridinyl	15.6/31.2
2e	4-pyridinyl	62.5/62.5
2f	4-methoxyphenyl	*
2g	4-methylphenyl	*
2h	4- chlorophenyl	*
2i	3,4-dichlorophenyl	*
3a	phenyl	15.6/31.2
3b	2-thiophenyl	15.6/31.2
3c	2-furanyl	*
3d	3-pyridinyl	15.6/31.2
3e	4-pyridinyl	15.6/15.6
3f	4-methoxyphenyl	*
3g	4-methylphenyl	*
3h	4-chlorophenyl	31.2/31.2
3i	3,4-dichlorophenyl	31.2/31.2
3j	2,6-dichlorophenyl	7.80/15.6
3k	3-chlorophenyl	62.5/62.5
3l	2-chlorophenyl	15.6/15.6
3m	4-fluorophenyl	15.6/31.2
3n	3-fluorophenyl	3.9/3.9
3o	2-fluorophenyl	7.8/7.8
3p	4-bromophenyl	31.2/31.2
3q	3-bromophenyl	62.5/62.5
3r	2-bromophenyl	62.5/62.5
3s	4-trifluoromethoxyphenyl	*
3t	3-trifluoromethyl-4-chlorophenyl	62.5/62.5
3u	4-nitrophenyl	*
3v	3-nitrophenyl	*

4a	phenyl	31.2/62.5
4b	2-thiophenyl	31.2/31.2
4c	2-furanyl	62.5/62.5
4d	3-pyridinyl	15.6/31.2
4e	4-pyridinyl	62.5/62.5
4f	4-methoxyphenyl	*
4g	4-methylphenyl	*
4h	4- chlorophenyl	*
4i	3,4-dichlorophenyl	*
amphotericin B		0.5/nd

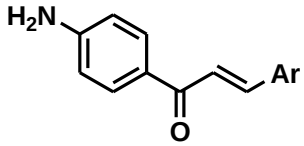

*MIC and MFC values higher than 62.5 μg/mL. nd = not determined.

Table 2. Antifungal effect of combination between **3n** and amphotericin B against *C. albicans*

Strain	**Combination**	**MIC (µg/mL)**				**FICI**	**Type of combination**
		Alone		**Combined**			
		3n	**d**	**3n**	**d**	**$FIC_{3n}+FIC_d$**	
C. albicans	**3n**+amphotericin (d)	3.9	0.5	0.9	0.1	0.4	Synergistic

Table 3. Mechanism of action of **3n** on the membrane of *C. albicans* expressed as MIC values in μg/mL

Compound	***C. albicans* MIC (μg/mL)**	
	MIC	MIC with Ergosterol
Chalcone **3n**	3.9	7.8
Amphotericin B	0.5	16.0

Table 4. Mechanism of action of **3n** on cell wall of *C. albicans* expressed as MIC values in μg/mL

Compound	***C. albicans* MIC (μg/mL)**	
	MIC	MIC with Sorbitol
Chalcone **3n**	3.9	3.9
Caspofungin	0.1	15.6

SUPPLEMENTARY MATERIAL

Antifungal activity of chalcones against *Candida albicans* planktonic cells and biofilms

Mayara A. R. Garcia[a], Mariana B. Santos[a], Ricardo A. Z. Bertani[a], Janaína de C. O. Sardi[b], Pedro L.Rosalen[b], Luis O. Regasini[a,*]

[a]*Department of Chemistryand Environmental Sciences, Institute of Biosciences, Humanities and Exact Sciences, São Paulo State University Júlio de Mesquita Filho, São José do Rio Preto, SP, Brazil.*

[b]*Department of Physiological Sciences, Piracicaba Dental School, University of Campinas, Piracicaba, SP, brazil.*

*** Corresponding author.**

E-mail addresses: regasini@ibilce.unesp.br (LO Regasini)

Figure S 1. ^{1}H NMR spectrum of compound **2a** (DMSO-d_6; 600 MHz)

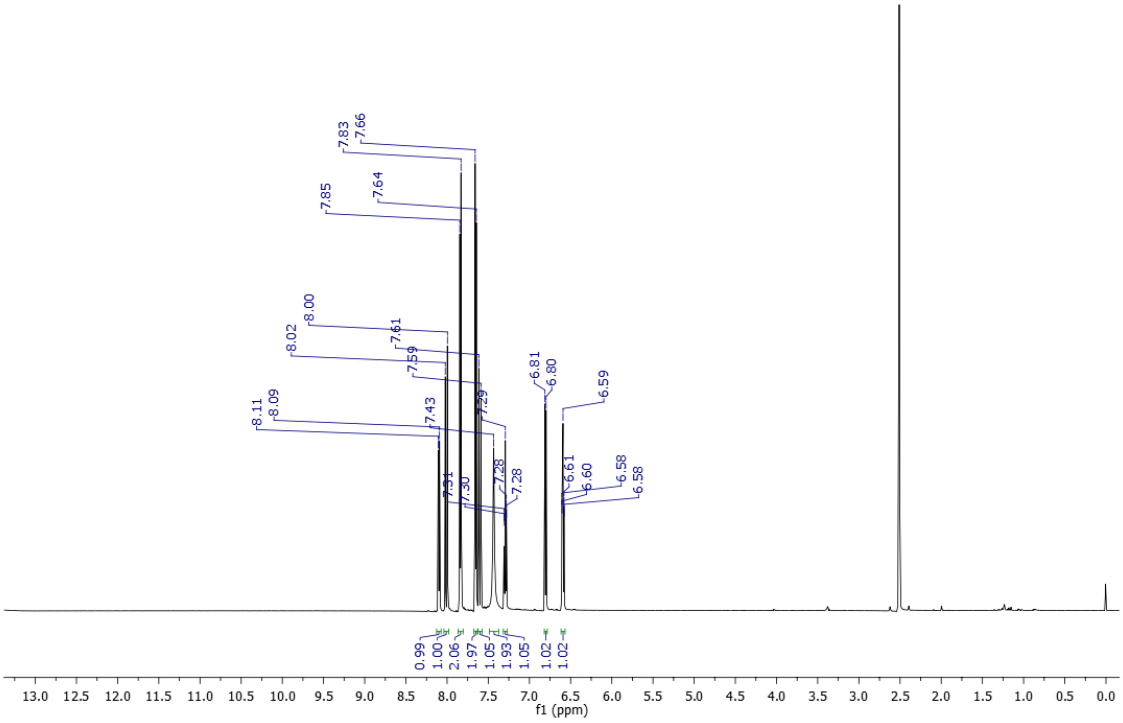

Figure S 2. ^{13}C NMR spectrum of compound **2a** (DMSO-d_6; 150 MHz)

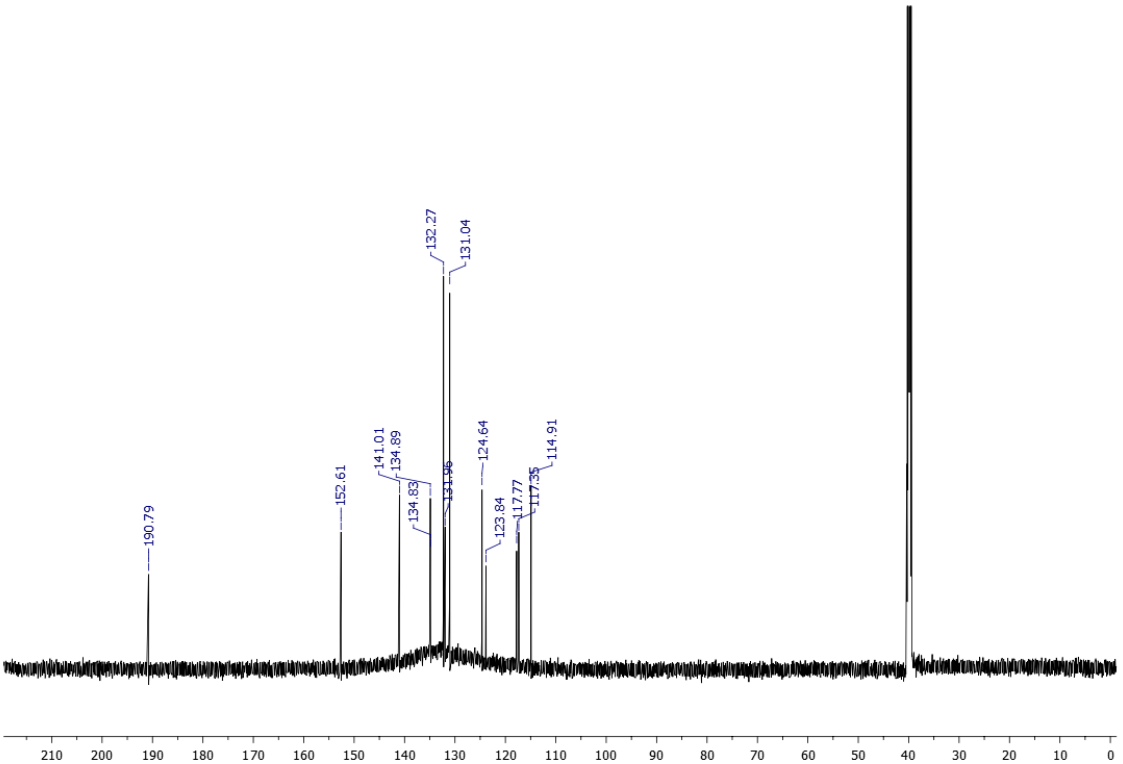

Figure S 3. HPLC chromatogram of compound **2a**

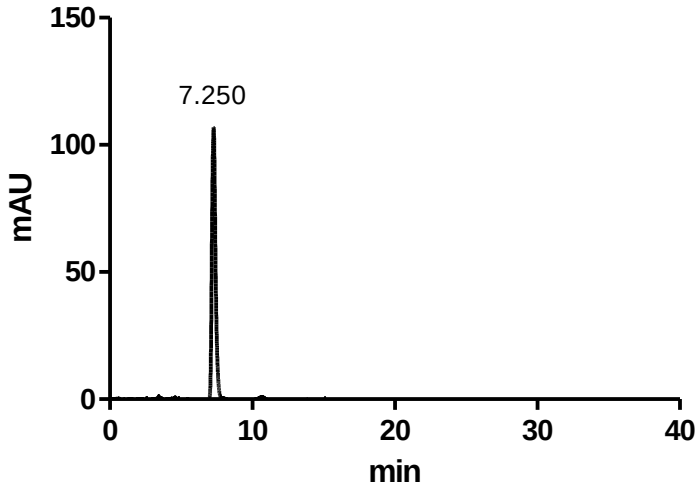

Figure S 4. UV-Vis spectrum of compound **2a**

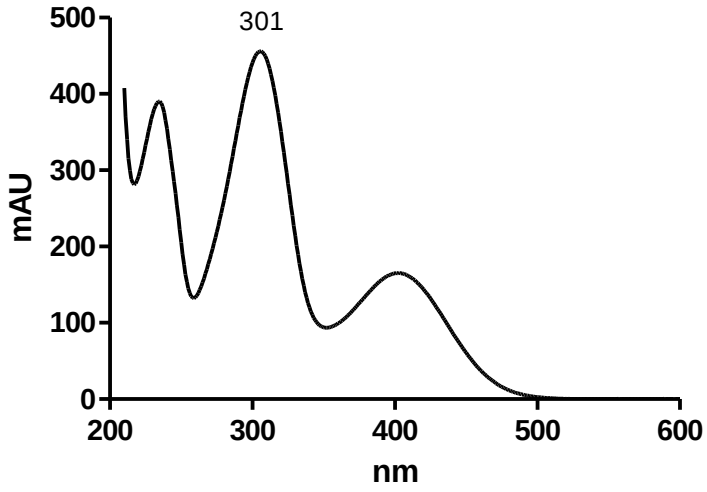

Figure S 5. ^{1}H NMR spectrum of compound **2b** (DMSO-d_6; 600 MHz)

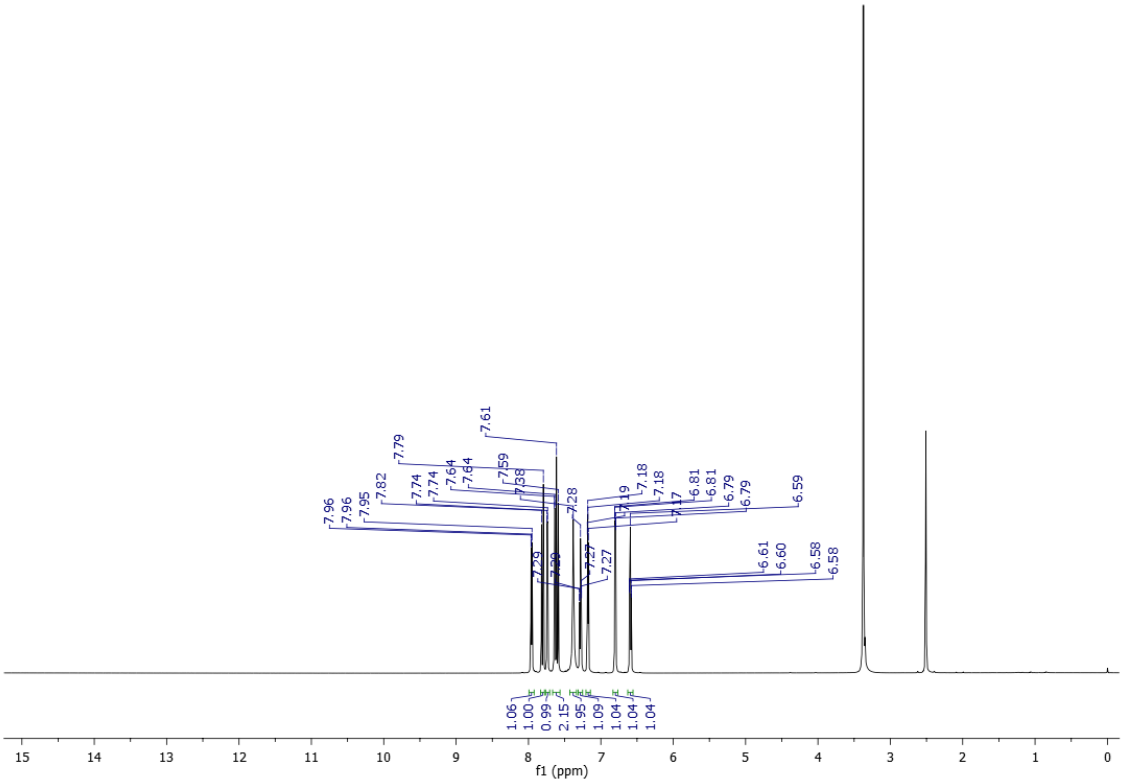

Figure S 6. ^{13}C NMR spectrum of compound **2b** (DMSO-d_6; 150 MHz)

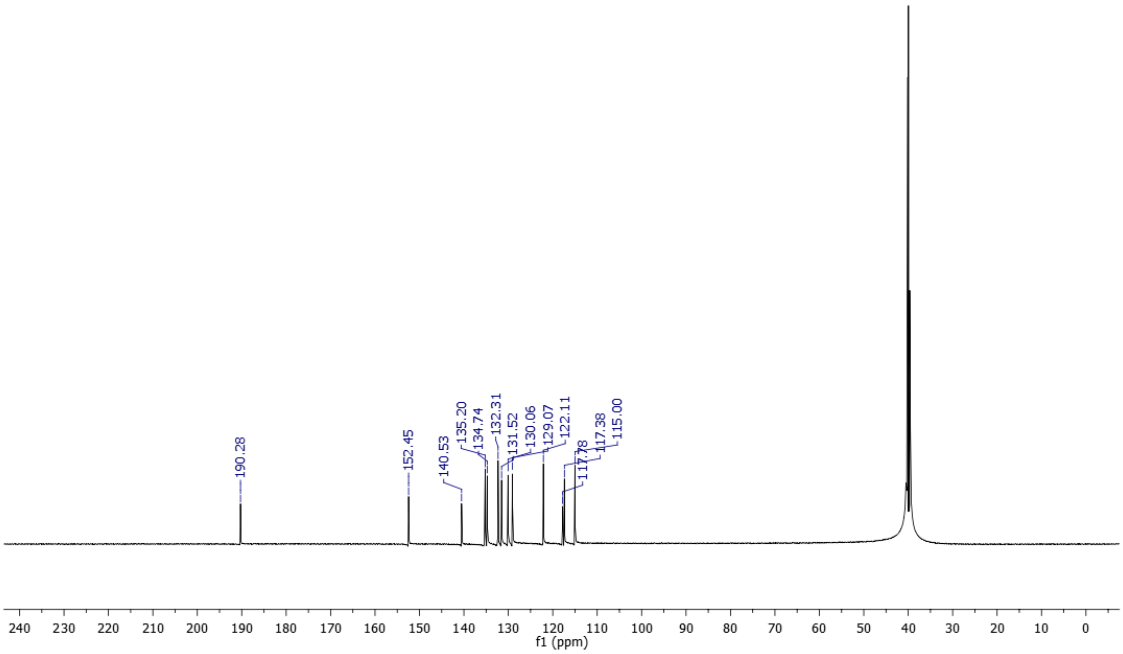

Figure S 7. HPLC chromatogram of compound **2b**

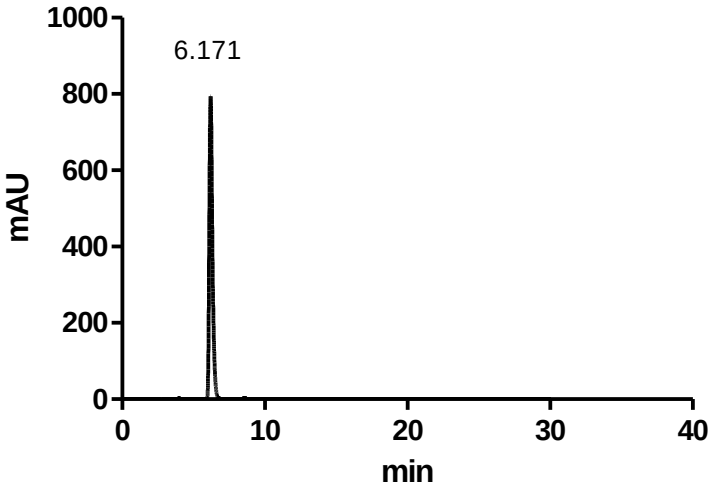

Figure S 8. UV-Vis spectrum of compound **2b**

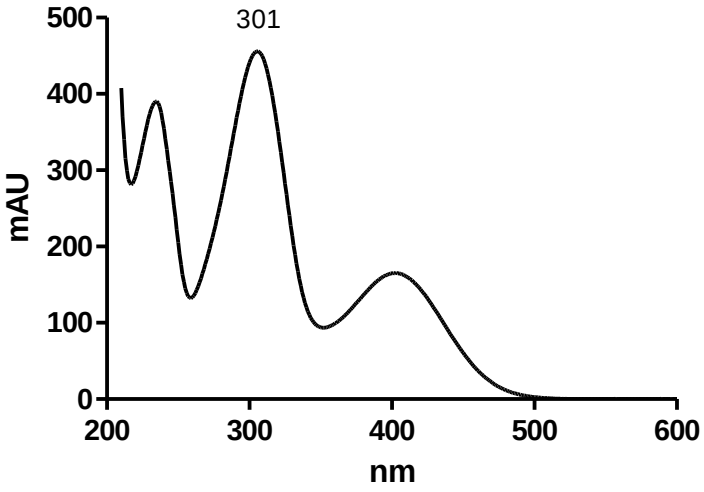

Figure S 9. ^{1}H NMR spectrum of compound **2c** (DMSO-d_6; 600 MHz)

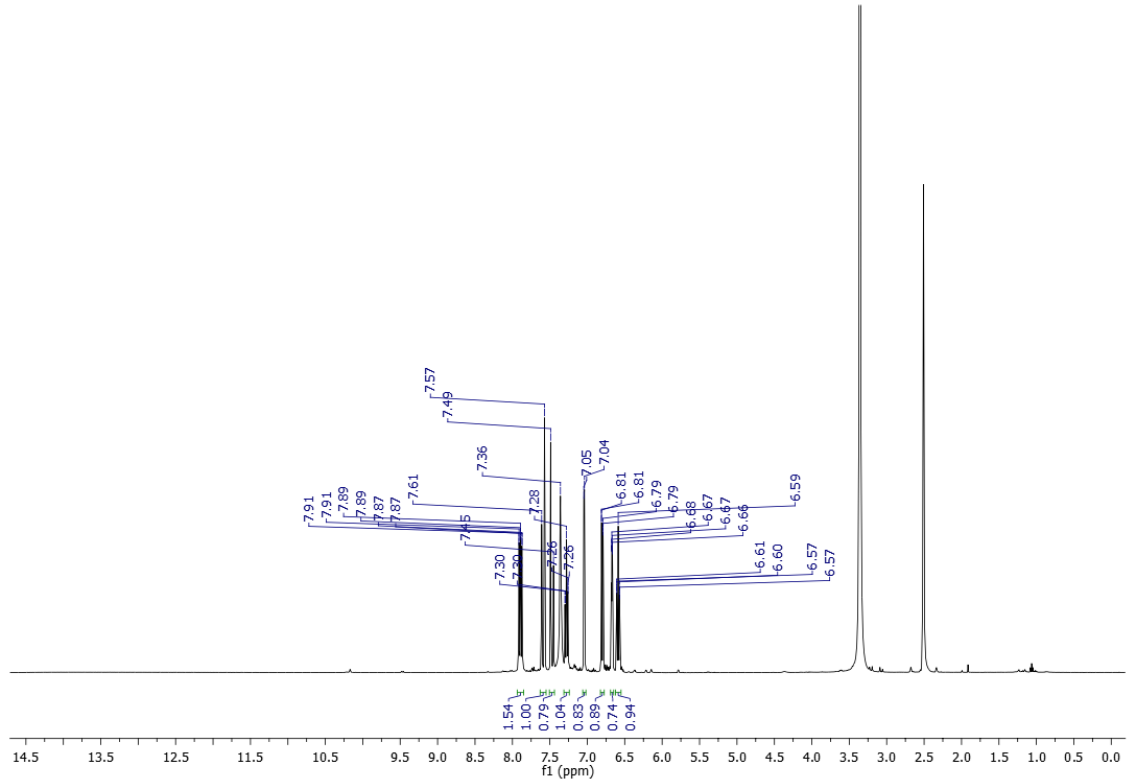

Figure S 10. ^{13}C NMR spectrum of compound **2c** (DMSO-d_6; 150 MHz)

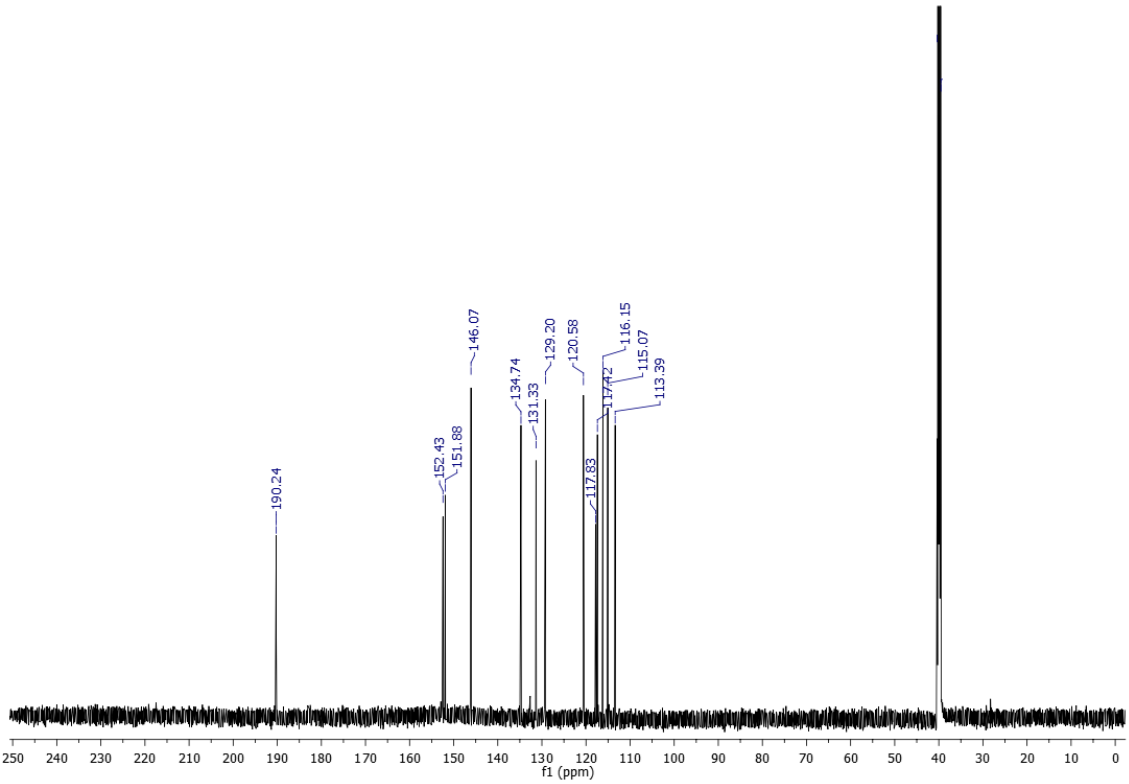

Figure S 11. HPLC chromatogram of compound **2c**

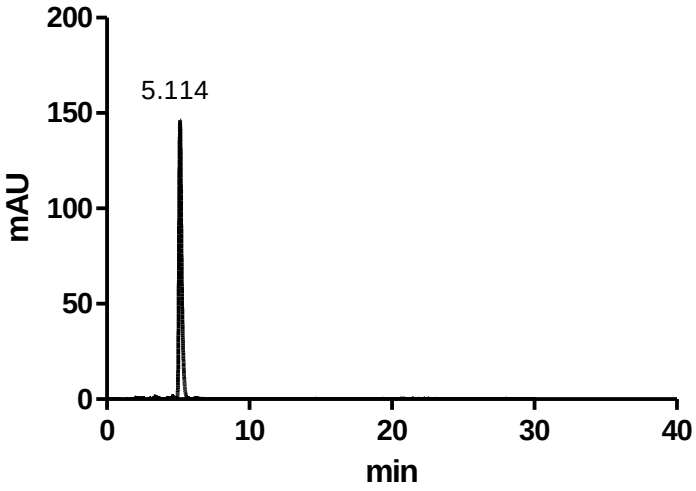

Figure S 12. UV-Vis spectrum of compound **2c**

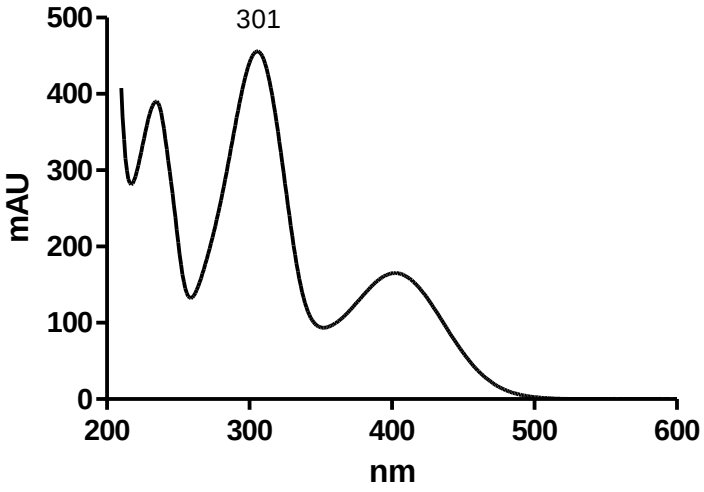

Figure S 13. ^{1}H NMR spectrum of compound **2d** (DMSO-d_6; 600 MHz)

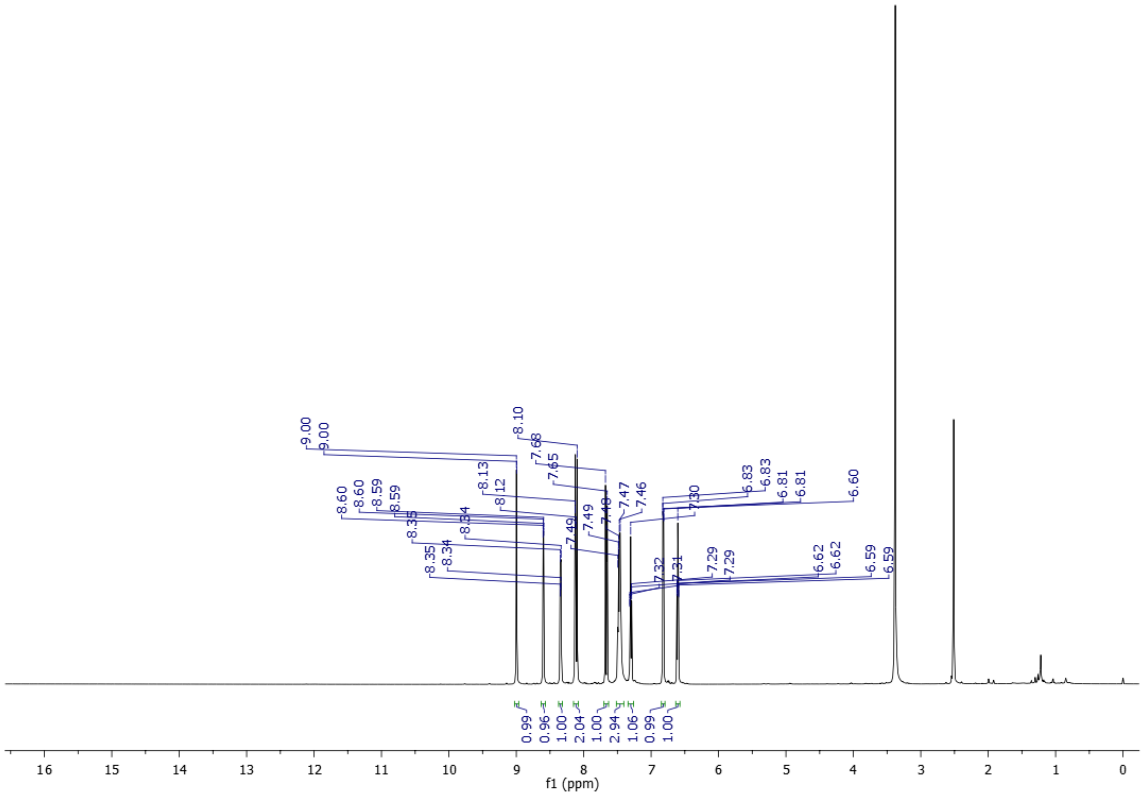

Figure S 14.^{13}C NMR spectrum of compound **2d** (DMSO-d_6; 150 MHz)

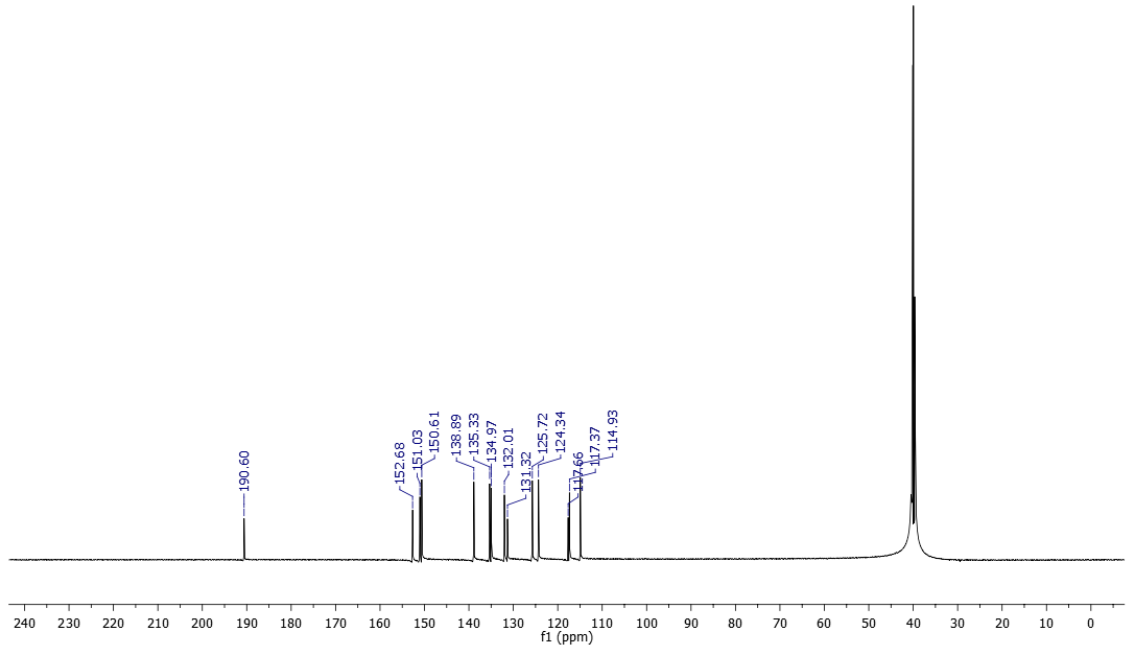

Figure S 15. HPLC chromatogram of compound **2d**

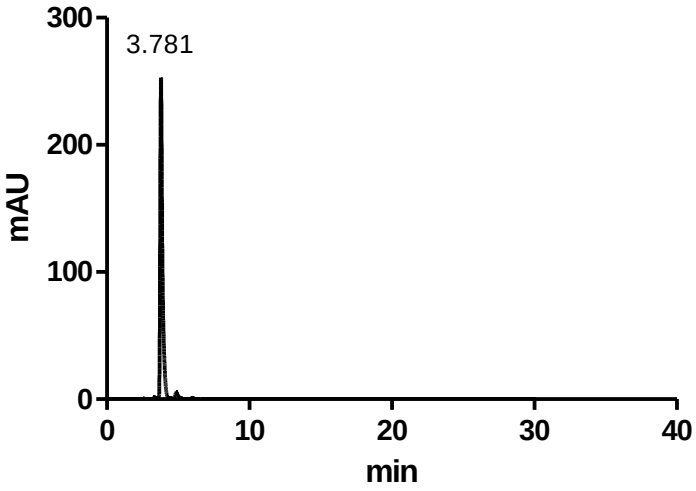

Figure S 16. UV-Vis spectrum of compound **2d**

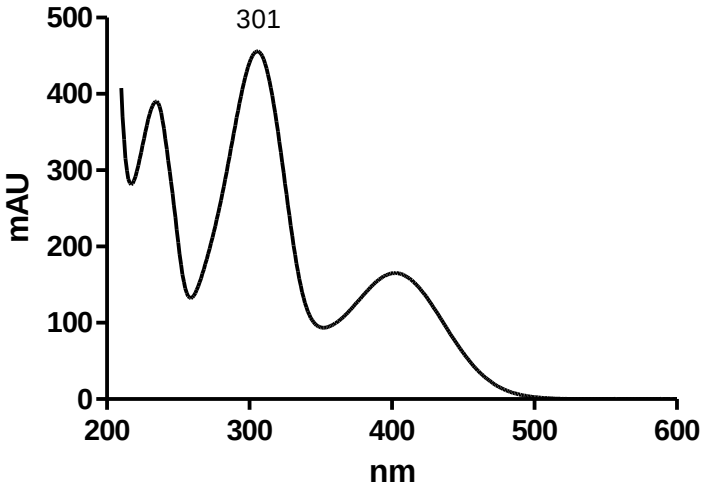

Figure S 17. ^{1}H NMR spectrum of compound **2e** (DMSO-d_6; 600 MHz)

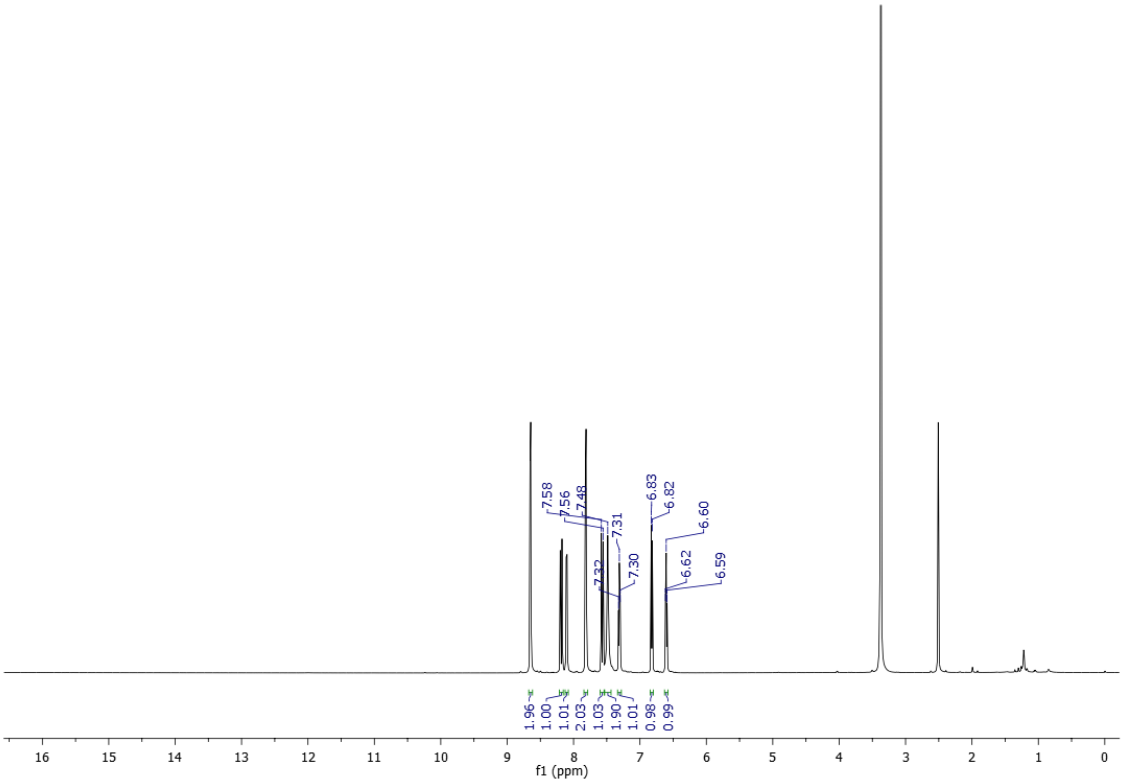

Figure S 18. ^{13}C NMR spectrum of compound **2e** (DMSO-d_6; 150 MHz)

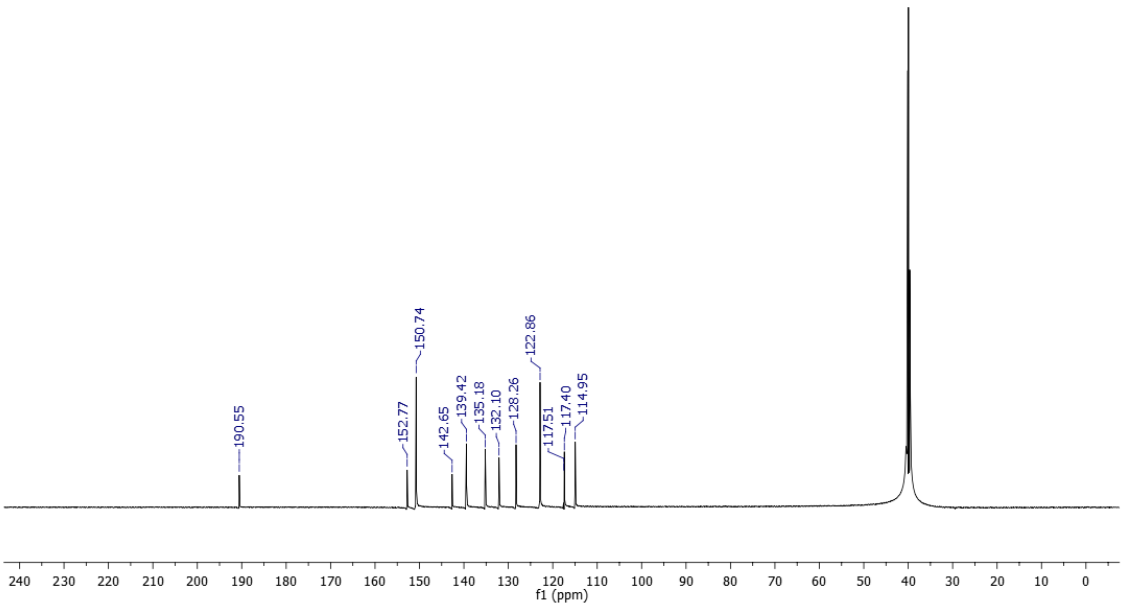

Figure S 19. HPLC chromatogram of compound **2e**

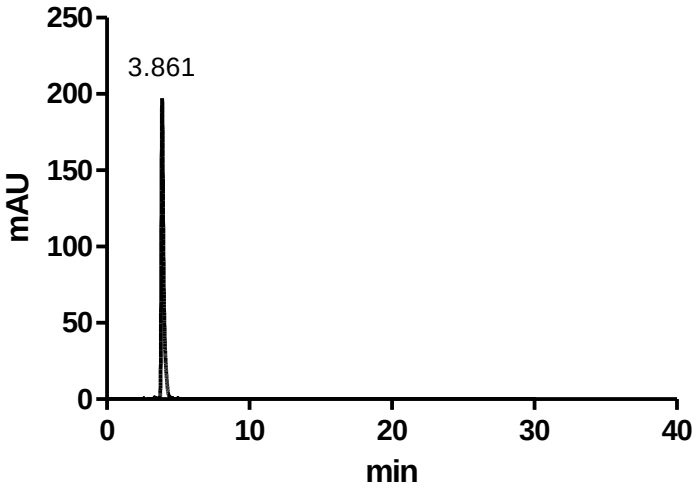

Figure S 20. UV-Vis spectrum of compound **2e**

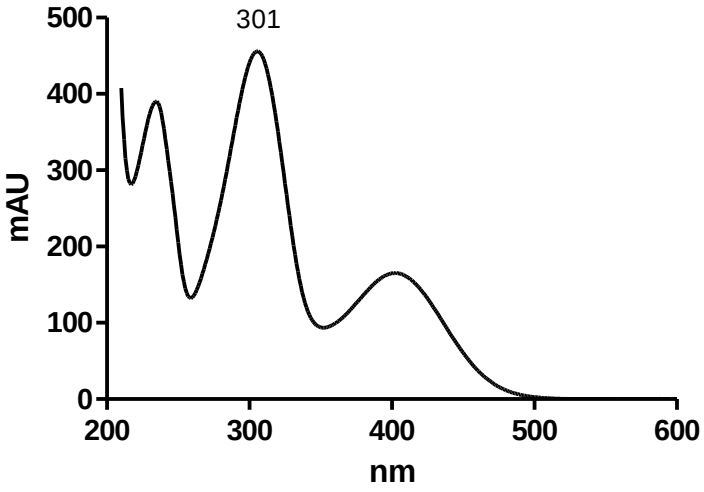

Figure S 21. ^{1}H NMR spectrum of compound **2f** (DMSO-d_6; 600 MHz)

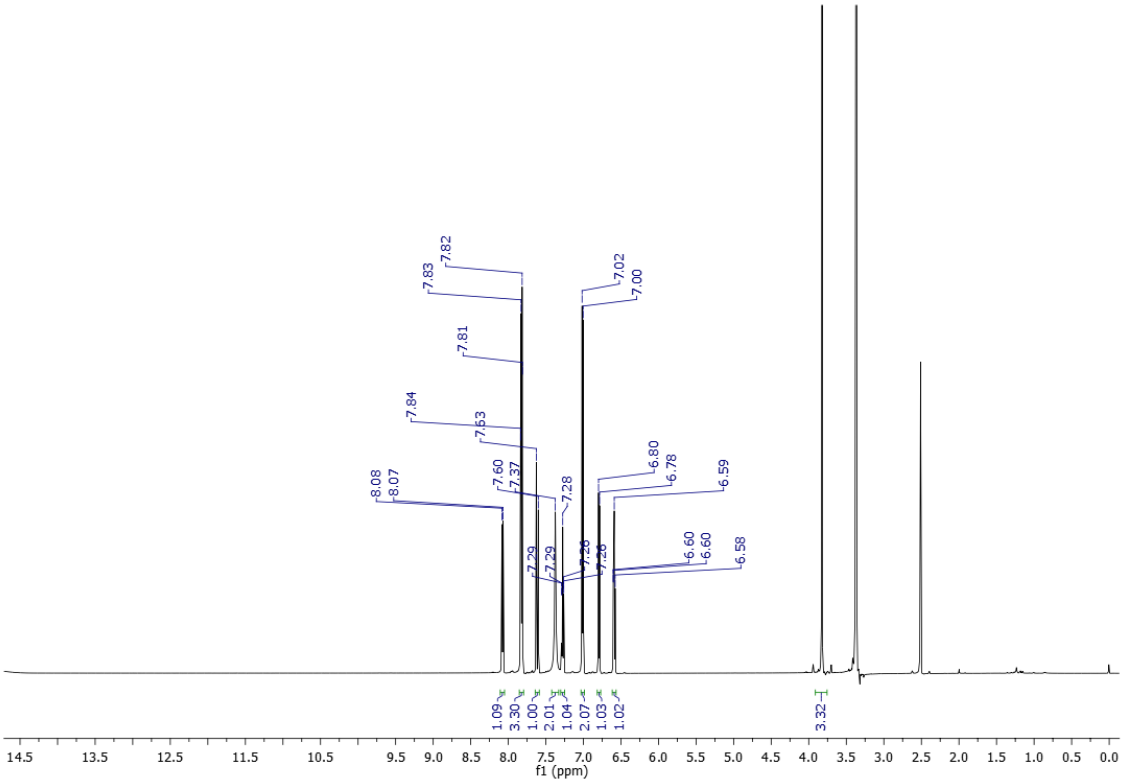

Figure S 22. ^{13}C NMR spectrum of compound **2f** (DMSO-d_6; 150 MHz)

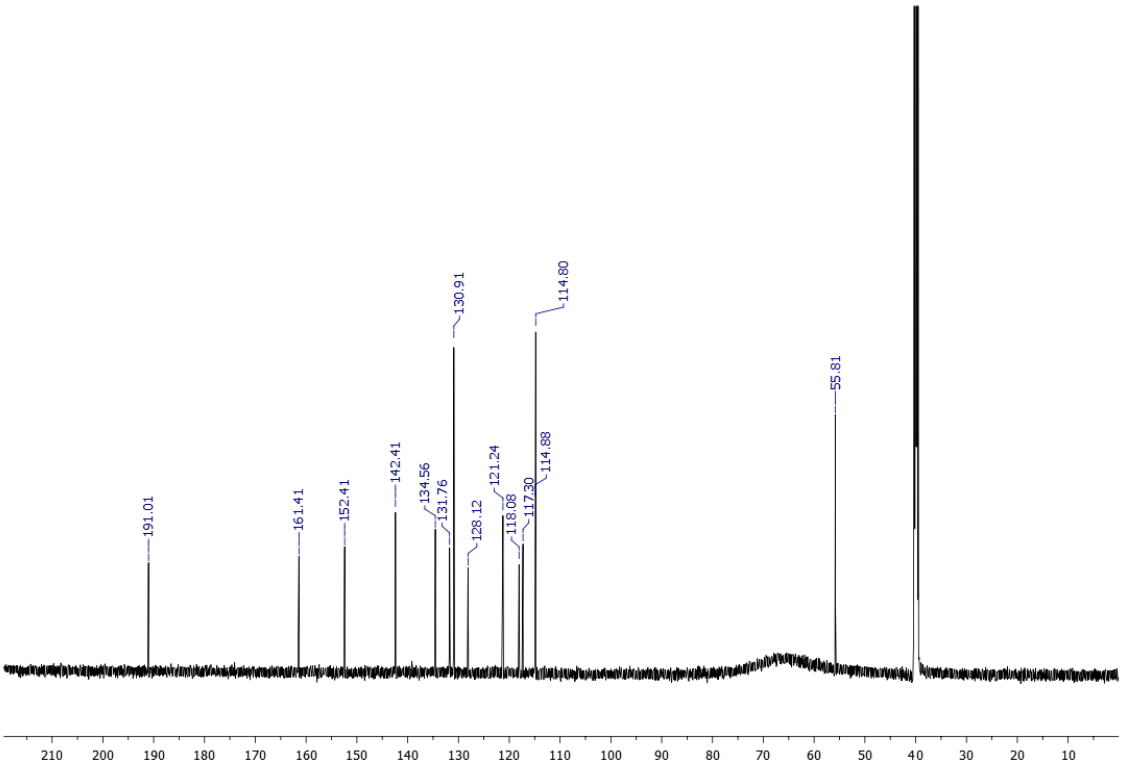

Figure S 23. HPLC chromatogram of compound **2f**

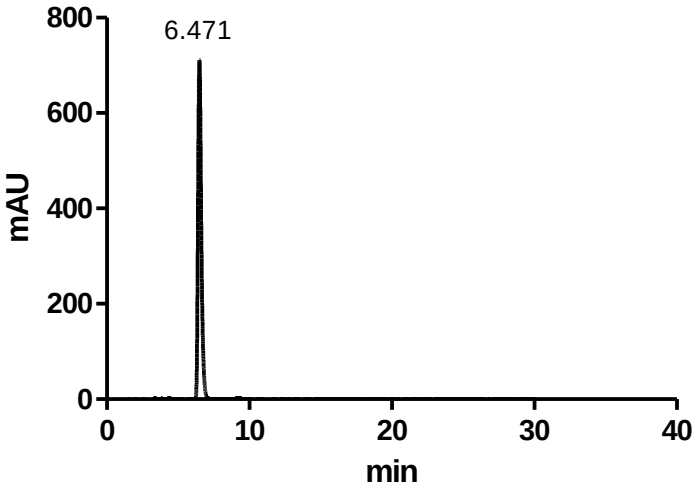

Figure S 24. UV-Vis spectrum of compound **2f**

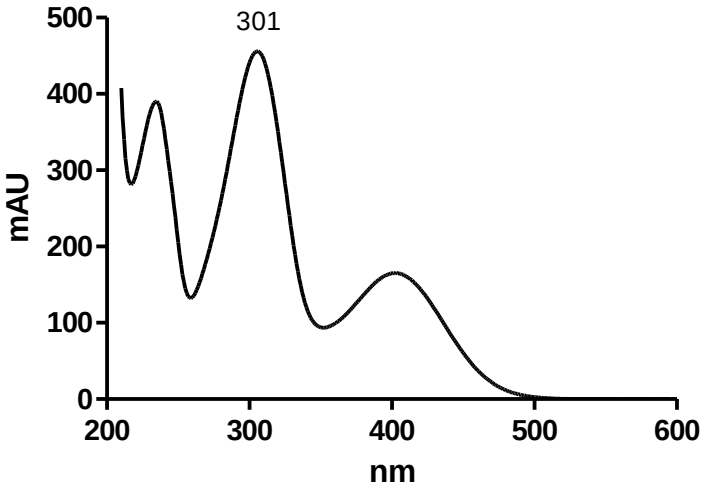

Figure S 25. ^{1}H NMR spectrum of compound **2g** (DMSO-d_6; 600 MHz)

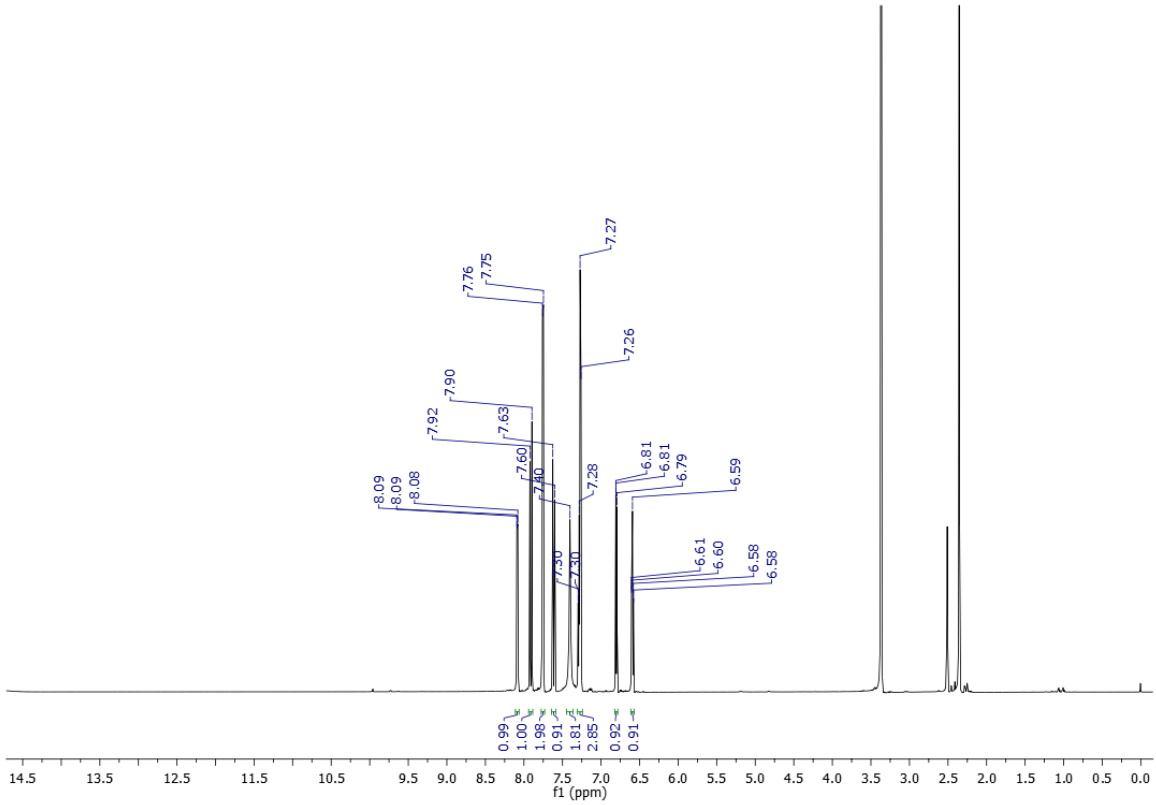

Figure S 26. ^{13}C NMR spectrum of compound **2g** (DMSO-d_6; 150 MHz)

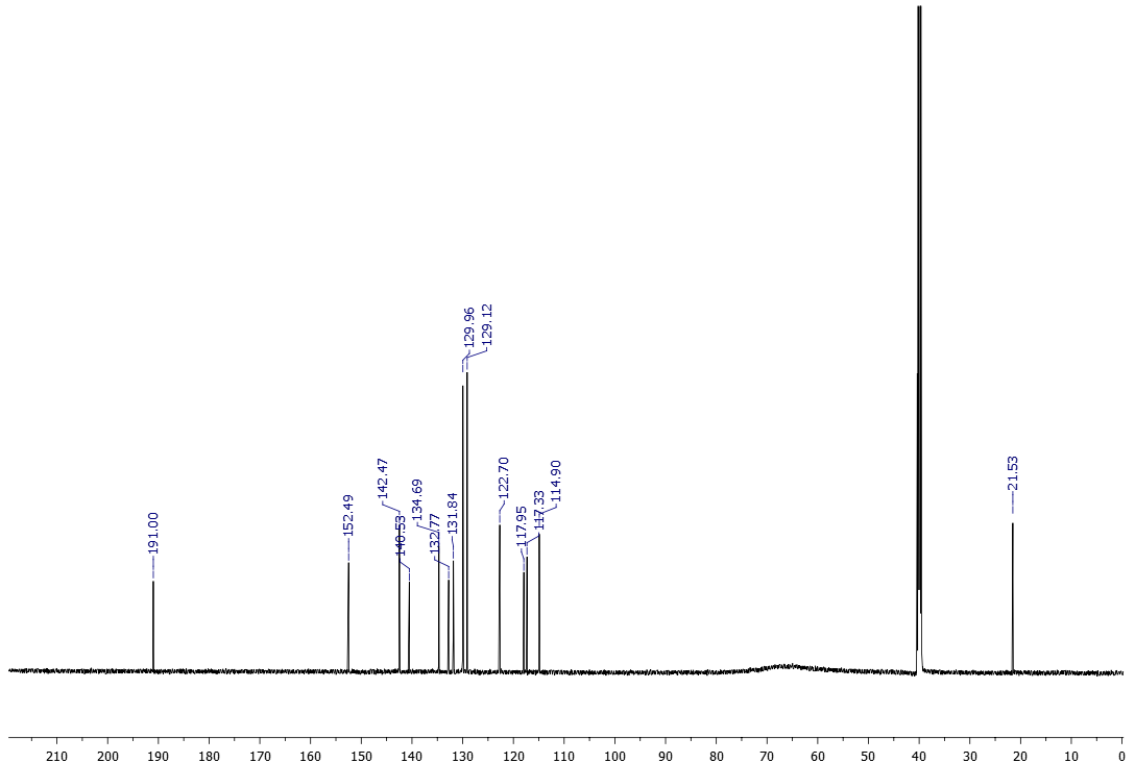

Figure S 27. HPLC chromatogram of compound **2g**

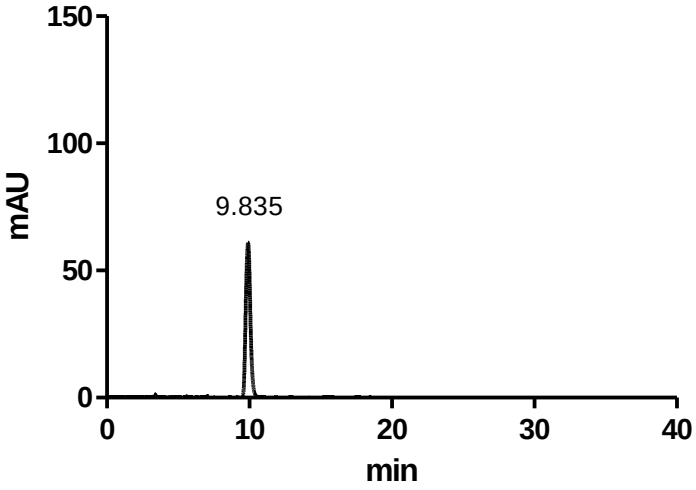

Figure S 28.UV-Vis spectrum of compound **2g**

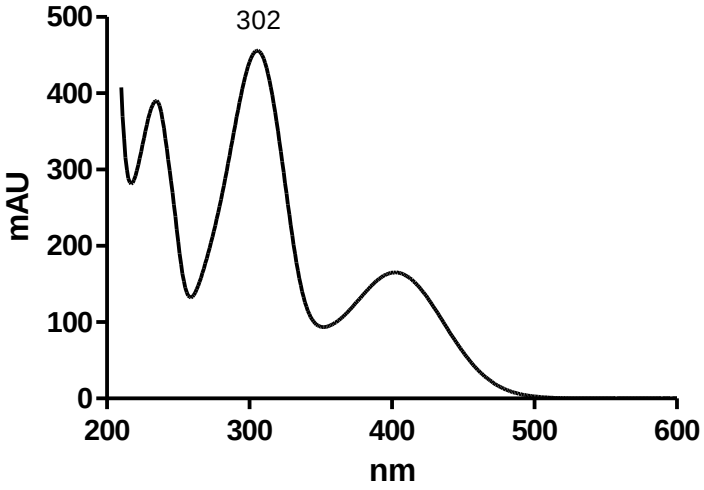

Figure S 29. ^{1}H NMR spectrum of compound **2h** (DMSO-d_6; 600 MHz)

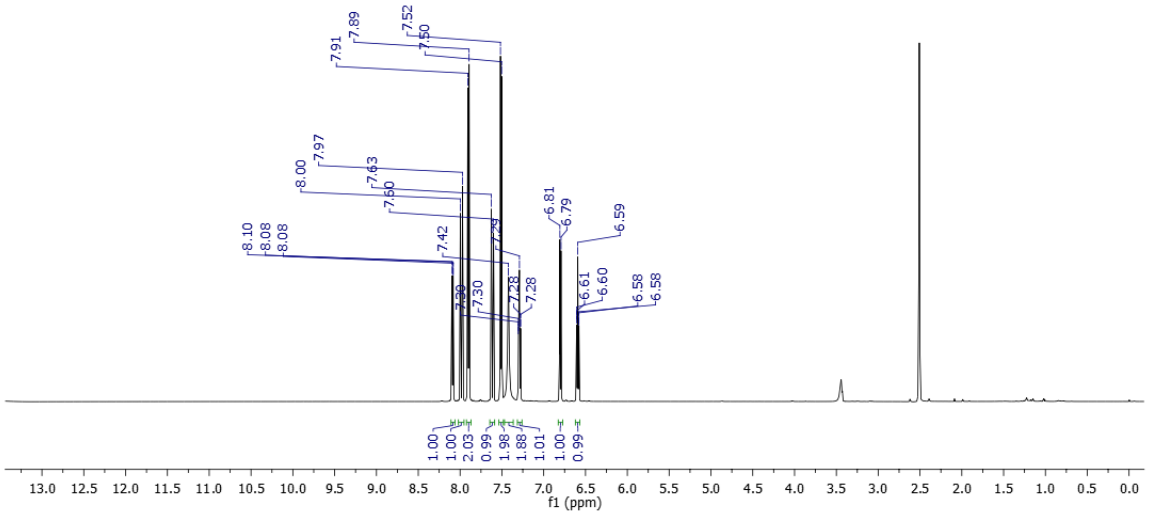

Figure S 30. ^{13}C NMR spectrum of compound **2h** (DMSO-d_6; 150 MHz)

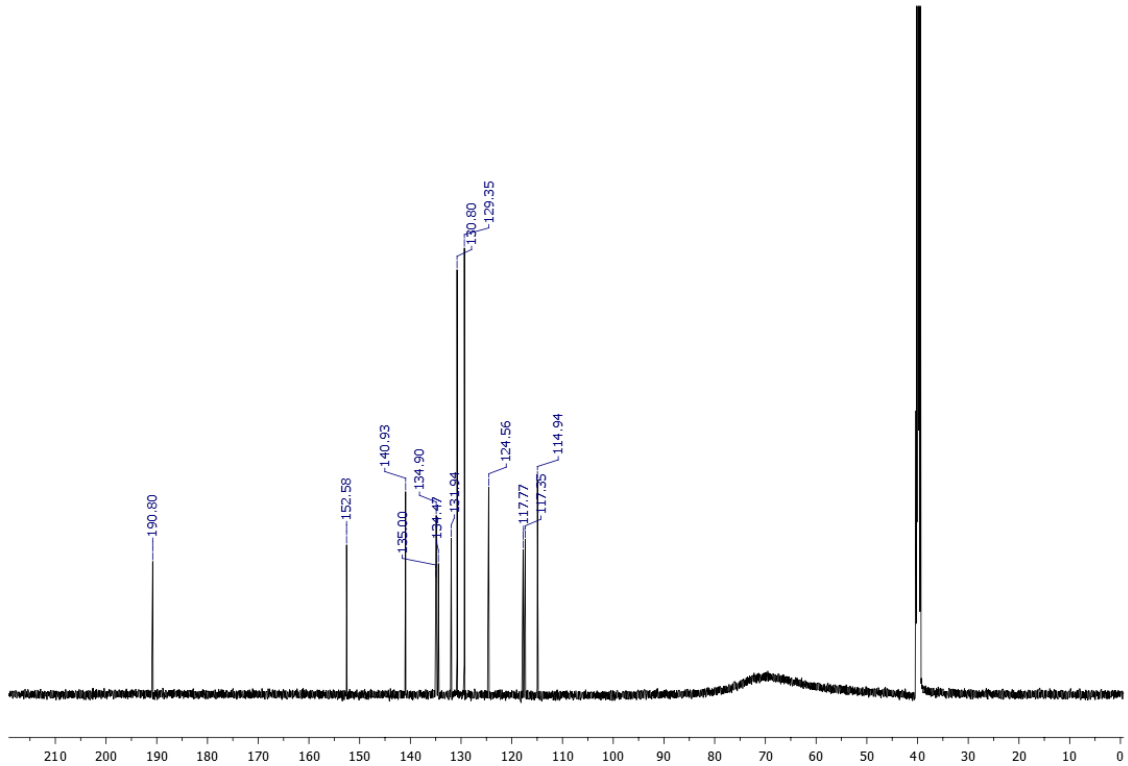

Figure S 31. HPLC chromatogram of compound **2h**

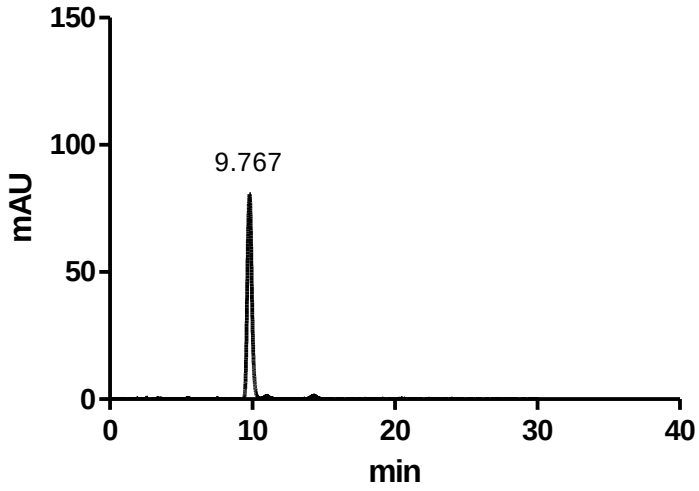

Figure S 32. UV-Vis spectrum of compound **2h**

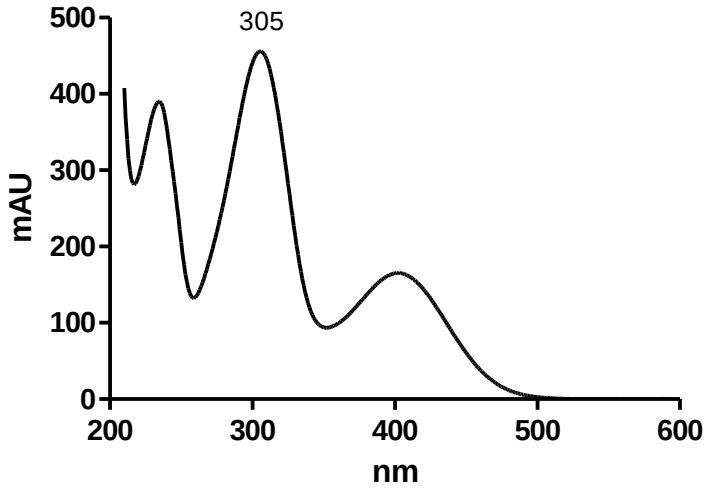

Figure S 33. ^{1}H NMR spectrum of compound **2i** (DMSO-d_6; 400 MHz)

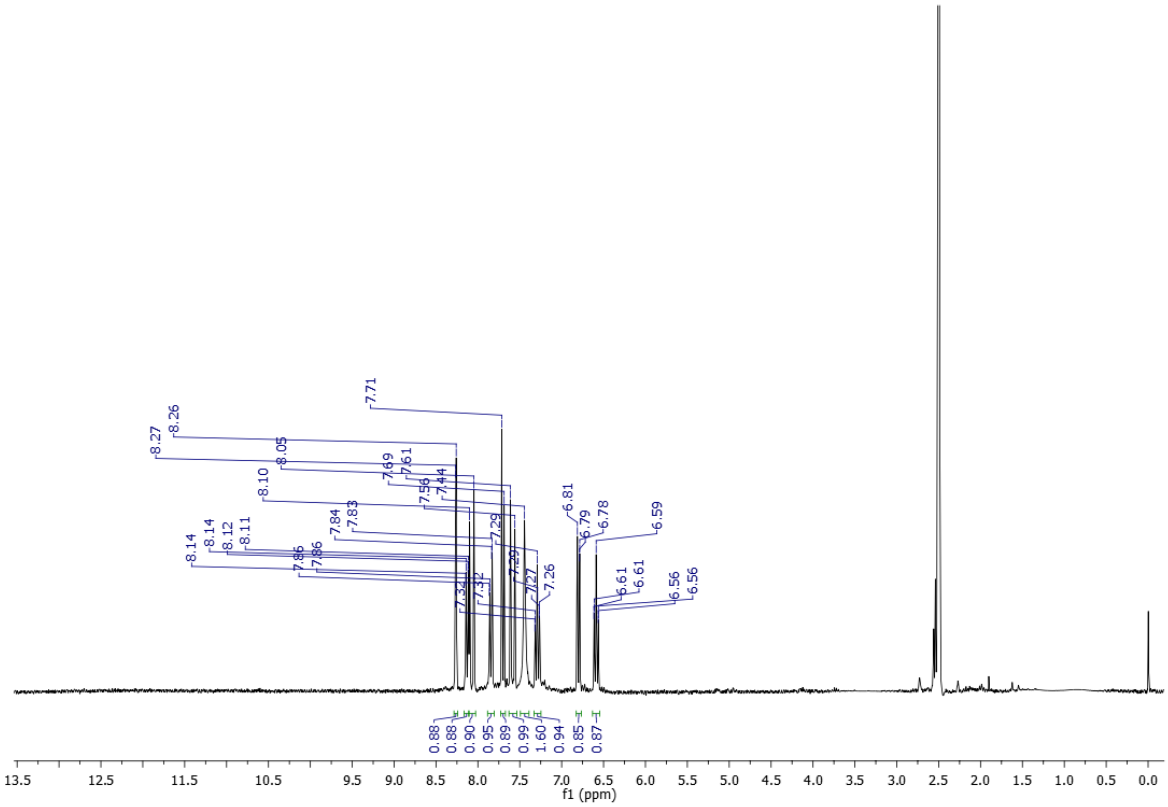

Figure S 34. ^{13}C NMR spectrum of compound **2i** (DMSO-d_6; 150 MHz)

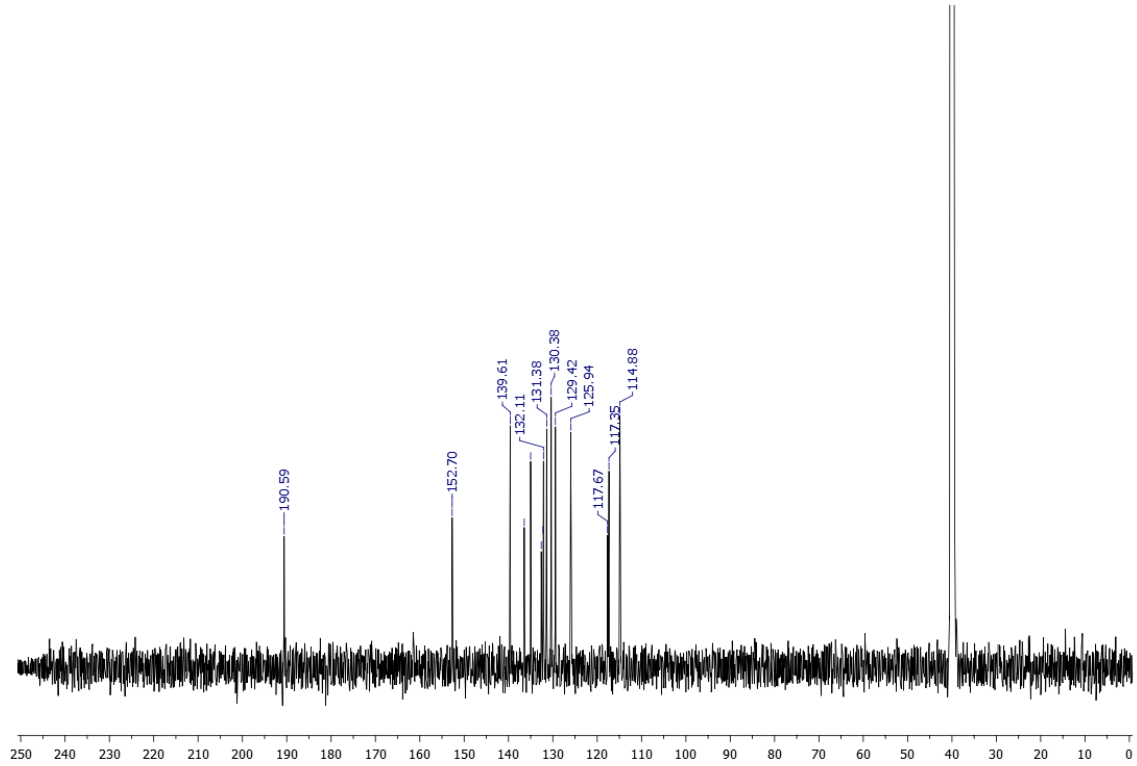

Figure S 35. HPLC chromatogram of compound **2i**

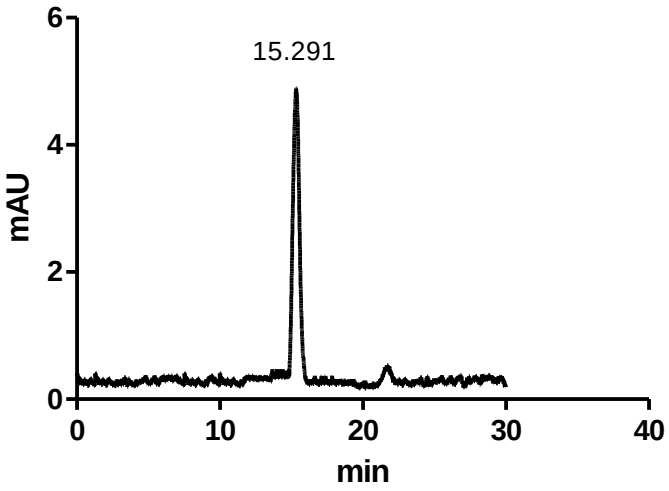

Figure S 36. UV-Vis spectrum of compound **2i**

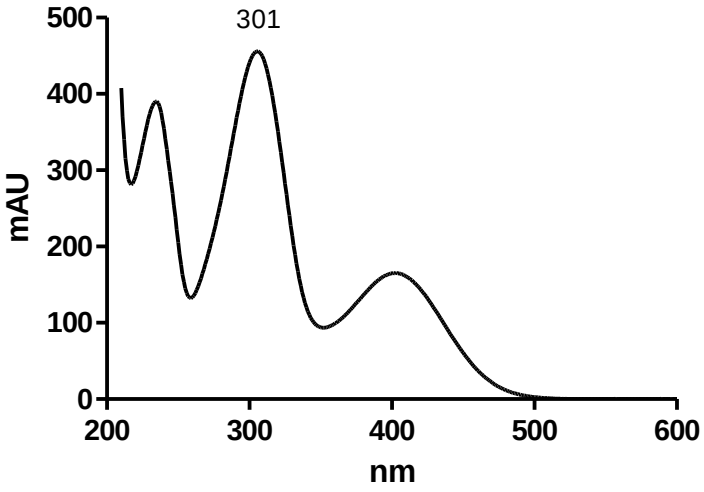

Figure S 37. ^{1}H NMR spectrum of compound **3a** (DMSO-d_6; 600 MHz)

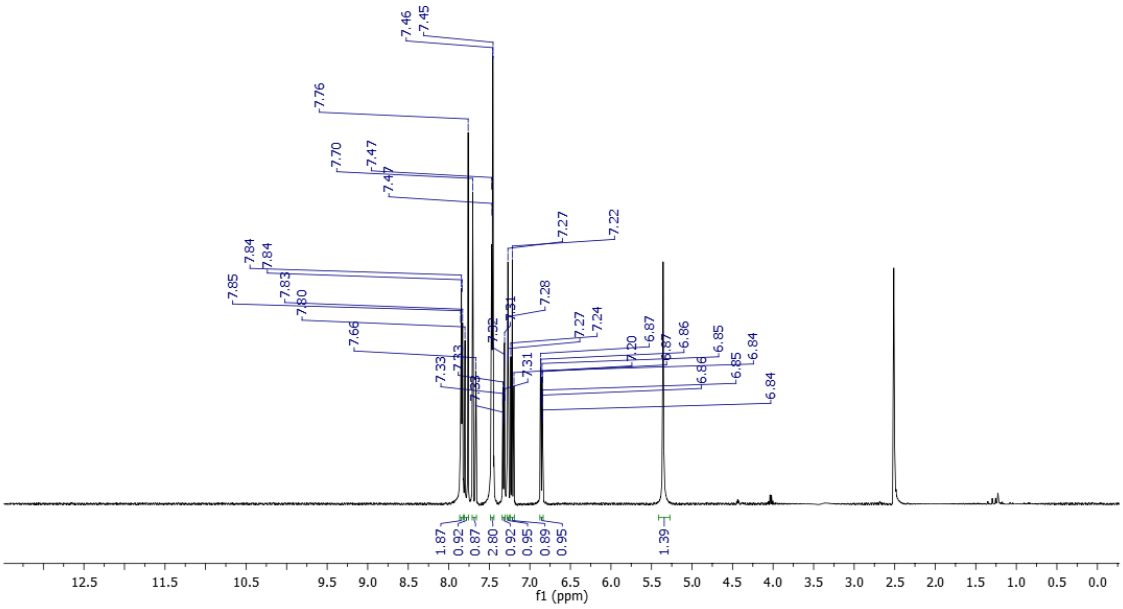

Figure S 38. ^{13}C NMR spectrum of compound **3a** (DMSO-d_6; 150 MHz)

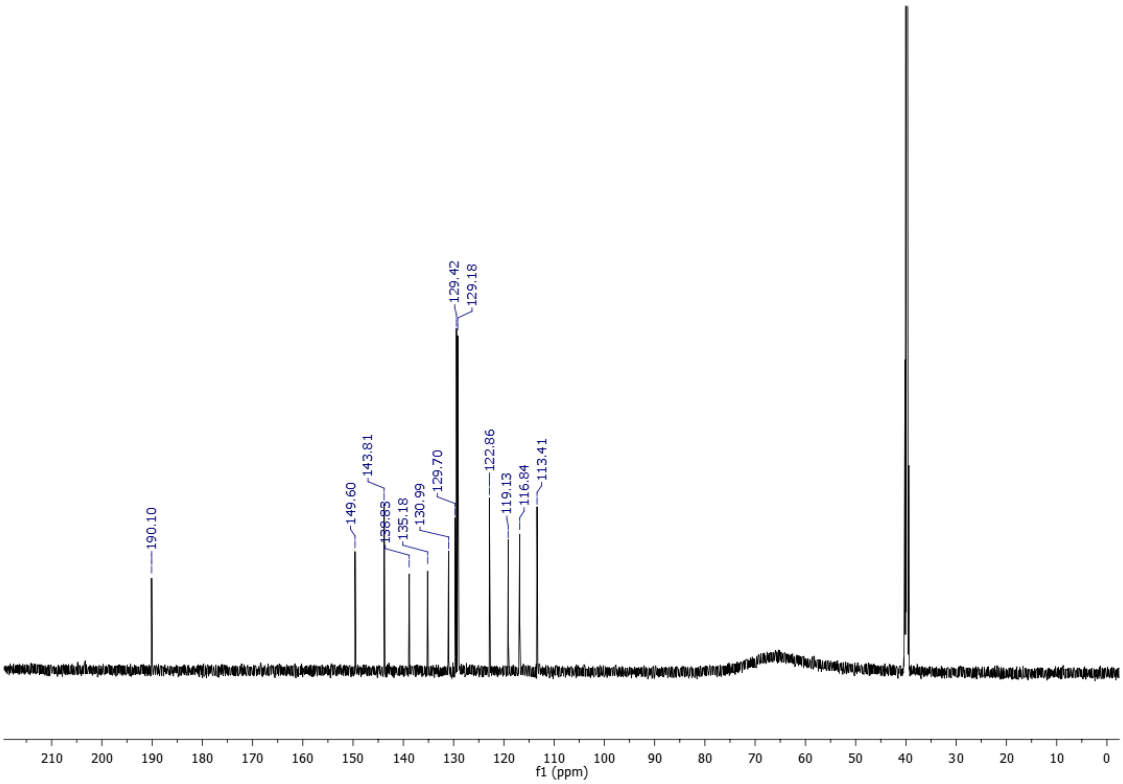

Figure S 39. HPLC chromatogram of compound **3a**

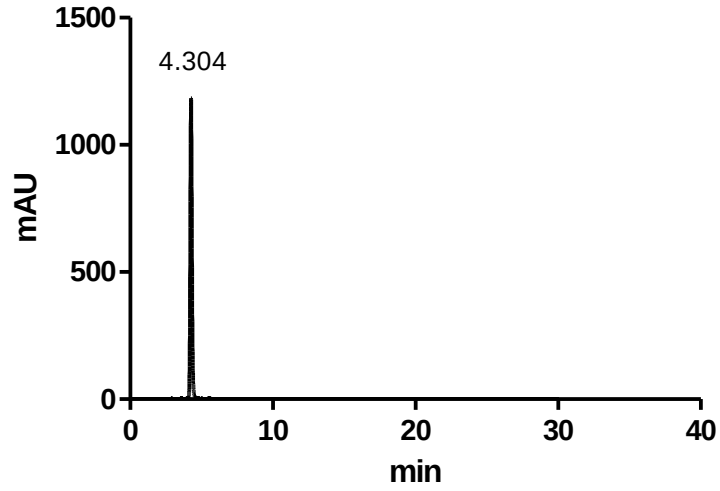

Figure S 40. UV-Vis spectrum of compound **3a**

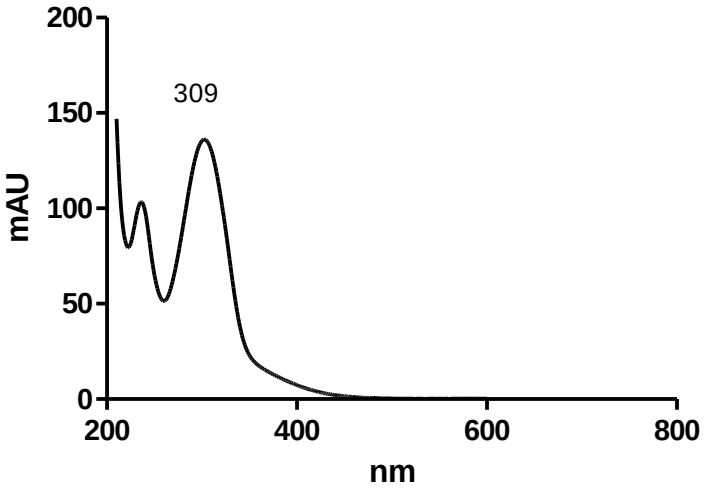

Figure S 41. ^{1}H NMR spectrum of compound **3b** (DMSO-d_6; 600 MHz)

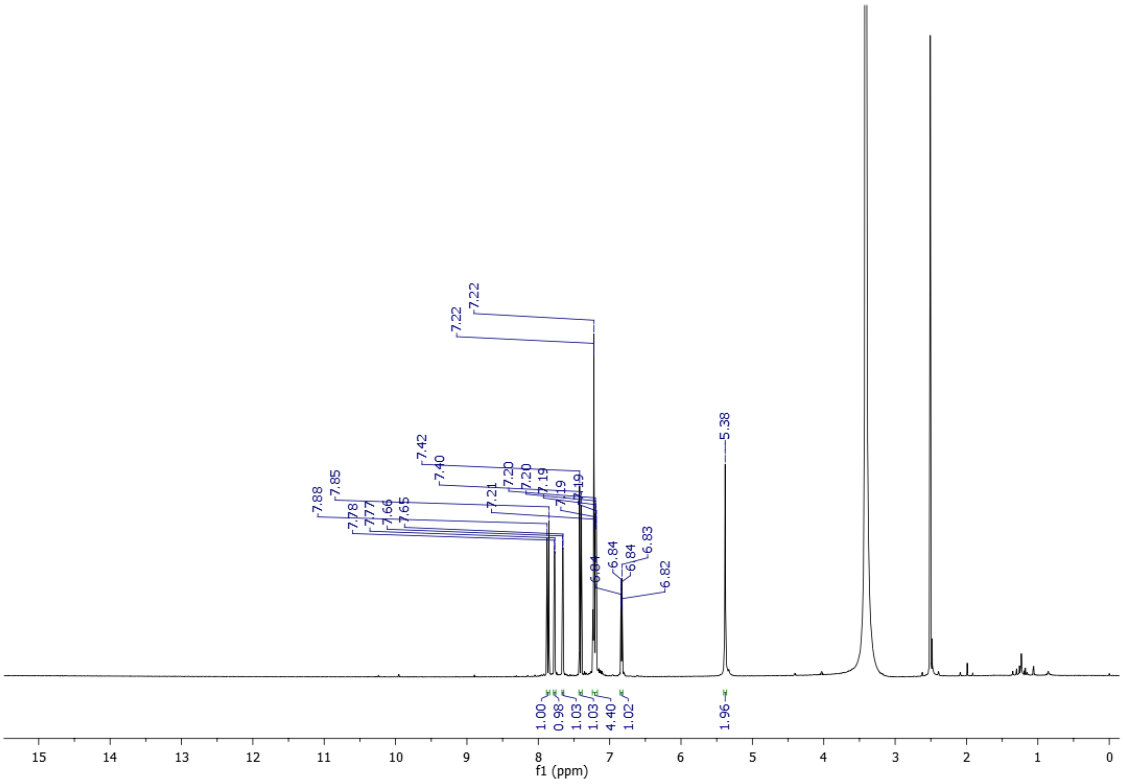

Figure S 42. ^{13}C NMR spectrum of compound **3b** (DMSO-d_6; 150 MHz)

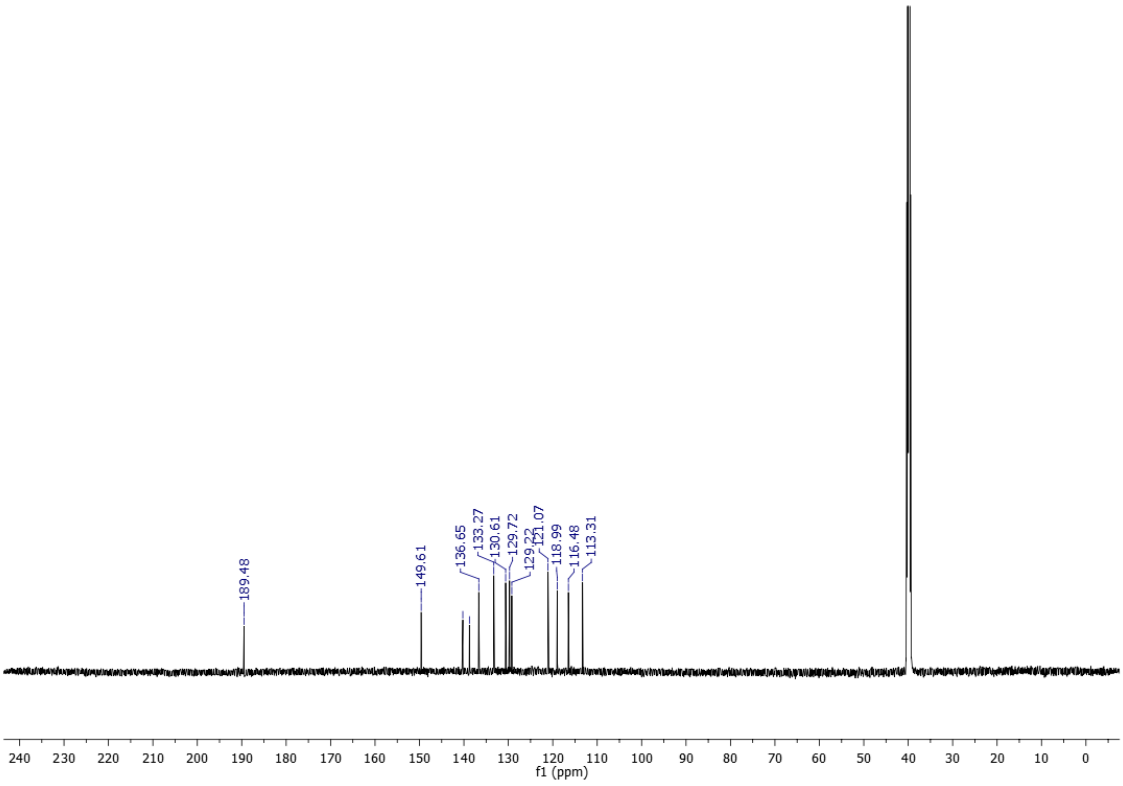

Figure S 43. HPLC chromatogram of compound **3b**

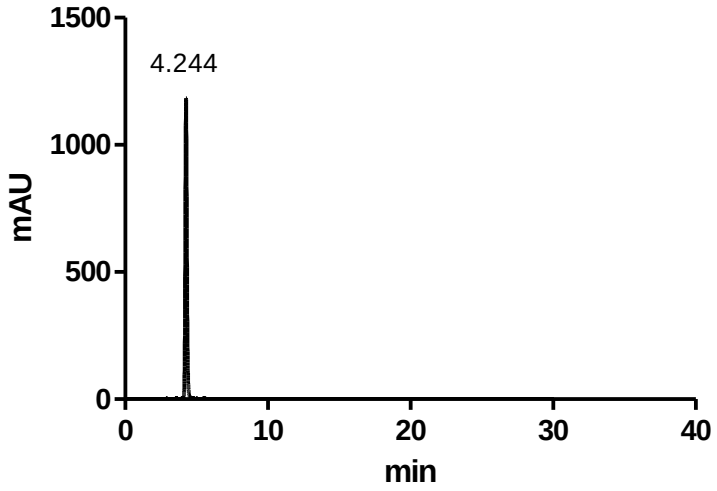

Figure S 44. UV-Vis spectrum of compound **3b**

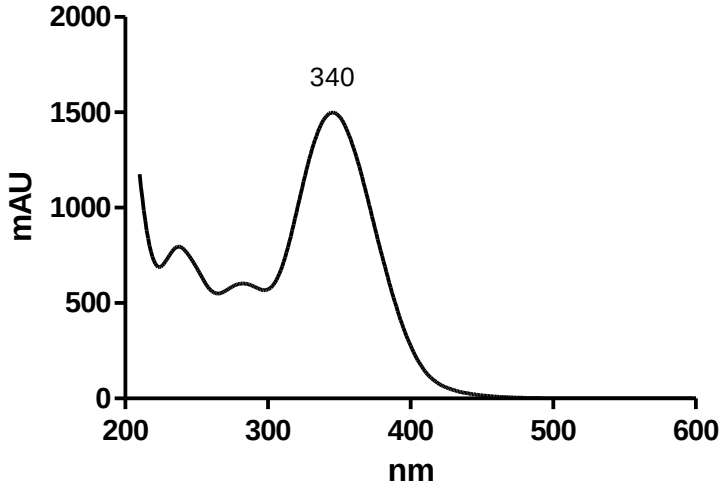

Figure S 45. ^{1}H NMR spectrum of compound **3c** (DMSO-d_6; 600 MHz)

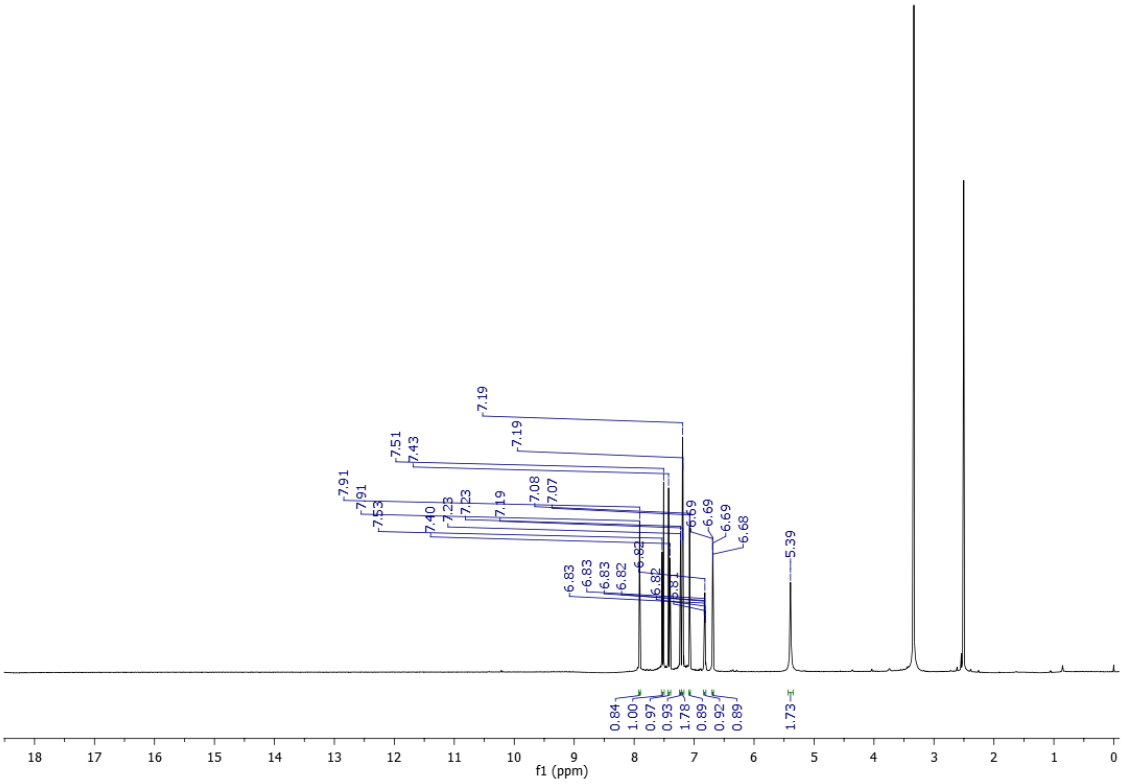

Figure S 46. ^{13}C NMR spectrum of compound **3c** (DMSO-d_6; 150 MHz)

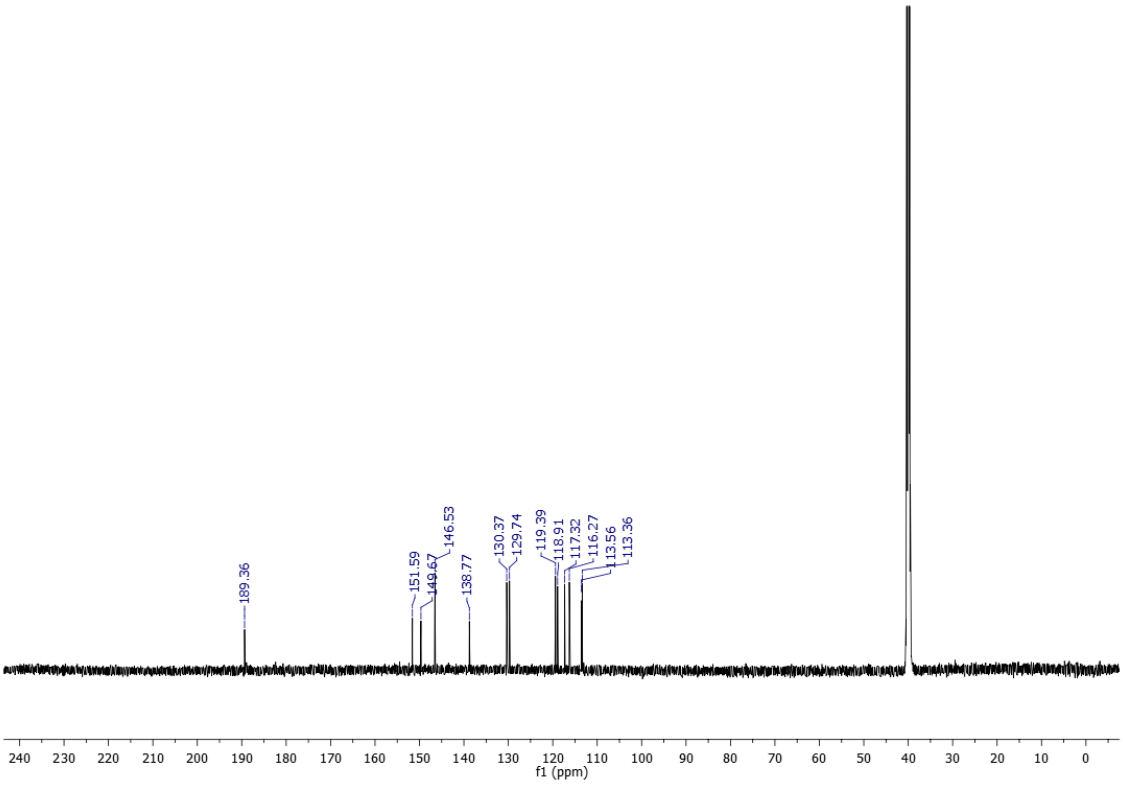

Figure S 47. HPLC chromatogram of compound **3c**

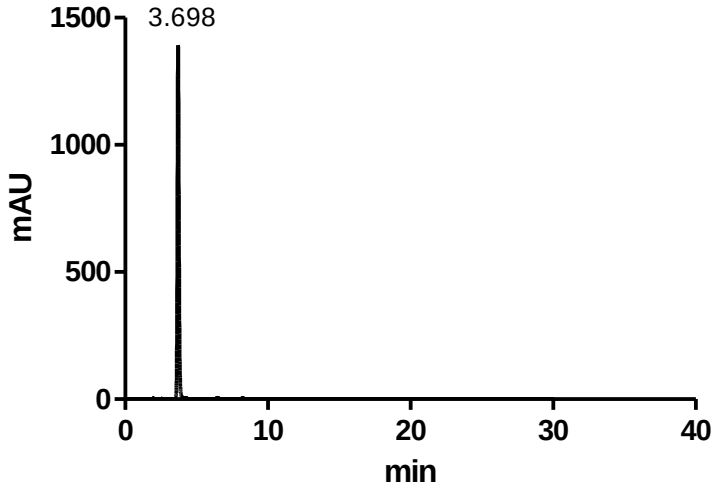

Figure S 48. UV-Vis spectrum of compound **3c**

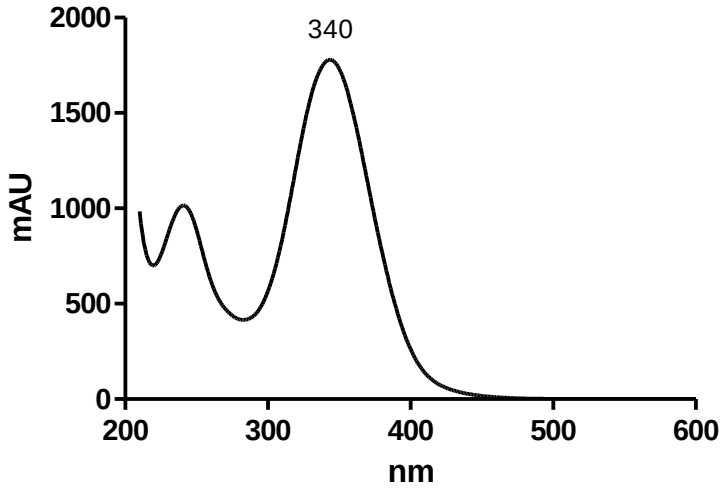

Figure S 49. ^{1}H NMR spectrum of compound **3d** (DMSO-d_6; 600 MHz)

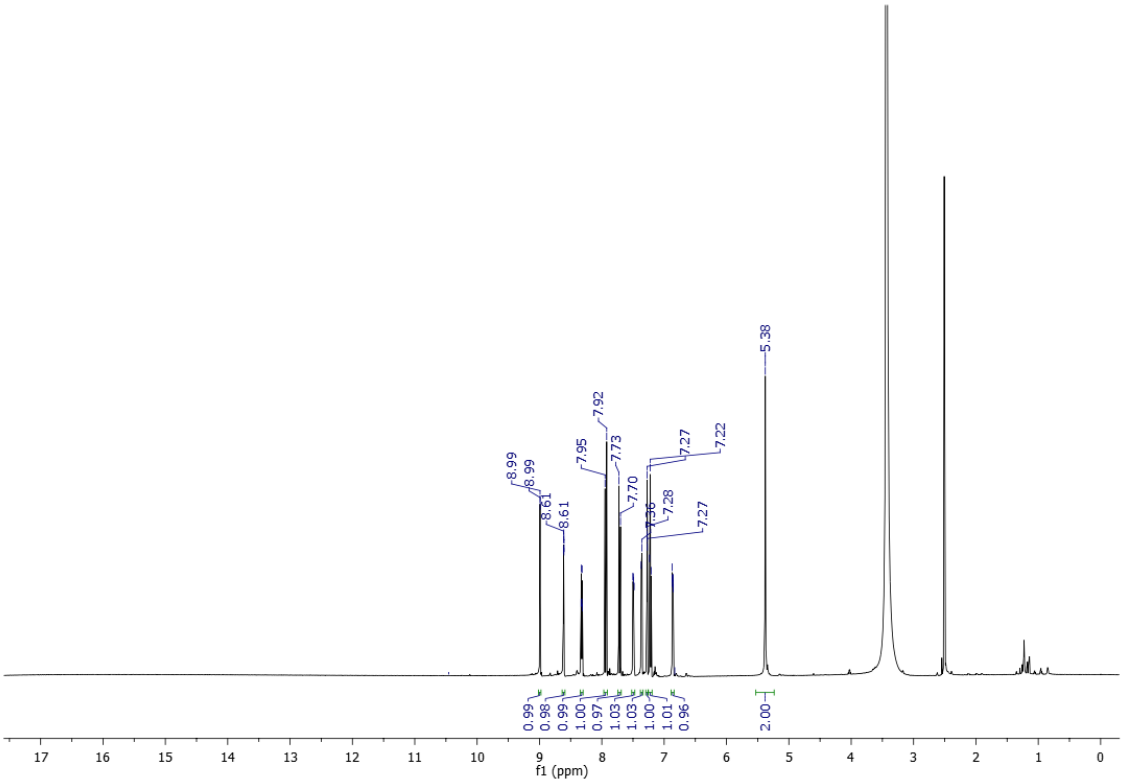

Figure S 50. ^{13}C NMR spectrum of compound **3d** (DMSO-d_6; 150 MHz)

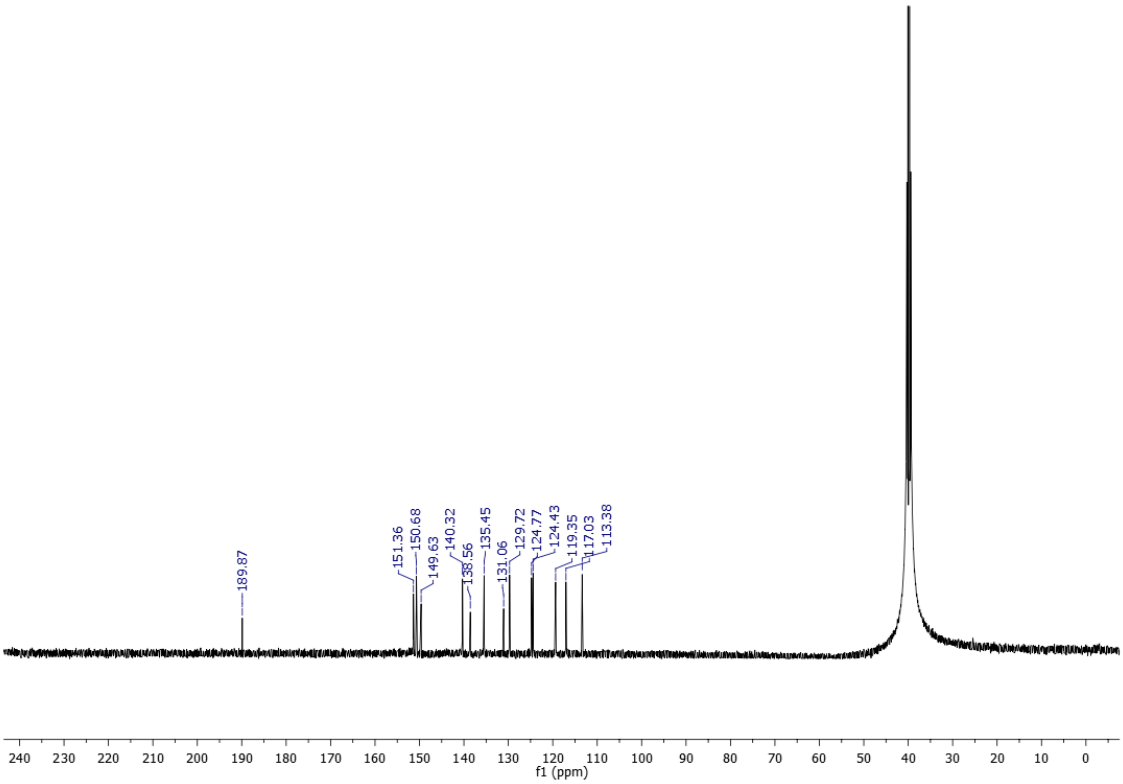

Figure S 51. HPLC chromatogram of compound **3d**

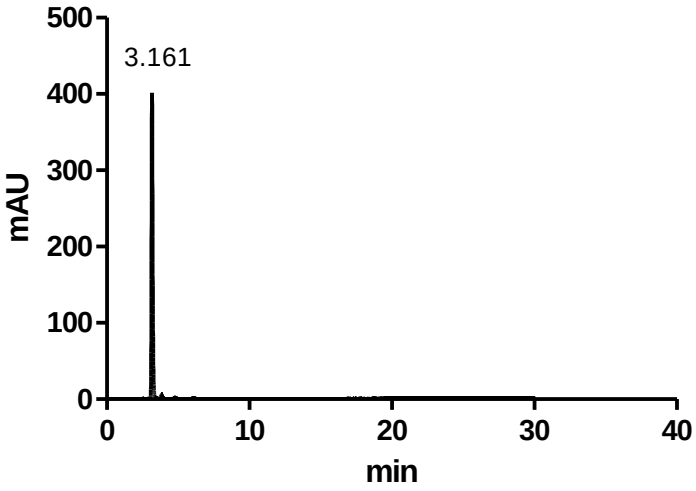

Figure S 52. UV-Vis spectrum of compound **3d**

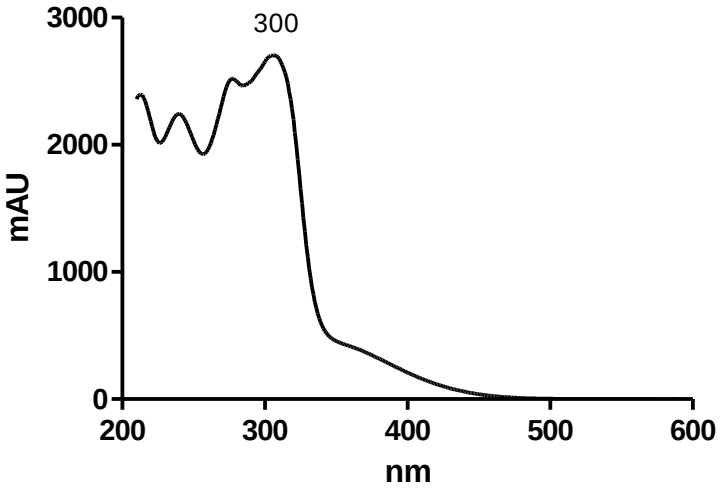

Figure S 53. ^{1}H NMR spectrum of compound **3e** (DMSO-d_6; 600 MHz)

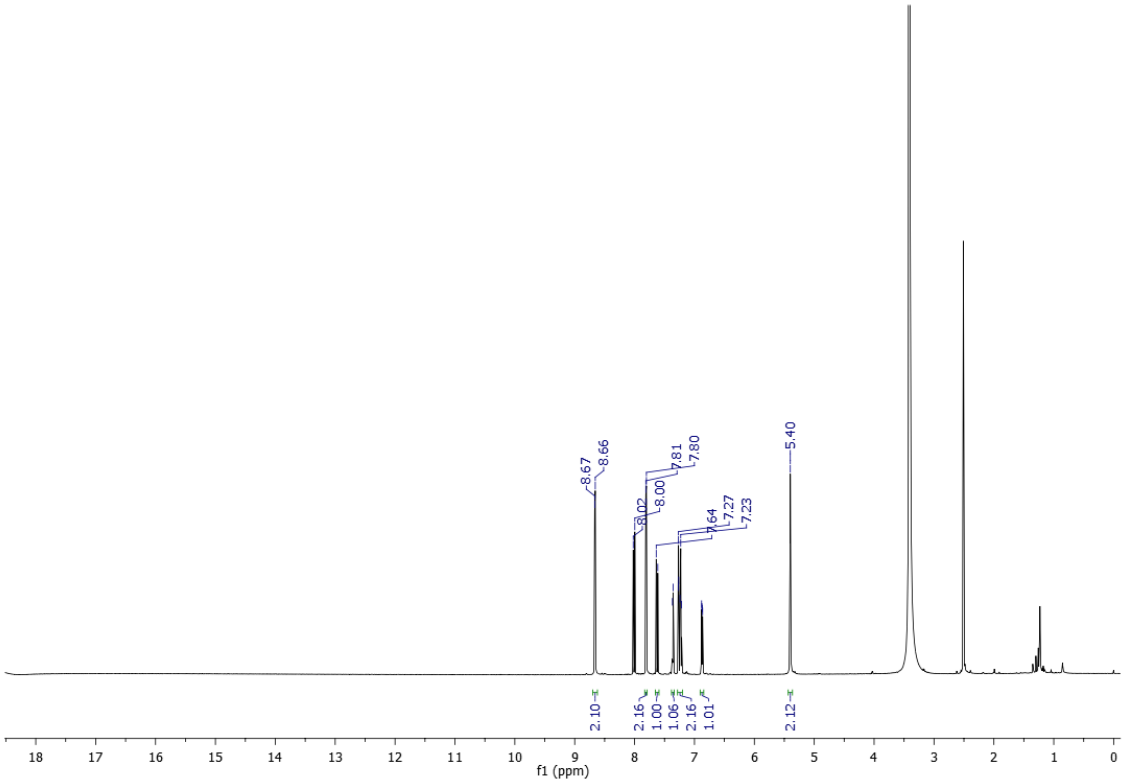

Figure S 54. ^{13}C NMR spectrum of compound **3e** (DMSO-d_6; 150 MHz)

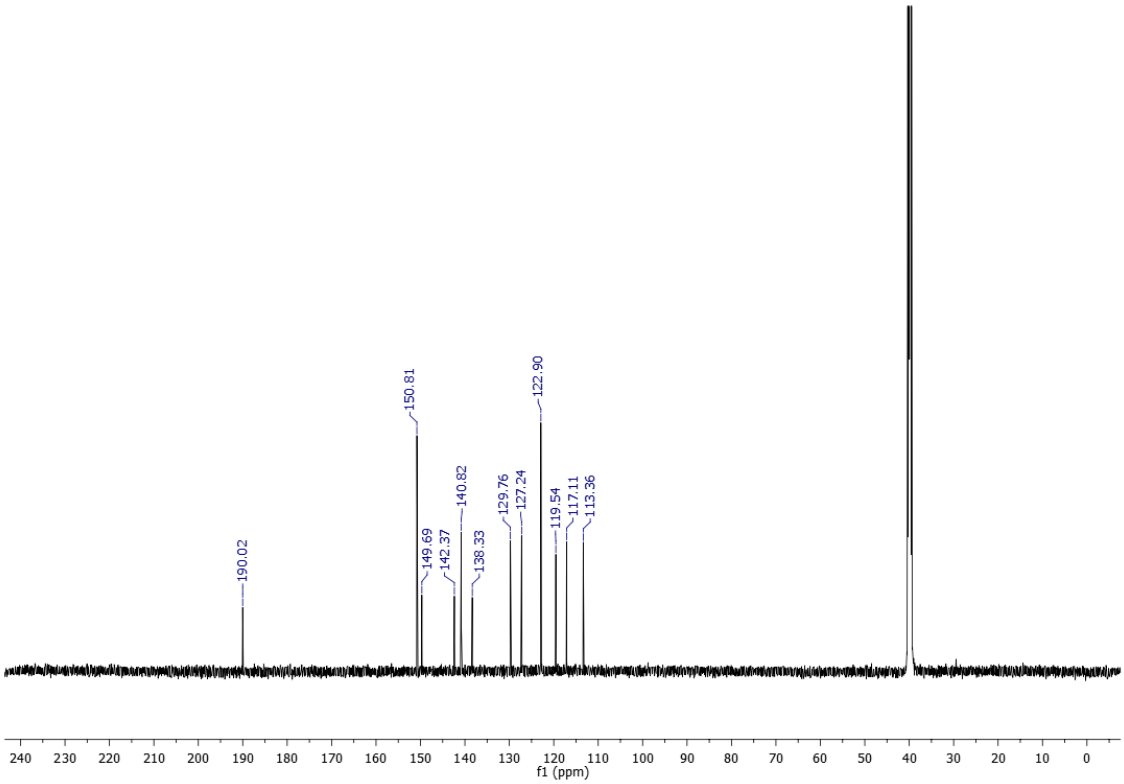

Figure S 55. HPLC chromatogram of compound **3e**

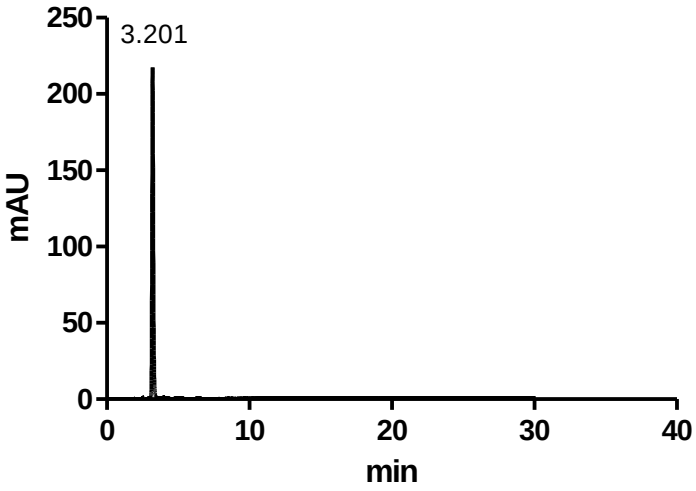

Figure S 56. UV-Vis spectrum of compound **3e**

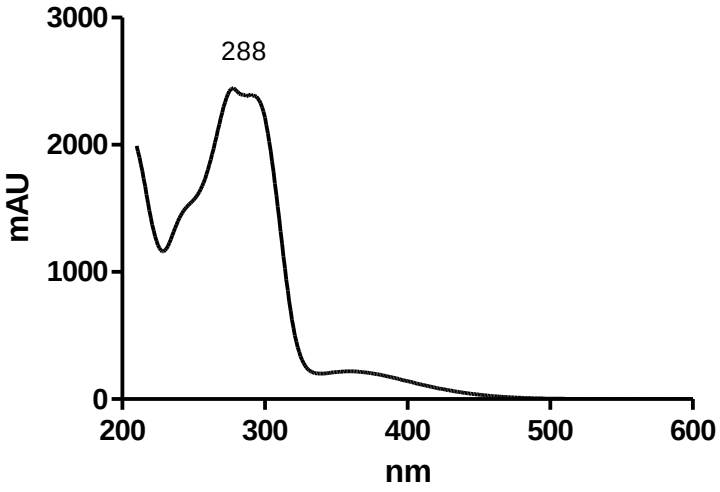

Figure S 57. ^{1}H NMR spectrum of compound **3f** (DMSO-d_6; 600 MHz)

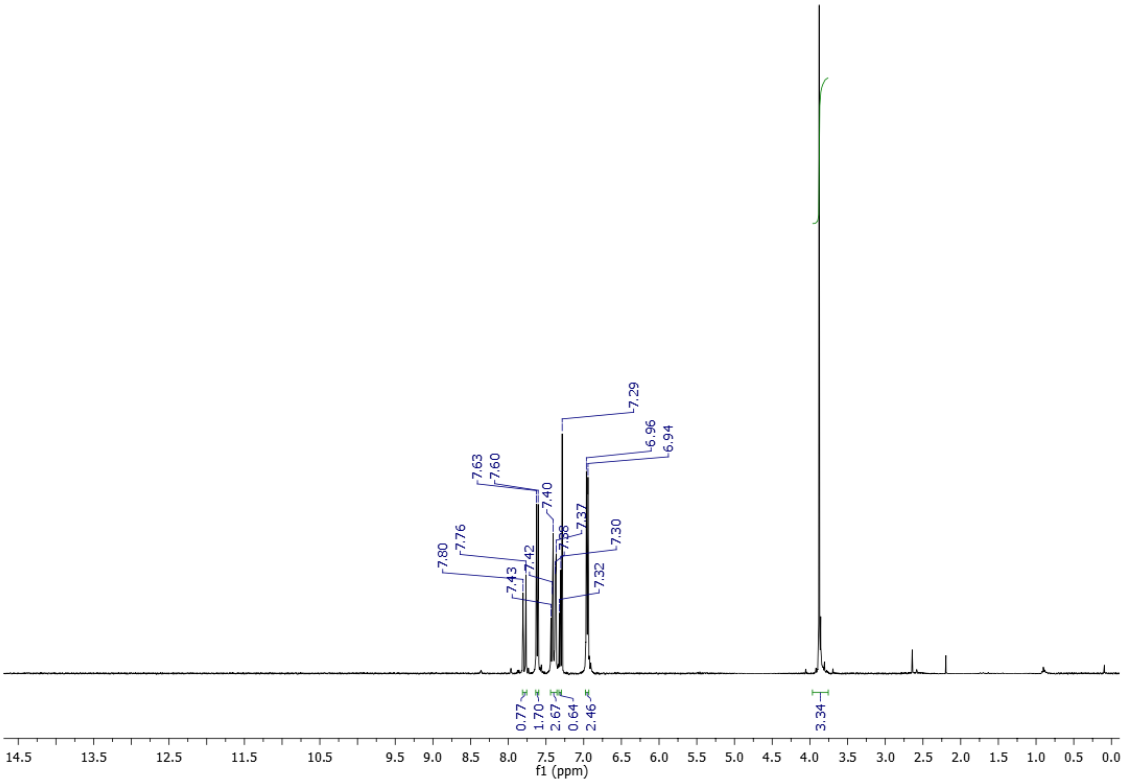

Figure S 58. ^{13}C NMR spectrum of compound **3f** (DMSO-d_6; 150 MHz)

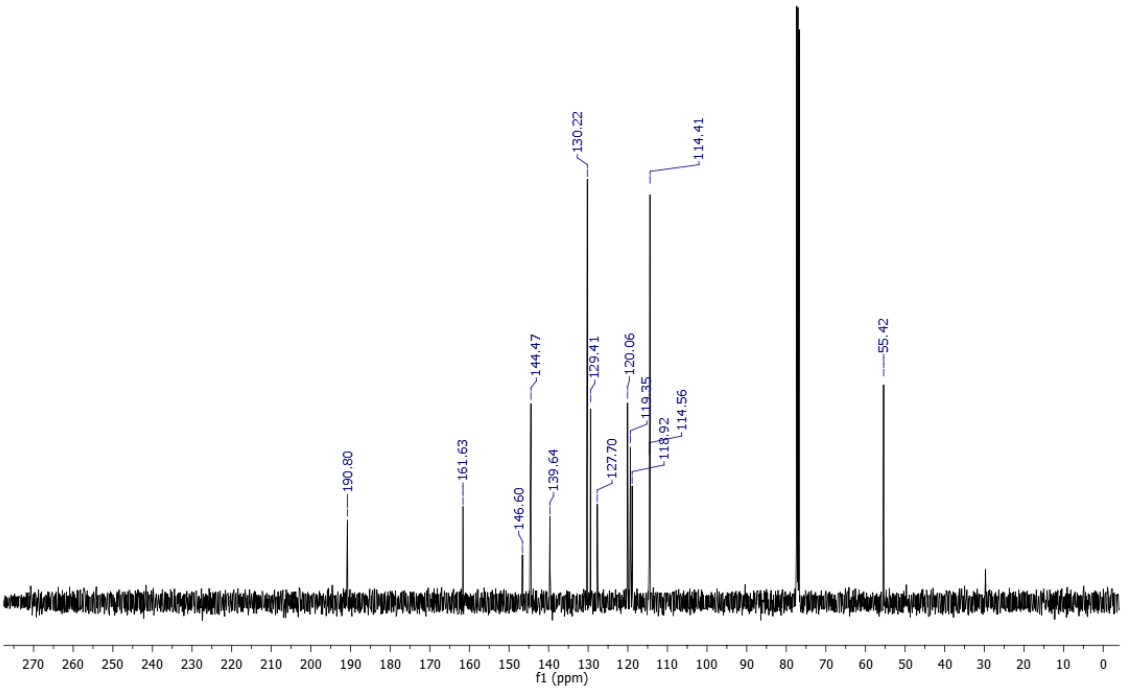

Figure S 59. HPLC chromatogram of compound **3f**

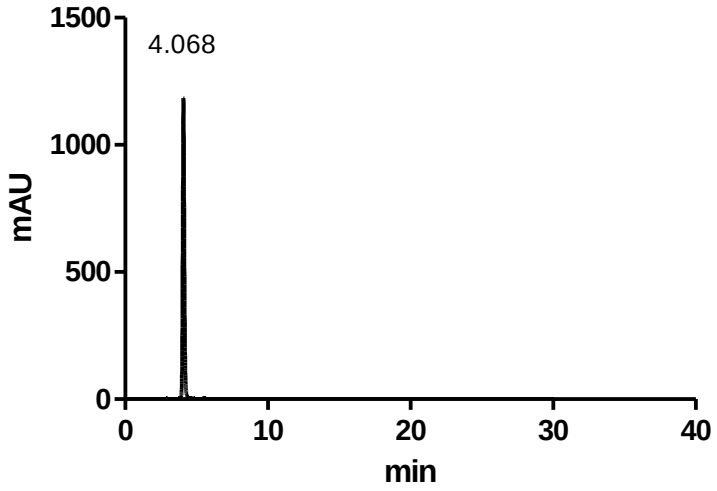

Figure S 60. UV-Vis spectrum of compound **3f**

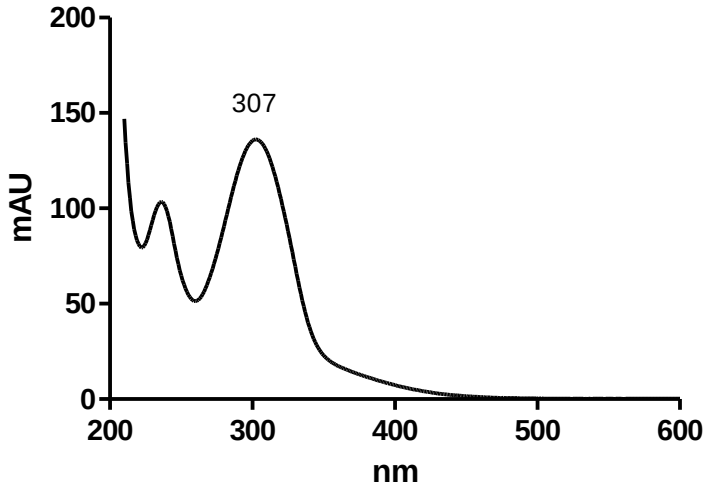

Figure S 61. ^{1}H NMR spectrum of compound **3g** (DMSO-d_6; 600 MHz)

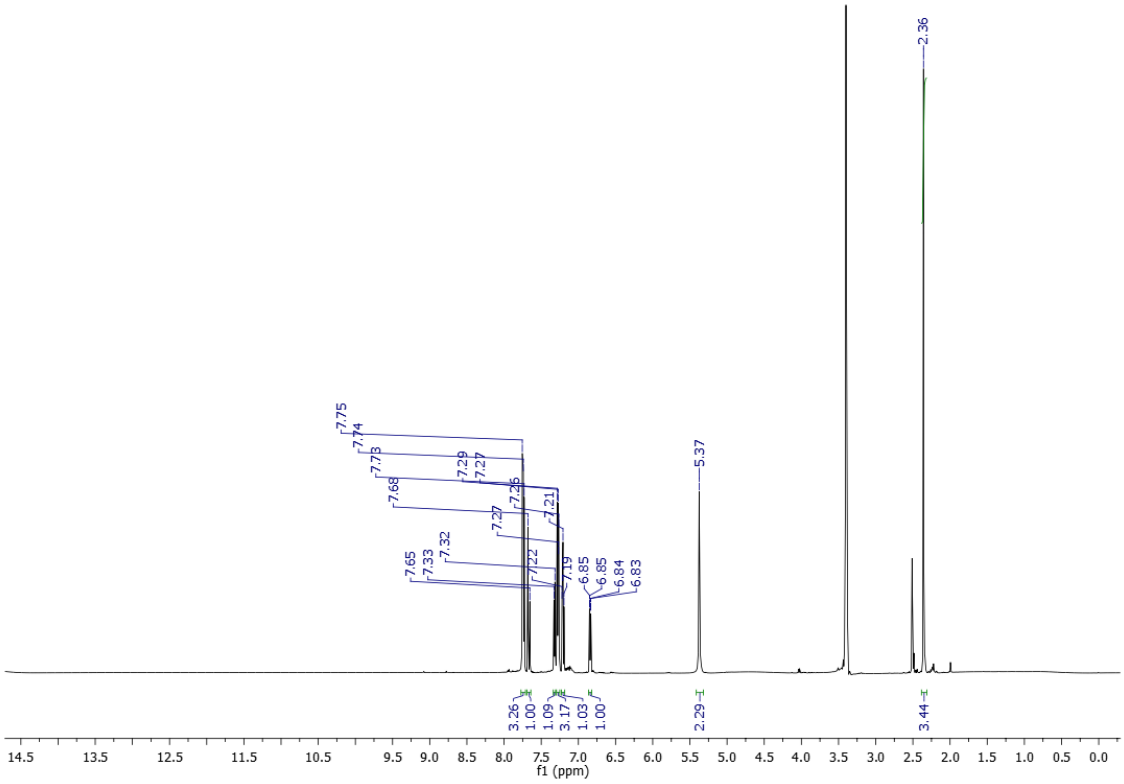

Figure S 62. ^{13}C NMR spectrum of compound **3g** (DMSO-d_6; 150 MHz)

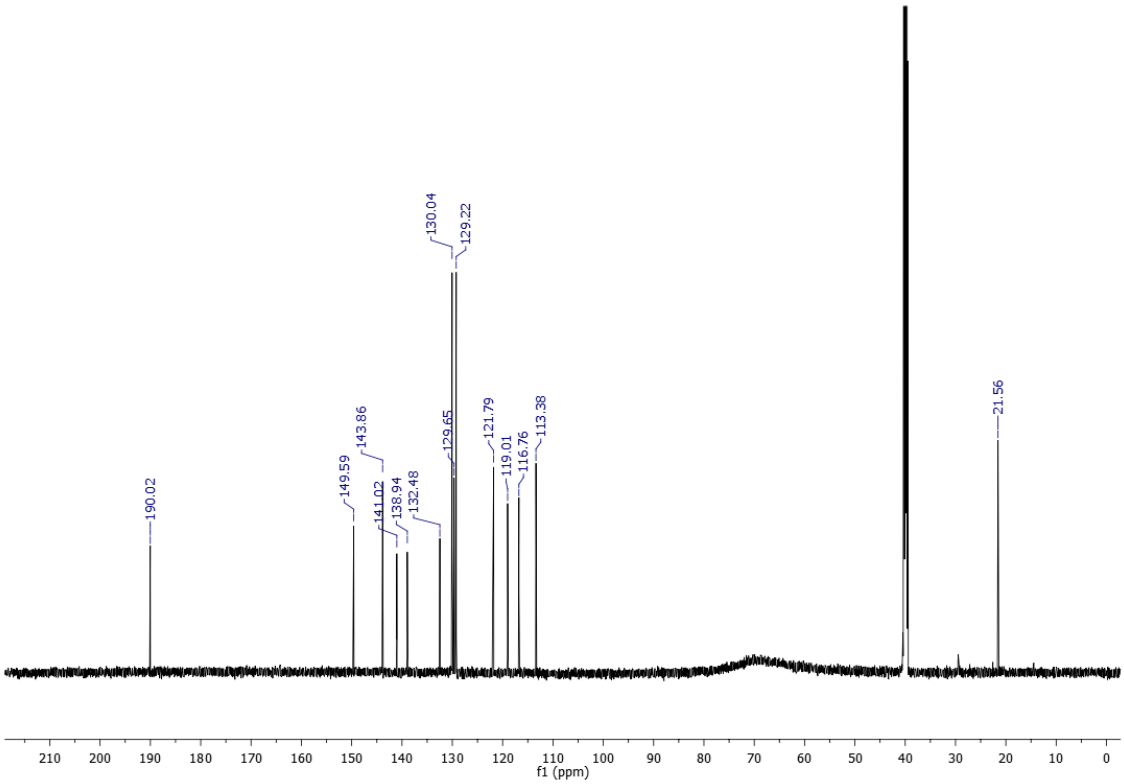

Figure S 63. HPLC chromatogram of compound **3g**

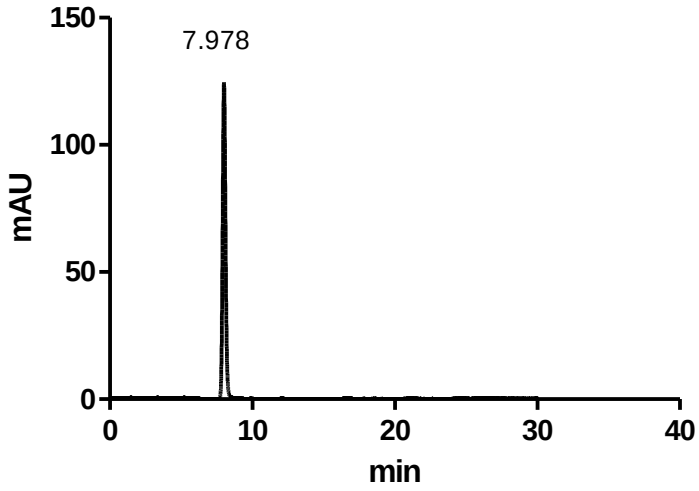

Figure S 64. UV-Vis spectrum of compound **3g**

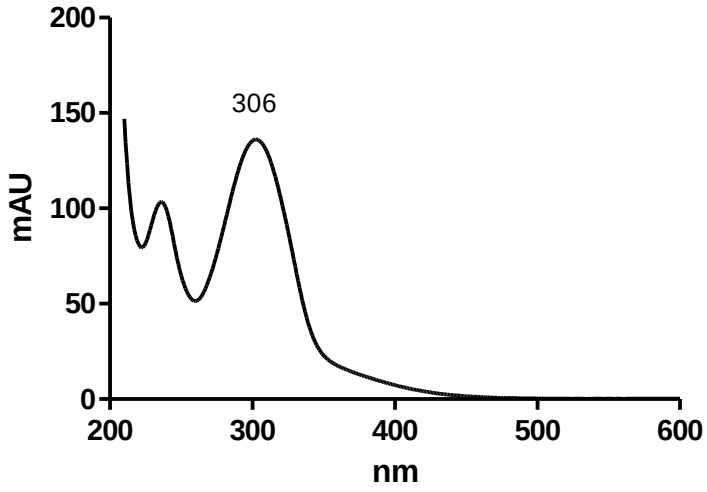

Figure S 65. ^{1}H NMR spectrum of compound **3h** (DMSO-d_6; 600 MHz)

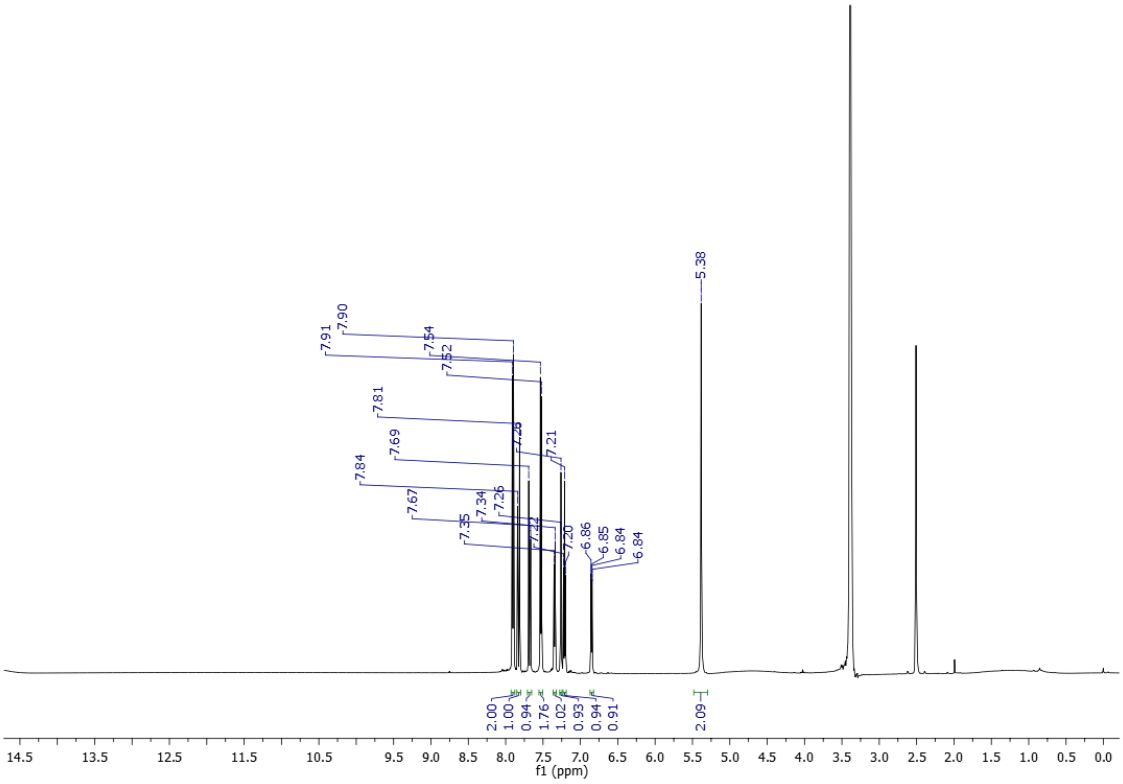

Figure S 66. ^{13}C NMR spectrum of compound **3h** (DMSO-d_6; 150 MHz)

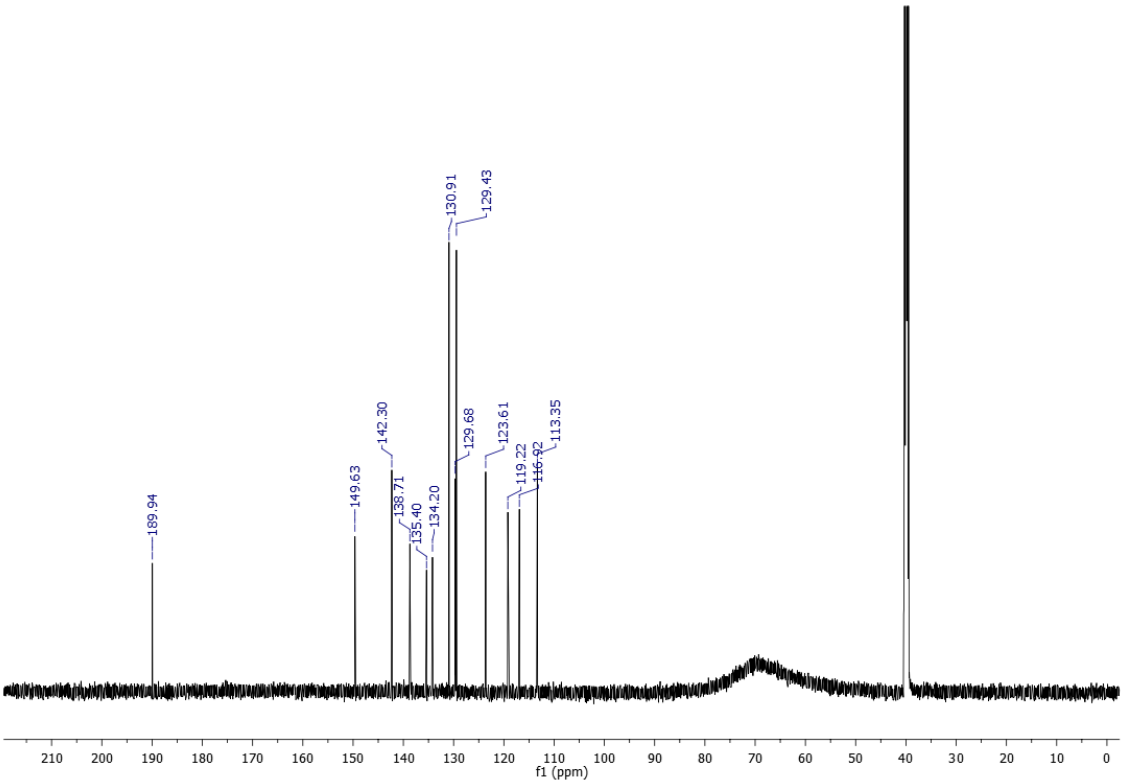

Figure S 67. HPLC chromatogram of compound **3h**

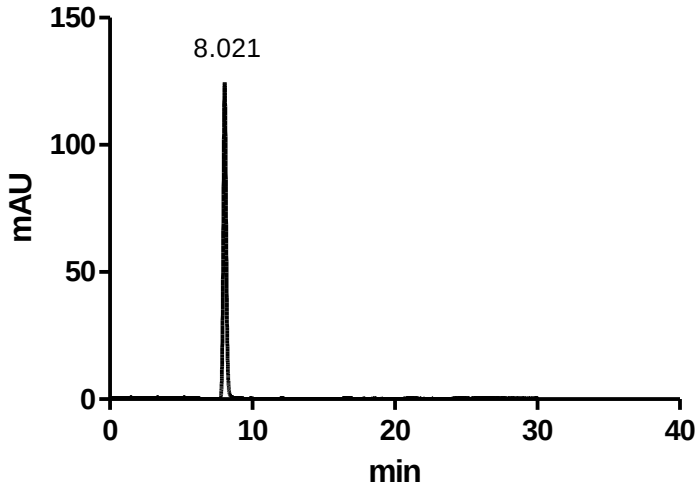

Figure S 68. UV-Vis spectrum of compound **3h**

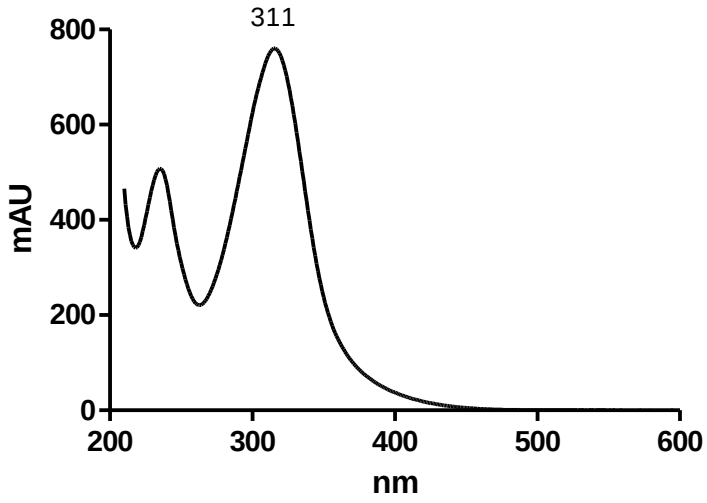

Figure S 69. ^{1}H NMR spectrum of compound **3i** (DMSO-d_6; 600 MHz)

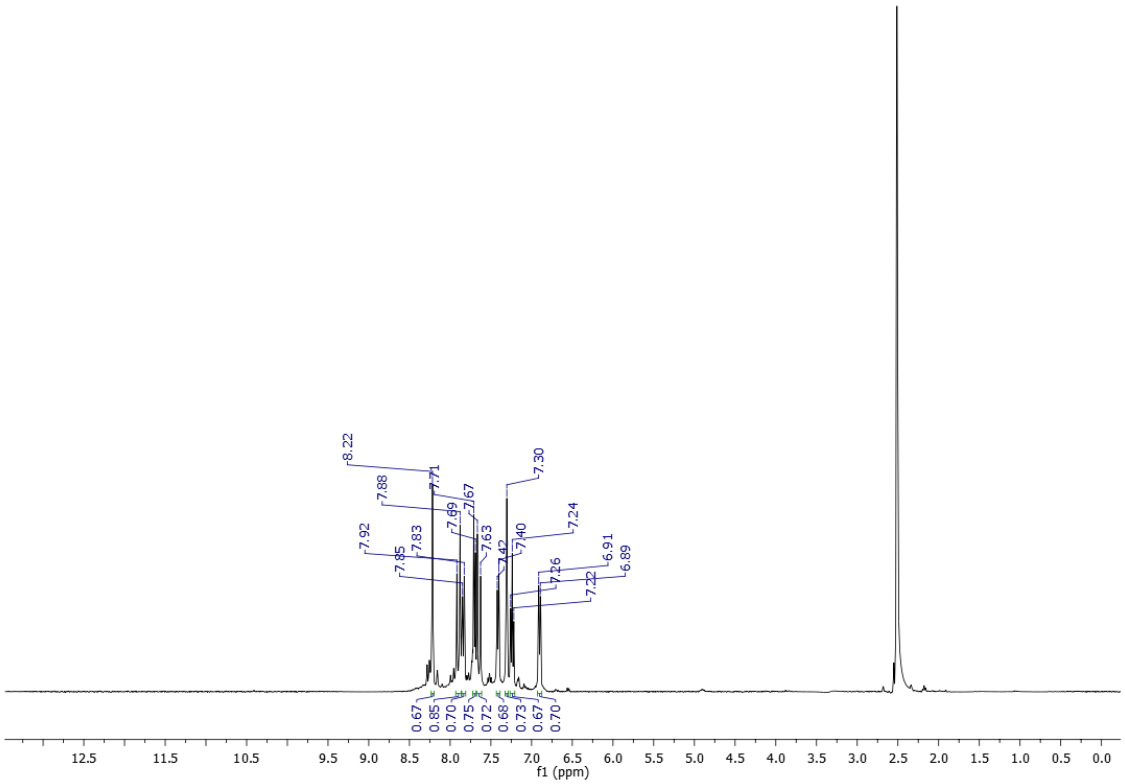

Figure S 70. ^{13}C NMR spectrum of compound **3i** (DMSO-d_6; 150 MHz)

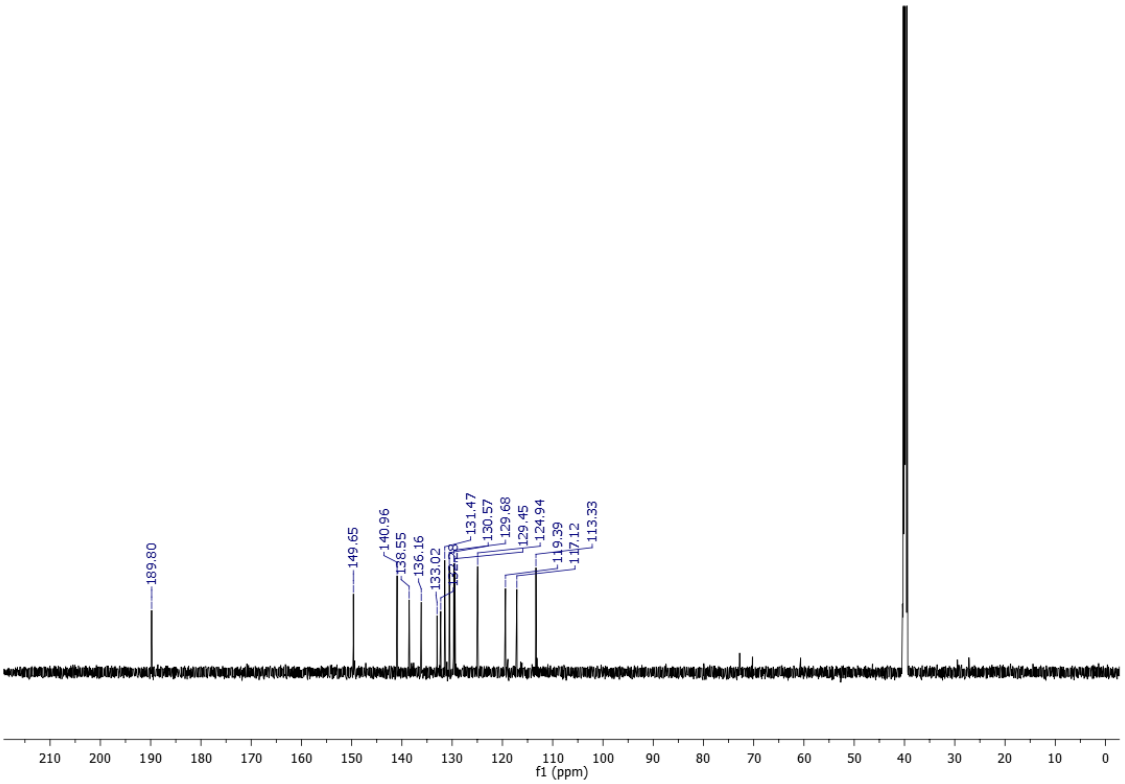

Figure S 71. HPLC chromatogram of compound **3i**

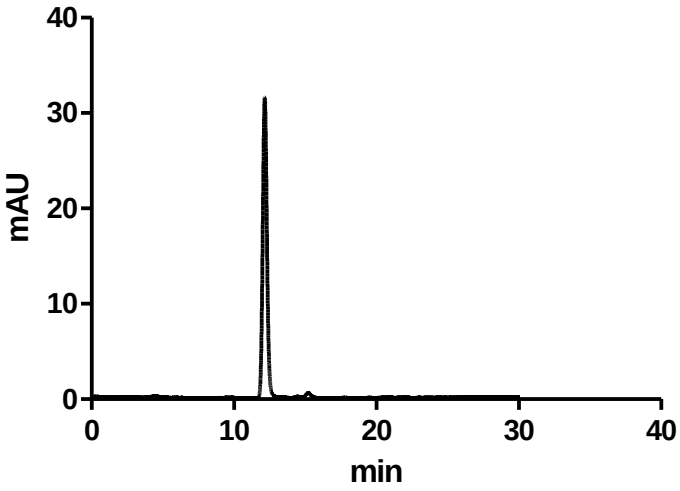

Figure S 72. UV-Vis spectrum of compound **3i**

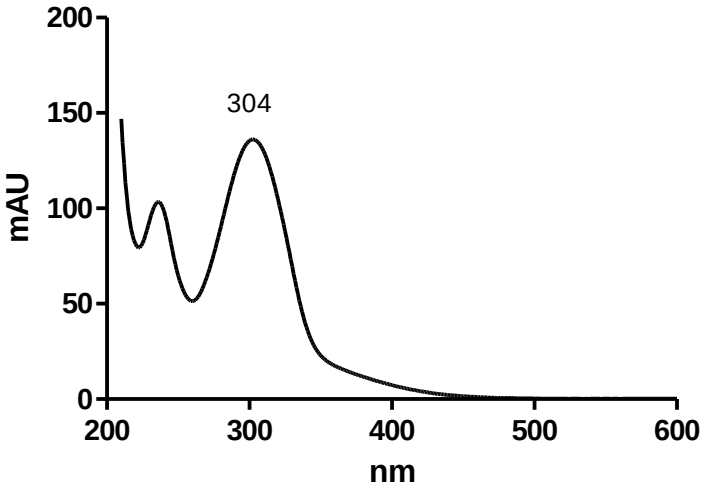

Figure S 73. HRMS of compound **3i**

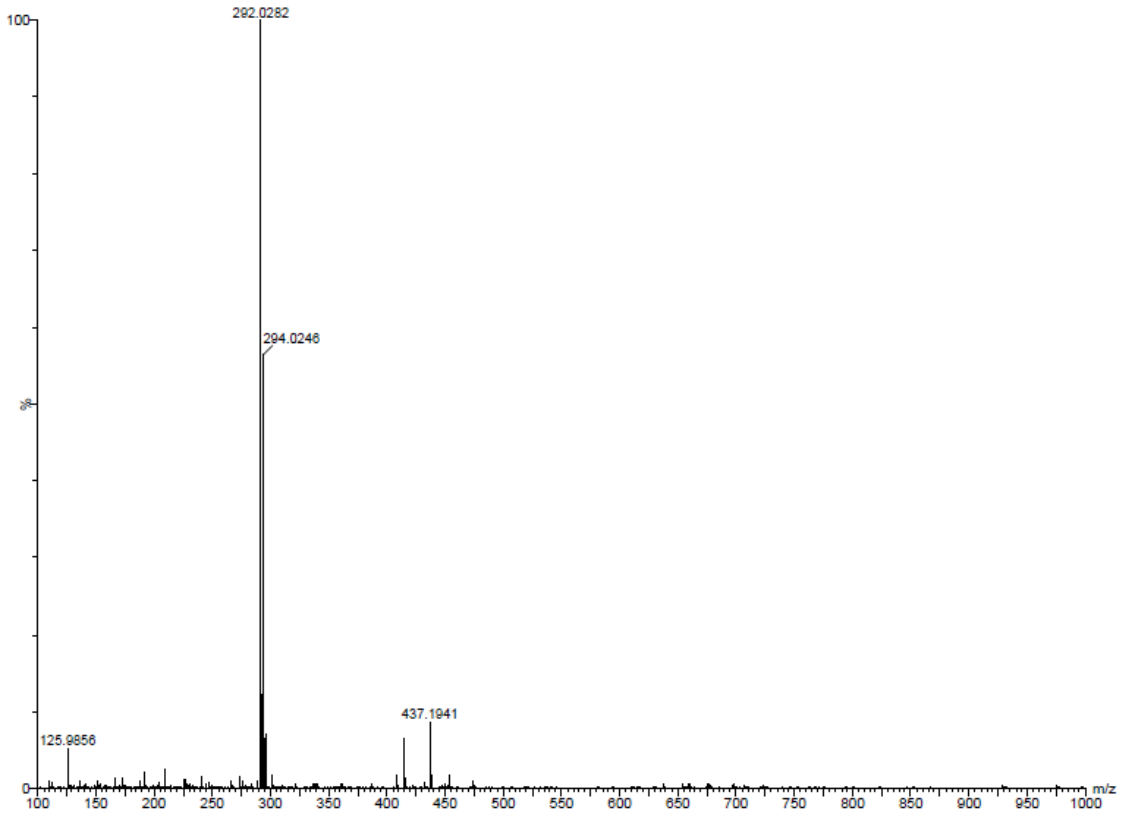

Figure S 74. ^{1}H NMR spectrum of compound **3j** (DMSO-d_6; 600 MHz)

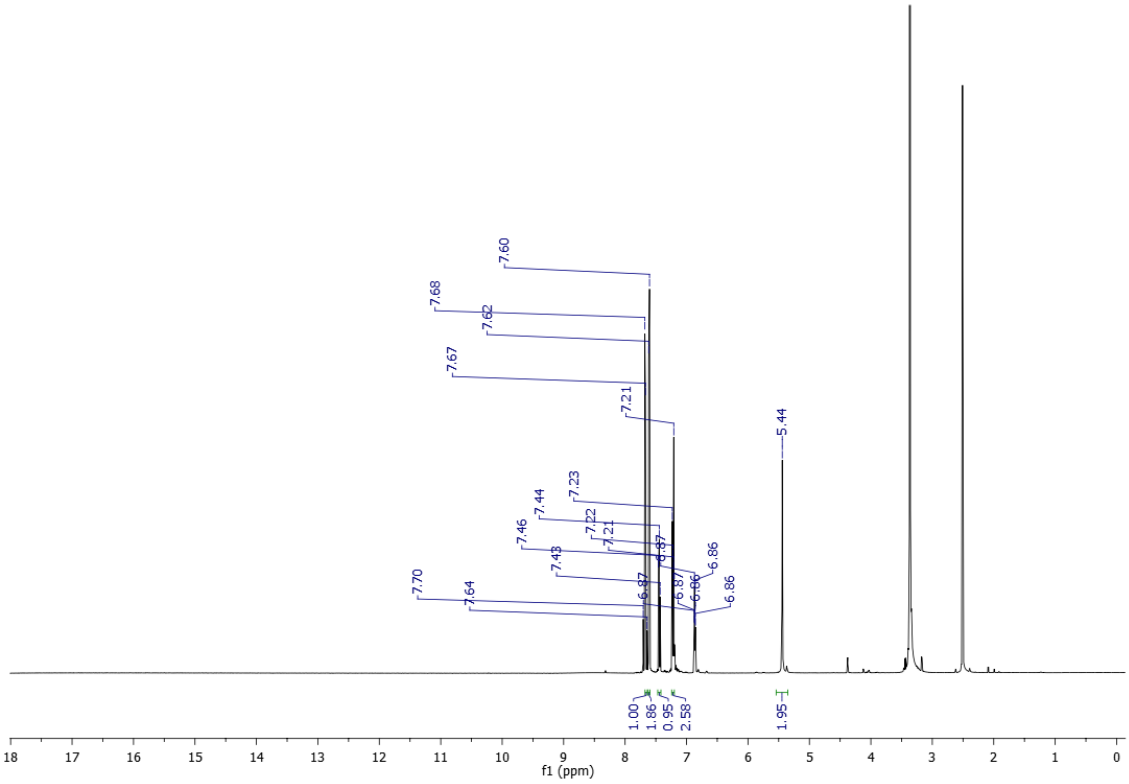

Figure S 75. ^{13}C NMR spectrum of compound **3j** (DMSO-d_6; 150 MHz)

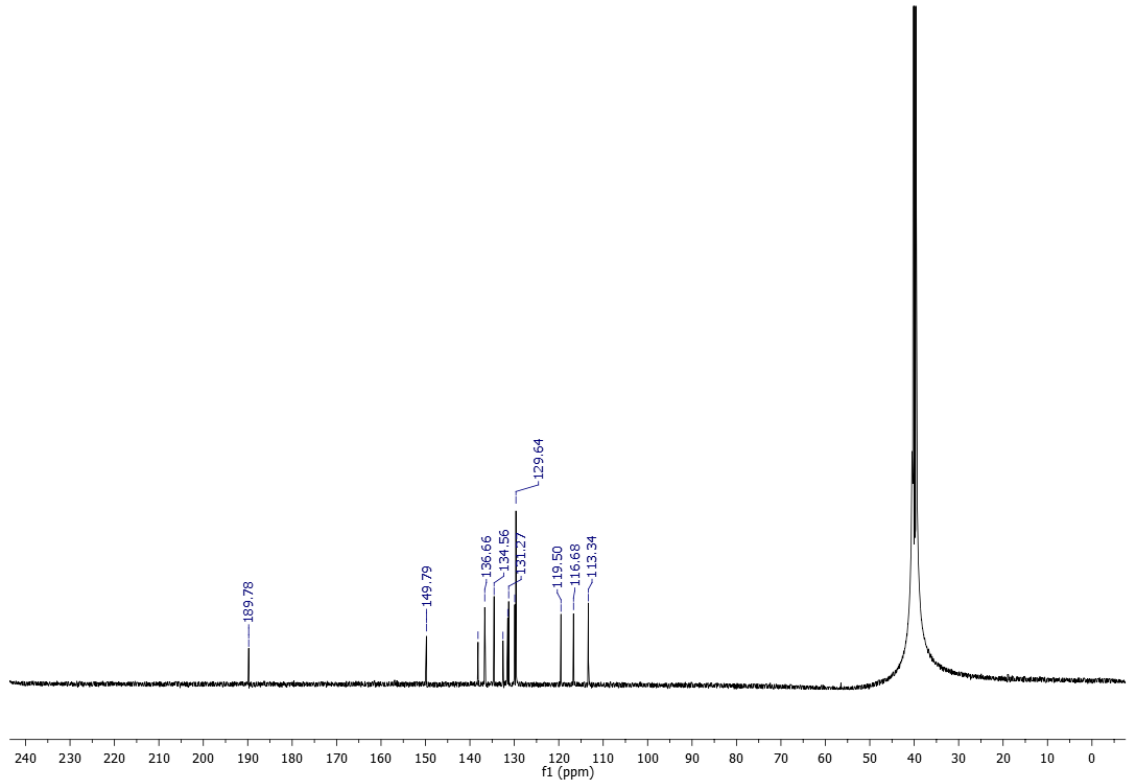

Figure S 76. HPLC chromatogram of compound **3j**

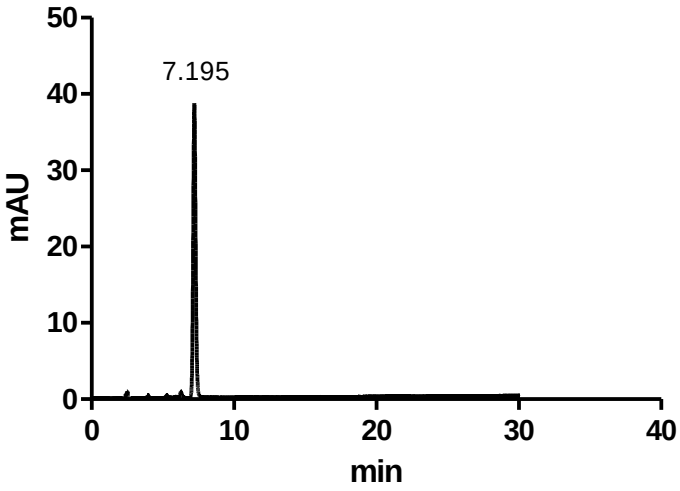

Figure S 77. UV-Vis spectrum of compound **3j**

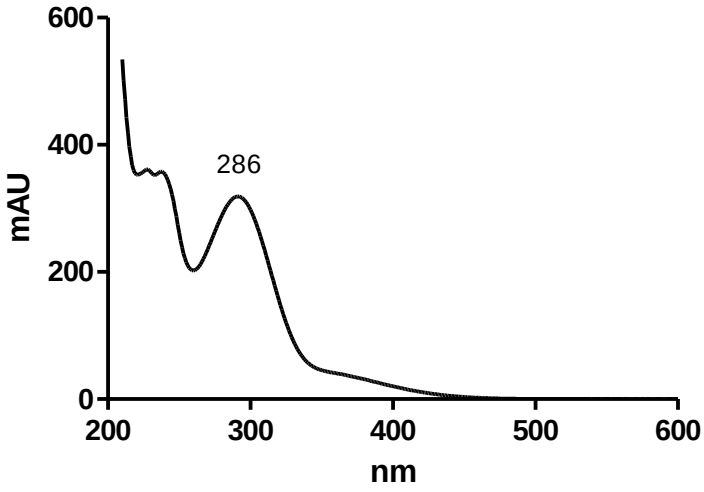

Figure S 78. HRMS of compound **3j**

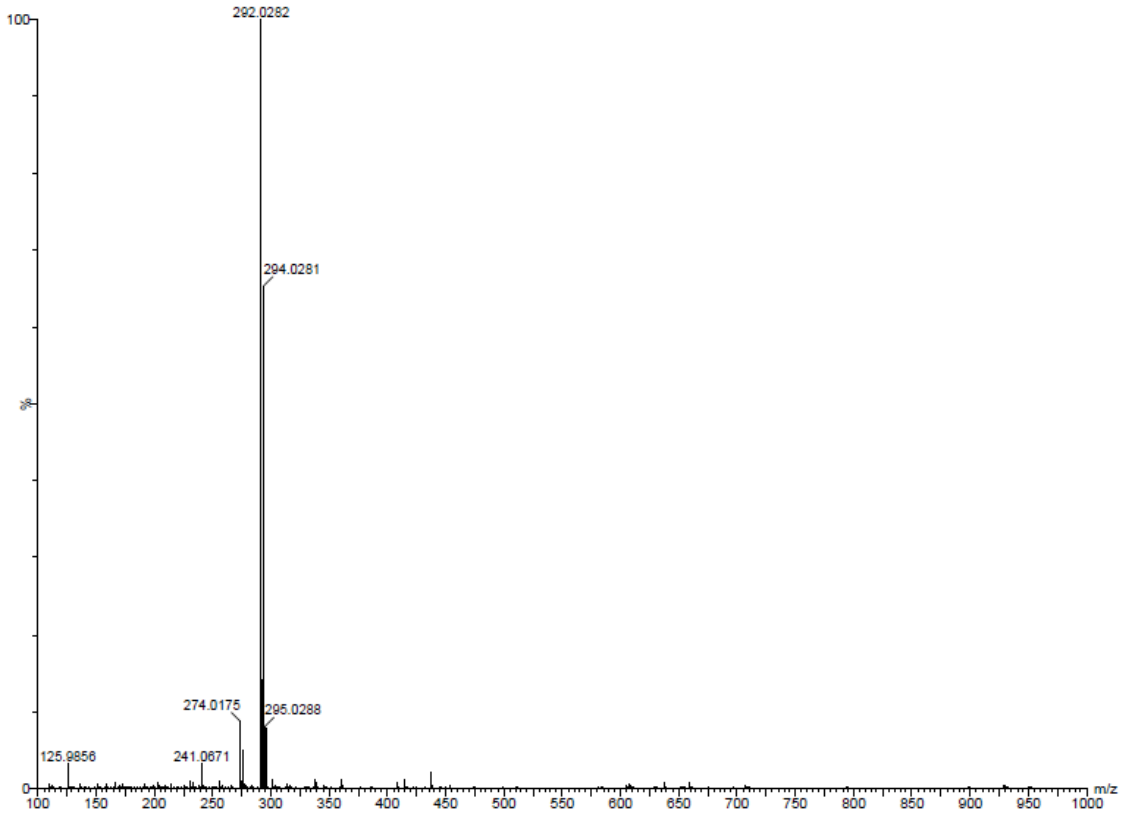

Figure S 79. ^{1}H NMR spectrum of compound **3k** (DMSO-d_6; 600 MHz)

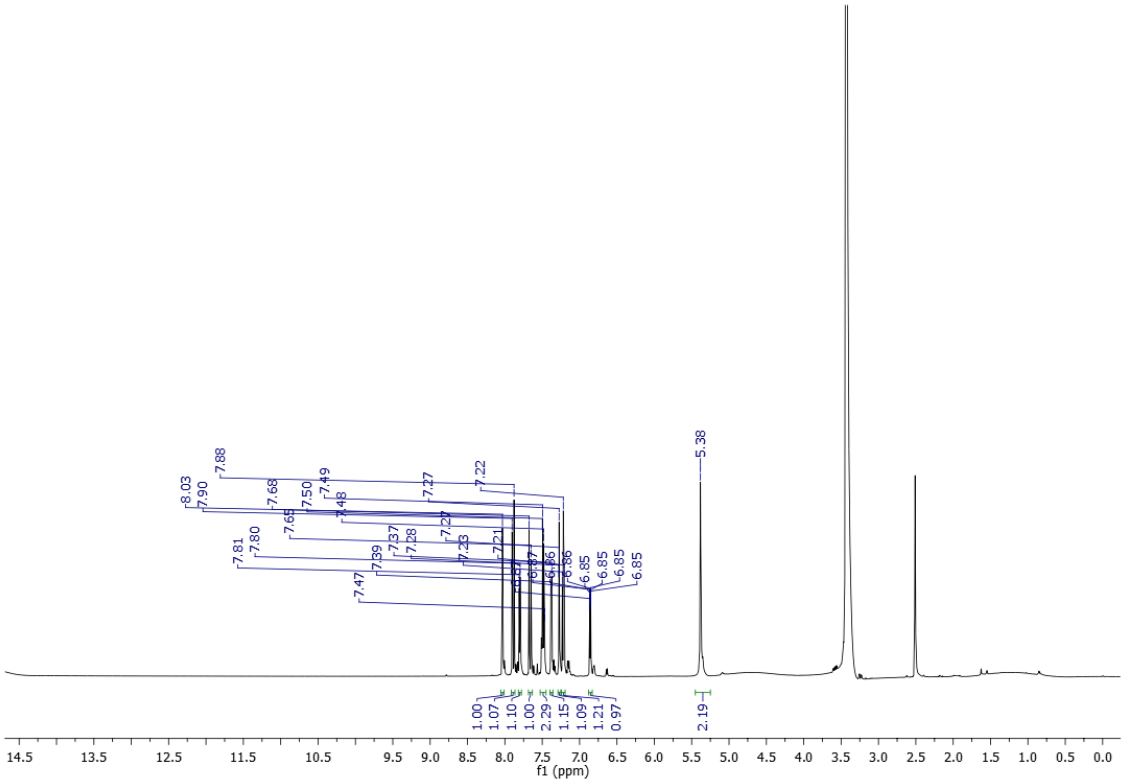

Figure S 80. ^{13}C NMR spectrum of compound **3k** (DMSO-d_6; 150 MHz)

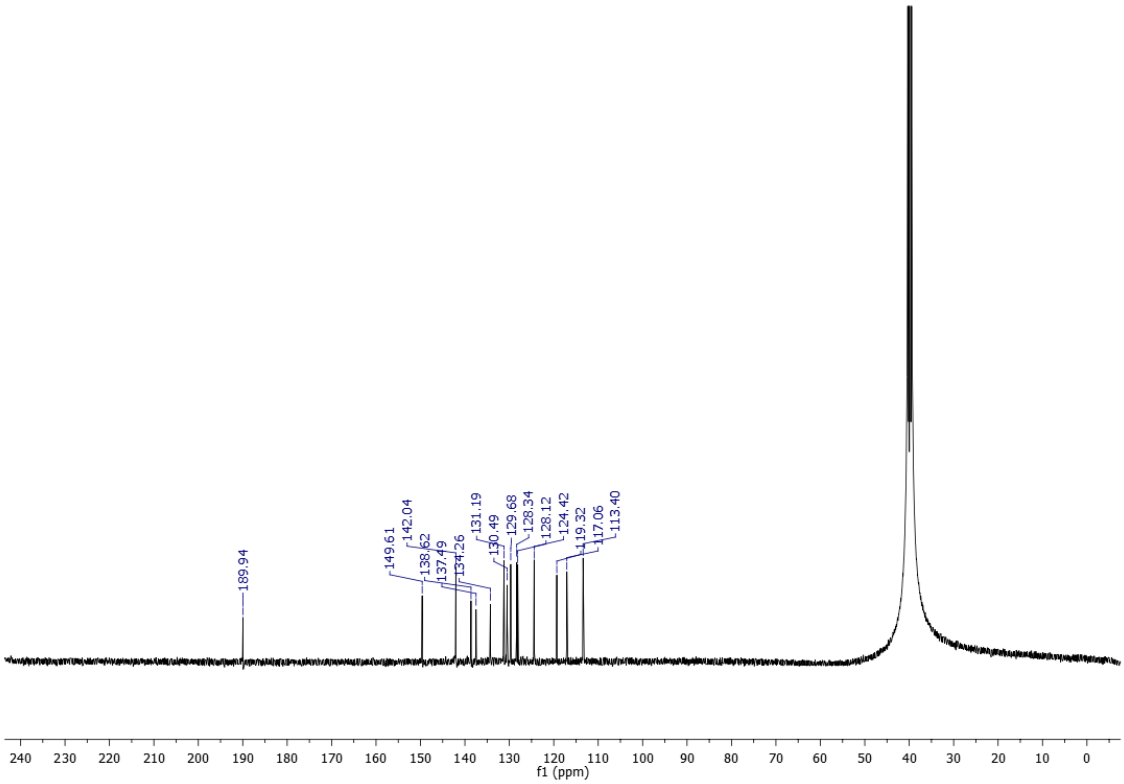

Figure S 81. HPLC chromatogram of compound **3k**

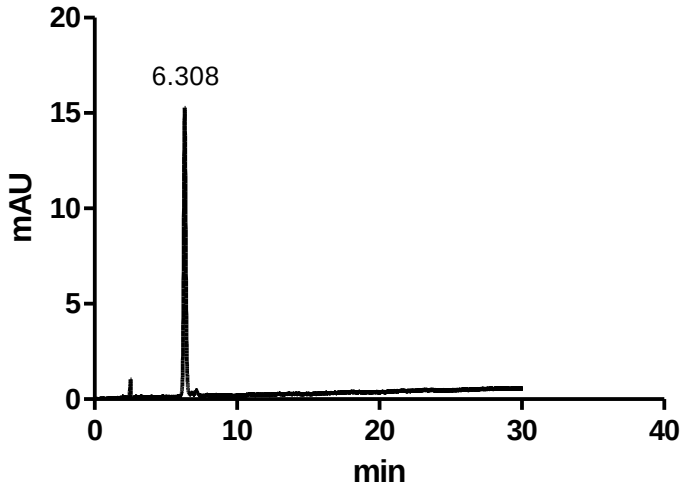

Figure S 82. UV-Vis spectrum of compound **3k**

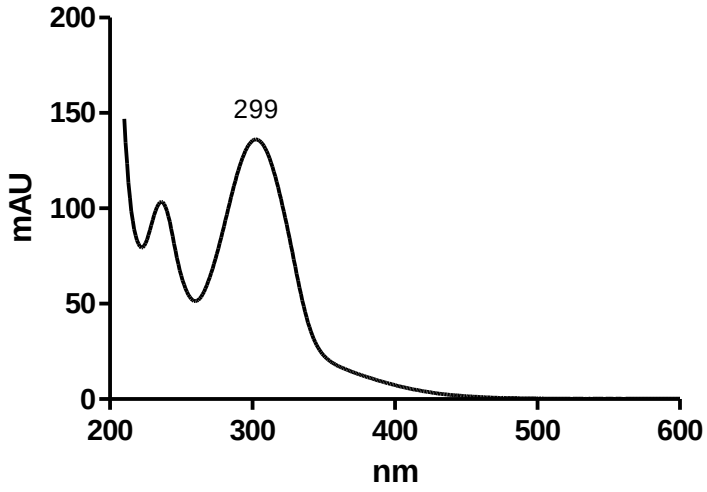

Figure S 83. ^{1}H NMR spectrum of compound **3l** (DMSO-d_6; 600 MHz)

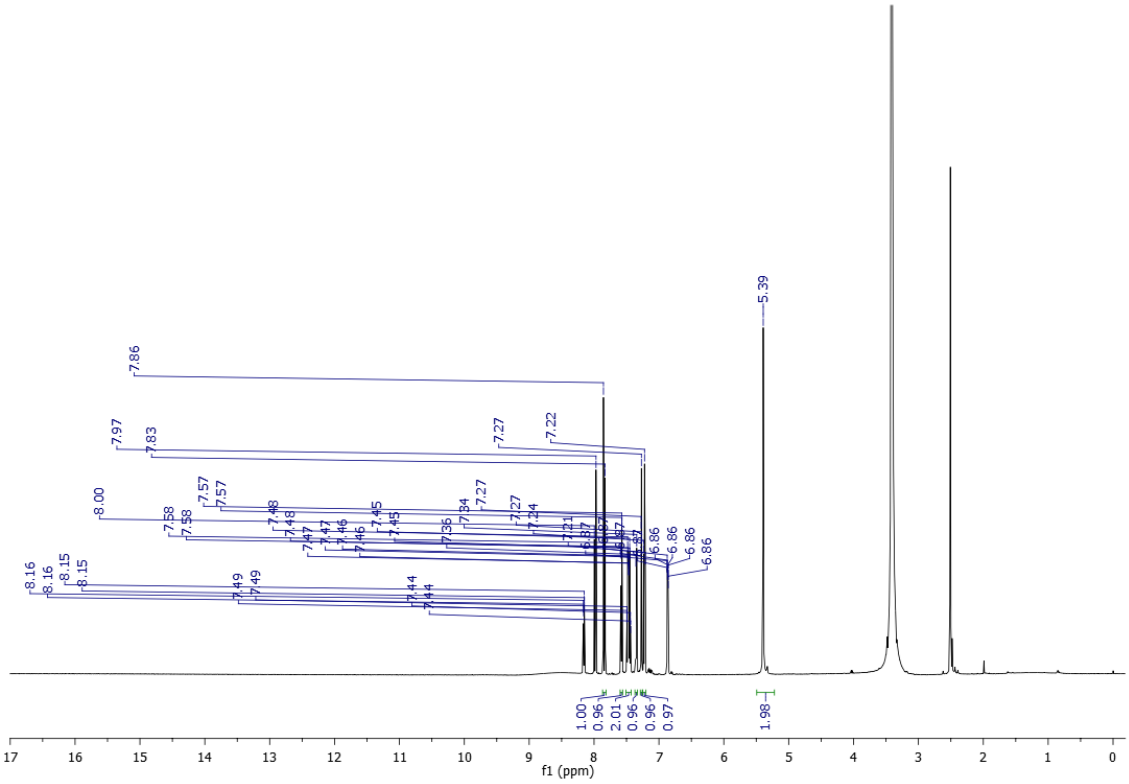

Figure S 84. ^{13}C NMR spectrum of compound **3l** (DMSO-d_6; 150 MHz)

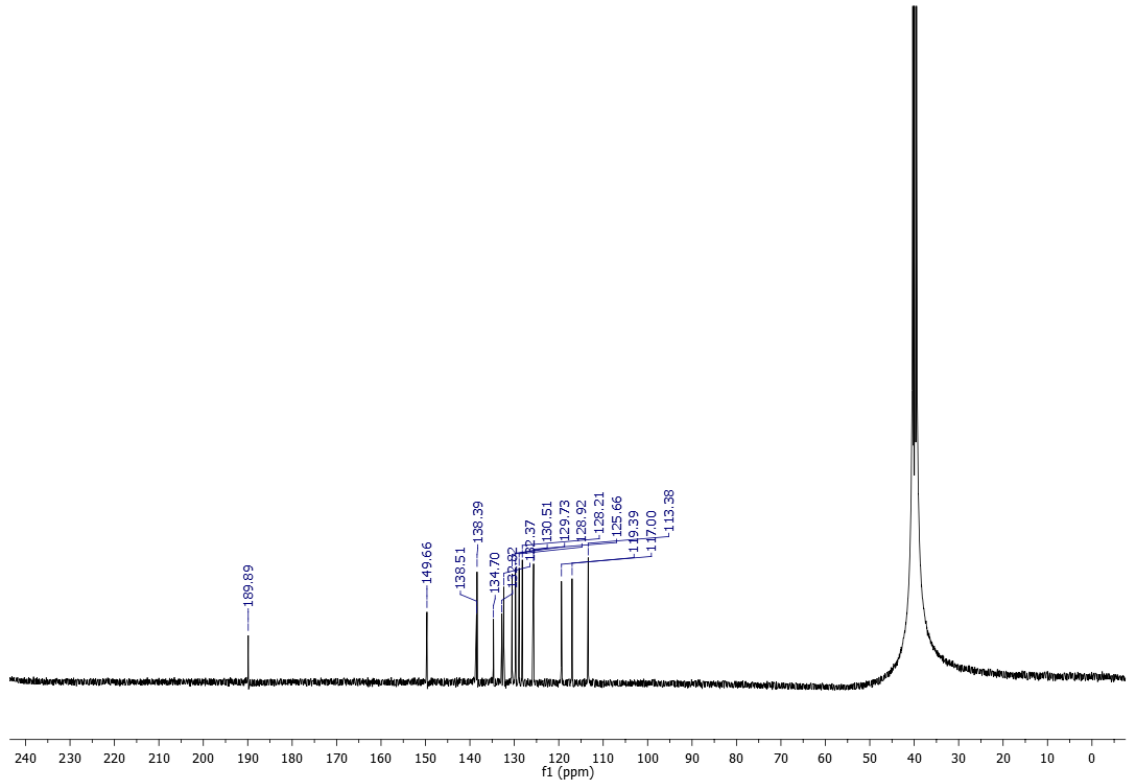

Figure S 85. HPLC chromatogram of compound **3l**

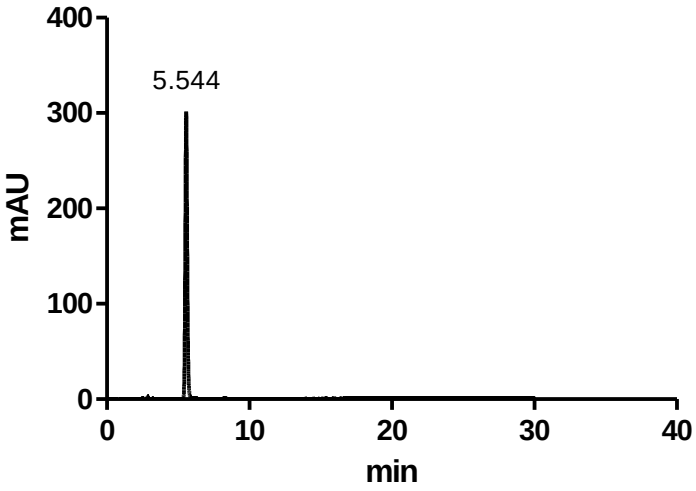

Figure S 86. UV-Vis spectrum of compound **3l**

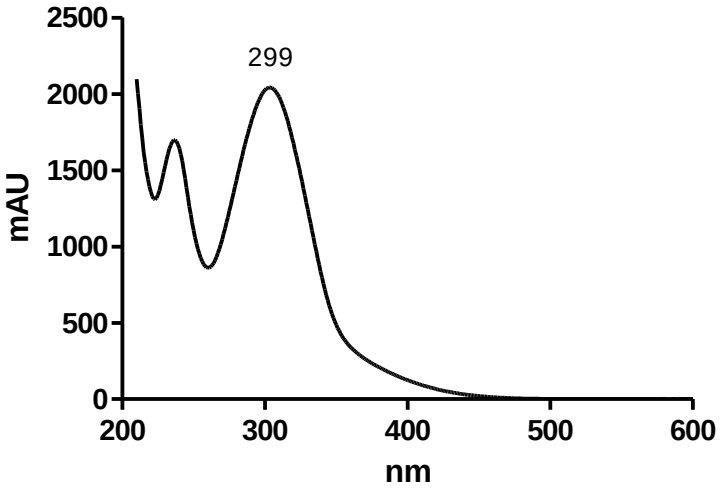

Figure S 87. ^{1}H NMR spectrum of compound **3m** (DMSO-d_6; 600 MHz)

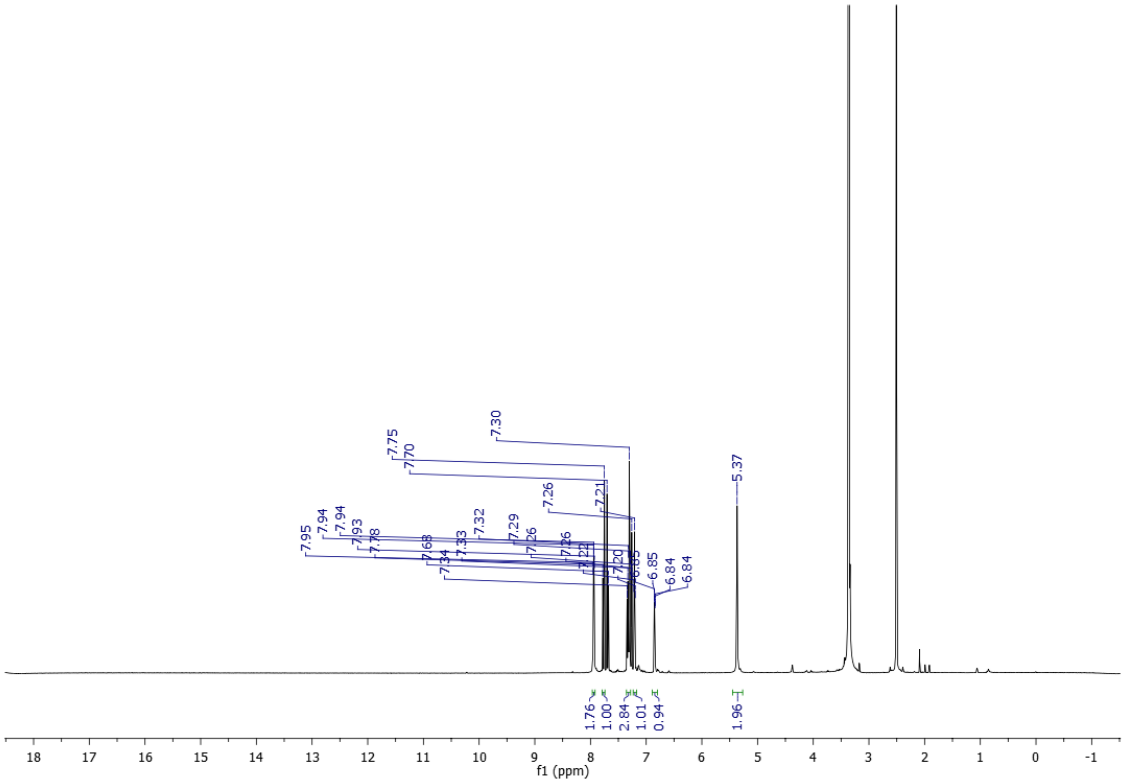

Figure S 88. ^{13}C NMR spectrum of compound **3m** (DMSO-d_6; 150 MHz)

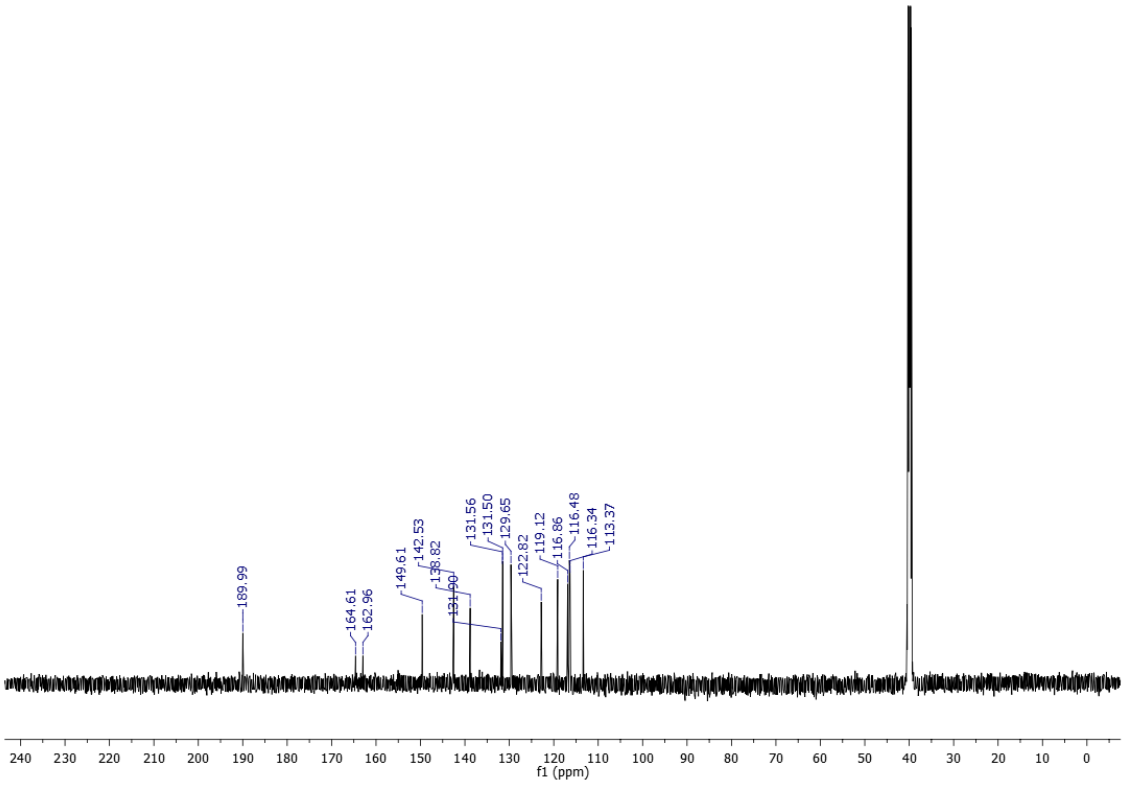

Figure S 89. HPLC chromatogram of compound **3m**

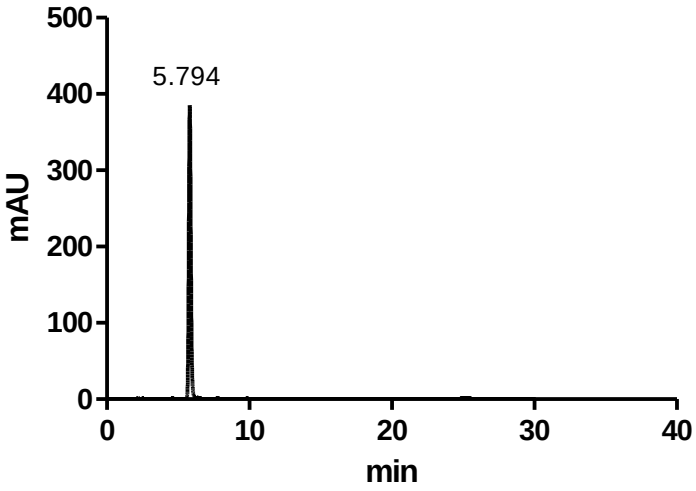

Figure S 90. UV-Vis spectrum of compound **3m**

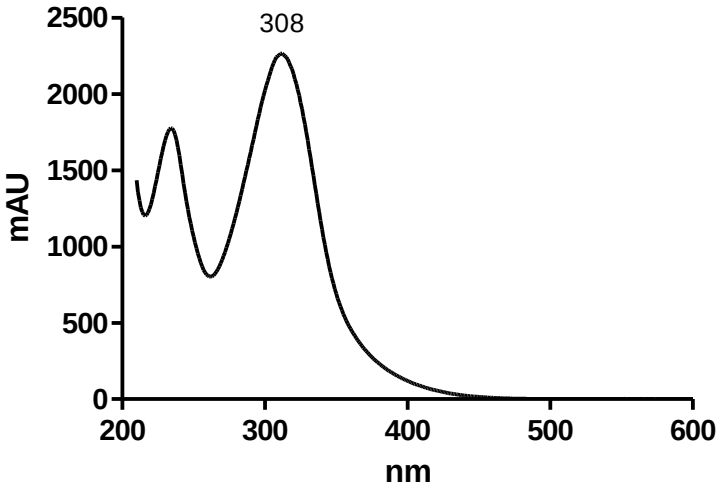

Figure S 91. ^{1}H NMR spectrum of compound **3n** (DMSO-d_6; 600 MHz)

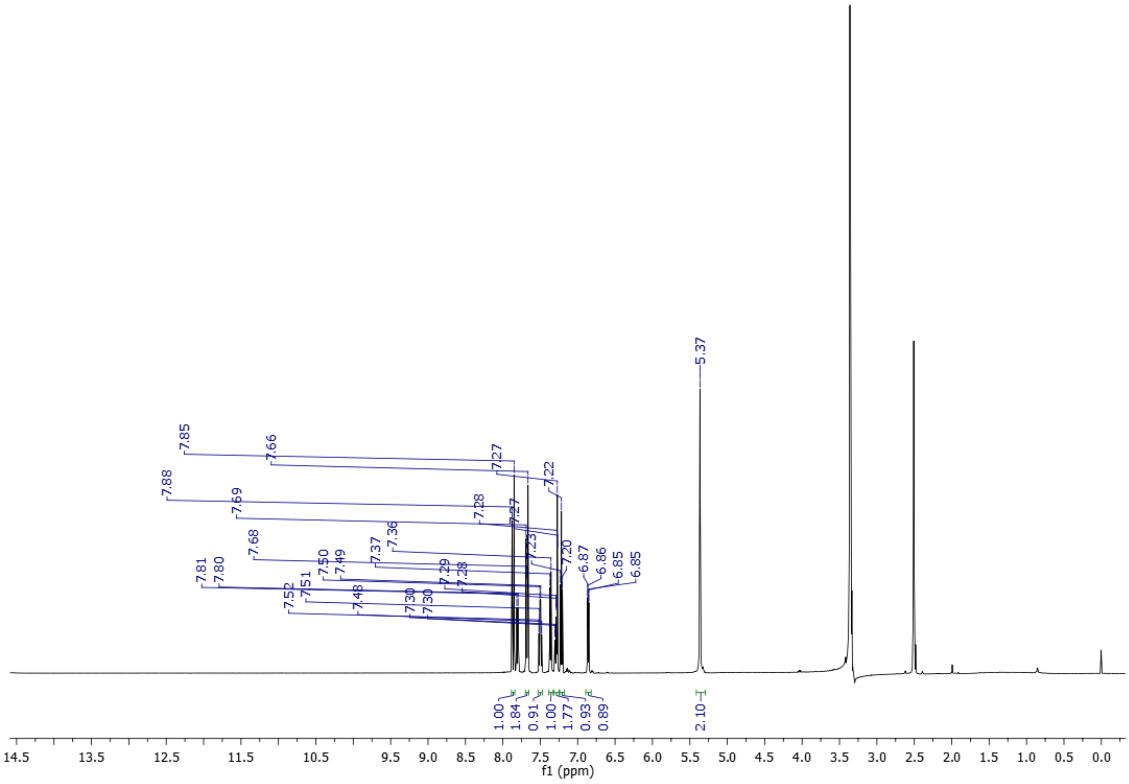

Figure S 92. ^{13}C NMR spectrum of compound **3n** (DMSO-d_6; 150 MHz)

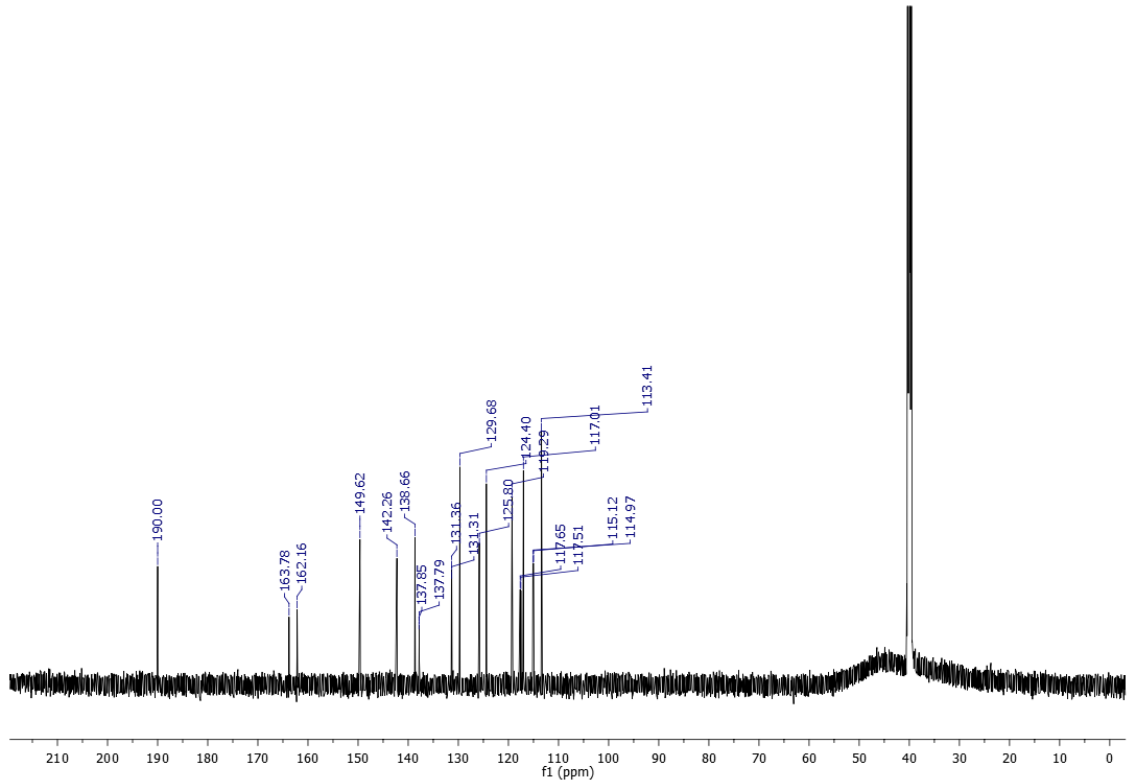

Figure S 93. HPLC chromatogram of compound **3n**

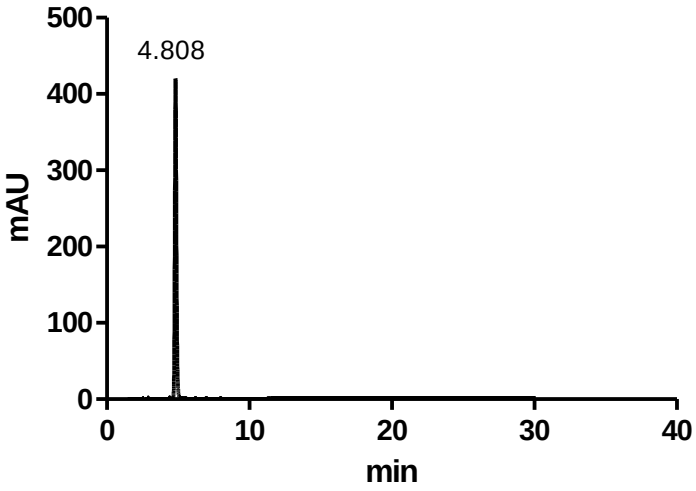

Figure S 94. UV-Vis spectrum of compound **3n**

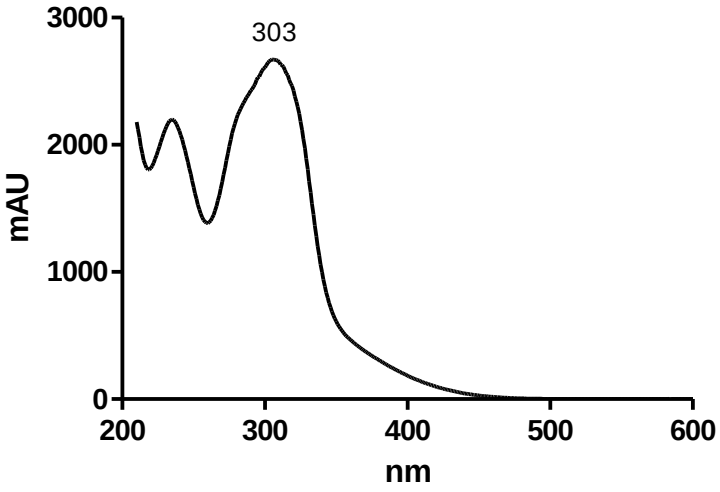

Figure S 95. ^{1}H NMR spectrum of compound **3o** (DMSO-d_6; 600 MHz)

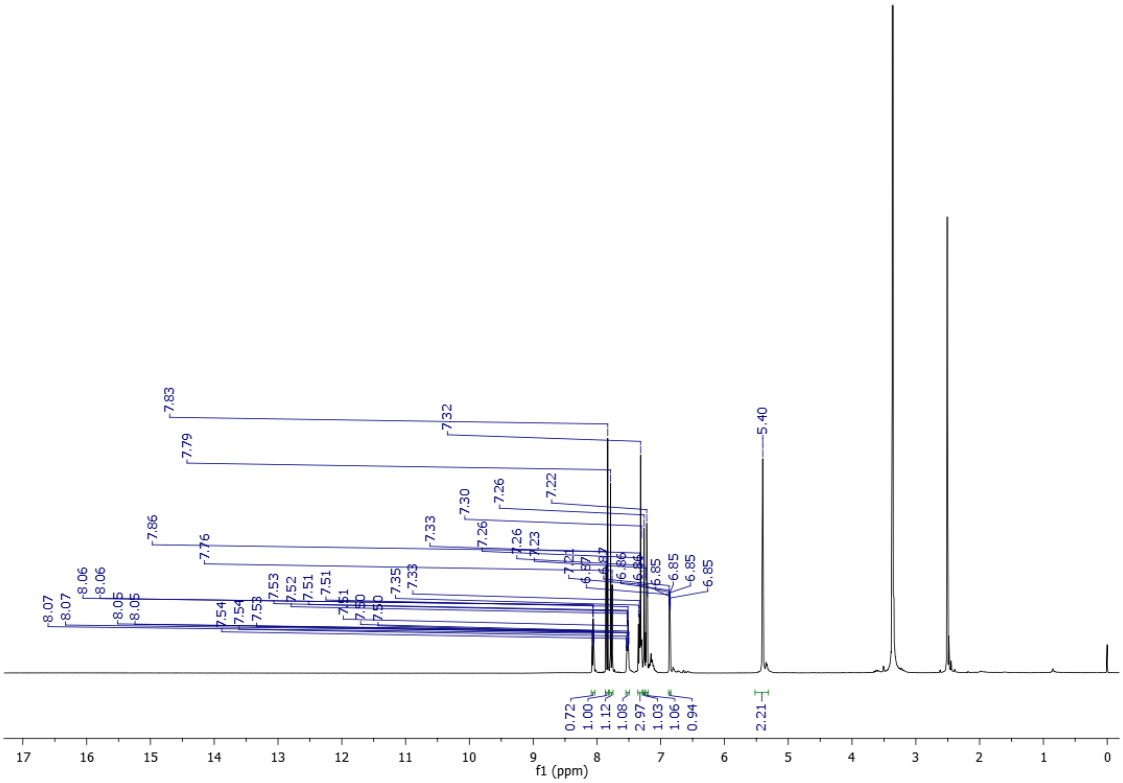

Figure S 96. ^{13}C NMR spectrum of compound **3o** (DMSO-d_6; 150 MHz)

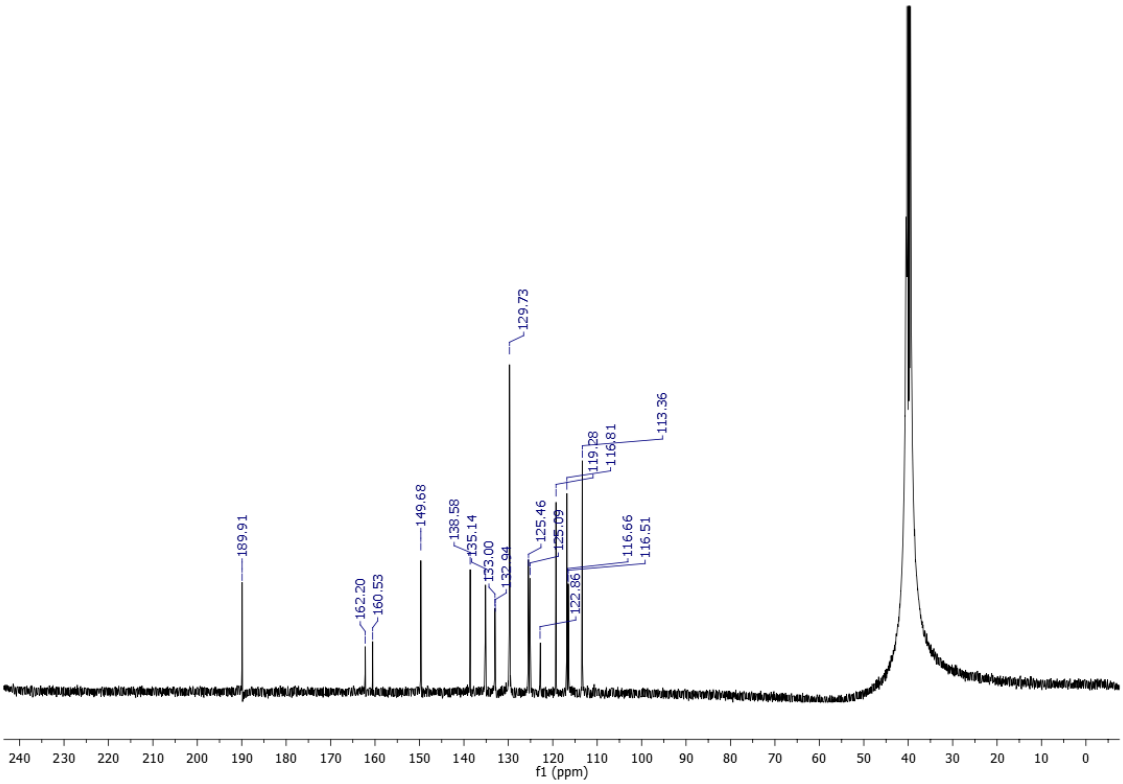

Figure S 97. HPLC chromatogram of compound **3o**

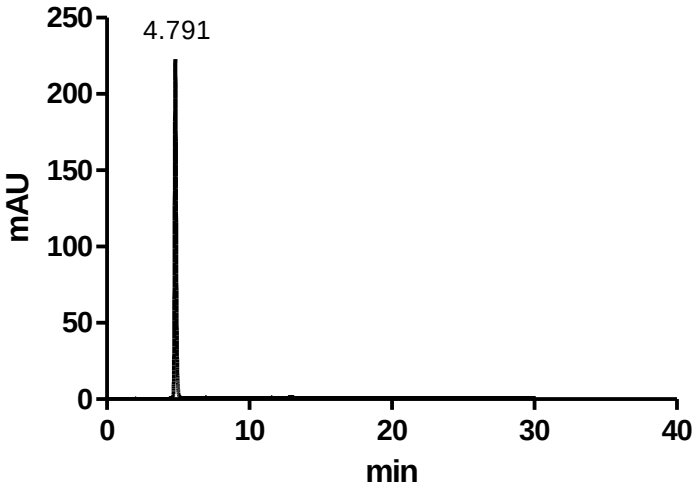

Figure S 98. UV-Vis spectrum of compound **3o**

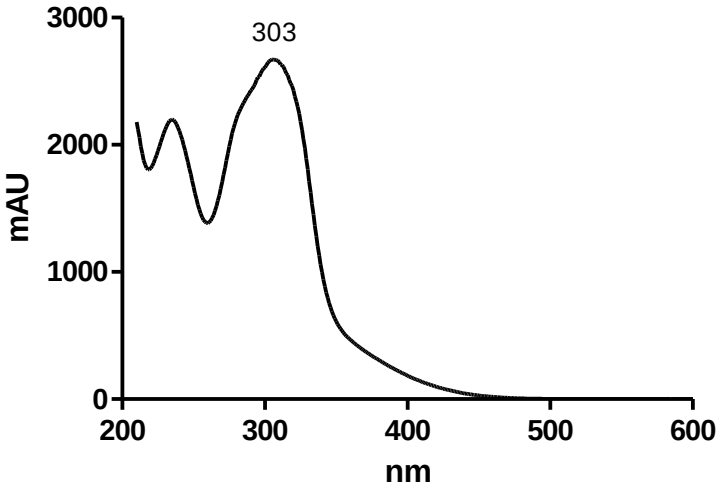

Figure S 99. HRMS of compound **3o**

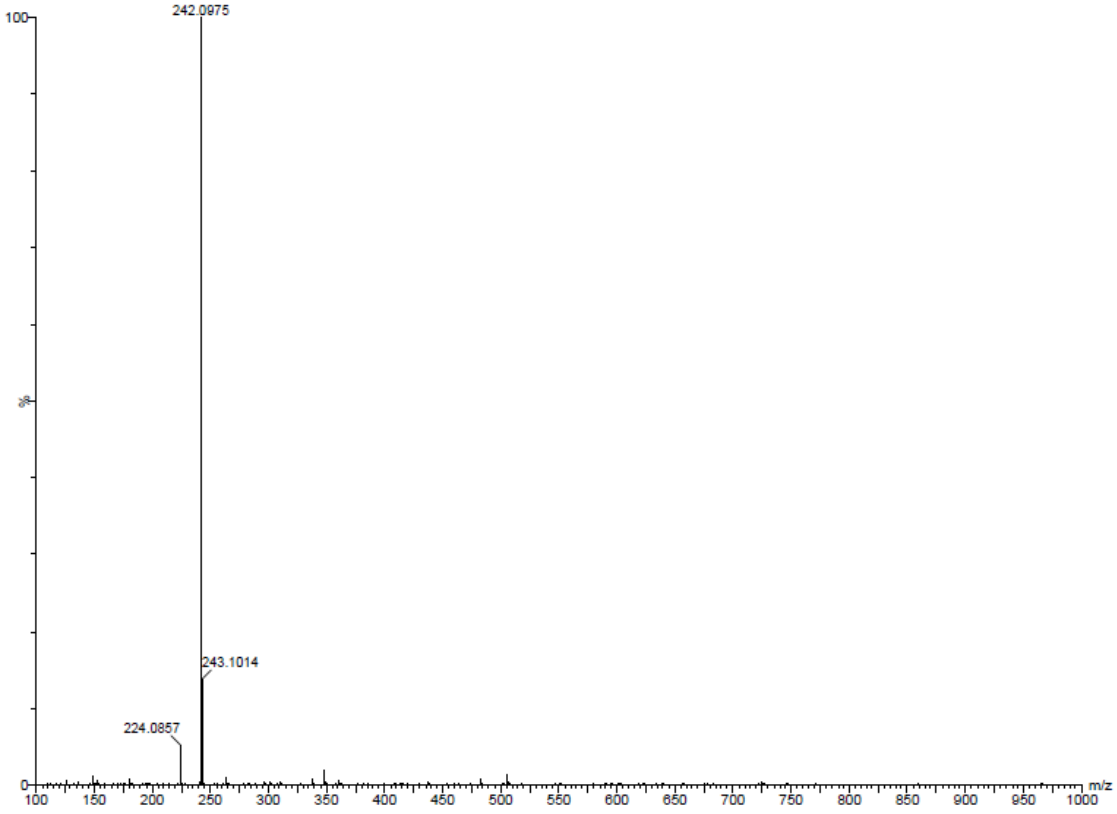

Figure S 100. ^{1}H NMR spectrum of compound **3p** (DMSO-d_6; 600 MHz)

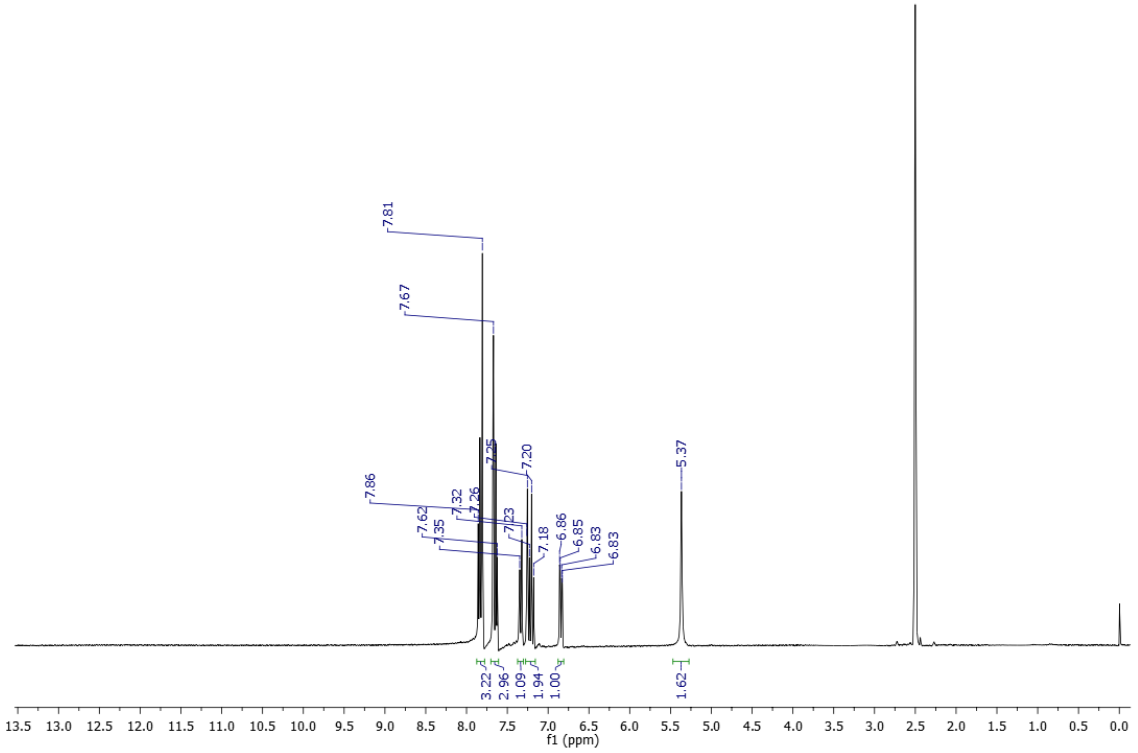

Figure S 101. ^{13}C NMR spectrum of compound **3p** (DMSO-d_6; 150 MHz)

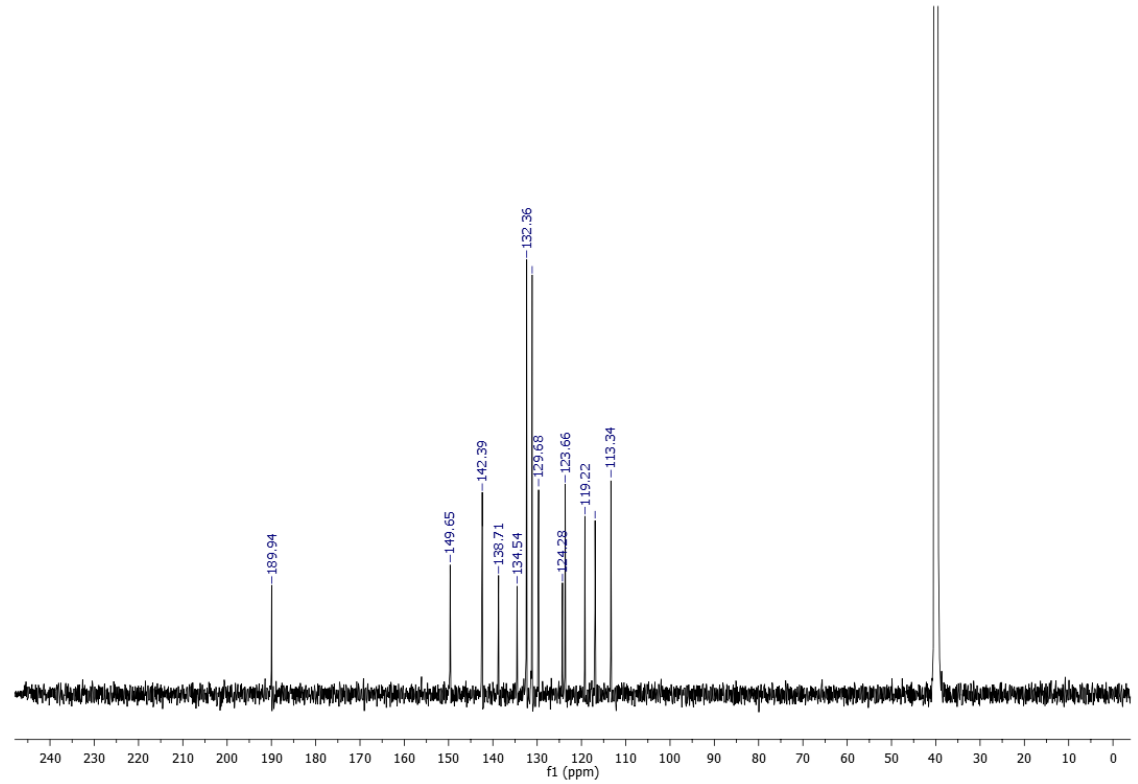

Figure S 102. HPLC chromatogram of compound **3p**

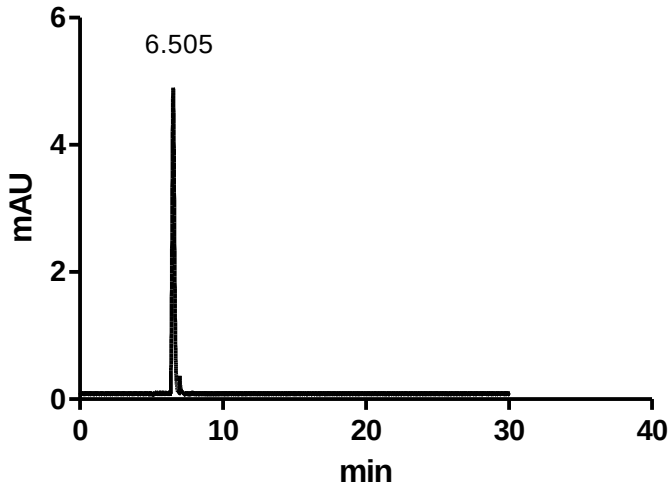

Figure S 103. UV-Vis spectrum of compound **3p**

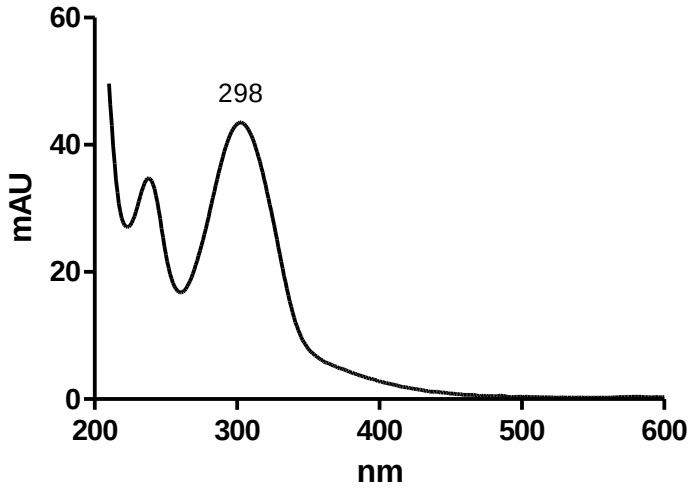

Figure S 104. ^{1}H NMR spectrum of compound **3q** (DMSO-d_6; 600 MHz)

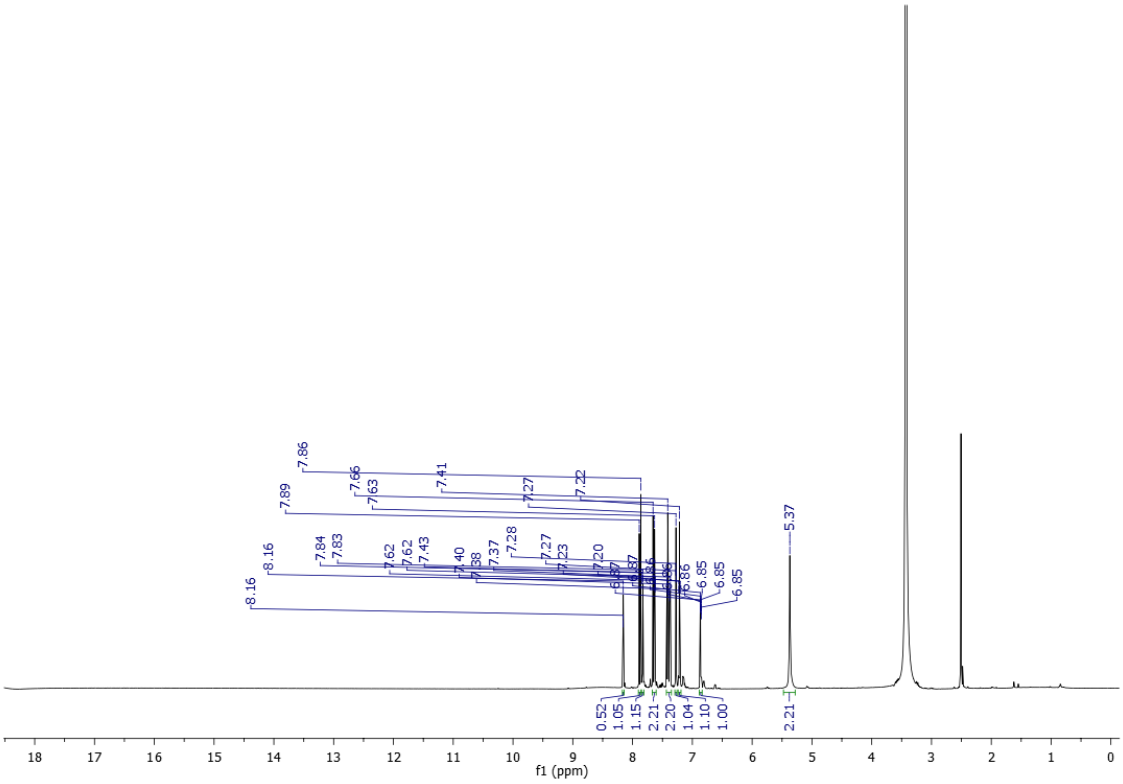

Figure S 105. ^{13}C NMR spectrum of compound **3q** (DMSO-d_6; 150 MHz)

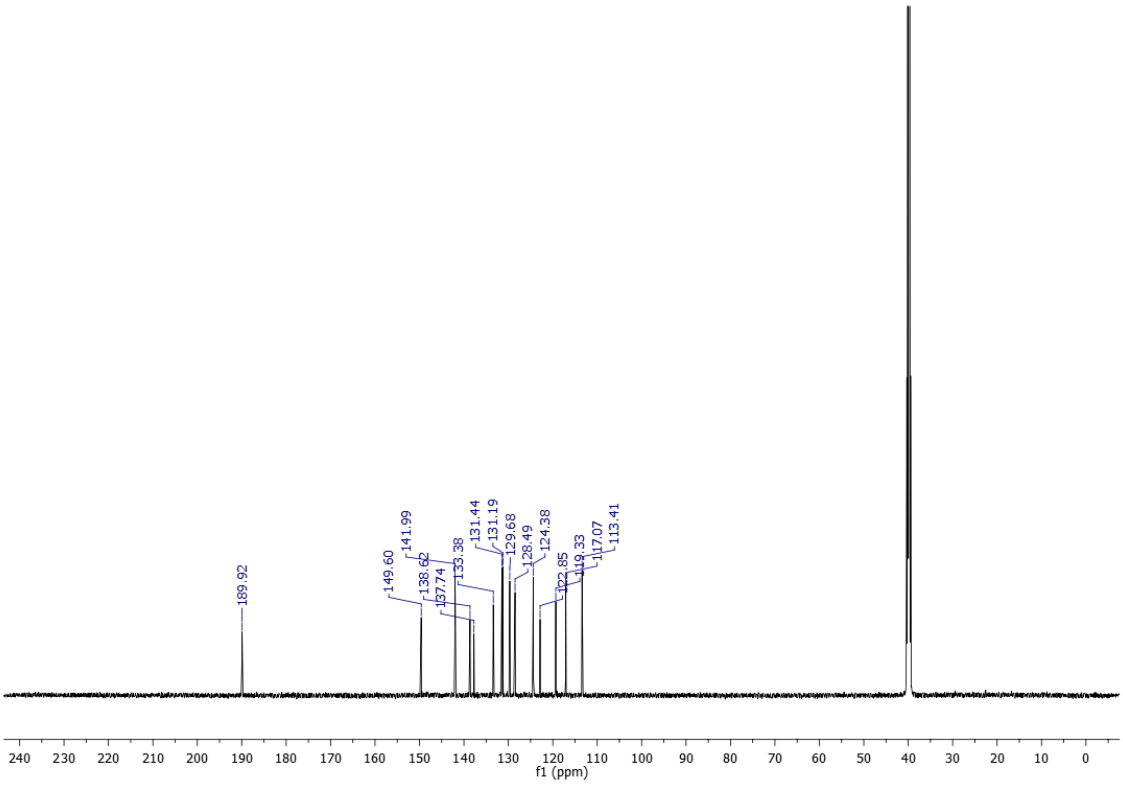

Figure S 106. HPLC chromatogram of compound **3q**

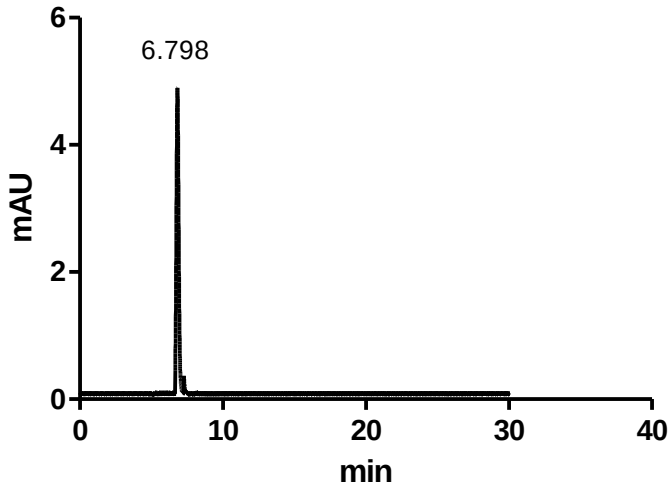

Figure S 107. UV-Vis spectrum of compound **3q**

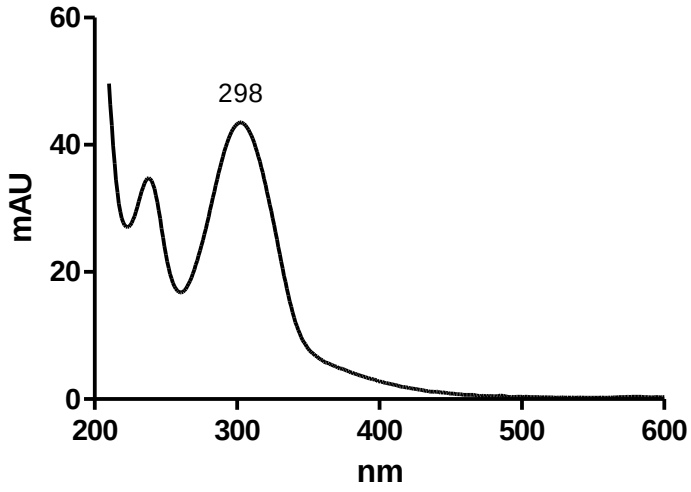

Figure S 108. ^{1}H NMR spectrum of compound **3r** (DMSO-d_6; 600 MHz)

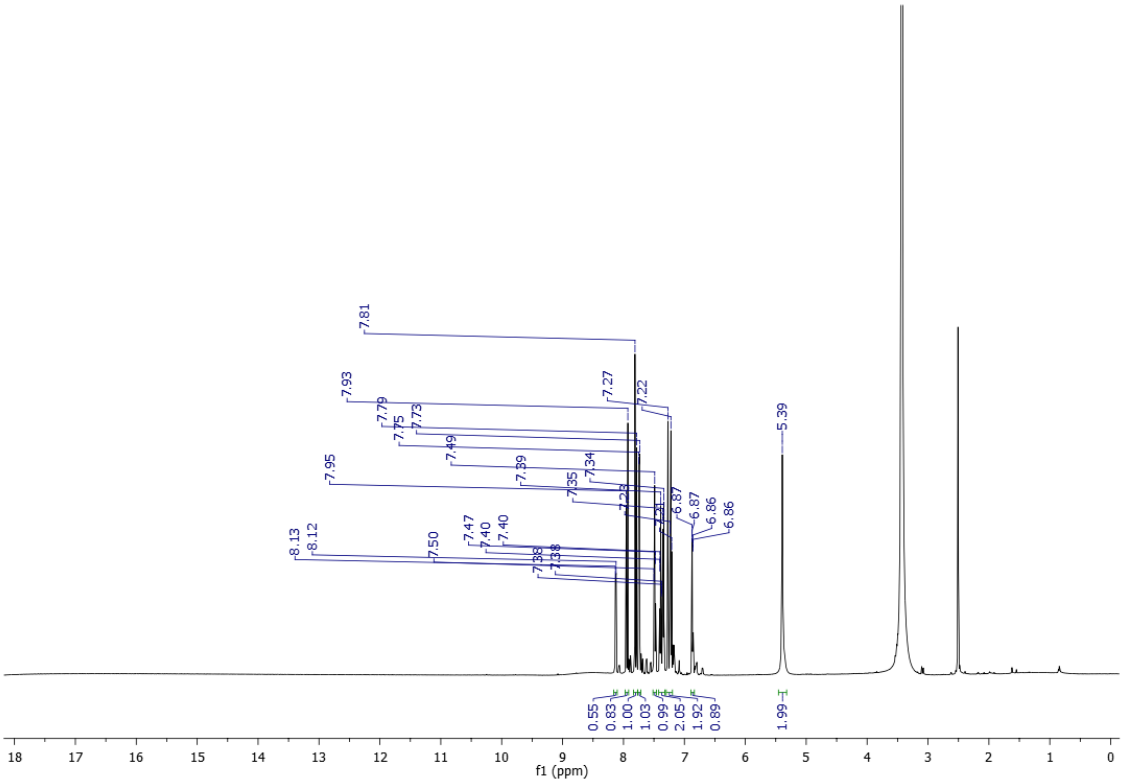

Figure S 109. ^{13}C NMR spectrum of compound **3r** (DMSO-d_6; 150 MHz)

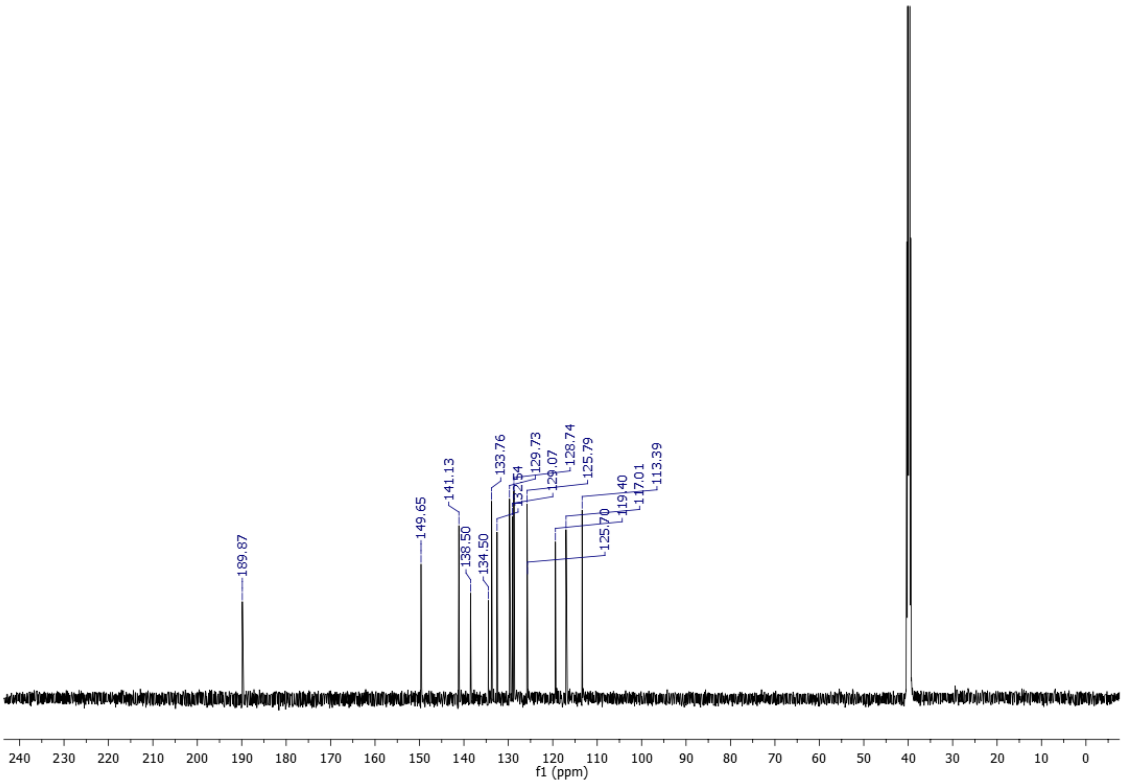

Figure S 110. HPLC chromatogram of compound **3r**

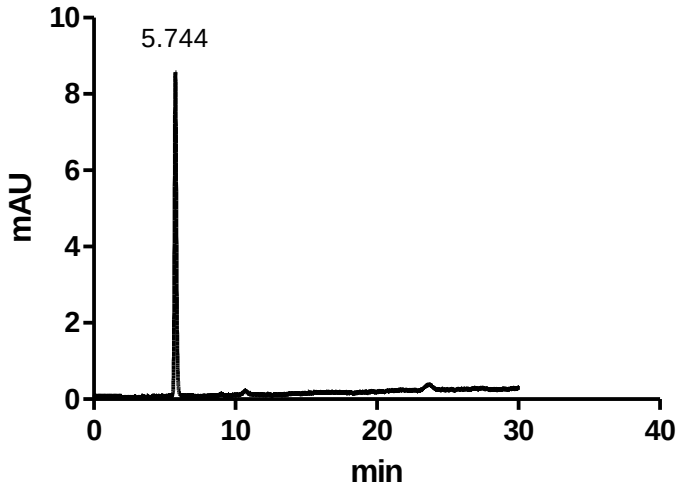

Figure S 111. UV-Vis spectrum of compound **3r**

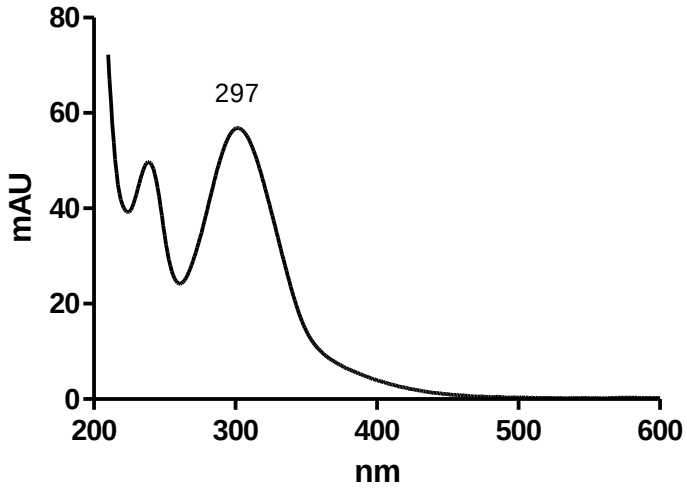

Figure S 112. HRMS of compound **3r**

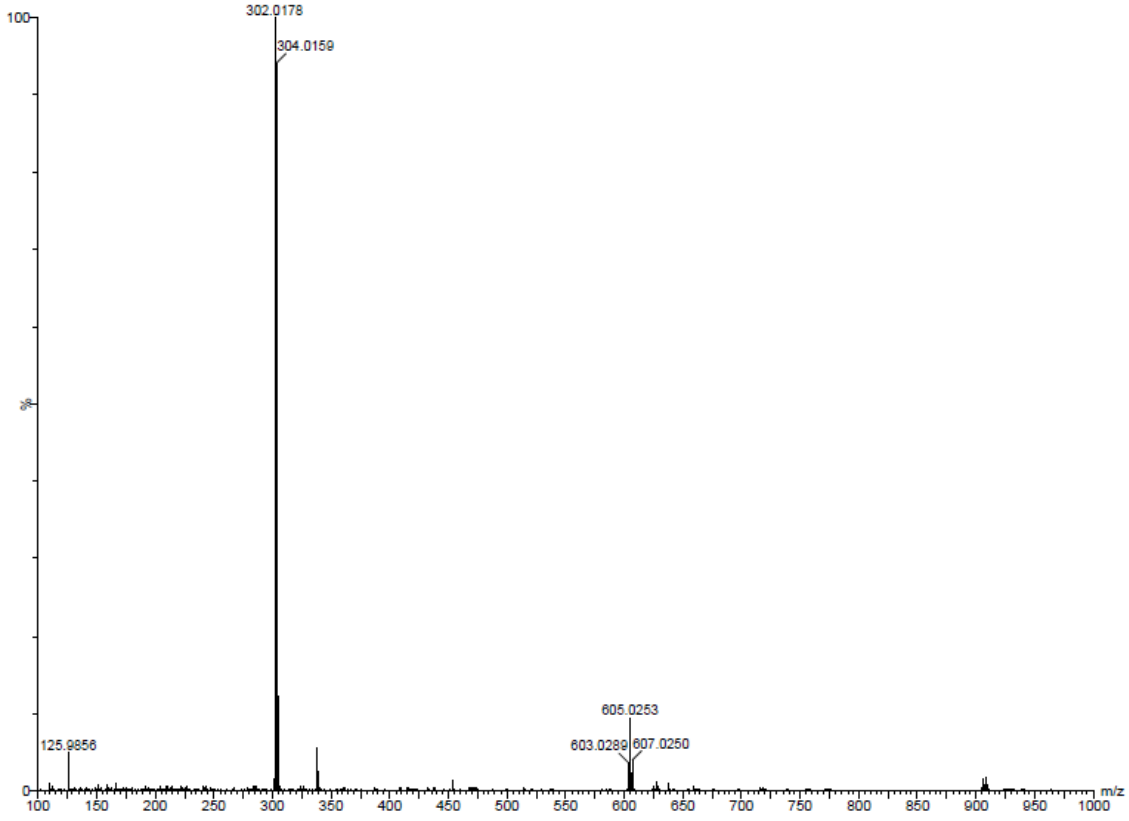

Figure S 113. ^{1}H NMR spectrum of compound **3s** (methanol-*d*$_4$; 600 MHz)

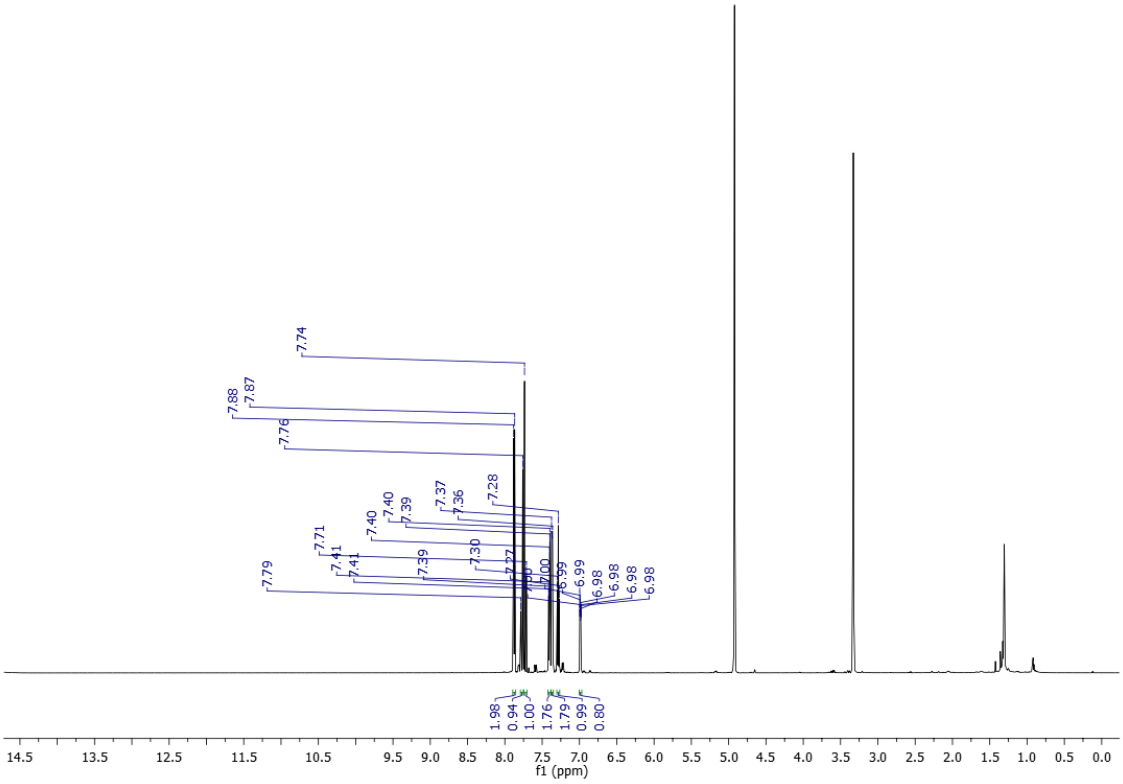

Figure S 114. ^{13}C NMR spectrum of compound **3s** (methanol-*d*$_4$; 150 MHz)

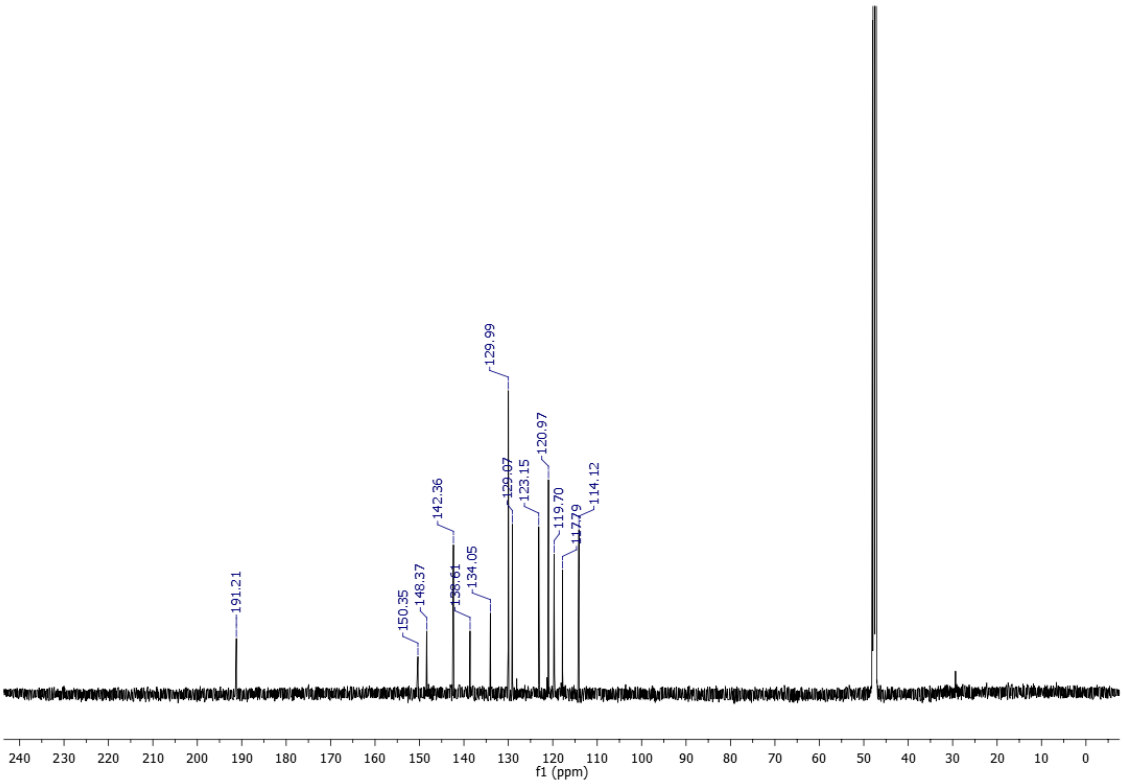

Figure S 115. HPLC chromatogram of compound **3s**

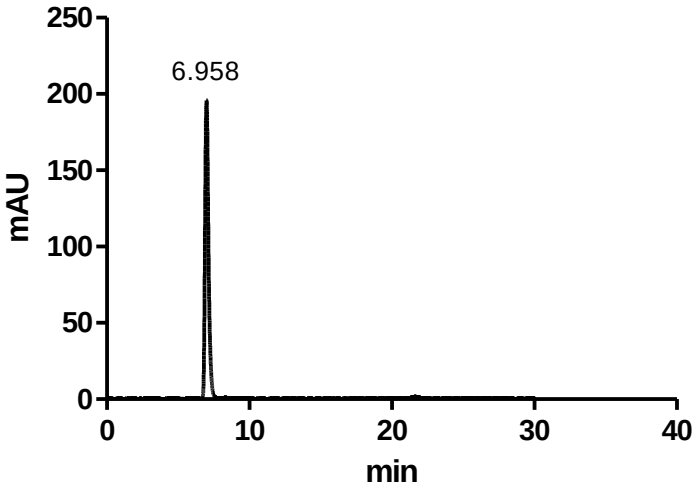

Figure S 116. UV-Vis spectrum of compound **3s**

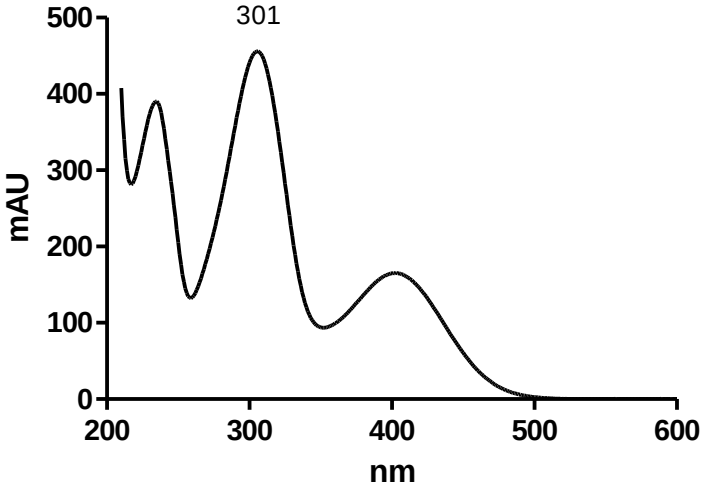

Figure S 117. HRMS of compound **3s**

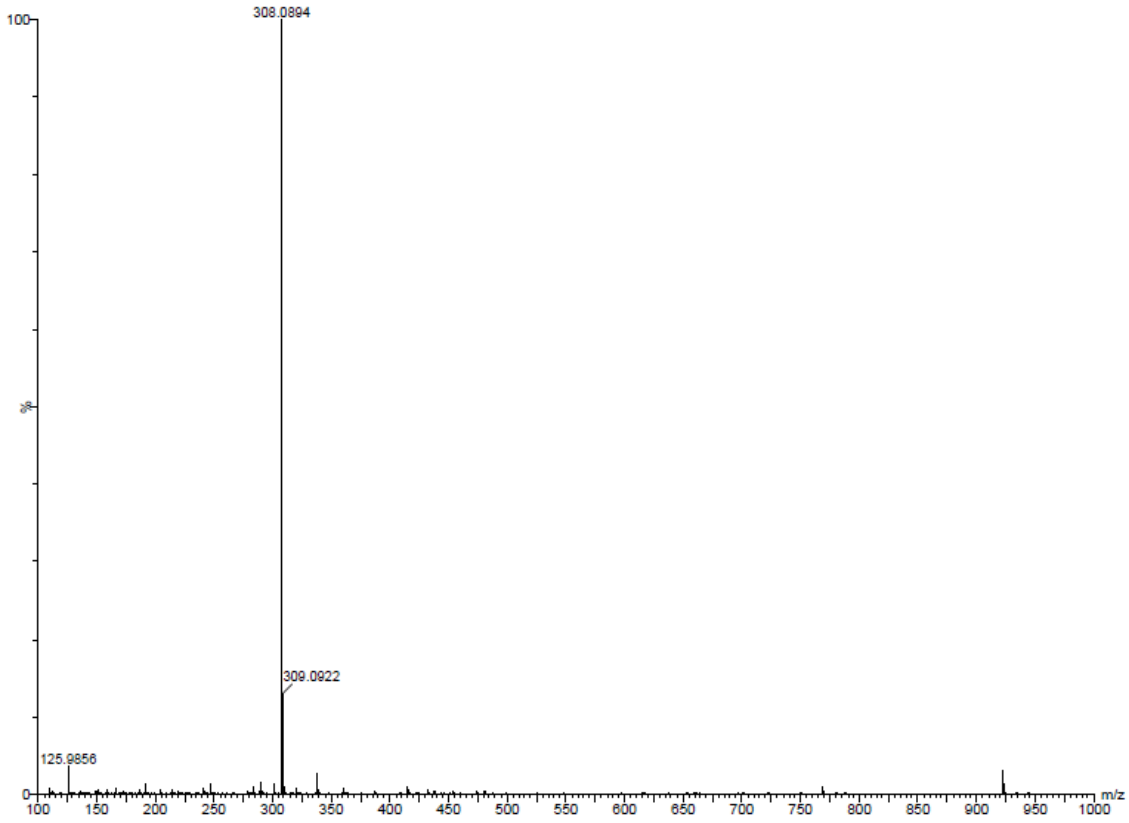

Figure S 118. ^{1}H NMR spectrum of compound **3t** (DMSO-d_6; 600 MHz)

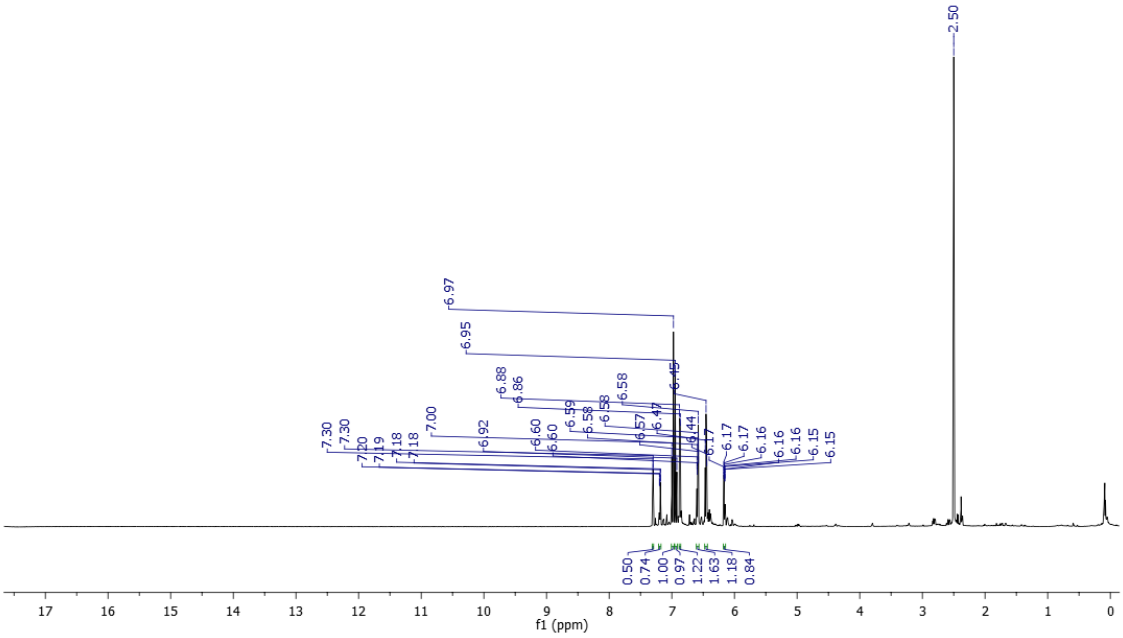

Figure S 119. ^{13}C NMR spectrum of compound **3t** (DMSO-d_6; 150 MHz)

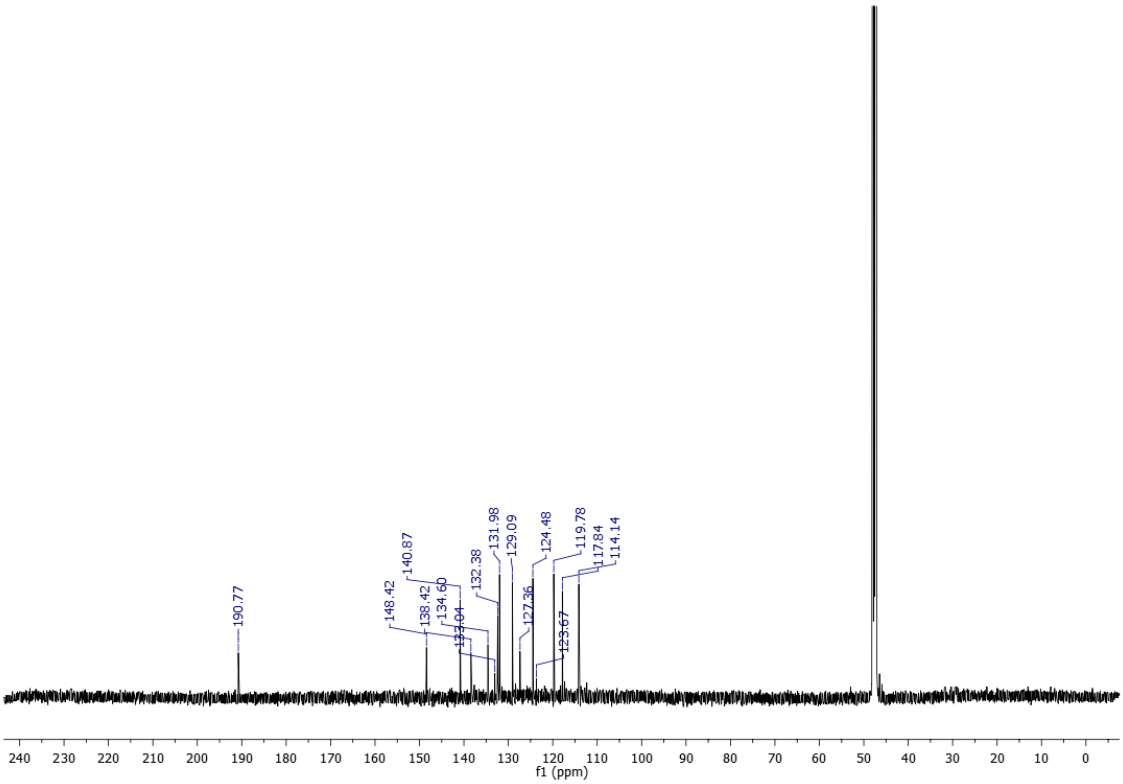

Figure S 120. HPLC chromatogram of compound **3t**

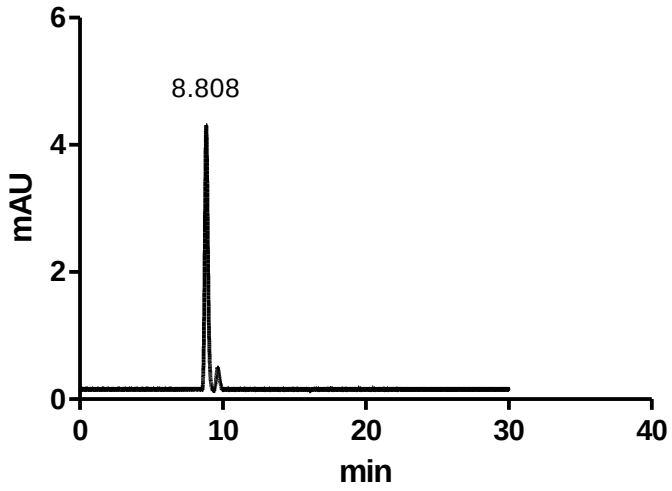

Figure S 121. UV-Vis spectrum of compound **3t**

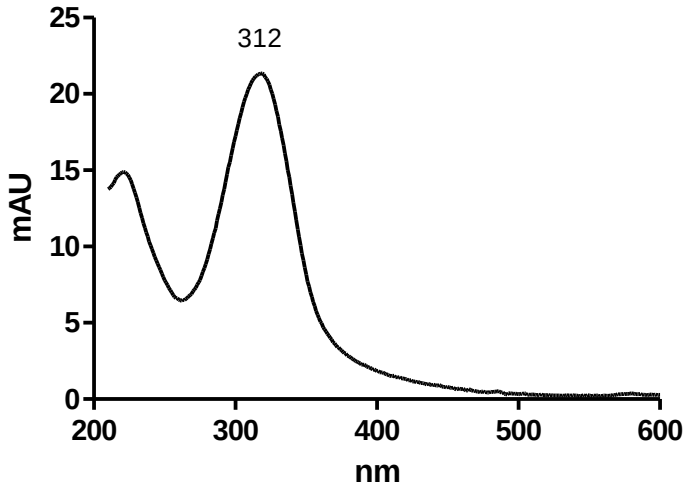

Figure S 122. ^{1}H NMR spectrum of compound **3u** (DMSO-d_6; 600 MHz)

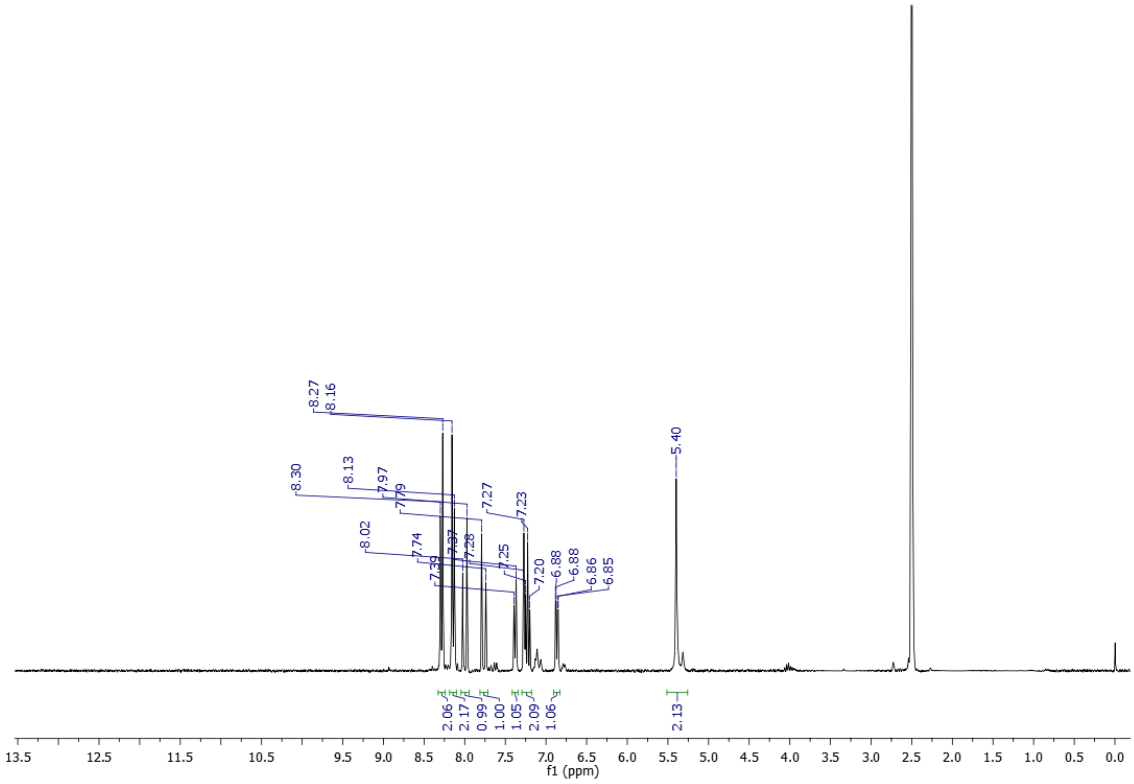

Figure S 123. ^{13}C NMR spectrum of compound **3u** (DMSO-d_6; 150 MHz)

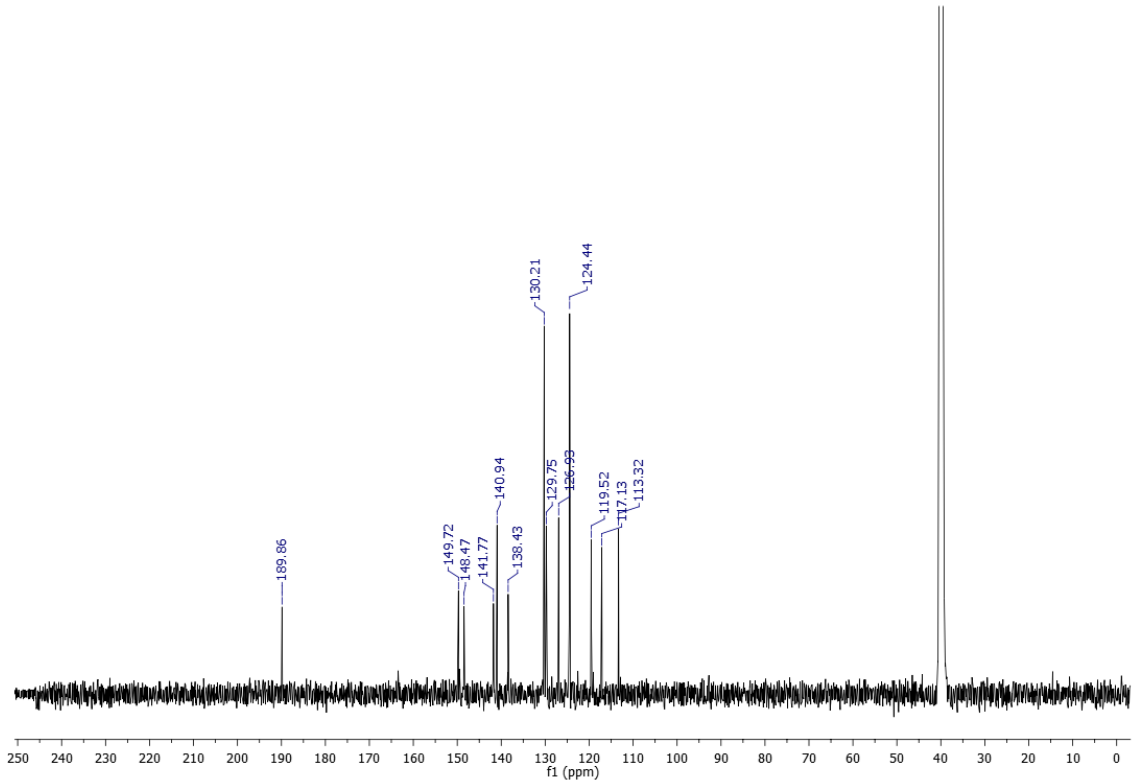

Figure S 124. HPLC chromatogram of compound **3u**

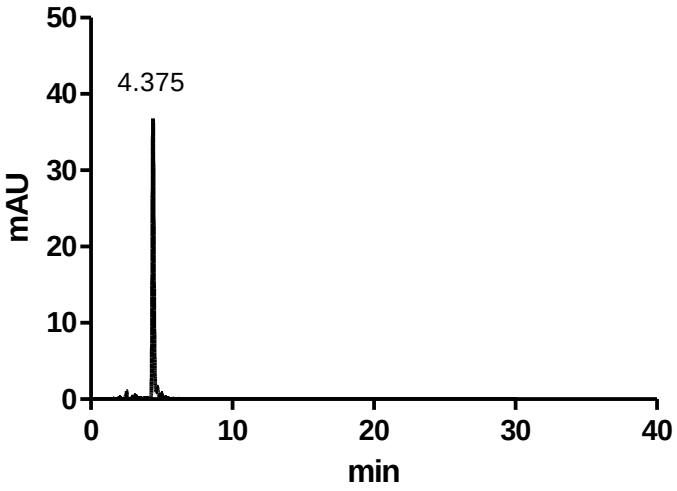

Figure S 125. UV-Vis spectrum of compound **3u**

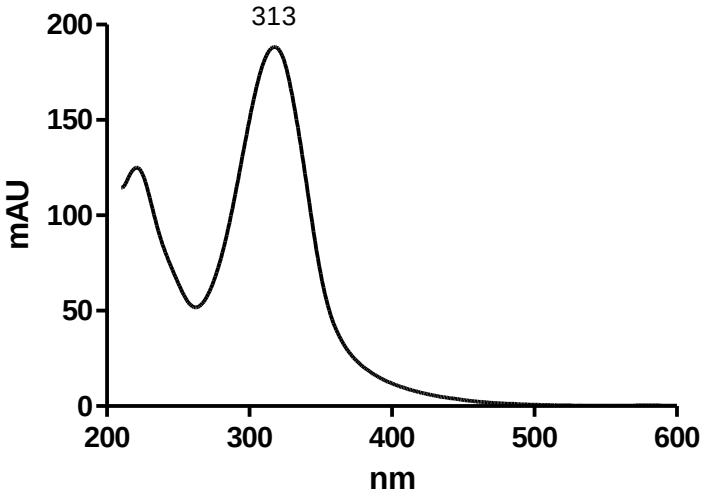

Figure S 126. ^{1}H NMR spectrum of compound **3v** (DMSO-d_6; 600 MHz)

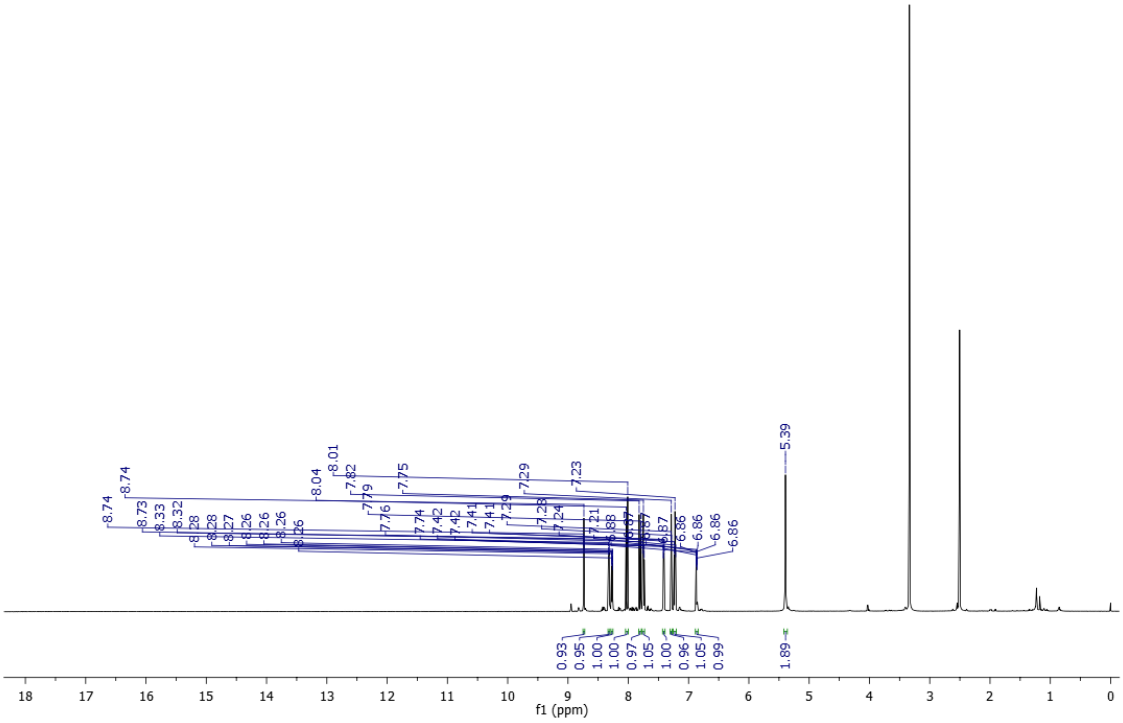

Figure S 127. ^{13}C NMR spectrum of compound **3v** (DMSO-d_6; 150 MHz)

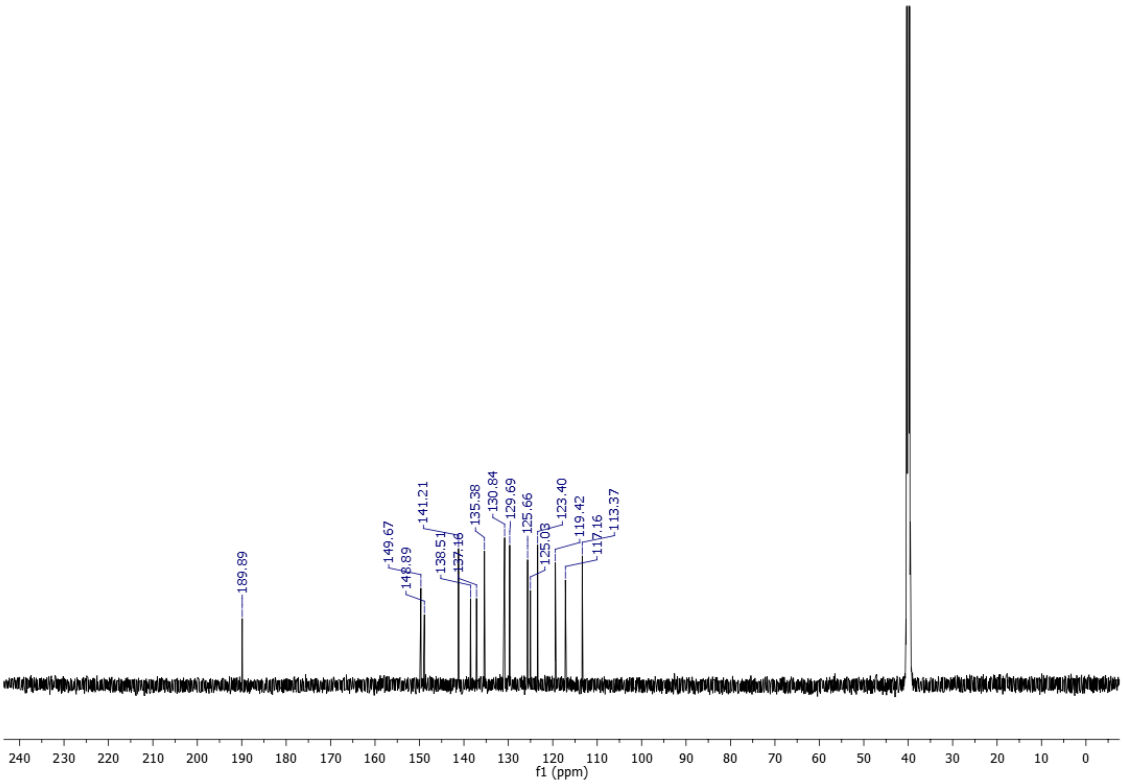

Figure S 128. HPLC chromatogram of compound **3v**

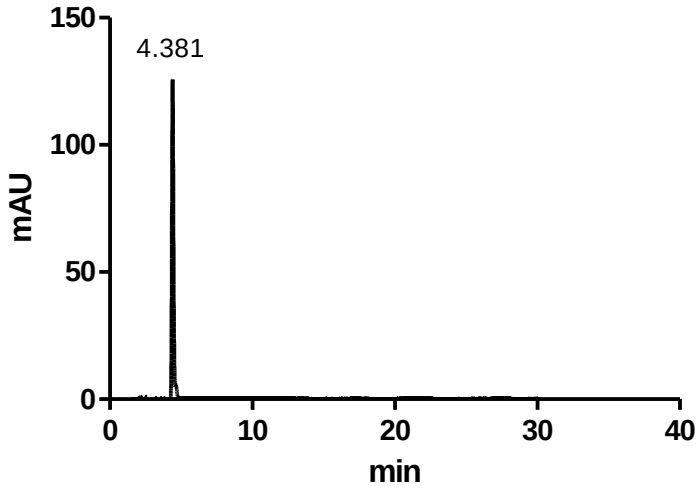

Figure S 129. UV-Vis spectrum of compound **3v**

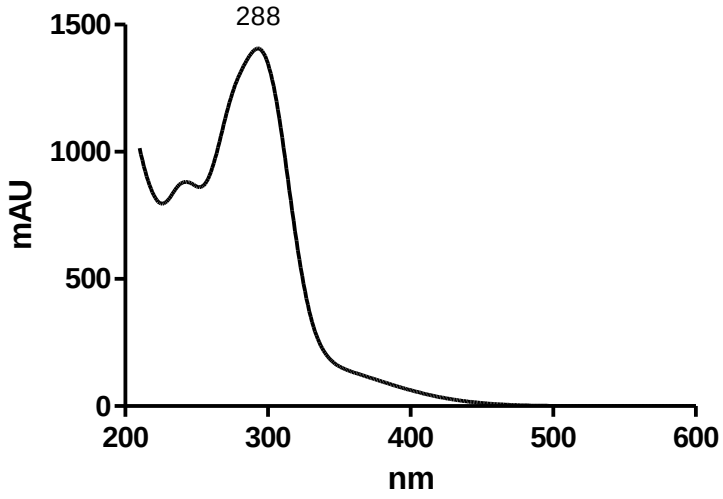

Figure S 130. ^{1}H NMR spectrum of compound **4a** (DMSO-d_6; 600 MHz)

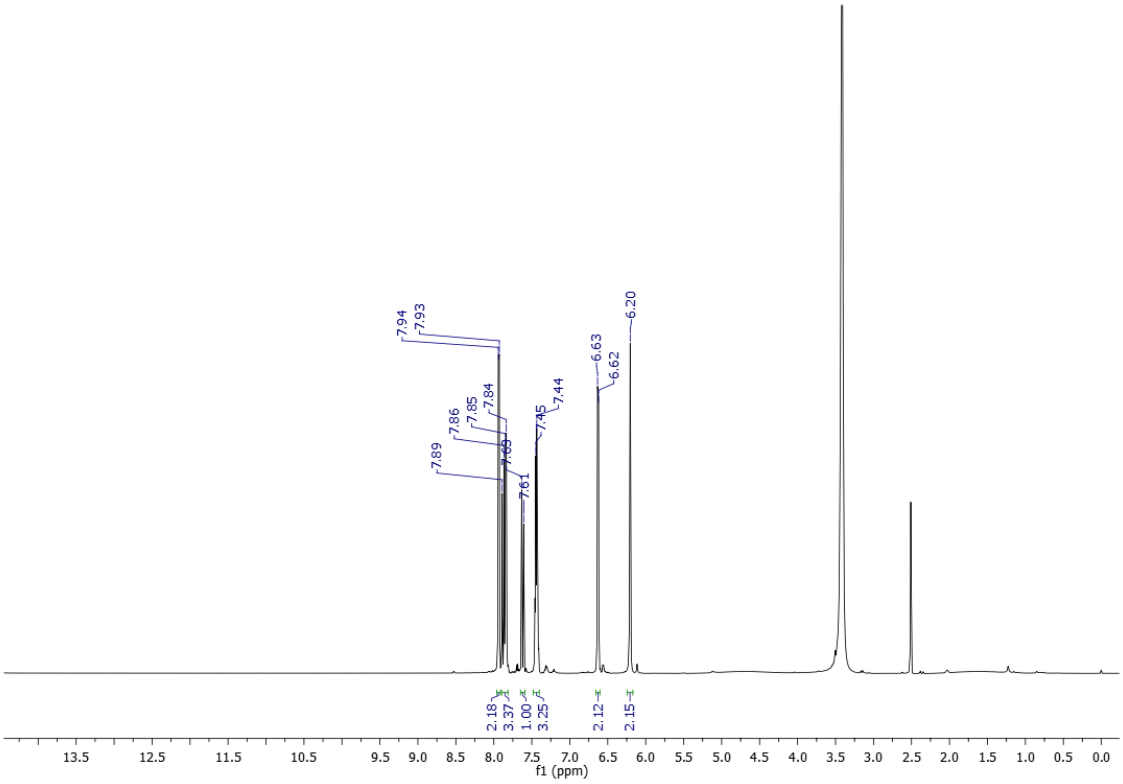

Figure S 131. ^{13}C NMR spectrum of compound **4a** (DMSO-d_6; 150 MHz)

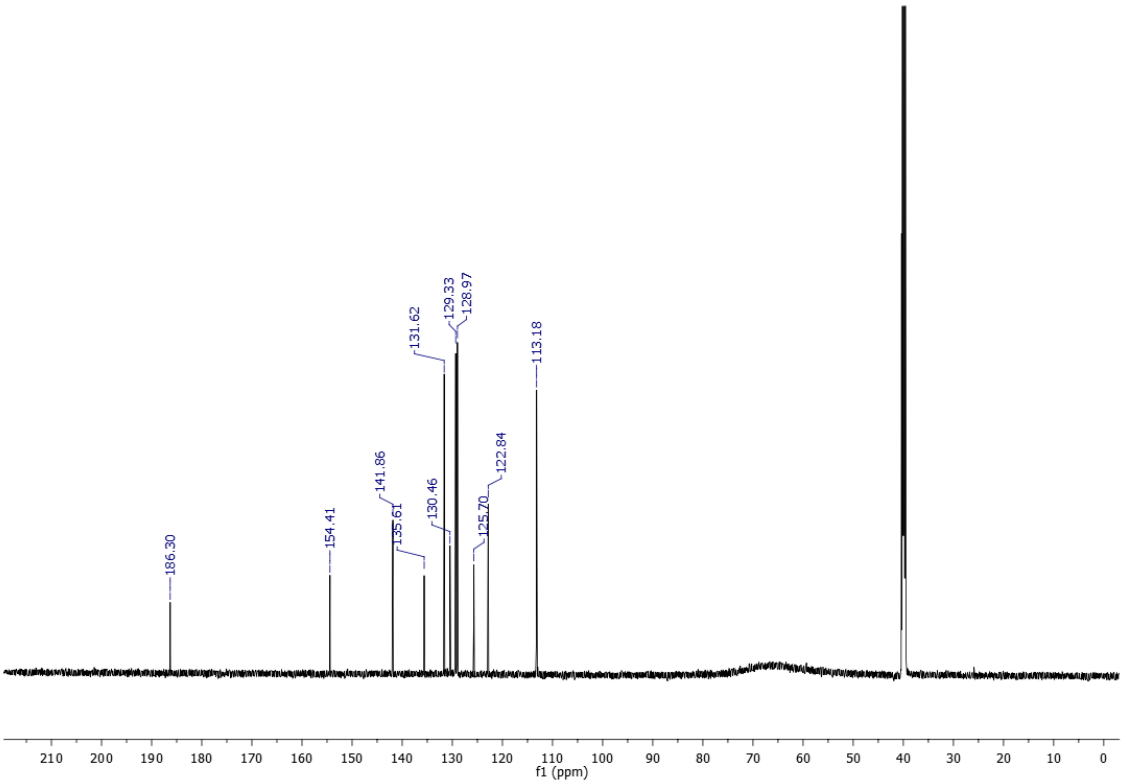

Figure S 132. HPLC chromatogram of compound **4a**

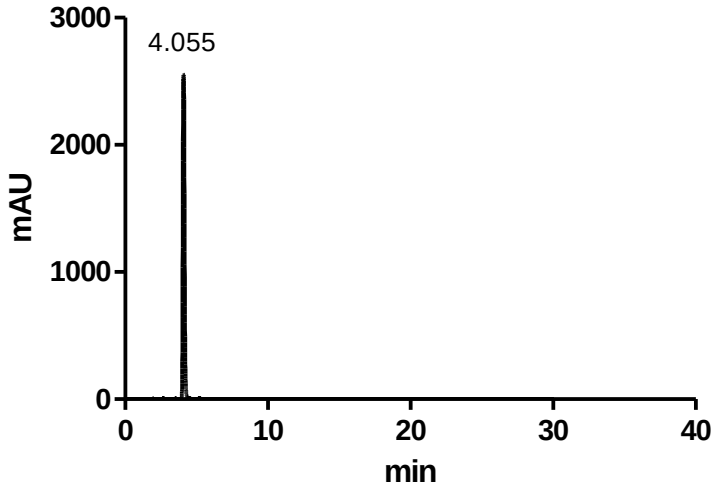

Figure S 133. UV-Vis spectrum of compound **4a**

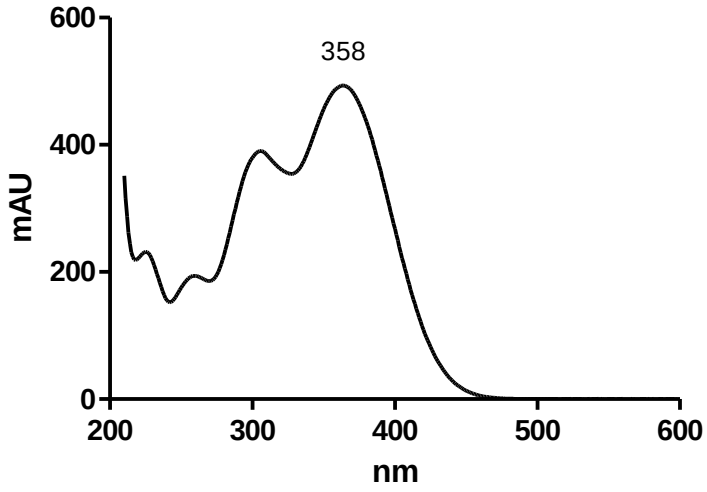

Figure S 134. ^{1}H NMR spectrum of compound **4b** (DMSO-d_6; 600 MHz)

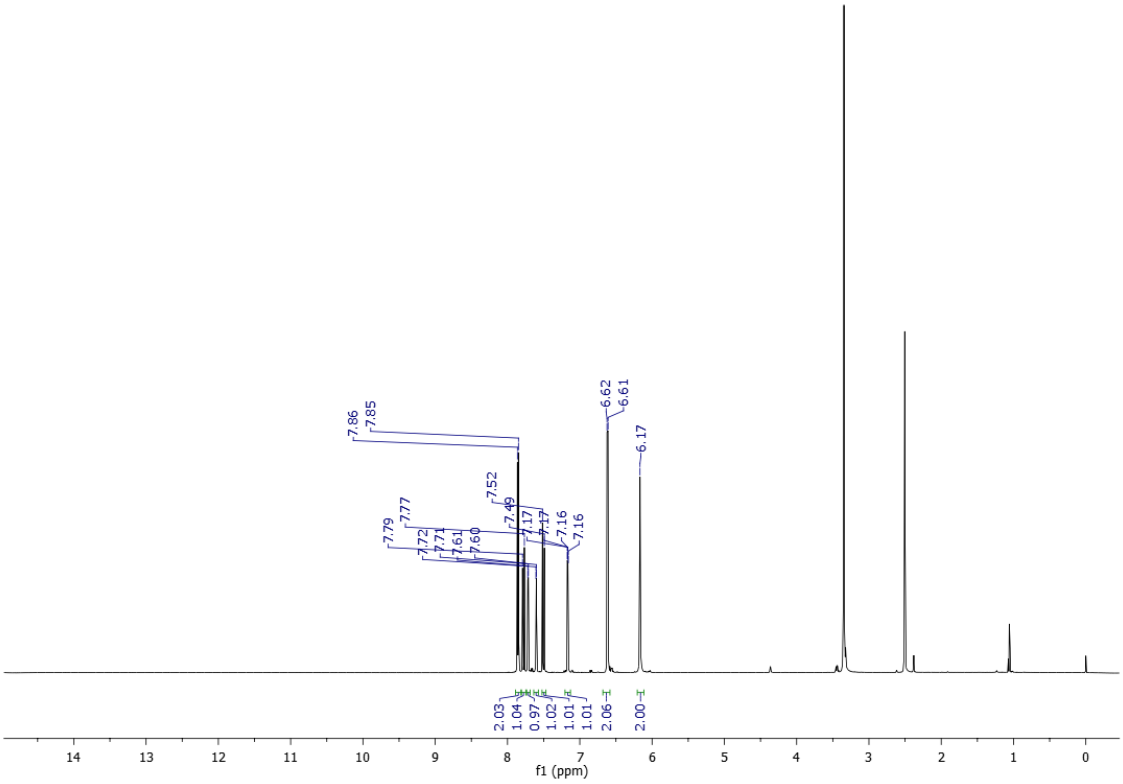

Figure S 135. ^{13}C NMR spectrum of compound **4b** (DMSO-d_6; 150 MHz)

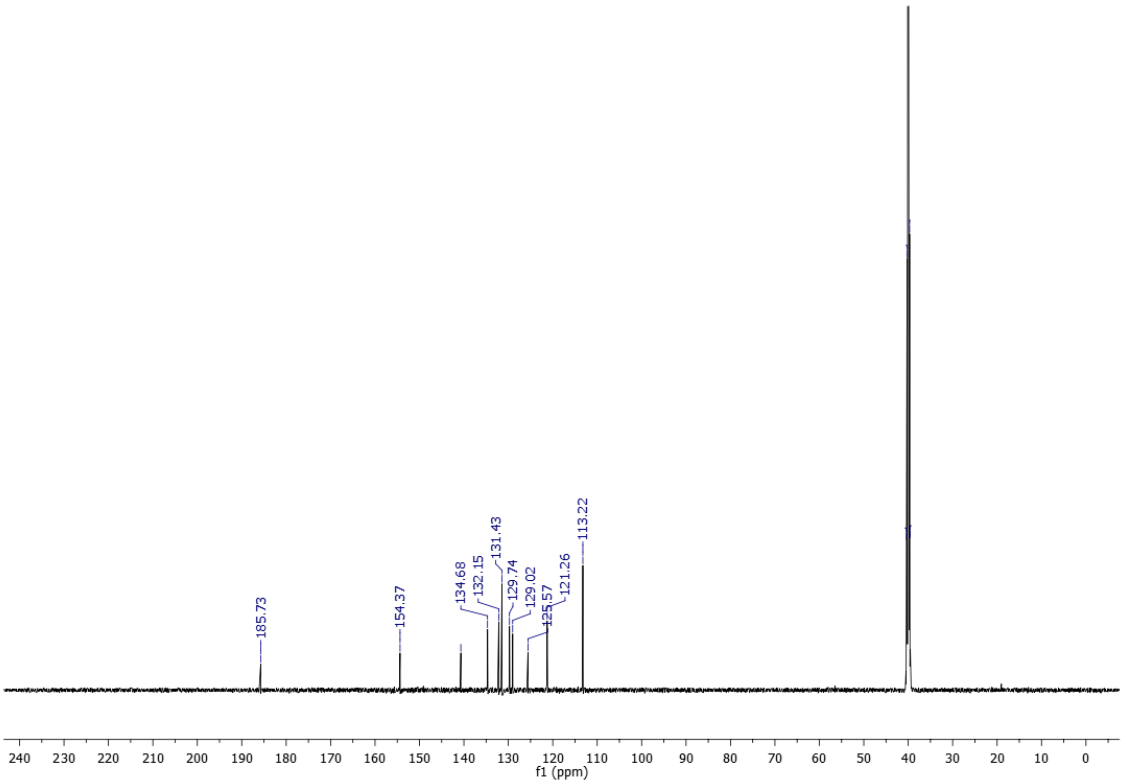

Figure S 136. HPLC chromatogram of compound **4b**

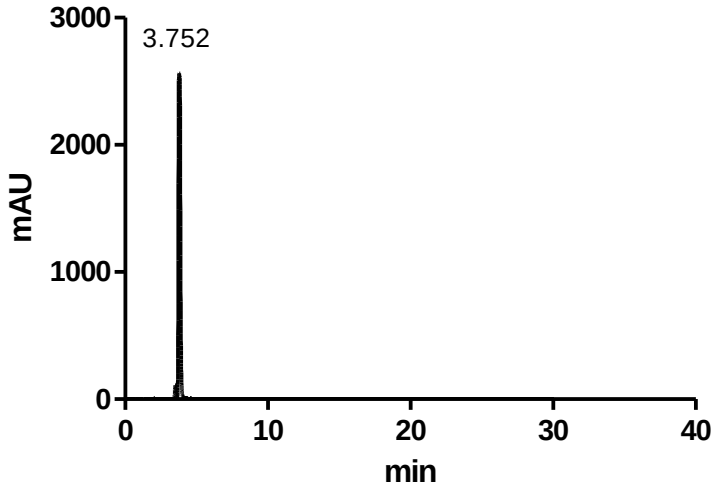

Figure S 137. UV-Vis spectrum of compound **4b**

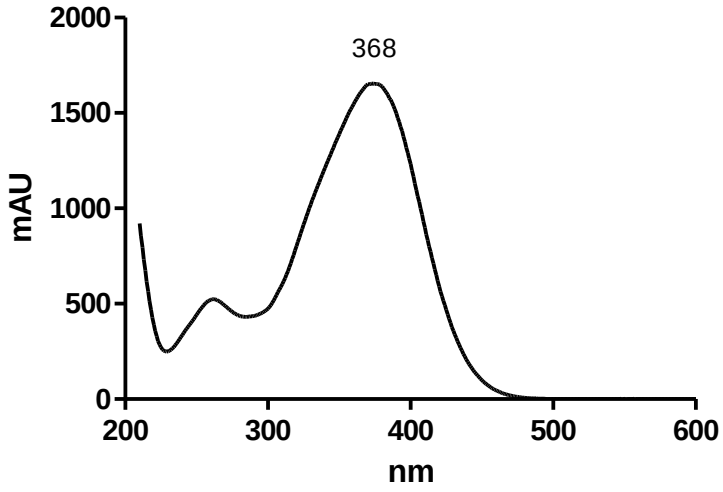

Figure S 138. ^{1}H NMR spectrum of compound **4c** (DMSO-d_6; 600 MHz)

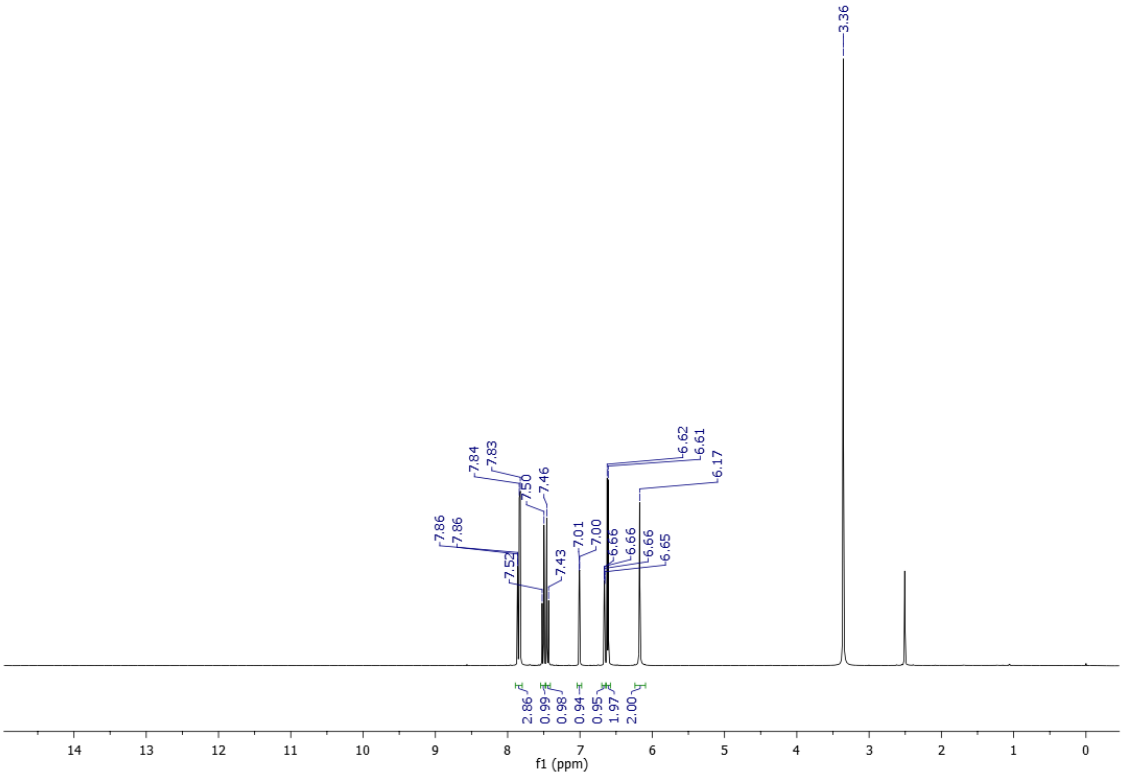

Figure S 139. ^{13}C NMR spectrum of compound **4c** (DMSO-d_6; 150 MHz)

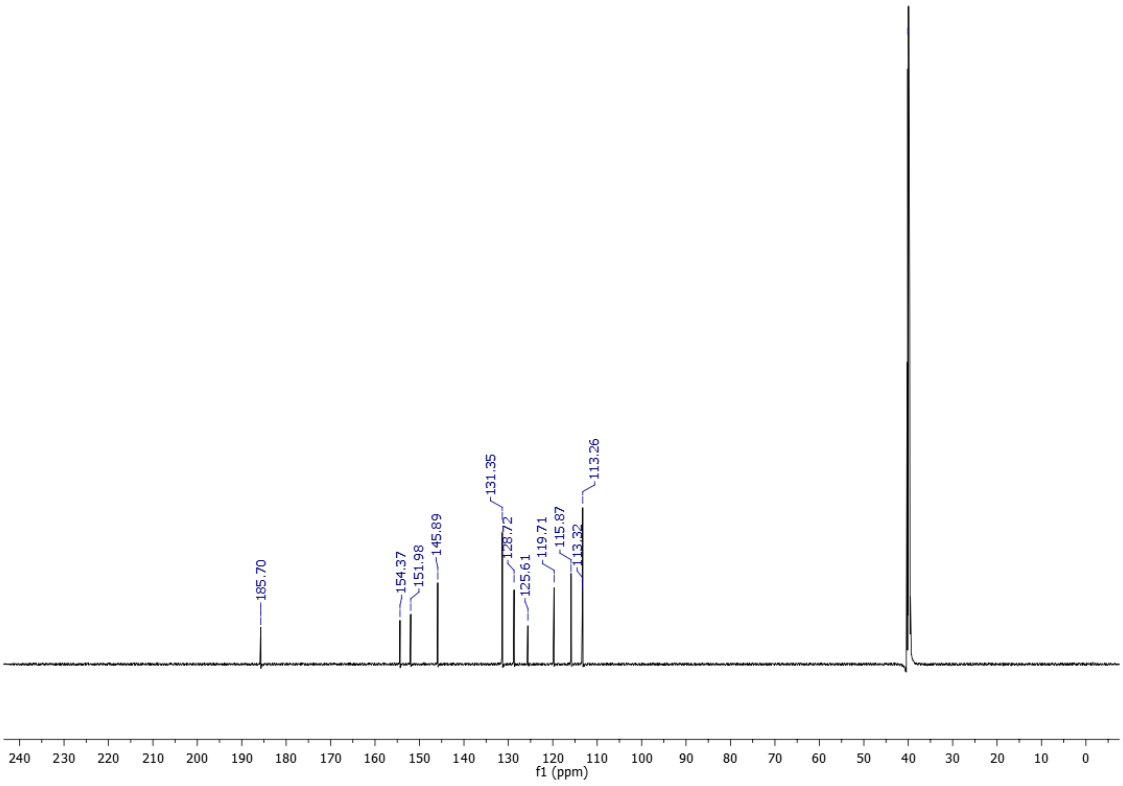

Figure S 140. HPLC chromatogram of compound **4c**

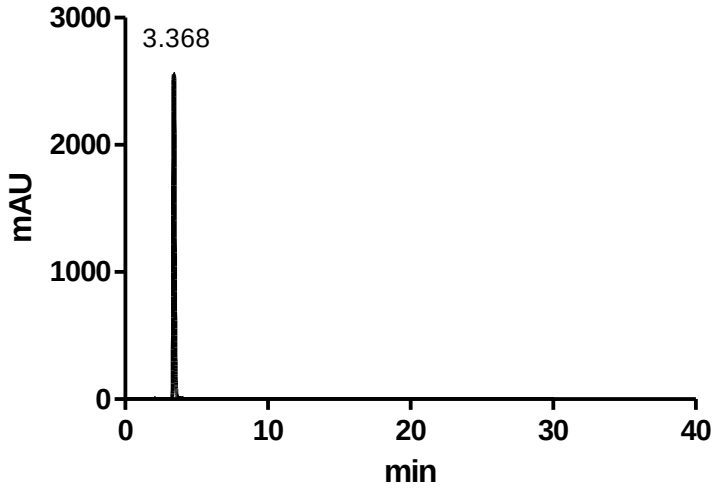

Figure S 141. UV-Vis spectrum of compound **4c**

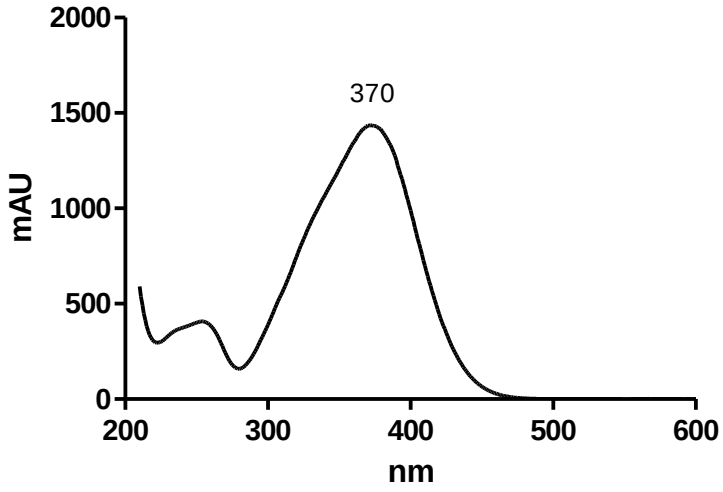

Figure S 142. ^{1}H NMR spectrum of compound **4d** (DMSO-d_6; 600 MHz)

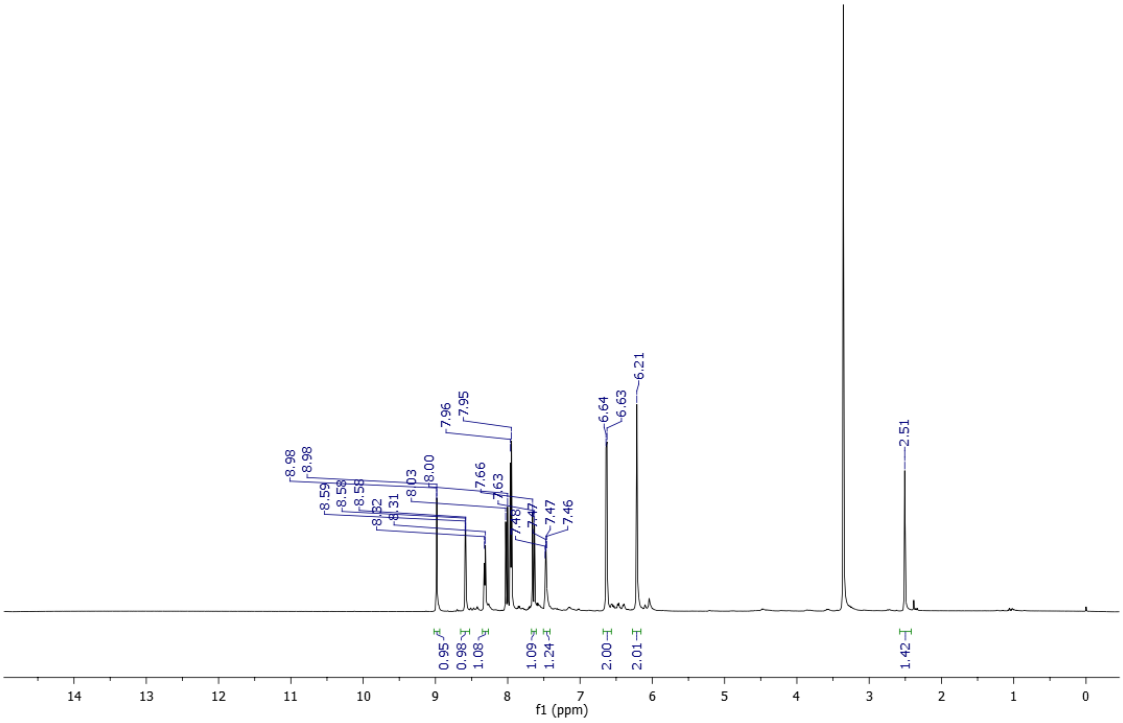

Figure S 143. ^{13}C NMR spectrum of compound **4d** (DMSO-d_6; 150 MHz)

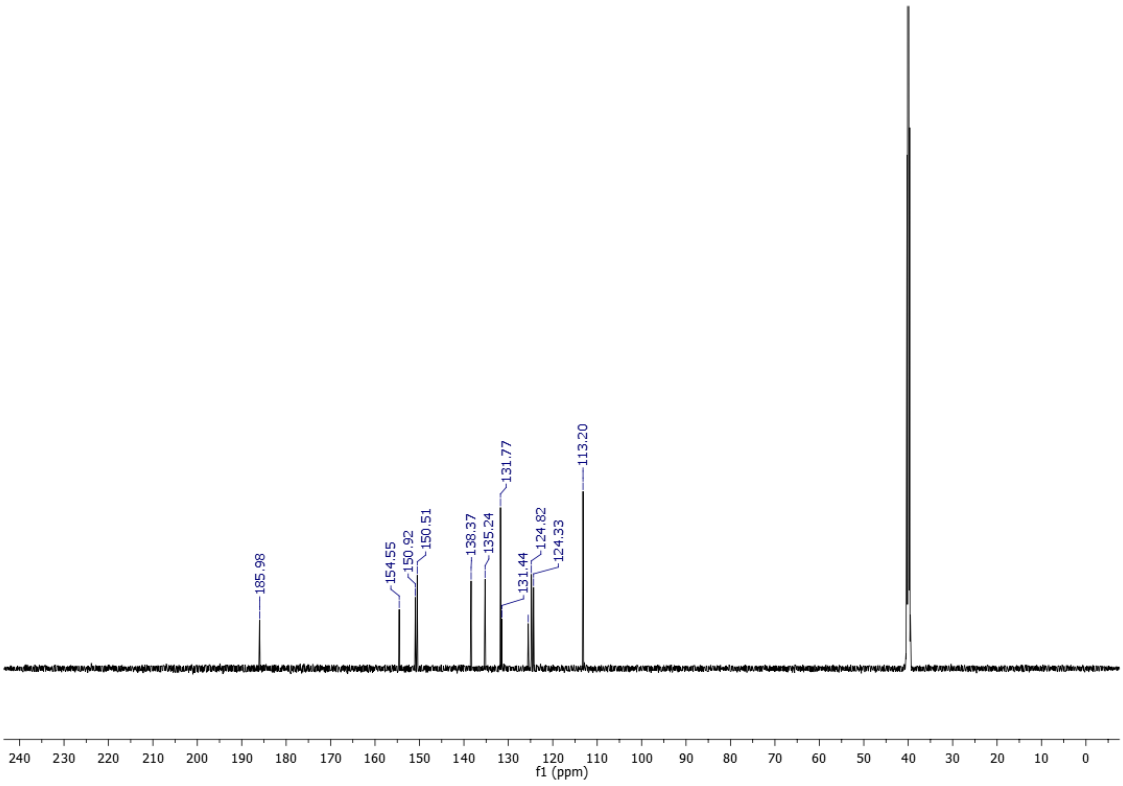

Figure S 144. HPLC chromatogram of compound **4d**

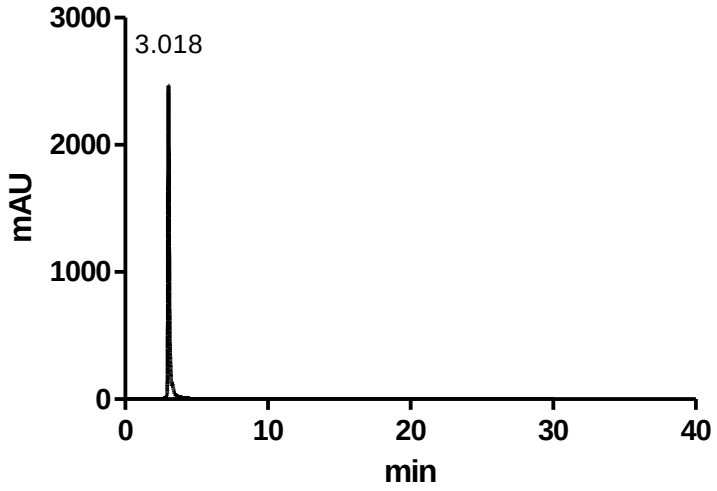

Figure S 145. UV-Vis spectrum of compound **4d**

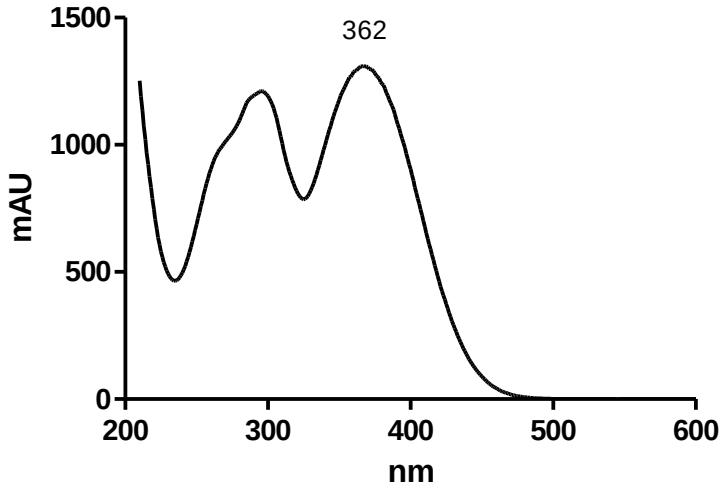

Figure S 146. ^{1}H NMR spectrum of compound **4e** (DMSO-d_6; 600 MHz)

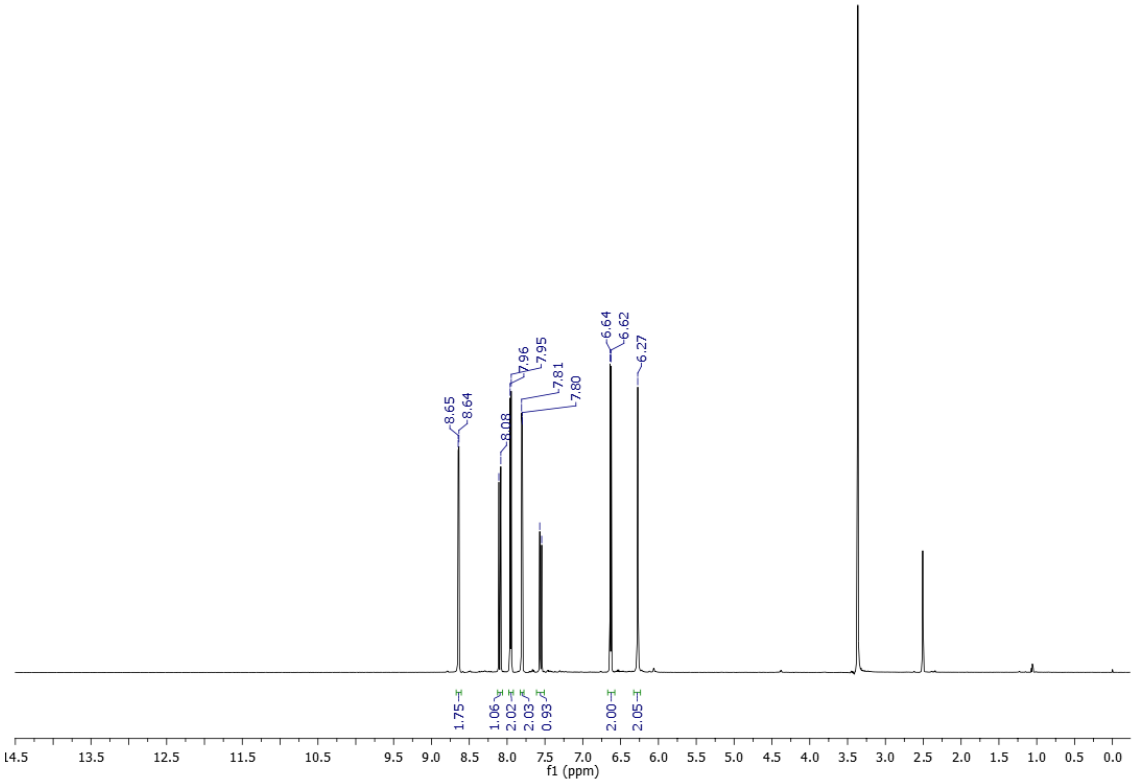

Figure S 147. ^{13}C NMR spectrum of compound **4e** (DMSO-d_6; 150 MHz)

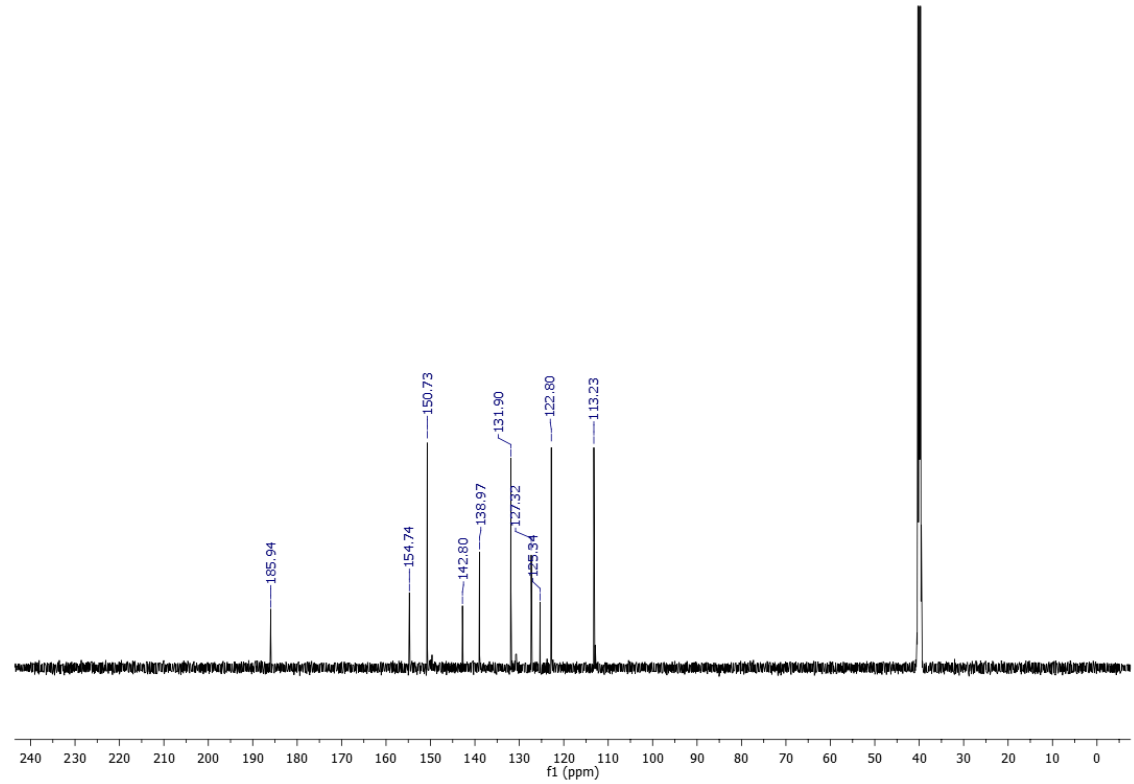

Figure S 148. HPLC chromatogram of compound **4e**

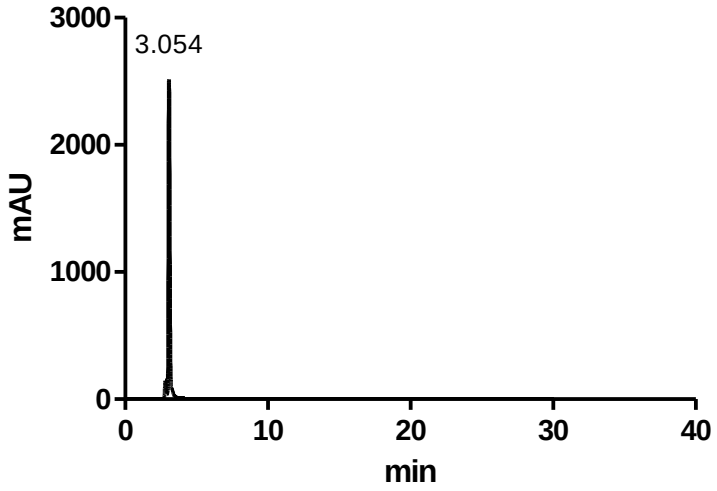

Figure S 149. UV-Vis spectrum of compound **4e**

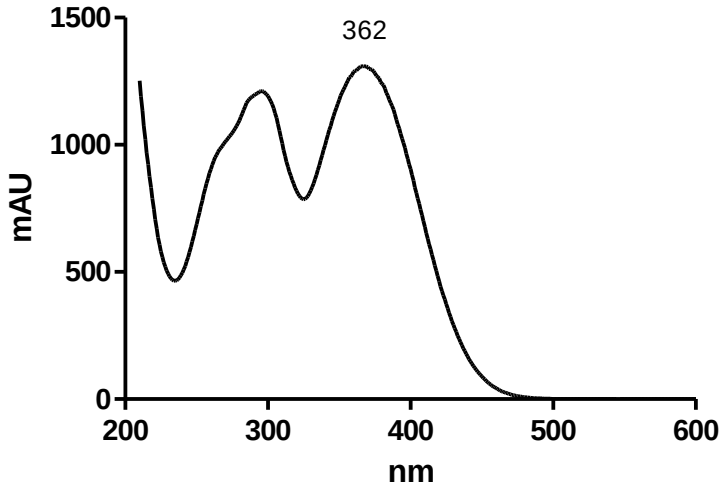

Figure S 150. ^{1}H NMR spectrum of compound **4f** (DMSO-d_6; 600 MHz)

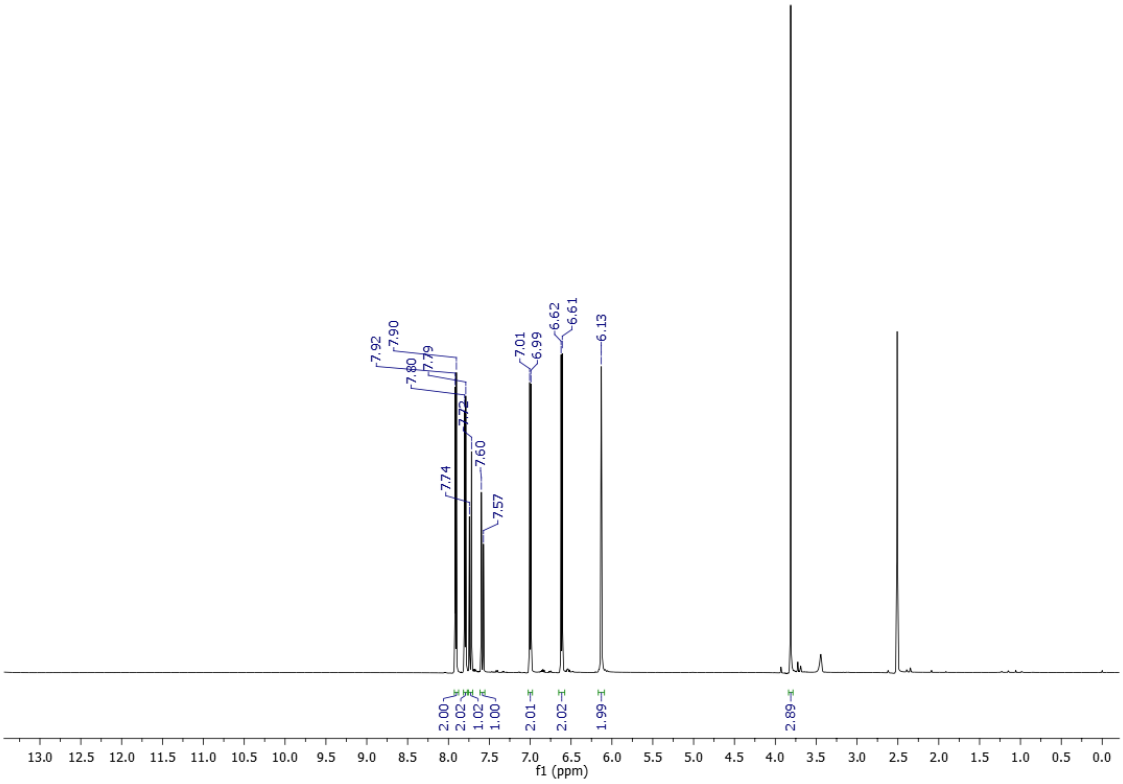

Figure S 151. ^{13}C NMR spectrum of compound **4f** (DMSO-d_6; 150 MHz)

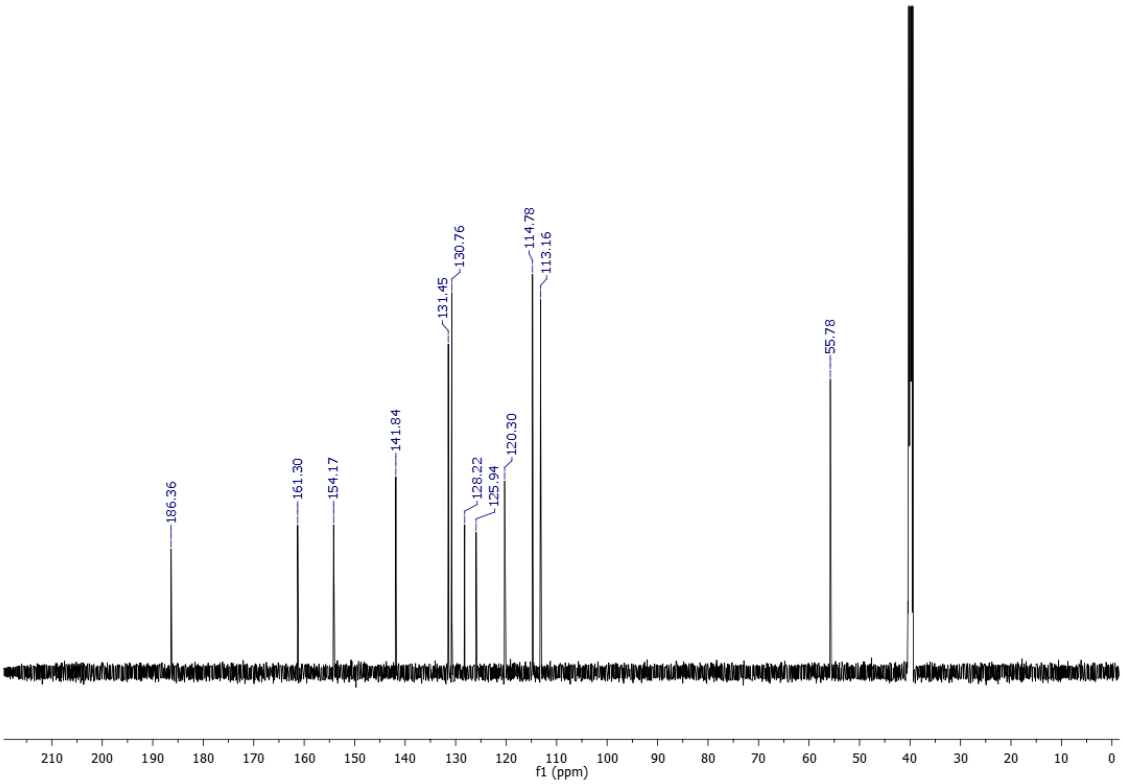

Figure S 152. HPLC chromatogram of compound **4f**

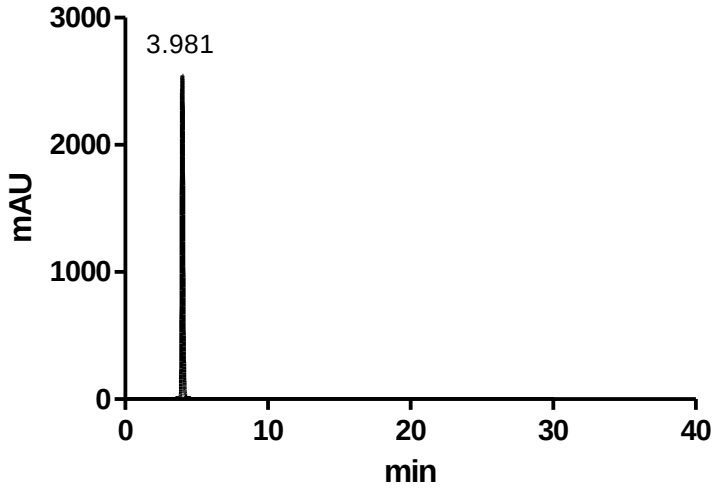

Figure S 153. UV-Vis spectrum of compound **4f**

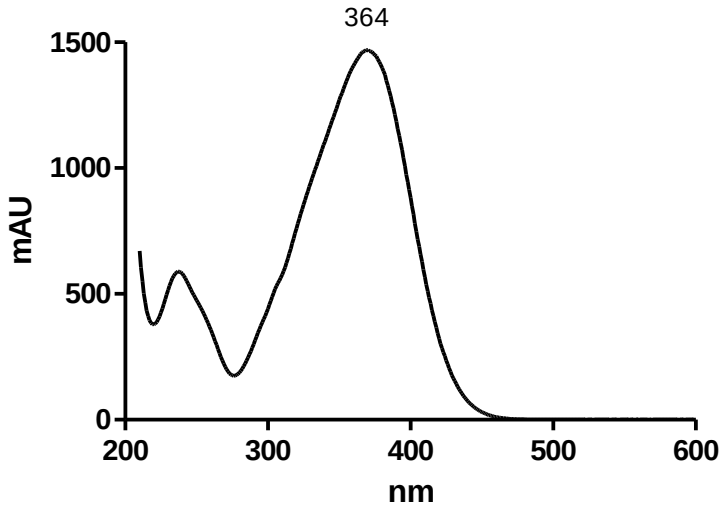

Figure S 154. ^{1}H NMR spectrum of compound **4g** (DMSO-d_6; 600 MHz)

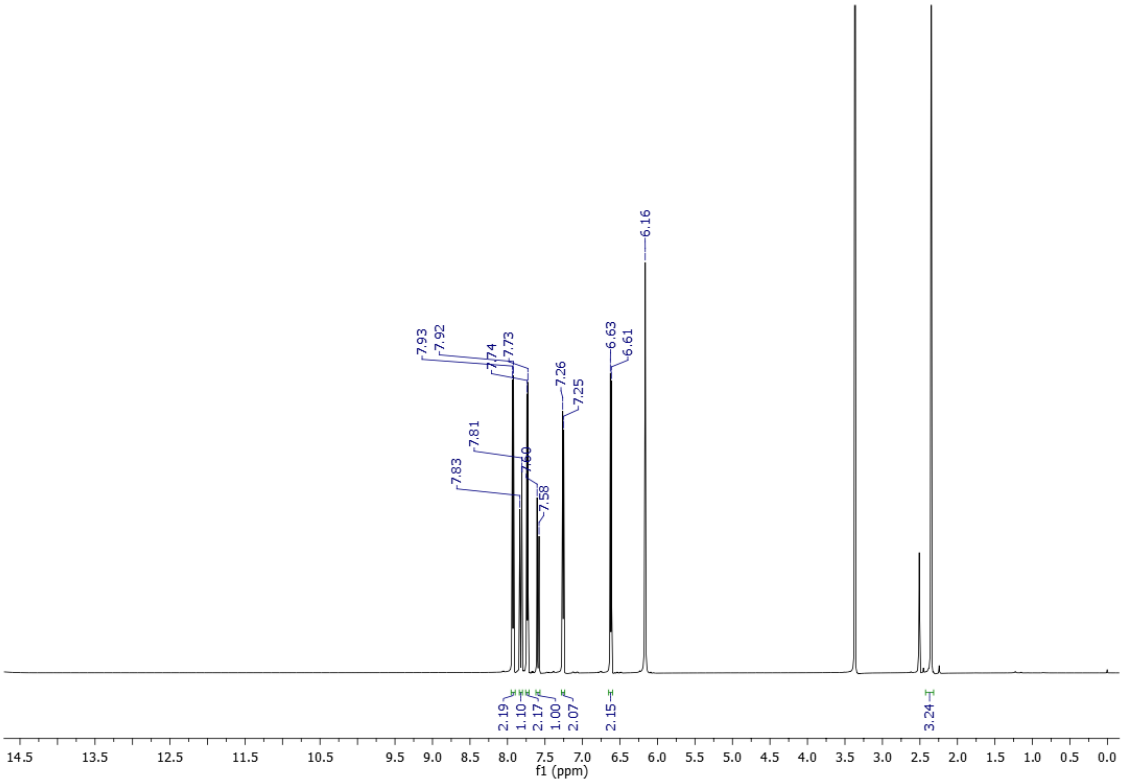

Figure S 155. ^{13}C NMR spectrum of compound **4g** (DMSO-d_6; 150 MHz)

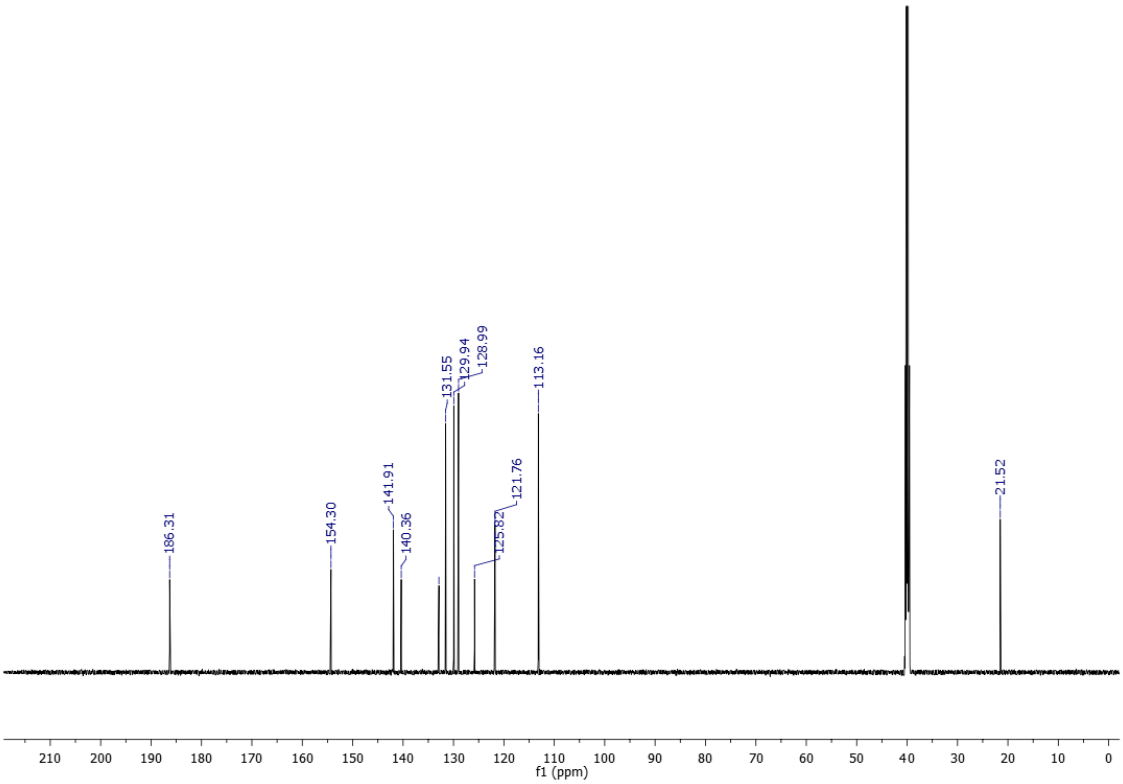

Figure S 156. HPLC chromatogram of compound **4g**

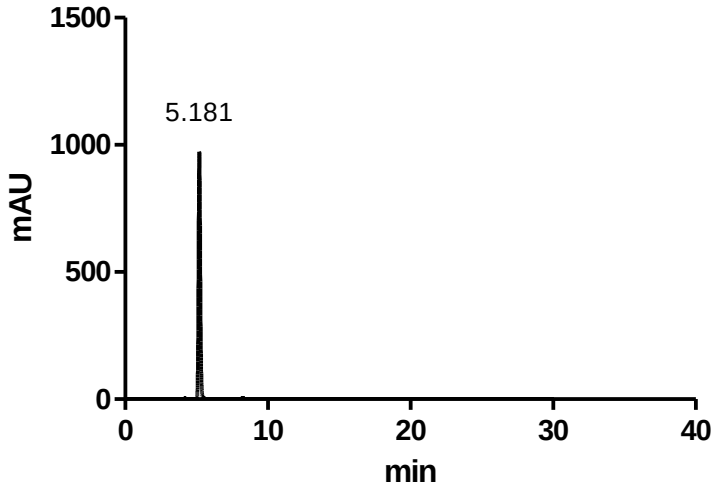

Figure S 157. UV-Vis spectrum of compound **4g**

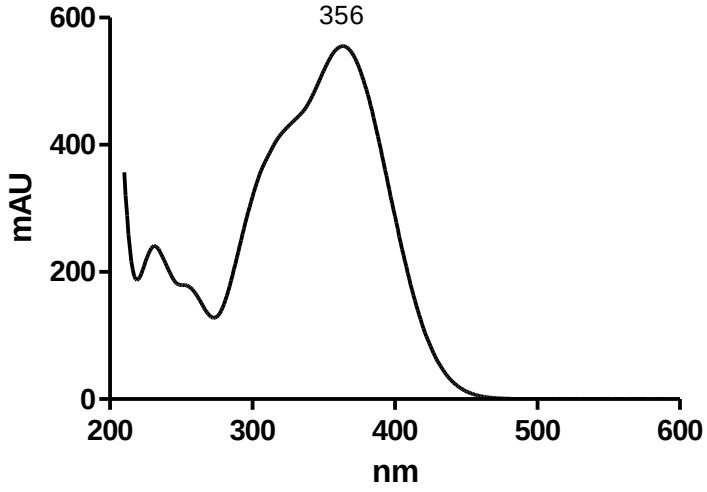

Figure S 158. ^{1}H NMR spectrum of compound **4h** (DMSO-d_6; 600 MHz)

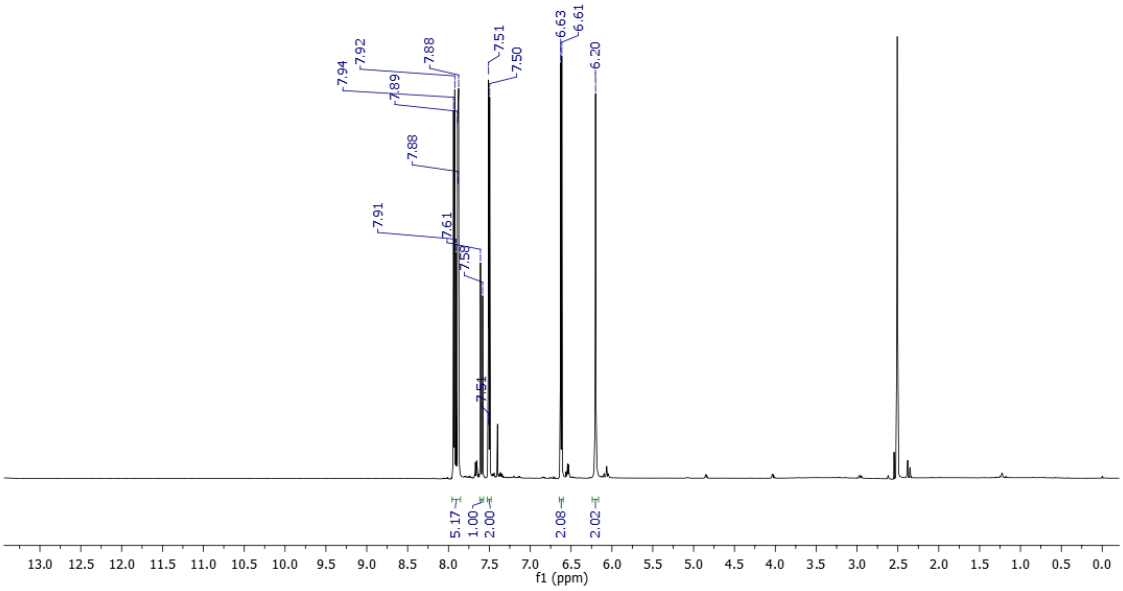

Figure S 159. ^{13}C NMR spectrum of compound **4h** (DMSO-d_6; 150 MHz)

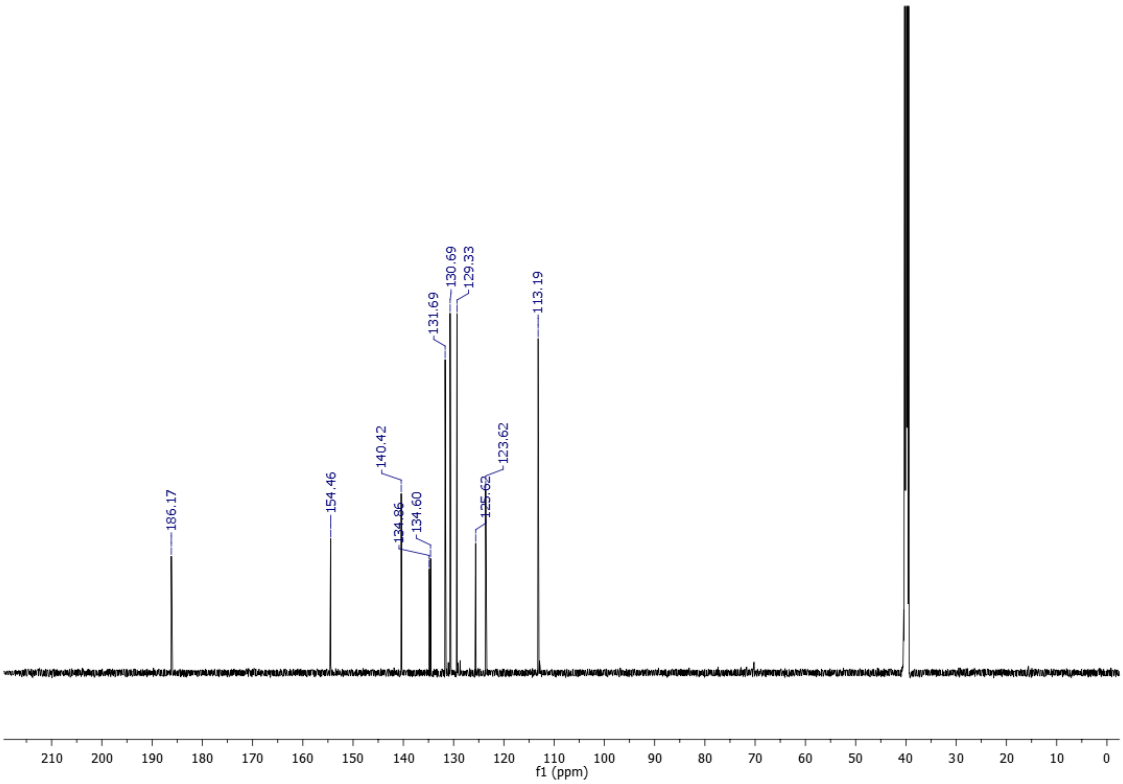

Figure S 160. HPLC chromatogram of compound **4h**

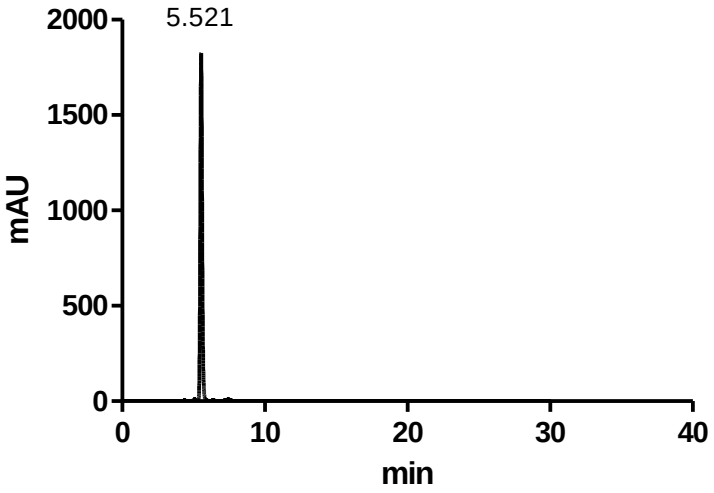

Figure S 161. UV-Vis spectrum of compound **4h**

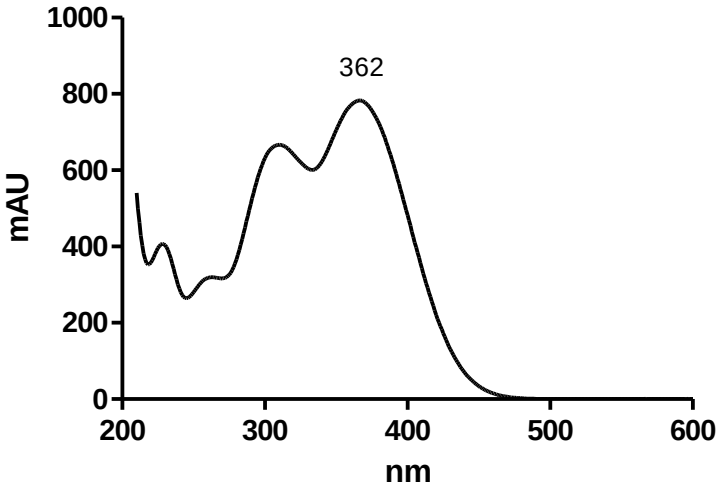

Figure S 162. ^{1}H NMR spectrum of compound **4i** (DMSO-d_6; 600 MHz)

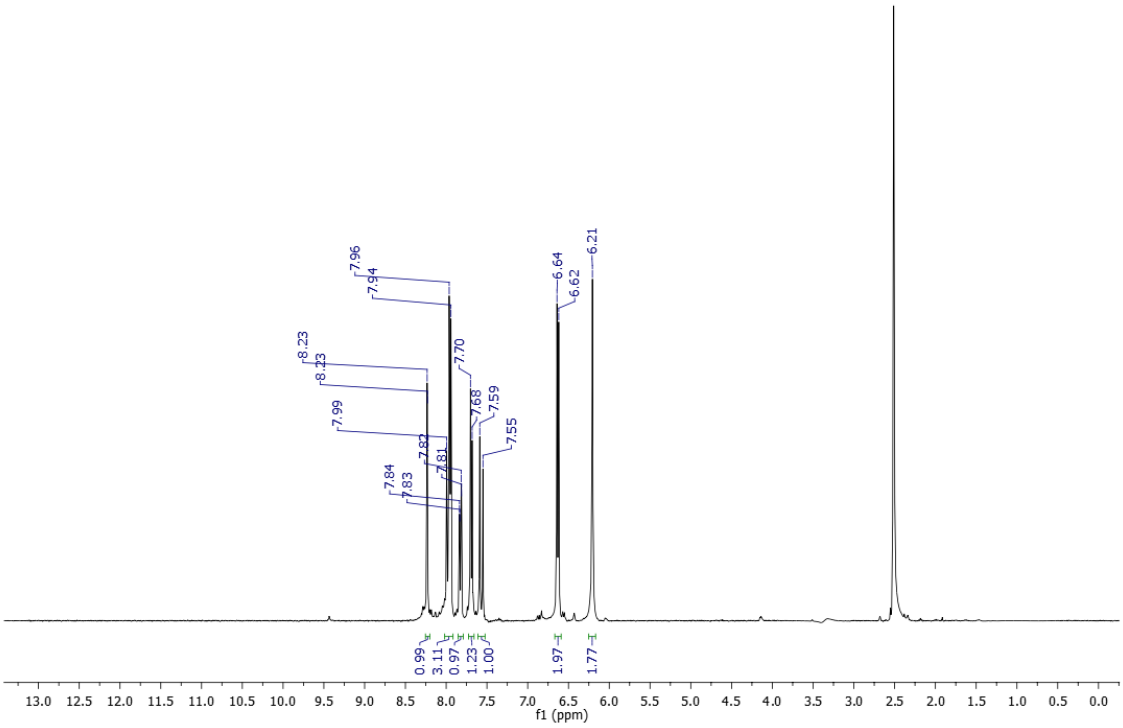

Figure S 163. ^{13}C NMR spectrum of compound **4i** (DMSO-d_6; 150 MHz)

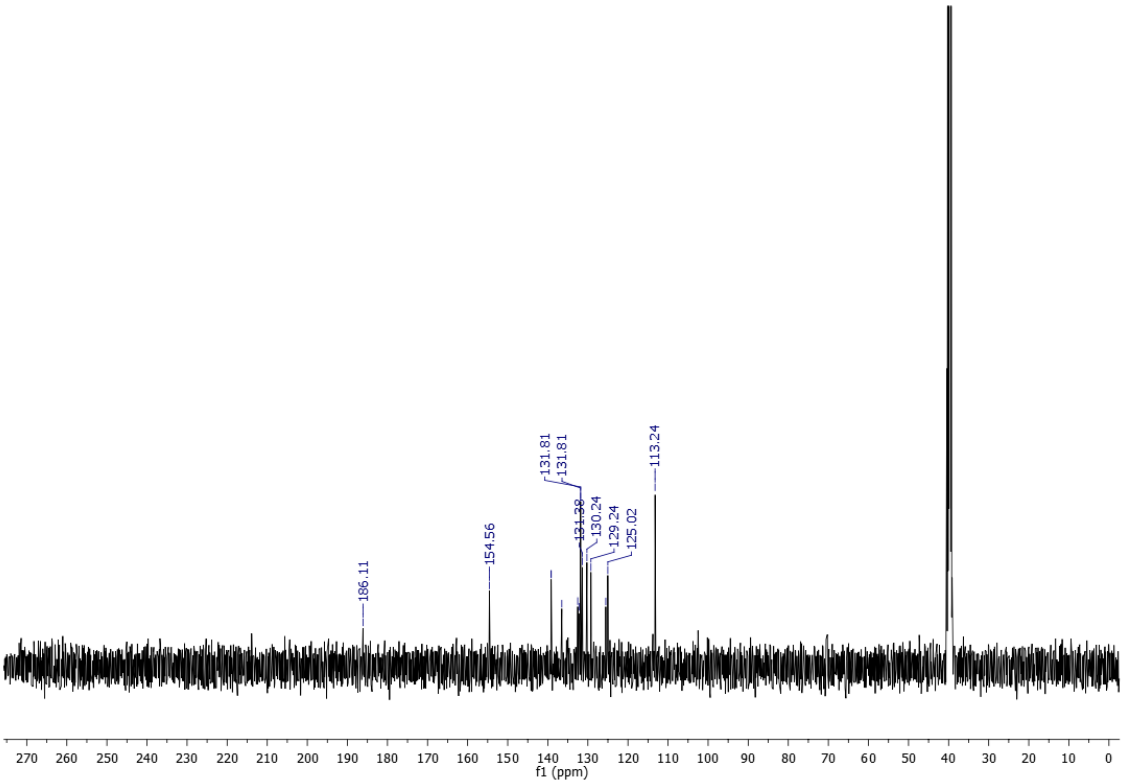

Figure S 164. HPLC chromatogram of compound **4i**

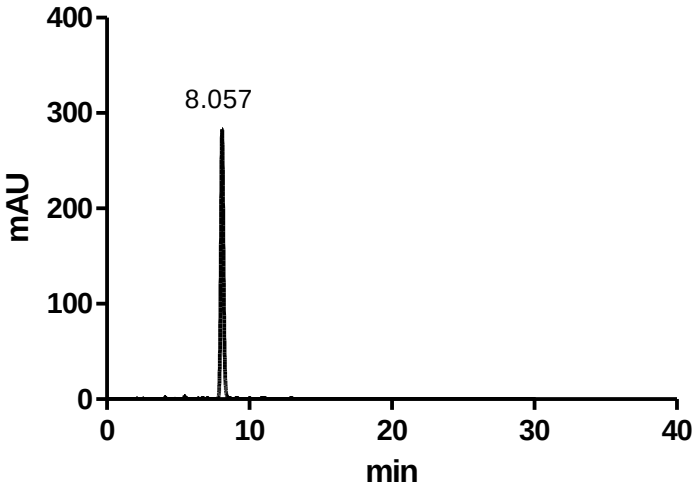

Figure S 165. UV-Vis spectrum of compound **4i**

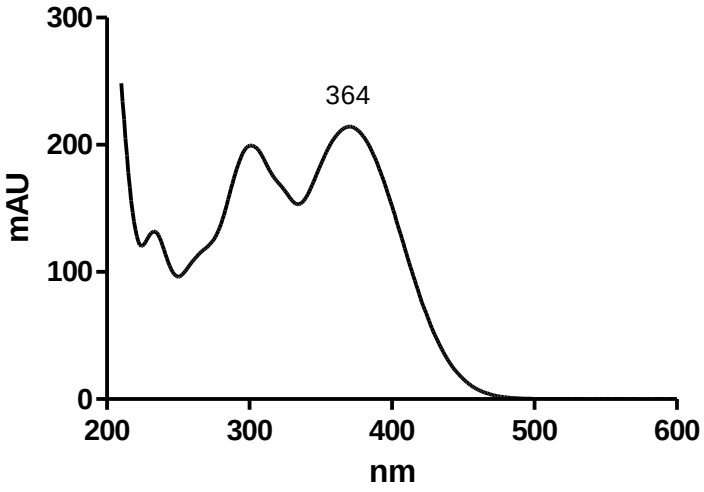

CAPÍTULO IV

1. CONCLUSÕES

O trabalho demonstrou a atividade antimicrobiana de 40 aminochalconas. As chalconas foram sintetizadas, purificadas e identificadas, com posterior avaliação antimicrobiana com foco na ação contra *S. aureus* sensível e resistente à meticilina (MSSA e MRSA) e *C. albicans*.

Os resultados de atividade antimicrobiana de aminochalconas permitiu concluir que a posição do grupo amino em 3' (anel A), bem como de grupos retiradores de elétrons e hidrofóbicos no anel B conduzem à obtenção de chalconas com atividade antimicrobiana potencializada. Dentre essas substâncias, a 3'-amino-4-bromochalcona (**3f**) que demonstrou potente atividade antibacteriana contra MSSA e MRSA com valores de CIM 1,95 e 7,80 µg/mL, foi selecionada para demais ensaios. A associação entre **3f** e vancomicina demonstrou efeito sinérgico contra MSSA. O tratamento com **3f** diminuiu a aderência de MSSA e MRSA em queratinócito humano. Após o tratamento com **3f**, verificou-se diminuição da formação de biofilme de MSSA e MRSA, similarmente à vancomicina. Além disso, **3f** demonstrou baixa toxicidade a 10 × CIM após 72 horas, com morte de 20% das larvas de *G. mellonella*. A chalcona **3f** demonstrou amplo espectro de ação antibacteriana, uma vez que foi ativa contra *E. faecalis*, *A. baumanii* e *M. tuberculosis*.

A 3'-amino-3-fluorchalcona (**3n**) demonstrou maior potência contra *C. albicans* com CIM de 3,90 µg/mL. A associação com anfotericina B demonstrou efeito sinérgico contra *C. albicans*. O tratamento com **3n** diminuiu a adesão de *C. albicans* à queratinócitos, além de ação antibiofilme em formação e maduro. O ensaio de tempo-morte indicou ação funcida da chalcona **3n**. Além disso, **3n** demonstrou interação com ergosterol de membrana, sendo um possível mecanismo de ação desta chalcona. A baixa toxicidade de **3n** a 100 × CIM levou a morte de 20% das larvas de *G. mellonella*. A chalcona **3n** demonstrou amplo espectro de ação anti-*Candida*, sendo a mais ativa da série contra *C. tropicalis*, *C. parapsilosis*, *C. glabrata* e *C. krusei*.

Com esses resultados, pode-se comprovar a atividade antimicrobiana de aminochalconas, encorajando o estudo nessa classe de substâncias na busca de novos agentes contra infecções nosocomiais.